Probe-based confocal endomicroscopy: technical challenges and clinical applications

Richard Charles Newton

MBChB BSc (Hons) MRCS

Supervisors:

Professor The Lord Ara Darzi of Denham KBE

Professor Guang-Zhong Yang

The Hamlyn Centre for Robotic Surgery,

Institute of Global Health Innovation,

Imperial College London

2014

This thesis is submitted to the Imperial College London in partial fulfilment of the requirements for the degree of Doctor of Philosophy. Except for where specifically described in the acknowledgements section, it presents entirely my own work and describes the results of my own research.

The copyright rests with the author and is made available under a Creative Commons Attribution Non-Commercial No Derivatives licence. Researchers are free to copy, distribute or transmit the thesis on the condition that they attribute it, that they do not use it for commercial purposes and that they do not alter, transform or build upon it. For any reuse or redistribution researchers must make clear to others the licence terms of this work.

Abstract

Probe based confocal laser endomicroscopy (pCLE) is an in vivo device which acquires high resolution superficial optical biopsies. Despite encouraging data on neoplasia identification in colorectal polyps and Barrett's oesophagus, there are many hurdles to pCLE advancement beyond the research arena. This thesis defines these challenges, and via 5 experimental chapters expounds four key requirements: 1) the effect of probe contact force upon the tissue needs assessing and harnessing; 2) the probe's diagnostic accuracy needs to be improved; 3) the probe's site of optical biopsy acquisition needs improved tracking; and 4) the ergonomics of pCLE optical biopsy need development.

These challenges are elucidated and elaborated upon using two short clinical studies. A library is created describing the differences between normal, inflammatory and neoplastic endobronchial pCLE images from 16 pCLE bronchoscopies, but an inability to distinguish between endobronchial carcinoma and carcinoma-in-situ is shown. The tolerability of pCLE imaging of the colorectum over five sessions during chemoradiotherapy for advanced rectal cancer is explored, and possible morphological changes are described.

The accuracy of bronchoscopic pCLE for diagnosing peripheral lung diseases is investigated. In 116 bronchopulmonary segments in 43 subjects pCLE safely provided video sequences for comparison with computed tomography, transbronchial biopsy, and bronchoalveolar lavage. With pCLE, non-emphysematous peripheral diseases tend to create diminishment of the distinct elastin alveolar microstructure, and distinction between microvessels and septal walls becomes more difficult. Alveolar septal wall density is reduced in severe emphysema, and the pleura is demonstrated beyond bullae in two patients. Though assessors have some consistency, they are shown to be unable to accurately judge the category of emphysema severity in this small study. Intravenous fluorescein is shown to cause "white-out" and thus provide no advantage for pCLE imaging of the pulmonary lobule.

At least in the laboratory, this thesis demonstrates that mucosal distension/colonic inflation and probe contact force significantly affect the consistency of pCLE images in terms of gland diameter and intergland separation. It also introduces the concept of pCLE elastography: if a device attaches to the probe to enable it to produce a sinusoidal force upon the tissue, the amount with which the glands individually expand/shrink and separate is altered if the mucosa is artificially stiffened to mimic disease.

It suggests there is potential for improving pCLE ergonomics, and tracking (at least within peripheral lung). A transvaginal flexible endoscopic robot is predicted to reach 88% of a human peritoneal cavity for pCLE periteoneoscopy; a porcine feasibility study provides interpretable abdominal cavity images. Probe tracking in the peripheral lung is especially difficult and important in heterogeneously distributed disease. A study using ex vivo porcine lung assesses the predictability of probe tip destination; it shows that only half of the probe deployments beyond the most distally visible bronchus have a single possible path.

Finally, a role for pCLE evaluation of chronic radiation proctopathy is proposed. 26 patients with symptomatic disease are pCLE sigmoidoscoped with correlative pinch biopsy. Macroscopically severe disease is associated with pCLE sequences showing glandular disruption and vasculopathy (dilated or absent vessels; “dilabscence”). A score from 16 histological features correlates with pCLE vessel dilabscence and glandular disruption suggesting pCLE may have a role in the longitudinal monitoring of this unpleasant disease.

Overall, the thesis approaches pCLE challenges from several angles in both laboratory and clinical settings, and the data are often descriptive and preliminary. However, it significantly expands upon the understanding of pCLE in peripheral and endobronchial lung disease, describes two novel clinical roles for pCLE (radiation proctopathy and evaluation of neoadjuvant therapy response), and contains the first description of two technical pCLE developments (elastographic interrogation and robotic actuation). The time is fast approaching when one of

these clinical niches capitalises on pCLEs enormous potential for mainstream deployment.

Acknowledgements

"The machine does not isolate man from the great problems of nature but plunges him more deeply into them."

Sixty years before the invention of the probe based confocal endomicroscope this comment was made by the French aristocratic aviator and author Antoine de Saint-Exupéry in his memoirs *Terre des Hommes* (1939); its pertinence became apparent during my PhD programme.

I am grateful to Professor Ara Darzi for accepting me onto this PhD programme, for his advice, and for him allocating me to have day to day supervision from Professor Guang-Zhong Yang. Professor Yang's broad knowledge, imagination, diverse academic experience and unfailing interest are enviable aids for a PhD student to have. His relentless enthusiasm and ambition are inspiring and have pushed me to plunge more deeply into the great problems of the confocal endomicroscope machine.

I am very grateful to Dr Pallav Shah and Dr Sam Kemp from the Royal Brompton Hospital for their eagerness, bronchoscopy experience and acquainting me with the rudiments of respiratory medicine and interventional bronchoscopy.

From the Royal Marsden Hospital Dr Jervoise Andreyev, Dr Andrew Wotherspoon (in particular for assessing the pinch biopsies in Chapter 7), and Dr Diana Tait have been extremely helpful.

My fellow surgical trainee colleagues Mr James Clark, Mr Mikael Sodergren, Mr David James and Mr Tou Pin Chang have been a valuable resource and have helped make the whole experience thoroughly enjoyable.

I can only hope that clinicians bring as much to the table as scientists and engineers in an academic collaboration, and I therefore express enormous gratitude for the academic rigour and dynamism of Dr David Noonan and Mr Christopher Payne (for jointly building the linear servoing device, and writing the LabVIEW programme in Chapter 5, and creating the endoscopic robot in Chapter 6), Dr Valentina Vitiello (especially for estimating the ability of the robot to navigate the workspace in Chapter 6), Dr Marco Visentini Scarzanella (in particular for processing the dynamic force videos and creating the raw data regarding gland area and separation in Chapter 5), Dr Johannes Totz (for performing the iterative optimisation of the probe tip coordinates in Chapter 6), Dr Karim Lekadir (for producing the enhanced still images in chapter 4), Dr Dan Elson, Dr Win Tun Latt, and Dr Kevin Koh.

Useful tips have also come from Professors Alexander Meining and David Hansell and thanks go to Miss Karen Kerr, Miss Raphaele Raupp, Dr Catherine Thomas and endoscopy teams at the Royal Brompton and Royal Marsden Hospitals.

As with any clinical projects, an invaluable contribution came from the brave, stoical, and usually very interested patients who offered their time, patience and orifices in the hopeful furtherment of medical science.

My mother, father, sister and friends have been inquisitive and supportive with each project, but the firmest encouragement and most lucid advice has, as always, come from my wife Shazia, who has ungrudgingly tolerated the “mistress” in our relationship for several years.

Contents

Abstract

Acknowledgements

Contents

List of Figures xv

List of Tables: xxiv

List of Acronyms: xxvi

Chapter 1 Introduction and Overview 1

1.1 Introduction - the Development of pCLE 1

1.2 A Synopsis of Each Chapter 2

1.3 The Main Original Contributions that Advance pCLE Understanding in this Thesis and their Clinical Impact 5

1.4 Main Publications Associated with this Thesis 7

Chapter 2 The brief history of probe-based confocal endomicroscopy 10

2.1 Introduction 10

2.1.1 Conventional tissue biopsy 10

2.1.2 Optical biopsy methods 11

2.3 Optical Biopsy with Optical Coherence Tomography 12

2.4 Optical Biopsy with Endocytoscopy 13

2.5 The Desktop Confocal Microscope 14

2.6 The Miniaturisation of the Confocal Microscope 16

2.7 Advantages of Conventional Tissue Biopsy over Optical Biopsy 19

2.8 Contrast Agents, Safety and Optimisation of pCLE Imaging Protocol 20

2.9 Optically Biopsying the Gastrointestinal Tract with pCLE 21

2.9.1 Imaging the large intestine with pCLE 21

2.9.2 Imaging the biliary tree with pCLE 30

2.9.3 Barrett's oesophagus and pCLE 31

2.10 Assessment of the Urological Tract with pCLE 36

2.11 Gynaecological Targets for pCLE 37

2.12 A role for pCLE in the Respiratory Tract? 39

2.12.1 Recent biophotonic developments in bronchoscopy 39

2.12.2 Adaptation of pCLE for the lung 40

2.12.3 pCLE of the upper airways 41

2.12.4 pCLE of the peripheral lung 43

2.13 The Peritoneal Cavity and pCLE 47

2.13.1 The evolution of peritoneoscopy 47

2.13.2 The integration of optical biopsy into peritoneoscopy 48

2.14 Confocal Endomicroscopy of Solid Viscera 48

2.15 CLE for the Assessment of Vasculature 50

2.16 The Ergonomics of pCLE 52

2.17 Tracking the pCLE Probe's Tip 55

2.18 Conclusion 56

2.18.1 Enhancing the F.A.T.E. of pCLE 56

Chapter 3 In Vivo Experimental Assessment of the Challenges Facing pCLE 58

3.1 Introduction to Both Studies 58

3.2 Introduction to pCLE for Endobronchial Disease Study 58

3.3 Methods for Endobronchial Study 58

3.3.1 Bronchoscopy 59

3.4 Results of Endobronchial Study 59

3.4.1 Healthy endobronchium 60

3.4.2 Inflammatory endobronchium 62

3.4.3 Neoplastic endobronchium 64

3.5 Introduction to Rectal Cancer Study - can pCLE identify Effects of Chemoradiotherapy? 65

3.5.1 A background to predicting tumour response 65

3.5.2 Pelvic radiotherapy side effects 66

3.5.3 Acute radiation proctopathy 66

3.5.4 Chronic radiation proctopathy 67

3.5.5 pCLE and acute radiation proctopathy 67

3.5.6 Aims of rectal cancer study 68

3.6 Methods for Rectal Cancer Study 68

3.7 Results of Rectal Cancer Study 69

3.7.1 Symptom severity and endoscopy procedure acceptability 69

3.7.2 Serial endoscopies 70

3.7.3 pCLE image interpretation 70

3.8 Conclusion 74

3.8.1 Force 74

3.8.2 Diagnostic accuracy 75

3.8.3 Tracking 75

3.8.4 Ergonomics 76

Chapter 4 Imaging Parenchymal Lung Diseases with pCLE 77

4.1 Introduction 77

4.1.1 Hypotheses - assessing and maximising the accuracy of a new niche for pCLE 77

4.2 Methods 78

4.2.1 Subjects 78

4.2.2 Bronchoscopy 79

4.2.3 BAL/TBB analysis and definitive diagnosis 79

4.2.4 pCLE image acquisition, processing and interpretation 80

4.3 Results 80

4.3.1 Subjects 80

4.3.2 Safety and acceptability 82

4.3.3 Mosaic function 84

4.3.4 Basic analysis of emphysema 84

4.3.6 Inflammatory cells 88

4.3.7 Intravenous fluorescein 89

4.4 Conclusion 90

4.4.1 Contact force and safety 90

4.4.2 Accuracy of pCLE 90

4.4.3 The role of fluorescein 92

4.4.4 Tracking 93

4.5 Quantification of Emphysema Severity: the Accuracy of pCLE Compared to HRCT 94

4.5.1 Introduction 94

4.5.2 Objectives and hypothesis 94

4.5.3 Methods 96

4.5.4 Results 97

4.5.5 Conclusion 99

Chapter 5 The Significance of Contact Force during pCLE Imaging 101

5.1 Introduction 101

5.1.1 Initial hypotheses 103

5.2 Methods 103

5.2.1 Colon inflation study 103

5.2.2 Static force study 103

5.3 Results 105

5.3.1 Colon inflation study 105

5.3.2 Static force study 105

5.4 Conclusion 107

5.5 Introduction - a Study in Dynamic Force 109

5.5.1 Diagnosis through assessment of a tissue's mechanical phenotype 109

5.5.2 Aims and hypothesis 110

5.6 Methods 111

5.7 Results 112

5.8 Conclusion 114

Chapter 6 Probe Manipulation – Improving the Ergonomics and Tracking of pCLE 116

6.1 Introduction 116

6.1.1 Probe manipulation for a larger optical biopsy 116
6.1.2 Precise tracking of probe tip location 117
6.1.3 The aims and hypotheses of the robotic manipulation and tracking studies . 119
6.2 Methods - Robotic Manipulation Study 120
6.2.1 Articulated robotic endoscope 120
6.2.2 Imaging probe and deployment 121
6.2.3 Estimation of clinical workspace 121
6.2.4 Projection of robotic pCLE in workspace 122
6.2.5 Study animal and in vivo imaging procedure 122
6.3 Results - Robotic Manipulation Study 123
6.3.1 Workspace analysis 123
6.3.2 pCLE peritoneoscopy 125
6.3.3 Interpretability of robotic actuated optical biopsies 126
6.4 Discussion - Robotic Manipulation Study 128
6.5 Methods – Tracking Study 131
6.6 Results - Tracking Study 132
6.7 Discussion - Tracking Study 135
6.8 Conclusion 137
Chapter 7 Chronic Radiation Proctopathy Assessment with pCLE 138
7.1 Introduction 138
7.1.1 pCLE and vascularity 138
7.1.2 Radiation proctopathy 139
7.1.3 Aims and hypothesis 139

7.2 Methods 140
7.2.1 Statistics 142
7.3 Results 143
7.3.1 Patient cohort 143
7.3.2 Biopsy sites 144
7.3.3 pCLE correlated with VRS 145
7.3.4 Histology 148
7.3.5 Correlation between histology and macroscopic appearance 149
7.3.6 Correlation between histology and glandular distortion on pCLE 150
7.3.7 Correlation between histology and pCLE vascular appearance 152
7.3.8 Correlation of symptoms with pCLE and endoscopic appearance 155
7.4 Conclusion 155
Chapter 8 Conclusion 158
8.1 The Ideal Optical Biopsy Device 158
8.2 Achievements of this Thesis and Future Work 159
8.2.1 Probe contact force – its importance in pCLE imaging 159
8.2.2 Assessing and trying to maximise the accuracy of pCLE 160
8.2.3 Tracking the probe 163
8.2.4 Ergonomics of probe manipulation 165
8.3 Closing Comments 166
References 168

List of Figures

Figure 1.1 The rapidly escalating interest in miniaturised confocal microscopy is demonstrated with a graph showing the number of new annual publications listed on PubMed. This is contrasted with titles containing "endoscopy", showing a more typical growth in other technological research. 1

Figure 1.2 The experimental chapters develop from four key themes identified in chapter 2. 5

Figure 2.1 Endobronchial OCT. A, B & C show mild moderate and severe dysplasia respectively with corresponding H&E histological images underneath (x20 magnification). Worsening dysplasia is demonstrated by increasing thickness of the epithelium (e) above the highly scattering basement membrane (bm). The epithelial nuclei become more visible as black dots with moderate and severe dysplasia (adapted from Lam et al. 2008[27]). Endocytoscope images using methylene blue as the contrast agent are shown of (D) healthy bronchial mucosa and (E) a right upper lobe endobronchial tumour with a marked heterogeneous epithelial appearance. The endocytoscope distal end is inset. The tumour's white light endoscope image (F) is shown with the autofluorescence image (G), with malignant area indicated by arrow. 14

Figure 2.2 A schematic representation of how the CLSM focuses light of a single wavelength upon the tissue under investigation and detects the fluorescence emitted. Only light from the required optical plane is detected; "out of focus" light is blocked from detection by the pinhole. 16

Figure 2.3 The histopathological features of colonic mucosa demonstrable with conventional haemotoxylin and eosin sections both vertically (A) and en-face (B) are illustrated in a schematic (C) and shown in a colour enhanced pCLE mosaic (D). 24

Figure 2.4 High-resolution pCLE mosaics showing normal (A) [100], hyperplastic (B)[100], and adenomatous mucosa (C)[100], with the typical morphological disorganisation of adenocarcinoma (D)[101]. 25

Figure 2.5 Attempts to improve diagnostic accuracy include measurement of the speed of absorption of topical fluorescein (A)[118], and the use of nuclear staining topical contrast agents like cresyl violet (B)[119]. Fluorescent molecular markers include heptapeptides

(C)[126], and anti-EGFR antibodies (D) applied topically to the tumour (E) [124]. Fluorescent labelled anti-endothelial antibodies under colour enhanced eCLE imaging ex vivo illustrate a thinner more regularly hexagonal microvascular structure in normal colonic biopsies (F) versus colorectal tumour biopsies (G)[127]..... 29

Figure 2.6 A stricture within the common bile duct is demonstrated using ERCP (A). pCLE images of healthy bile duct show thin dark bands (B), whereas large black cells and tortuous fluorescent vessels are evident in malignant areas (C and D)[143, 144]. 31

Figure 2.7 In (A), argon plasma coagulation marks the Barrett's segment of the distal oesophagus to enable optical and pinch biopsies to be obtained from the same site, immediately above the burn marks. On the end of the endoscope, the transparent mucosectomy cap is visible to enable suction stabilisation[157]. The pCLE appearance of regular columnar epithelium in non-dysplastic Barrett's mucosa, interspersed with mucin filled goblet cells is shown in B[158]. Features of dysplasia or cancer include epithelial inhomogeneity with large dark cells, and fluorescein leakage (C&D) [157, 160]. Desktop confocal microscopy images of non-dysplastic (E) and, as denoted by hyperfluorescent glands, high grade dysplastic oesophageal pinch biopsies (F) incubated in 2-NBDG[164]. 35

Figure 2.8 Healthy urothelium is shown in (A) in the form of a single pCLE image, also expanded into a panoramic mosaic. These "umbrella" cells appear more crowded in low-grade carcinoma (B), and display increasing pleomorphism in (D) which is taken from high-grade carcinoma. In (F), taken from chronically inflamed urothelium, there are small monomorphic cells. (C), (E) & (G) are the equivalent haemotoxylin and eosin stained histology images. Adapted from Wu et al. 2011[59]. 37

Figure 2.9 A schematic showing a novel device for confocal image acquisition during laparoscopy is shown in (A). Ovarian images obtained using this microlaparoscope were superior using topical acridine orange (C-F) compared to topical fluorescein (B). The distribution and size of nuclei are more heterogeneous in adenocarcinoma (D) than in healthy epithelium (C). Epithelium can be easily denuded with accidental mechanical scraping during imaging (E) and when the device is used in vivo, uniform contact is more difficult to achieve (F). Cervical CLE with topical acriflavine can easily differentiate healthy epithelium (G) from CIN3 (I) on the basis of nuclear density, but distinguishing CIN1 (H) from healthy epithelium is more problematic. Adapted from[175] and [177].. 39

Figure 2.10 The arrangement of the elastin network beneath the airway epithelium autofluoresces and, it has been suggested, characteristically in different areas; dense, homogeneous without crosshatching in the anterior trachea (A), compact cross hatchings close to bronchial gland openings near lobar carinae (B), increasingly loose cross-hatchings of membranous trachea (C), and distal airways (D and E), and a "ringlike" appearance to noncartilagionous bronchioles (F). Disrupted basement membrane appearance is shown with carcinoma-in-situ (G), metaplasia (H) and sarcoidosis (I). Using topically applied cresyl violet in vivo at 561nm, it is possible to differentiate between normal epithelium (J) and dysplasia (K&L), but not between grades of dysplasia; mild (K), and severe (L). Adapted from [47] and [198]. 42

Figure 2.11 Confocal alveoscopy in a non-smoker demonstrates (a) the elastin scaffold of the lobule with a green arrow showing the alveolar mouth diameter, and (b) a microvessel. The alveolus is stuffed with autofluorescent macrophages in healthy smokers (c), and in amiodarone-induced interstitial lung disease (d). In PAP 100-300μm lipoproteinaceous globules are present (e). In rat models of bleomycin induced ALI, the parenchymal walls are thickened, as illustrated by type 1 epithelial cell fluorescent labelling in normal lung (f) and bleomycin induced ALI (g). Fluorescent labelled neutrophils are also drawn into the peripheral lung in ALI; healthy (h) and ALI (i). Adapted from [48, 204, 208, 212] 46

Figure 2.12 Transthoracic pCLE signal in rats showing no discernible fluorescence over a healthy area even after peptide injection (A). When imaging an aspergillus microabscess small specks were evident before peptide injection (B), becoming larger fluorescent patches after peptide injection (C). A similar appearance to (B) was seen overlying inflammatory areas, and *Geosmithia argillacea* microabscesses before and after peptide injection[213]..... 47

Figure 2.13 The nCLE consists of a probe similar to a cholangioflex deployed through a 19 or 22 gauge needle (A). nCLE images of porcine liver (B), appear to delineate sinusoids shown with H&E staining in (C). nCLE of the pancreas after EUS sometimes shows a reticular pattern similar to that found with biliary pCLE, suggesting the pancreatic duct has been abutted (D). A non-mucinous pancreatic neoplasm (E), and an intraductal papillary mucinous neoplasm showing papillary proliferation (F&G) are shown. The highly vascular histology of a mixed serous/acinar cell pancreatic cystadenoma is shown in (J) with corresponding blood vessels (H) and acinar cells (I) demonstrated on nCLE. Adapted from [67] and [227]..... 50

Figure 3.1 Representative still images from pCLE video sequences in 12 subjects; all taken from endobronchium that appears normal during white light bronchoscopy. The yellow ovals indicate where bronchial gland ducts penetrate the elastin rich basement membrane. Sequence 11a demonstrates a short mosaic. 61

Figure 3.2 pCLE images of inflammatory endobronchium. Yellow ovals once again highlight bronchial glands. The reticular elastin pattern appears to be at least partly preserved in mild inflammation or nodularity, but a "cotton wool" appearance is seen in the more dramatic nodularity of tracheobronchopathia osteochondroplastica and tracheobronchial amyloidosis. These conditions are illustrated in the CT scans and bronchoscopic images. Endobronchial biopsies of the mucosa affected by amyloid show acellular pink material underlying the respiratory epithelium after haemotoxylin and eosin staining; viewing this material with polarised light after congo red staining demonstrated apple-green birefringence. 63

Figure 3.3 pCLE images of endobronchium affected by dysplasia and neoplasia. To highlight the subtlety of these lesions sometimes, the arrow within the autofluorescence bronchoscopy image points to an area of mild dysplasia. 64

Figure 3.4 Representative pCLE still images and mosaics of the tumour during treatment demonstrating mostly disorganisation and loss of recognisable structure. Yellow and blue ellipses respectively highlight frames which include recognisable glands, and those containing vessels with flowing blood. The white light endoscopy images are taken with the endoscope retroflexed, and show the tumour shrinking during treatment. (For simplicity, images from the fourth endoscopy session have been omitted). 72

Figure 3.5 pCLE images of the posterior wall of the rectum during treatment. Blue ellipses highlight vessels; these are usually approximately10µm , but larger diameter ones are present after a couple of weeks of radiotherapy (20µm). 73

Figure 3.6: The glandular and vascular morphology of descending colonic mucosa (control) imaged with pCLE during neoadjuvant treatment did not seem to alter significantly. Blue ellipses once again highlight vessels. 74

Figure 4.1 Still pCLE images in A,B & C are from healthy BPSs and show fine undistorted septal wall elastin architecture (<10µm thickness), though age seems to play a role in the septal wall fluorescence intensity (A and B are from a 52 year old patient; C was aged 29). Mosaicing was able to increase the FOV in 64/116 BPSs: D shows the

longest mosaic created (1268µm); the oval highlights a 150µm microvessel with a small branch (from a BPS with grade 1 emphysema). 82

Figure 4.2: Free ends of septal walls, observed on video loops to flutter loosely, were apparent in 28/116 BPSs (highlighted with circles in A, B, C and D). This phenomenon could be partly illustrative of the primary disease, however, in 6 BPSs, individual septal walls were observed to fracture, separate and then their blind ends swing freely, presumably from the axial pressure of the probe (demonstrated in C, and in D across 3 sequential frames; each separated by 83ms). Microvessels were also observed to snap under axial pressure in 4 BPSs (highlighted by an oval in C, and sequential frames shown in E). A is from a grade 1 emphysema BPS, B, C and E are from different grade 3 and 4 BPSs, and D is from a patient with respiratory bronchiolitis. 83

Figure 4.3: A schematic (A) shows the loss of of alveolar septal wall density in emphysema, often in the apices. White light microscopic images of emphysematous (B) and healthy (C) transbronchial lung biopsies are shown. The number of visible septal walls on pCLE tends to reduce as emphysema worsens: grade 1 emphysema (D&E), grade 4 (F). G and H are images near large bullae. The ellipse in G highlights probable distorted thickened septal wall that on discrimination by thickness could be confused with a microvessel. H shows a probable vessel but minimal septal wall. I and J are images of pleura beyond bullae..... 85

Figure 4.4: Many PLDs cause a non-specific loss of fluorescence and distinctiveness. This is demonstrated with a peripheral metastatic fibrosarcoma deposit (A), an organising pneumonia (B), and an area of lung affected by a lymphocytic infiltration secondary to a peri-chemotherapy pneumonia (F). In a patient with bronchioloalveolar carcinoma, HRCT showed severely affected upper lobes (D), and pCLE provided virtually no recognisable autofluorescence within the right upper lobe (C) whereas the spared right lower lobe showed distinct alveolar structures with greater autofluorescence (G). E was acquired from maximal distal cannulation of LB6 in a patient with tracheobronchial amyloidosis: the “cotton wool like” autofluorescence was similar to that observed in pCLE of endobronchial amyloid deposits[282]..... 87

Figure 4.5: In health, differentiation between microvessels and septal walls (Figure 2.11A&B) is done on diameter and shape characteristics[48]. This is not as straightforward in diseased BPSs, and here the circles show indeterminate structures from diseased BPSs which cannot be identified as either structure on the basis of their shape or

intermediate calibre. A-E are from emphysematous BPSs (grades 2, 3, 3, 4, and 4 respectively) and F is from a BPS with drug-induced pneumonitis. 87

Figure 4.6: Bright indeterminate 3μm specks are common on approach to the acinus regardless of smoking status (A is from a patient with pneumonia). Apparent mucus blobs or bubbles are non-specific (B is from a resolving pneumonia, and C is from a BPS with grade 3 emphysema). Whilst some very faint cells are suggested even in non-smokers, brightly autofluorescing alveolar macrophages are exclusive to smokers (or those with a recent smoking history) regardless of disease (D&E are from RB4 and RB6 of a recently quit heavy ex-smoker with chronic bronchitis). F shows that these macrophages sometimes "drown out" the alveolar walls (respiratory bronchiolitis). 88

Figure 4.7: Compared to standard biopsy, there is reduced resolution/diagnostic information with conventional elastin autofluorescence pCLE: from the same sarcoid BPS, compare the H&E stained TBB (autofluorescent microscopy x200) (A) of a pathognomonic non-necrotising granuloma to the non-specific disruption seen with pCLE (B). Could the administration of intravenous fluorescein help? It causes a general white appearance of the mucus/surfactant (C shows a healthy BPS following injection of 5ml of 1%) with bubbles displacing the contrast agent. All other acinar structures are disguised. Even when tiny quantities are used (such as 0.4ml of 1% in D), the microvessels (marked by the ellipse) are no more distinct, but bubbles are still evident where the newly fluorescing mucus is being disturbed. 89

Figure 4.8 A few of the unenhanced collated still images (CSI) selected from the pCLE video loops of the BPSs of healthy and emphysematous BPS. Whilst it would appear that the most abnormal/destroyed lobules on pCLE fall within the worst two radiological classifications, there do seem to be multiple "false negative" grade 4 images that have good septal wall density compared to the destruction evident upon HRCT. 95

Figure 4.9: Prior to being asked to grade the BPS on each of the two occasions, each assessor was given general background information about the essence of emphysema and pCLE, and shown examples on slides of G0, G2, G3 and G4 emphysema in the form of VS (A), CSI (B) and CESI (C). 97

Figure 4.10 A shows the prevalence of BPSs identified for the study of each different NETT emphysema grade. Over half of the BPS were of normal density, perhaps contributing to the assessors overscoring them by a mean of 0.73, 0.63, and 0.61 grades for VS, CSI and CESI respectively (B). 98

Figure 4.11: In each format there was a disappointing accuracy for the assessors correctly predicting the actual emphysema grade of the BPSs (A). B shows the interobserver agreement coefficient for each format, and C shows the intraobserver reliability. 99

Figure 5.1: The effect of contact force alterations to pCLE images was mostly evident upon sea sponge. 102

Figure 5.2: For each image, every gland was counted and its maximum diameter measured (E). Imaging conditions were altered in an ex vivo experiment by changing the contact force using a bespoke programmable actuator to drive the probe into porcine colon (A, B & C), and altered in an in vivo experiment by changing the colon diameter using occluded insufflation. 104

Figure 5.3: The result of colonic inflation on gland density and diameter. 105

Figure 5.4 The number of glands and their maximum diameter was easily calculated for each image although a few of the 0.005N images had to be repeated due to shadows, perhaps due to incomplete contact (A). Some of the 0.5N glands had less distinct boundaries (C) than those observed at the smaller forces (B). 106

Figure 5.5: The effects of contact force on gland density and diameter in an ex vivo set-up. 107

Figure 5.6: An example of the temporal effect of a sinusoidal force on the mean separation of five tracked glands in a fresh piece of colon with the corresponding area of one of the glands (marked in red). Formalin pre-treatment toughens the tissue and appears to condense more glands into the field of view (bottom right). 113

Figure 5.7: Columns demonstrating that for the same additional axial force, the pre-treated tissue's glands did not enlarge or separate to the same degree as the fresh tissue. 114

Figure 6.1: LB6 was cannulated with the probe (A), in an attempt to image the circled lesion on CT in (G). It is suspected that the probe was able to pass either inferiorly (B) and image relatively normal lung (C&D) or pass superiorly (E) to image abnormal parenchyma (F&G). 119

Figure 6.2 The 7 degrees-of-freedom robotic articulated endoscope (a) has two operating channels for the camera and interchangeable instruments (eg. pCLE probe). In the linear

translation mechanism schematic (b), the components which translate to servo the probe (rack, slider, clamp and pCLE probe) are shaded in red. 120

Figure 6.3: The top diagram projects the configurations required by the robot to target three regions of the pneumoperitoneum workspace during transvaginal deployment. Underneath it are heatmaps which illustrate the areas of the workspace that could be pCLE biopsied at particular angles (proceeding downwards is a lateral view from the left; a view of the parietal peritoneum from the outside; and a view of the visceral surface from below the workspace). Dark blue, lighter blue/yellow, and red areas can be abutted at a maximum of 90°, 45-90° and <45° respectively by the probe. 124

Figure 6.4: The robot was inserted transvaginally and navigated around the abdominopelvic cavity (a). Optical biopsies were obtained of spleen (b), peritoneum of anterior abdominal wall (c), and liver (d). (e) shows the onboard camera view of the liver during pCLE imaging. 126

Figure 6.5 Robotically acquired pCLE optical biopsies of peritoneum, liver and spleen. Courtesy of slow and controlled movements of the distal robotic joint, it was possible to use mosaicing software to expand the field-of-view by up to 4 times (approximately 2mm) to create more representative and interpretable optical biopsies (a, d & h show the expansion). The parietal peritoneum of the anterior abdominal wall shows 10 to 100µm blood vessels (a-c). The liver images show distinct features of liver parenchyma, with mildly fluorescent hepatocytes contrasted against dark sinusoids (particularly prominent in (g)), arranged into hexagonal lobules (d-f) each surrounded by fluorescent vascular septa with highly fluorescent branches of the portal vein at the hepatic triad present at each lobule corner (marked by circles). The splenic parenchyma shows dark cords of billroth surrounded by extracellular space containing fluorescent blood. Larger diameter sinusoids are clearest in j. The 100µm vessel in i is likely to be a penicillar arteriole (a straight arteriolar branch of one of the central arteries)[333]. 127

Figure 6.6 The argon blue laser light appearing subpleurally after probe deployment down a dorsal branch of the pig's left caudal lobar bronchus is circled in white (left). Fiducial markers, circled in yellow, were stuck to the inflated lung (middle). An axial slice of the mid pig lung is viewed from below (right). 131

Figure 6.7: A schematic representation of the pig lung's bronchial tree at bronchoscopy with the number of terminal destinations possible (in parentheses) for each starting point 1-19. 133

Figure 7.1 The typical vascular pattern of normal colonic mucosa (G_0) is demonstrated with normal descending colon in A, and undergoes pCLE optical biopsy in B. C shows G_2 VRS proctopathy of the lower rectum with an oedematous mucosa containing multiple non-confluent telangectasia. G_3 mucosa of the upper rectum with confluent telangectasia is shown in D. 142

Figure 7.2 The biopsy sites in the lower rectum were generally affected by the higher VRS grades of radiation proctopathy. Only one descending colon was macroscopically unhealthy (in a very symptomatic patient 72 months post brachytherapy and external beam radiotherapy for cervical cancer). 144

Figure 7.3 A chart demonstrating that VRS G_2 and G_3 areas were much more likely to display no obvious vessels on pCLE videos. pCLE mosaics provide examples whereby external beam radiotherapy for prostate cancer appears to have disrupted the normal vascular appearance. 146

Figure 7.4 In proctopathic tissue, where vessels *are* seen, there is a (non-significant) tendency for the vessels to have a larger calibre; some examples are shown. 147

Figure 7.5 Morphological changes appear more commonly in G_2 and G_3 disease. An irregular ridge-lined epithelial layer ($p<0.0001$) is more common. Fluorescein leakage seemed particular marked in the G2/G3 disease but its categorical presence was not statistically different across the groups ($p=0.25$). Included are some examples of G_3 disease displaying fluorescein leakage into the crypt lumen (A and B) and epithelial ridges (C and D). 148

Figure 7.6: For each of the 16 histological features analysed, stacked columns showing the interpreted frequency of severity for the 75 biopsy pairs. 149

Figure 7.7 For those sequences with a visible vessel, graphs showing the mean largest vessel diameter with pCLE imaging, for each grade of the four vascular histological features assessed. Only histological vessel dilatation was significantly correlated, positively, with largest vessel diameter on pCLE. 153

List of Tables:

Table 2.1 A summary of the specifications of the main commercially available confocal endomicroscopes for clinical use. Pre-clinical devices are also commercially available. 19

Table 2.2: Studies assessing accuracy of pCLE for the diagnosis of colorectal polyps. IVF = intravenous fluorescein; TA = topical acriflavin; TI = topical indigocarmine 26

Table 3.1 pCLE image description and interpretation of 20 different endobronchial surfaces. 60

Table 3.2 Radiation induced side-effects during the study were most severe at week 2, but no endoscopy sessions were considered particularly uncomfortable by the patient. 70

Table 4.1: Quantification of percentage of lung affected by emphysema on HRCT 78

Table 4.2: The main diagnosis of the 42 subjects bronchoscoped, providing the 116 BPSs that were imaged. 81

Table 4.3: A summary of the observations and measurements from the 116 BPSs analysed. Whilst the elastin scaffold morphology with emphysema is most likely to appear distorted, structures tend to be vivid and brightly autofluorescent. Diminution of both autofluorescence and recognisable distinct structure is common in other PLDs. The few BPSs displaying autofluorescent macrophages were from the only two current smokers in the study, both with PLDs [a], and a COPD patient who had only quit smoking 2 weeks previously[b]. (Using ANOVA for mosaic length, and 2-sided chi-square tests for the other observations $p<0.05^{S}$, $p\geq0.05^{NS}$) 86

Table 6.1: The proportion of the workspace mesh surface that would be reached for different angles of the pCLE probe. 123

Table 6.2 A table outlining the length of probe deployment from each starting point to terminal destination, and the maximum distances between possible probe tip terminal destinations (the 3 destinations 9a, 18b, 19a were removed from the data table as their computed coordinates would have required their measurements to fiducials to change by ≥ 11mm). 134

Table 7.1: The VRS score was provided for each area of mucosa. 141

Table 7.2 Normal histological appearance was designated zero. The degree of severity of any deviation from normal (-, +, ++, +++), was ascribed -1, 1, 2, 3 respectively for the purposes of a) creating an average to compare each VRS group, and b) to enable Kruskal-wallis tests to assess whether there were any trends in histological features across the four VRS groups. Averages have been tabulated with mean rather than median to avoid an excess of zeros. 150

Table 7.3 The relationship between histological factors and glandular disruption on pCLE. 151

Table 7.4 A table showing the presence or absence of visible vessels on pCLE for each grade of the four vascular histological features assessed. 152

Table 7.5 The relationship between histological variables and pCLE dilabsence. 154

Table 7.6 Apart from when measured by RTOG, the severity of a patient's symptoms has no correlation with their most severely proctopathic segment of colorectum as determined by VRS. Similarly, no pCLE feature was discovered that correlated with any of the four symptom scores. Kruskal-Wallis, Fisher's Exact Test, Spearman's Rank Correlation Coefficient (SRCC), and Mann-Whitney U tests were used as appropriate. 155

List of Acronyms:

ACS	Abdominal compartment syndrome
AFB	Autofluorescent bronchoscopy
ALI	Acute lung injury
ANOVA	Analysis of variance
BAL	Bronchoalveolar lavage
BPS	Bronchopulmonary segment
CESI	Collated enhanced still images
CIN	Cervical intraepithelial neoplasia
CIS	Carcinoma-in-situ
CLE	Confocal laser endomicroscopy
CLSM	Confocal laser scanning microscopy
COPD	Chronic obstructive airways disease
CPAP	Continuous positive airways pressure
CPR	Complete pathological response
CSI	Collated still images
CT	Computed tomography
EBUS	Endobronchial ultrasound
eCLE	Endoscopic confocal laser endomicroscopy
EGFR	Epidermal growth factor receptor
EMR	Endoscopic mucosal resection
ERCP	Endoscopic retrograde cholangiopancreatography
FCFM	Fibered confocal fluorescent microscopy
FDA	Food and drug administration (USA)
FICE	Fujinon intelligent colour enhancement
FITC	Fluoroscein isothiocyenate
FNA	Fine needle aspirate
FOV	Field of View
GvHD	Graft versus host disease
H&E	Haemotoxylin and Eosin
HAL	Hexylaminolevulinate
HD	High definition
HRCT	High resolution computed tomography
IBDQ	[modified] Inflammatory bowel disease questionairre
IBDQ-B	IBDQ [bowel specific]
JPEG	Joint photographic experts group
MRI	Magnetic resonance imaging
NBI	Narrow band imaging

nCLE	needle based confocal laser endomicroscopy
NETT	National emphysema treatment trial
NHLI	National heart and lung institute
NIR	Near infrared
NOTES	Natural orifice translumenal endoscopic surgery
NPV	Negative predictive value
OCT	Optical coherence tomography
PAP	Pulmonary alveolar proteinosis
pCLE	Probe-based confocal laser endomicroscopy
PD	Peritoneal dialysis
PET	Positron emission tomography
PLD	Parenchymal lung disease
PPV	Positive predictive value
ROI	Region of interest
RP	Radiation proctopathy
RTOG	Radiation therapy oncology group [late proctitis score]
SCLC	Small cell lung cancer
SILS	Single incision laparoscopic surgery
SPN	Solitary pulmonary nodule
TBA	Tracheobronchial amyloidosis
TBB	Transbronchial biopsy
TBOP	Tracheobronchopathia osteochondroplastica
VAI	Volume air index
VEGF	Vascular endothelial growth factor
VRS	[Wachter's] Vienna Rectoscopy Score
VS	Video sequences
WLE	Wide local excision

Chapter 1 Introduction and Overview

1.1 Introduction - the Development of pCLE

The scanning confocal microscope is a well established laboratory imaging tool that provides optical sections with superior resolution to conventional microscopes courtesy of its confocal pinhole that rejects out of focus light. However, being relatively unwieldy, its in vivo application is limited to externally accessible tissues such as skin, eye and the oral cavity[1]. Improvements in optic fibre technology have enabled the probe based confocal endomicroscope (pCLE) to be developed in the last decade; thousands of fibres individually act as a light source and detection pinhole. By inserting the probe through the working channel of an endoscope, pCLE provides impressive, near histological grade images of mucosal surfaces. It is therefore one of several technologies competing to provide clinically useful “optical biopsies” - nondestructive in vivo in situ assessment of mucosal microarchitecture and function using light to provide realtime tissue diagnosis.

The scientific and clinical communities are keen for CLE to fulfil its potential (Figure 1.1) and have described typical pCLE imaging in health and disease of several organs including most areas of the gastrointestinal and respiratory tracts.

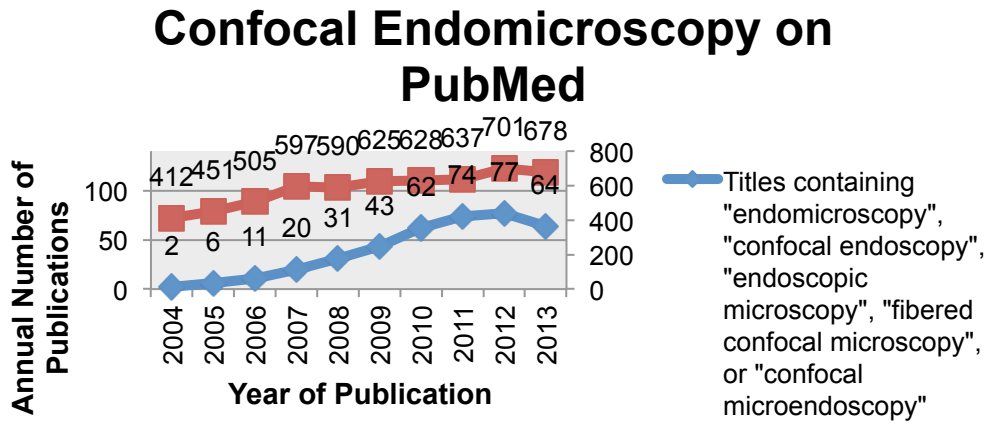


Figure 1.1 The rapidly escalating interest in miniaturised confocal microscopy is demonstrated with a graph showing the number of new annual publications listed on PubMed. This is contrasted with titles containing "endoscopy", showing a more typical growth in other technological research.

Nevertheless, as with most optical biopsy technologies, there are several hurdles that are still obstructing its expansion from a fascinating but expensive toy used by academics in the research setting to a device with widespread uptake that has genuine impact on patient management. Indeed, a survey of gastroenterologists from the 31 North American institutions listed by Mauna Kea Technologies as using pCLE in September 2010 showed that 40% considered the technology an experimental/research tool and 63% felt it was not ready for primetime[2]. The technical challenges and optimal clinical applications of pCLE form the subject of this thesis. It aims to identify (and attempt to address) the main challenges to pCLEs development, and in so doing, identify new niches for its advancement.

1.2 A Synopsis of Each Chapter

Chapter 2: This includes a comprehensive review of pCLE, describing its historical development, and the state of the art for pre-clinical and clinical applications. The chapter discusses the challenges which pCLE present to the scientific and clinical community, amongst which are:

1. *Force* (probe contact force is currently difficult to control and this may affect the resulting image)
2. *Accuracy* (the device is useless without adequate confidence in its diagnostic abilities)
3. *Tracking* (the operator must be able to define exactly from where the optical biopsies have been obtained)
4. *Ergonomics* (the probe must be easily manipulated to the relevant target)

Chapter 3: Here, two largely descriptive clinical studies are used to explore the ubiquity of these four challenges in vivo. For the first study, healthy and diseased endobronchium were pCLE imaged and pinch biopsied during 16 bronchoscopies. For the second study, a patient undergoing neoadjuvant chemoradiotherapy for an advanced rectal tumour underwent flexible sigmoidoscopy on five separate occasions with pCLE imaging of tumour, and healthy mucosa within and outwith the radiation zone. It is shown that in these two clinical situations the effect of probe contact pressure needs further evaluation

(*force*), that many tissue differences are not always sensitively and specifically identified by the probe (*accuracy*), that it is difficult to accurately obtain from the same identical mucosal target either a) correlative pCLE and pinch biopsies, or b) pCLE biopsies at sequential endoscopies (*tracking*), and that unpredictability with image output may relate to *ergonomics*.

Chapter 4: The pCLE images of healthy peripheral lung are particularly striking. This chapter aimed to see if diagnostic *accuracy* could be enhanced by focussing on the imaging of parenchymal lung diseases (with or without the addition of intravenous fluorescein – a contrast agent that is employed in gastrointestinal pCLE). pCLE sequences were safely acquired from 116 bronchopulmonary segments of healthy lung, or lung affected by emphysema or other inflammatory/neoplastic conditions diagnosed using radiology, histology and microbiology. With pCLE, alveolar septal wall density was less with severe emphysema, and the lung pleura was observed beyond bullae which had been entered with the probe. However, despite *some* intrassessor consistency, it was not possible for briefly trained assessors to reliably discern different grades of emphysema. Other parenchymal lung diseases caused a marked non-specific loss in the overall autofluorescence, and a reduction in the discriminability between alveolar septal walls and microvessels. Fluorescein did not improve accuracy. In terms of *tracking*, it was apparent that there is an occasional inability to ascertain if "no image" is due to the arrival of the probe in a bullous, or due to inadequate probe deployment.

Chapter 5: Evidence in the literature (mostly circumstantial) and in previous chapters implies that probe contact *force* may have an effect upon the pCLE image captured in different tissues, potentially with consequences for standardisation of the technique for image acquisition, to ensure image differences can be reliably assumed to be exclusively caused by altered tissue microarchitecture. In this chapter, in an in vivo pig study it was shown that the mean diameter doubles and the mean number of glands per field decreases threefold between collapsed and hyperinflated colon. In a carefully controlled ex vivo experiment, increasing probe contact force produced images with glands that were larger in diameter but fewer in number.

Aware that information regarding tissue characteristics is gleaned from manual palpation or compression during ultrasonography, it was next ascertained whether pCLE could produce similar elastographic information regarding mechanical phenotype to potentially enhance diagnostic *accuracy*. Indeed, with a sinuisoidally varied contact force, the percentage change in gland area was 2½ times greater for fresh ex vivo tissue than formalin soaked tissue (a simple disease model). The percentage change in intergland separation was fivefold greater in fresh tissue.

Chapter 6: The pCLE probe must be easily and accurately navigated to the tissue target, often for very gentle translation across the tissue surface to create "mosaics". *Ergonomic* obstacles to this are in the literature and preceeding chapters, leading to the hypothesis that robotic actuation could be advantageous. This chapter starts with a theoretical analysis of human pCLE peritoneoscopy and then describes a transvaginal porcine feasibility study in which a seven degree of freedom robot is manipulated within the peritoneal cavity to obtain interpretable mosaics of liver, spleen and abdominal wall.

For reliable image interpretation, the site from which the optical biopsy has been taken must be clear. This probe *tracking* is especially difficult within the peripheral lung, and particularly problematic in a heterogeneously diseased segment. The second part of this chapter is designed to assess the predictability of the probe tip destination in an ex vivo lung porcine model (it does not confront gastrointestinal pCLE tracking). It concludes that only half of deployments beyond the most distally visualised part of the bronchial tree have a single possible path.

Chapter 7: Having shown in chapter 3 feasibility for pCLE imaging in acute radiation proctopathy, with excellent displays of vascularity, the intention in this chapter was to establish if pCLE *accuracy* can be maximised by focussing on the assessment of chronic radiation proctopathy, a poorly understood condition with (at least in part) a vascular aetiology. 26 patients with symptomatic disease underwent multiple pCLE and pinch biopsies during flexible sigmoidoscopy. Macroscopically more severely diseased areas were associated with pCLE sequences showing dilated or absent vessels ("dilabscence"), and morphological distortion of glandular structure. Following detailed microscopic analysis of the biopsies, a score from 16 histological features correlated with pCLE vessel

dilabscence and glandular disruption, suggesting pCLE could have a role in the assessment of this debilitating condition.

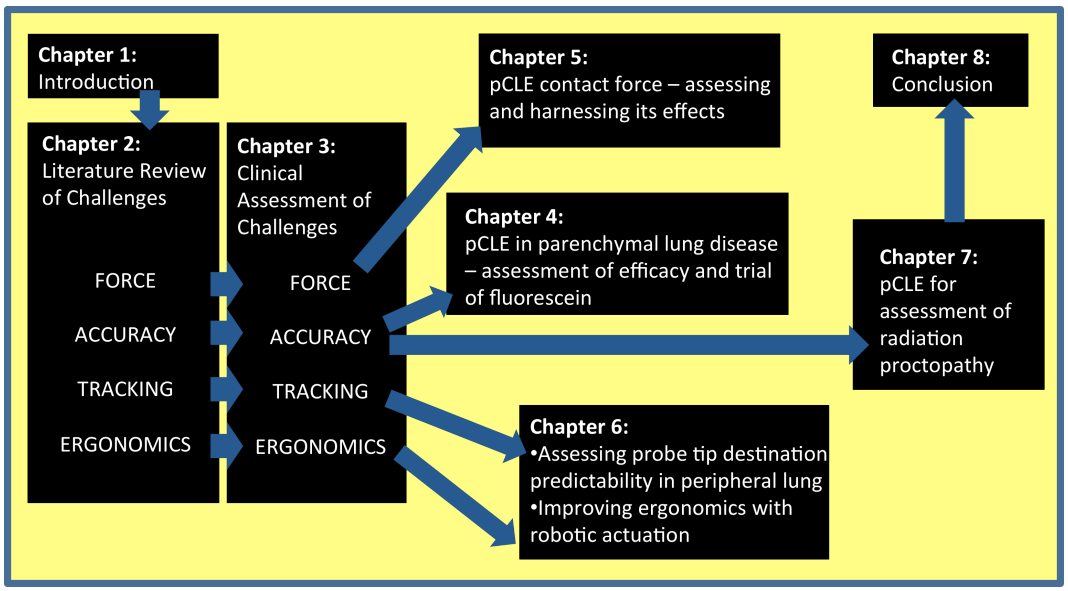


Figure 1.2 The experimental chapters develop from four key themes identified in chapter 2.

1.3 The Main Original Contributions that Advance pCLE Understanding in this Thesis and their Clinical Impact

pCLE is a new technology with the majority of publications centred around colorectal polyps and Barrett's oesophagus. This thesis was highly original, focussing on novel or relatively unexplored avenues; therefore data are often preliminary and of a hypothesis generating nature. Nevertheless, it significantly contributes to the understanding of pCLE in both endobronchial disease and different peripheral lung diseases, leading the way for safer realtime more accurate diagnosis in respiratory medicine. It outlines two completely novel clinical roles for pCLE (the evaluation of efficacy of neoadjuvant chemoradiotherapy towards rectal cancer, and the assessment of chronic radiation proctopathy), and contains the world's first description of two technical pCLE developments (robotic actuation and the assessment of tissue phenotype using the principles of elastography) which have the clinical potential for enhancing pCLE ergonomics and accuracy respectively.

The ten main contributions of this thesis are:

1. The creation of a library of normal, inflammatory and neoplastic endobronchial pCLE images.
2. The first description of pCLE imaging in endobronchial amyloidosis and tracheobronchopathia osteochondroplastica.
3. The ascertainment that pCLE is a feasible and tolerated technique for longitudinal colorectal imaging during neoadjuvant chemotherapy for advanced rectal cancer, but that any temporal superficial histological changes are not easily discernible with pCLE.
4. The thesis shows that despite showing realtime imaging of the destruction of septal walls with the probe, pCLE imaging in peripheral lung diseases is tolerated and safe. Severe emphysema and bullae cause obvious alterations to pCLE images of the peripheral lung but trained image interpreters cannot accurately distinguish between grades of disease. Other peripheral diseases cause a non-specific attenuation of septal wall clarity. Fluorescein has no role in peripheral lung disease imaging.
5. The finding that tissue taughtness affects the images generated; in a porcine in vivo study, by increasing colonic inflation, the mean gland diameter increased, but the number of glands per field of view decreased.
6. Quantification of the effects of extremes of probe contact force upon ex vivo colonic mucosa, with regards to the gland diameter and number of glands per field of view.
7. The first description of pCLE elastography as a feasible future direction; a cyclical contact force upon colonic mucosa alters gland area and interglandular separation to a far greater extent in fresh tissue than tissue that has been toughened.
8. The finding that transvaginal pCLE peritoneoscopy with a robotic endoscope is feasible and safe in a pig and produces interpretable images of abdominal organs.
9. The conclusion that there is inherent unpredictability of the terminal destination in peripheral lung of a 1.4mm diameter pCLE probe. In an ex vivo porcine model, half of the deployments into the distal bronchial tree beyond the furthest bronchoscopically visualised branch have multiple possible routes to an acinus.

10. A detailed analysis of a future role of pCLE in the assessment of chronic radiation proctopathy. Glandular disruption, and microvessel dilatation or absence on pCLE correlate with severity of disease as defined by either the endoscopic view or a novel histological score.

1.4 Main Publications Associated with this Thesis

Only peer reviewed journal publications, first name international/national presentations and a book chapter have been included in this list.

Chapter 2

- Newton R, Yang G-Z. In Vivo Imaging for Cell Therapy. In: Cell Therapy for Lung Disease. Ed. Pollack J. Ch 15, Imperial College Press, 2010.
- Newton RC, Kemp SV, Shah PL, Elson D, Darzi A, Shibuya K, Mulgrew S, Yang G-Z. Progress toward optical biopsy - bringing the microscope to the patient. Lung 2011 Apr;189 (2):111-9.

Chapter 3

- Newton RC, Kemp SV, Yang G-Z, Darzi A, Sheppard MN, Shah PL. Tracheobronchial Amyloidosis and Confocal Endomicroscopy. Respiration. 2011 July. 82(2):209-11.
- Newton R, Kemp S, Zoumot Z, Yang GZ, Darzi A, Shah PL. An unusual case of haemoptysis. Thorax. April 2010: 65:309, 353

Chapter 4

- Newton RC, Kemp S, Elson DS, Yang G-Z, Thomas CMR, Shah PL Confocal Endomicroscopy In Diffuse Lung Diseases - Initial Results And Future

Directions. American Thoracic Society Conference, New Orleans, 2010. Am J Respir Crit Care Med 2010; 181:A6620-

- Newton RC, Kemp SV, Yang G-Z, Ellson D, Darzi A, Shah P. Imaging parenchymal lung diseases with confocal endomicroscopy. Respiratory Medicine. 2012 Jan: 106(1): 127-37

- *Shah PL, Von der Thusen J, Newton RC, Elson DS, Yang G-Z, Nicholson AG. Clinical correlation between real time endocytoscopy, confocal endomicroscopy and histopathology. To be submitted to Journal of Thoracic Oncology.*

Chapter 5

- Newton RC, Noonan D, Payne C, Andreyev J, Di Marco A, Visentini Scarzanella M, Darzi A, Yang G-Z. Probe contact force and bowel distension affect crypt morphology during confocal endomicroscopy. British Society of Gastroenteroloigsts Conference, Birmingham, March 2011, Gut; 60; A12-13

Chapter 6

- Newton RC, Noonan DP, Clark J, Vitiello V, Payne CJ, Shang J, Sodergren M, Darzi A, Yang G-Z. Robot-assisted transvaginal peritoneoscopy using confocal endomicroscopy: feasibility study in a porcine model. Surgical Endoscopy. 2012 Sep;26(9):2532-40

- Newton RC, Noonan D, Payne C, Clark J, Sodergren M, James D, Darzi A, Yang G-Z. LB86: Towards diagnostic peritoneoscopy with a force adaptive probe-based confocal endomicroscope via a transvaginal robotically controlled articulated endoscope. A poster presentation at the National Cancer Research Institute Cancer Conference, Liverpool, 2010. (online at www.ncri.org.uk/ncriconference/2010abstracts/abstracts/LB86.htm)

Chapter 7

- *Newton RC, Andreyev J, Wotherspoon A, Tait D, Yang GZ, Darzi, A. Probe based confocal endomicroscopy for the assessment and characterisation of radiation proctopathy. To be submitted to Colorectal Disease*

Other relevant peer reviewed publications (content not included within thesis)

- Tun Latt W, Newton R, Visentini-Scarzanella M, Noonan D, Payne C, Shang J, Yang G. A Hand-held Instrument to Maintain Steady Tissue Contact during Probe-Based Confocal Laser Endomicroscopy. IEEE Trans Biomed Eng. 2011 Sept: 58(9):2694-703.

- Noonan DP, Payne CJ, Shang J, Sauvage V, Newton R, Elson D, Darzi A, Yang G-Z. Force adaptive multi-spectral imaging with an articulated robotic endoscope. Med Image Comput Comput Assist Interv 2010;13(part 3): 245-52.

Chapter 2 The brief history of probe-based confocal endomicroscopy

2.1 Introduction

2.1.1 Conventional tissue biopsy

The concept of acquiring samples of internal tissue for subsequent analysis has been around since the tenth century when the Arabic physician Abulkasim distinguished between different types of goitre using a hollow needle to puncture the thyroid[3]. A millennium later, the definitive diagnosis of many human diseases still requires analysis of tissue obtained from biopsy. This interrogation of tissue and cellular anatomy within thin slices (sections) of biopsy material using a light microscope, or an electron microscope, is the science of histopathology; where aspirated lone cells are studied it is known as cytology. Usually, tissue biopsy material is preserved (fixed) using formalin or glutaraldehyde to cross-link proteins. It is then dehydrated with ethanol, before being embedded in wax or acrylic resin, enabling it to be typically visualised as 5μm thick vertical slices cut with a microtome. Conducting microscopy using visible light, these biological tissue slices have little inherent contrast; therefore stains are used, the industry standard being haemotoxylin and eosin: haemotoxylin is blue, and being alkaline it has a resulting affinity for staining nuclei; the acidic eosin stains cytoplasm pink.

However, depending on the method employed and the organ being sampled, there are risks to the patient including bleeding, perforation, and infection. Furthermore, there are inherent delays and cost implications with the preparation and reporting of tissue samples. Due to a lack of quantitative parameters in many fields of histological analysis, interobserver and intraobserver variability is an inherent problem. Even intraoperative "frozen sections", sent for histopathological analysis to exclude metastatic deposits, confirm adequate clearance of a tumour, or provide lymph node staging information to guide the operation, take around 30 minutes to process and do not always provide adequate accuracy[4]. Molecular analysis of biological specimens during surgery is yielding some promising results: for example, one-step nucleic acid amplification (OSNA) to intraoperatively assess axillary sentinel lymph nodes for the mRNA of cytokeratin 19[9], and therefore evidence of breast cancer metastasis, shows an excellent

concordance with subsequent histopathology but again takes over 30 minutes to perform[5]. Extracted histology specimens are also susceptible to sampling error, false negatives[6], as well as minor morphological alterations from dehydration and chemical fixation and they can never retain information about dynamic in vivo processes such as blood perfusion or cardiorespiratory movement. For some target organs, less invasive alternatives to tissue biopsy are being pursued. For example, liver biopsy is particularly risky[7], and a proposed alternative could be the creation of a scoring scheme based around variables such as serum biomarkers, cross-sectional imaging, liver stiffness measurement, and portal pressure measurement[8]. Such an approach would theoretically enable longitudinal assessment but is not sufficiently accurate to be used alone at present.

2.1.2 Optical biopsy methods

The exploitation of the properties of light has always been an integral part of medicine and surgery ever since Celsus described rubor (redness) as being one of the cardinal signs of inflammation 2000 years ago; anaemia, jaundice, and cyanosis are further obvious examples. Bozzini's "Lichtleiter" in 1806 allowed these observations to be extended into body cavities, and provided the basic principle of endoscopy[9]. Modern white light endoscopy provides in-situ imaging, but in its purest form only displays reflected visible light, which limits diagnostic power, often acting as a means to survey and direct tissue biopsy.

Developments in fibre optics, light sources, detectors, and molecular biology have enabled a plethora of techniques that provides non-destructive in situ evaluation and assay of epithelial surfaces, and in some cases underlying structures. This study of the interaction between light and tissue to acquire information about morphology and function without subjecting the patient to the risks of extracting tissue is the subject of "optical biopsy" research[10]. Many of these biophotonic technologies are integrated within endoscopes, or designed as a probe for use with conventional endoscopes. They can be imperfectly dichotomised into wide-field and narrow-field devices.

Wide-field surveillance methods to highlight potential pathology include a) chromoendoscopy, where absorptive or contrast agents are applied topically to mucosal surfaces, b) techniques which narrow the bandwidth of light components to preferentially highlight blood vessels such as narrow band imaging[11, 12] or "Fujinon Intelligent

Colour Enhancement" system (FICE)[13], c) autofluorescence endoscopy which displays the fluorescence from endogenous fluorophores[14-16], and d) high definition/resolution or high magnification endoscopy[17].

Narrow-field devices, often probe-based, that can only interrogate smaller areas, provide either a spectroscopic assessment[18], or an image with a magnification and spatial resolution close to that of histology. These high resolution imaging devices include optical coherence tomography (OCT), endocytoscopy and confocal endomicroscopy which are now discussed in more depth.

2.3 Optical Biopsy with Optical Coherence Tomography

OCT is being explored for several clinical niches including gastroenterology[19], ophthalmology[20], dermatology[21] and vascular medicine[22, 23]. Analogous to ultrasonography, a catheter tip transmits broadband near infrared (NIR) light through an optical fibre to detect the reflectance and backscattering properties of the tissue, each of which is influenced by changes in tissue density or refractive index boundaries such as cell membranes or structures[24]. By measuring the echo time delay between transmission and detection using a technique called low coherence interferometry, an optical depth scan may be recorded. A B-scan may then be performed by translating the optical probe, allowing for instance a circumferential transluminal cross-sectional tomographic image to be constructed[25]. Current technology only provides 2-3mm of penetration, which is adequate to image the mucosa and basement membrane within most organs. As the diffraction limit and coherence length of the light source is a fraction of the acoustic waves' used in ultrasound, the lateral and axial resolution of OCT can be as good as 5μm, which is 10-20 times better than high frequency ultrasound[26], though commercially 15μm resolution is more realistic, which still enables OCT to image to the level of individual nuclei[27]; for comparison, the human eye can only discriminate to a resolution of about 76 microns at 25cm.

OCT displays particular promise in the lung; ex vivo the layered structure of the bronchial tree is visible, demarcating the mucosa, lamina propria, and the underlying perichondrium and cartilage. The boundary of the epithelium and cartilage is particularly distinct, and it also has sufficient resolution to outline mucous glands and layers of smooth muscle within the submucosa[28]. The structure of the alveoli adjacent to

peripheral airways has also been shown[29]. In vivo, Michel et al. showed that these tissue boundaries are destroyed by endobronchial tumours[30], and during fluorescence bronchoscopic examination by Lam et al., radial OCT enabled accurate measurement of the respiratory epithelium thickness[27]. Breaches of the highly scattering basement membrane allowed differentiation between invasive neoplasia (although not histological subtype), carcinoma-in-situ, dysplasia and metaplasia (Figure 2.1). However, the resolution is currently inadequate to differentiate between grades of dysplasia.

2.4 Optical Biopsy with Endocytoscopy

The endocytoscope is a system by which real-time in vivo imaging of tissues at a cellular level can be achieved under white light conditions. It relies upon the principle of contact microscopy, where an image is seen for as long as the probe remains in contact with the tissues, and was first used for microhysteroscopy[31]. It has since been used predominantly as a research tool in the investigation of cancer in the gastrointestinal tract[32-34], and also in the urinary tract[35]. Detailed images of the nuclei allow clear distinctions between normal and malignant cells, with sharp borders between atypical and normal epithelium, differences in cellularity, and differences in the sizes and shapes of the nuclei[36]. The technique seems particularly effective in the colon and oesophagus[37].

Application of a 0.5-1% methylene blue (MB) solution to the area of interest allows sharp visualisation of cellular structures down to the level of the nucleolus. Mucous and blood can impair the contrast agent application and prevent suitable images being obtained. This can be partly overcome by the use of mucolytic agents[38].

More recently, endocytoscopy of the airways has shown promise[39] (XEC-300-U/F, Olympus, Tokyo, Japan), and is available either as an integrated system with normal and endocytoscope functions (Figure 2.1), or as a dedicated ultrafine probe with a diameter of 3.2mm that can be used via the biopsy channel of a larger bronchoscope[40]. Both systems have a spatial resolution of 4.2µm and a magnification of x570, with fields of view of 400µm x 400µm and 300µm x 300µm respectively.

Contrasting with OCT, endocytoscopy can only image the most superficial 50µm of the tissue. Early work suggests in vivo endocytoscopic images of endobronchial tumours,

sprayed with MB, resemble conventional histology, with an increase in cellular density, polymorphic cells and an increased nuclear to cytoplasm ratio when compared to images of normal mucosa[40, 41].

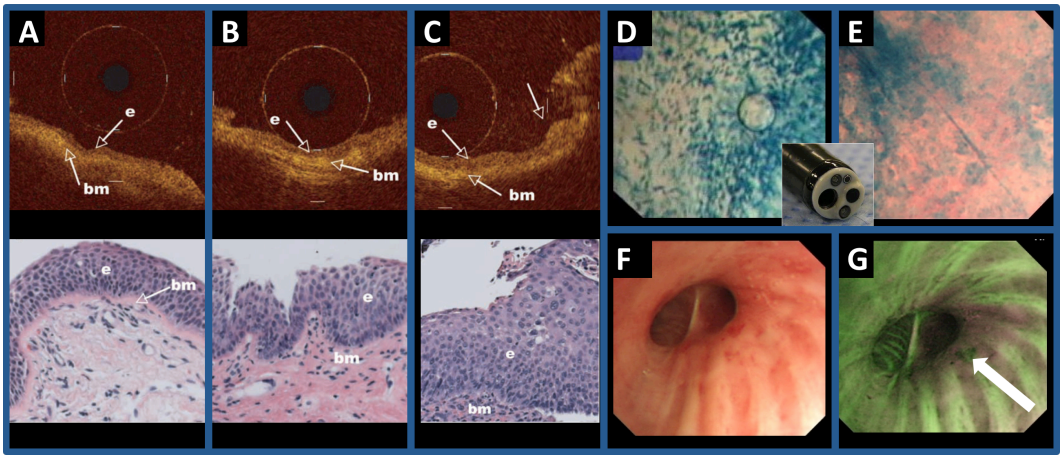


Figure 2.1 Endobronchial OCT. A, B & C show mild moderate and severe dysplasia respectively with corresponding H&E histological images underneath (x20 magnification). Worsening dysplasia is demonstrated by increasing thickness of the epithelium (e) above the highly scattering basement membrane (bm). The epithelial nuclei become more visible as black dots with moderate and severe dysplasia (adapted from Lam et al. 2008[27]). Endocytoscope images using methylene blue as the contrast agent are shown of (D) healthy bronchial mucosa and (E) a right upper lobe endobronchial tumour with a marked heterogeneous epithelial appearance. The endocytoscope distal end is inset. The tumour's white light endoscope image (F) is shown with the autofluorescence image (G), with malignant area indicated by arrow.

There have been many successful attempts at using a "red flag" wide-field technique to highlight areas for closer inspection by narrow field optical biopsy methods. For example, Kiesslich et al. showed that in colonoscopic surveillance for ulcerative colitis, by using confocal endomicroscopy at sites flagged by chromoendoscopy, the numbers of biopsies required could be reduced, but the yield of neoplasia increased [42].

2.5 The Desktop Confocal Microscope

Marvin Minsky developed the confocal laser scanning microscope (CLSM) in 1955 whilst he was a junior fellow at Harvard University[43]. As a desktop instrument it became popular in the 1980s to perform high resolution, blur free fluorescence microscopy and immunohistochemistry on excised tissues. These sharp images representing a thin cross-section of tissue are created by using pinhole apertures in front

of both the light source and the detector to exclude most of the light from the specimen that is not from the microscope's focal plane (Figure 2.2)[44]. The pinholes reduce the number of detectable photons, thus necessitating the provision of an intense light - initially a zirconium arc lamp and now a laser. Some CLSM machines record reflected photons, but most record the fluorescence from endogenous or exogenous fluorophores. The wavelength of the photons emitted from the laser in the CLSM is often adjustable but will always remain shorter than the lower energy photons emitted by the fluorescing specimen as the fluorophore electrons return to their ground state from their singlet excited state. As an example, fluorescein, a widely used exogenous fluorophore, featuring heavily in the subsequent chapters, emits green light when illuminated/excited by shorter wavelength blue light. Whilst the dichroic (dichromatic) mirror transmits the outgoing laser beam, the longer wavelength fluorescence that returns is reflected to a detector such as a photomultiplier tube. At any instant only one point is being examined, so standard visualisation of a complete optical plane requires scanning in two axes, with subsequent image computation. To scan the specimen, Minsky initially used solenoids to translate the stage in x and y axes, obtaining a new frame every 10 seconds. Nowadays, rapidly oscillating mirrors are used to provide point-by-point illumination and detection of fluorescence over the specimen. By assembling multiple optical slices obtained at narrow intervals up the vertical (z) axis, modern CLSM software can then create a 3-dimensional representation of the specimen.

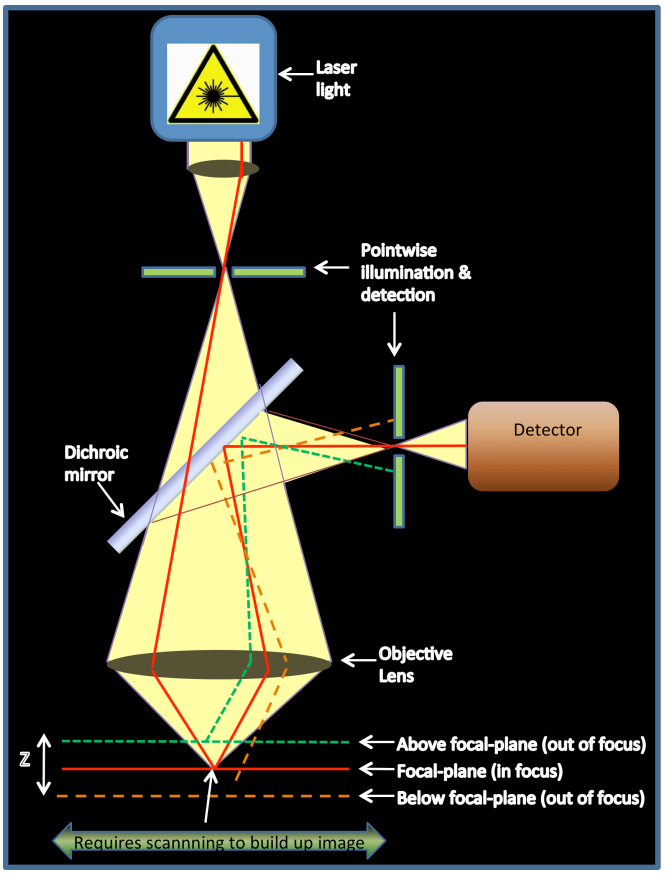


Figure 2.2 A schematic representation of how the CLSM focuses light of a single wavelength upon the tissue under investigation and detects the fluorescence emitted. Only light from the required optical plane is detected; "out of focus" light is blocked from detection by the pinhole.

2.6 The Miniaturisation of the Confocal Microscope

Over the last decade, miniaturisation of the CLSM has enabled it to be used as an in vivo device to take the microscope to the patient, and provide real-time virtual histology. In 1999, Rajadhyaksha et al. developed a CLSM with a mechanical arm and a rotatable head to image skin, lip and tongue[1]. Then in Yokohama in 2003, one hundred colonic mucosal specimens and one healthy volunteer's rectum were examined ex vivo and in vivo respectively with a CLSM probe that was thin enough to be passed down the working channel of an endoscope; both architecture and some pathological differences were identifiable[45]. The enormous possibilities of the technology were quickly appreciated, and whilst miniaturised CLSM, otherwise known as confocal laser endomicroscopy (CLE), is still not in mainstream use, in vivo CLE investigation has been considered for most areas of the gastrointestinal tract[46], lung[47, 48], ovary[49], cervix[50], bladder[51], peritoneal cavity[52], human skin[53], and oral cavity[54].

.

Two, fundamentally different, commercially competing clinically certified Communauté Européenne (CE)-marked and Food and Drug Administration (FDA)-approved systems have been developed, and are compared in Table 2.1.

1. **eCLE:** The first system, created as a Pentax (Tokyo, Japan)/Optiscan (Notting Hill, Victoria, Australia) collaboration, integrates a miniature objective lens and pair of scanning mirrors into the distal end of an endoscope to provide "distal scanning"[55]. This is sometimes termed endoscopic confocal laser endomicroscopy (eCLE). The EC3870CILK is a gastroscope eCLE; the EC3870CIFK is a colonoscope eCLE; and the ISC-1000 is the endoscopic stack.

2. **pCLE:** The second system houses the scanning mirrors within the endoscopic stack, and thousands of optical fibres form a probe to deliver the excitation photons into the patient and return the fluorescence photons to the main unit for processing (Cellvizio; Mauna Kea Technologies®, Paris)[56]. Each microfiber is scanned one at a time by the laser light and acts as its own pinhole. This proximal scanning system is termed fibered confocal fluorescent microscopy (FCFM)[47], or more commonly probe-based confocal endomicroscopy (pCLE). There are several pCLE probes available (Table 2.1), but all except the MiniOProbe used for small animal imaging are deployed down the operating channel of an endoscope. In most pCLE units, the probe relays 488nm wavelength blue excitation laser light to the tissue, and any radiation between 500nm and 650nm from fluorescing tissue is collected. At 12 frames per second pCLE is faster than eCLE, so in theory suffers from less movement artefact.

   With pCLE the focal plane depth is fixed for each probe, whereas with eCLE, at the press of a button, the image's focal plane depth along the z-axis is advanced in 7µm increments anywhere from 0-250µm. With current systems, pCLE has inferior resolution, even with the highest resolution probe, and whilst its initial capital outlay is less, its running costs are much greater, with human probes being limited to twenty uses and costing several thousand pounds. However, their small size provides better accessibility in vivo and they are sufficiently versatile to be used with most endoscopes including cholangioscopes and ureterosocopes. Therefore, as is frequently flaunted by the manufacturer, the pCLE probe can be used on-demand during a procedure if and when required; though in practice all

current clinical pCLE probes require a fifteen minute "warm-up" before calibration and use.

Although the field of view is even slightly smaller than the surface area of the probes, if the probes can be slid slowly over the biopsy site, video mosaicing software can "stitch" adjacent dynamic frames together to create a larger panoramic static image of the tissue being analysed[57, 58]. Mosaicing is a computational function to juxtapose overlapping video frames, acquired as the probe translates across the tissue, into one single composite image, thereby creating an increased field of view panorama of the microarchitecture. In a relatively unrestricted environment such as the bladder, Wu et al. found that the field of view can be increased up to fivefold (0.24mm to 1.27mm)[59] (Figure 2.8).

Mosaicing has other theoretical benefits. pCLE is a laser scanning device, consequently each whole frame represents a period, and not a single time point. This causes motion artefact when the probe moves. Also, probe abutment causes small non-rigid deformations of the tissue. However, video mosaicing for pCLE follows a hierarchical framework algorithm which identifies the motion of the probe relative to the tissue allowing distortions and motion artefacts to be removed. pCLE mosaicing was initially a function provided post-procedure, but can now be done realtime. It is important to appreciate that any dynamic information, such as moving red blood cells, is lost in the mosaics.

	eCLE (distal scanning)		pCLE (proximal scanning)			
Location of Scanning Mirrors	Distal to light guide fibres at end of endoscope; therefore fat		Proximal to light guide fibres; therefore narrow			
Commercial Manufacturer	Pentax/Optiscan		Cellvizio, Mauna Kea Technologies			
Laser Wavelength (nm)	488		488 or 660			
Endoscopes/ Probes	Colonoscope EC-3870CIK	Gastroscope EC-3870CIK	S Probe (alveoflex®)	Z Probe (gastroflex and coloflex)	Z Probe (UHD gastroflex & UHD coloflex)	CholangioFlex
Target Tissue	Large Intestine	Oesophagus & Stomach	Proximal and Distal Lung	Upper and lower GI tract	Upper and lower GI tract	Biliary Tree
Diameter (mm)	12.8	12.8	1.4	2.5	2.5	1
Compatible Operating Channel (mm)	2.8	2.8	>2.2	>2.8	>2.8	>1.2
Length (m)	N/A	N/A	3	3	3	4
Depth of Imaging (μm)	0-250 in 7μm increments	0-250 in 7μm increments	0-50 (no distal optics)	70-130	55-65	40-70
Diameter of Field of View (μm)	475x475	475x475	600	600	240	325
Lateral Resolution (μm)	0.7	0.7	3.5	3.5	1	3.5
Axial Resolution (μm)	<1	<1	15	15	15	15
Imaging Rate (images/sec)	0.8 or 1.2	0.8 or 1.2	12	12	12	12

Table 2.1 A summary of the specifications of the main commercially available confocal endomicroscopes for clinical use. Pre-clinical devices are also commercially available.

2.7 Advantages of Conventional Tissue Biopsy over Optical Biopsy

Whilst optical biopsy is exciting, novel and has many potential advantages, there remain fundamental benefits of conventionally extracting tissue for subsequent ex vivo analysis, in addition to avoiding the large capital outlay of many optical biopsy technologies. Whilst the in vivo information will often be assessed realtime with the obvious time pressures inherent in this approach, ex vivo tissue can be carefully prepared at leisure and the pathologist allowed sufficient time for full analysis. This assessment can incorporate many more types of histological evaluation than can be performed realtime. For example,

in addition to H&E stains, the pathologist can stain other sections of the same biopsy with "special stains" such as congo red, toluidine blue, or masson's trichrome, or indeed can use histochemistry (Perls Prussian blue demonstrates iron deposits in haemochromatosis) or use labelled antibodies to test for specifically expressed proteins (immunohistochemistry). Whilst the integration of more than one optical biopsy method into the procedural workflow or even a single device is achievable [18, 60], the diversity of tests feasible for a chunk of ex vivo tissue is unlikely to be achievable in vivo.

This introduces another issue of who should interpret the information. Whilst remote visualisation via "telepathology" may play a role[61], the pathologist cannot be present during each examination and therefore the clinician or endoscopist is required to develop interpretative skills. Whilst endoscopists are less familiar with assessing tissue structure, pCLE images are fundamentally different to those normally assessed by pathologists, especially with them being en face rather than orthogonal cross-sections. It is well known that even expert histopathologists disagree over interpretation of traditional biopsies[62], and Meining et al. found that a pathologist was no more accurate at interpreting pCLE images than a gastroenterologist[63]. Just as hepatobiliary surgeons have learned to interpret intraoperative cholangiograms and ultrasound during laparoscopy, endoscopists can probably adequately learn the rudiments of pCLE image interpretation, and as is demonstrated in the next chapters, the learning curve appears to be fairly short[64-66].

2.8 Contrast Agents, Safety and Optimisation of pCLE Imaging Protocol

If pCLE is ever to become a commonplace device, it must have an excellent safety profile. As a narrow, stiff but smoothly bevelled probe there are no reports of it causing any significant bleeding or visceral injury, although it is appreciated that minor traumatic bleeding is possible; indeed, blood absorbs the laser light and impairs the images obtained[67].

Ethics committees in pCLE clinical studies therefore focus more on the contrast agent employed. The majority of clinical pCLE is performed using intravenous sodium fluorescein as the contrast agent of choice, probably owing to its long history of clinical applications. Fluorescein is FDA approved for diagnostic fluorescein angiography or

angioscopy of the retinal vasculature. Whilst severe adverse reactions to intravenous fluorescein contrast agent are very rare, many patients report transient (1-2 hours) yellowish discolouration of the skin and mucous membranes, and bright yellow coloured urine for 1-2 days. In a study of 11898 patients given intravenous fluorescein for ophthalmological procedures, nausea and vomiting occurred 0.7% and 0.4% respectively[68]. There were no complications more significant than an urticarial rash (0.2%). A smaller safety study of intravenous fluorescein in pCLE showed no serious complications in 410 consecutive patients[69], and a study of 2272 patients in 16 centres undergoing CLE procedures yielded no serious events, with mild events such as nausea and vomiting, injection site erythema, transient hypotension without shock, diffuse rash or mild epigastric pain occurring in 1.4%[70]. At pH 7.6, fluorescein maximally absorbs photons of 490nm[71]. This explains why the most frequently used pCLE laser unit produces 488nm wavelength blue excitation laser light; this is relayed via the optical fibres in the probe to fluoresce the tissue, to return and record any emitted radiation between 500nm and 650nm from fluorescing tissue. It can be applied topically, but the main advantage of its clinical safety is its more frequently described intravenous administration which delineates vasculature by staying in large part well bound to serum albumin. To obtain the best contrast and signal to noise ratio with intravenous fluorescein, there is some evidence that at least 5mls of 10% should be used[72, 73], and that owing to ongoing extravasation of unbound fluorescein into the extracellular matrix and beyond, image quality gradually deteriorates from 8 minutes after injection[74]. Whilst topical or extravasated fluorescein readily diffuses through extracellular matrix, it is unable to stain nuclei. With nuclear size and pleomorphism featuring heavily in many categorisations of cellular dysplasia in different organs, the inability to describe nuclear morphology is potentially limiting. Whilst several agents such as acriflavin hydrochloride, acridine orange, and cresyl violet outline nuclei, their use within clinical pCLE has been restricted to topical application, and even then, ongoing concerns regarding mutagenicity restrict their use in some countries.

2.9 Optically Biopsying the Gastrointestinal Tract with pCLE

2.9.1 Imaging the large intestine with pCLE

In 2008, there were 39 991 new cases of colorectal cancer in the UK[75-78]. Despite major advances in surgical treatment[79] and chemoradiotherapy[80, 81], the overall 5

year survival is still only about 50%, making it the second leading cause of malignancy-related deaths after lung cancer[82]. The outcome is highly dependent upon the stage at which the disease is identified and treated, with 5 year survivals of greater than 90% reported for those tumours confined to the mucosa and submucosa (T1)[83]. Whilst it is increasingly realised that some colorectal cancers develop de novo, most are the product of pre-malignant adenomas (polypoid or flat) acquiring additional mutations; a process which probably takes 10-15 years[84] and has been well studied since it was described by Morson in 1968[85]. Thus, it is logical to screen for adenomas and early cancers before they become symptomatic, especially as most adenomas, and, albeit with controversy, some very early cancers[86] can be removed endoscopically. As a result, the NHS Bowel Cancer Screening Programme was introduced in 2006, inviting those who have a positive faecal occult blood test for colonoscopy[87]. Nevertheless the sensitivity for detection of neoplasia by faecal occult blood testing is less than 50%[88], prompting some authors to proffer that a better strategy would be to offer routine colonoscopy[89], or perhaps virtual colonoscopy with computed tomography[90] to everyone above a certain age. A simpler alternative which avoids the need for full bowel preparation is flexible sigmoidoscopy[91]. Indeed, in a recent UK study, a one-off sigmoidoscopy, with polypectomy where necessary, offered to asymptomatic men and women between the ages of 55 and 64, reduced colorectal cancer incidence by 23% [91].

However, this strategy has two key problems. Firstly, nearly half of all polyps are regenerative/inflammatory (hyperplastic)[92], and therefore display negligible neoplastic potential, especially if small, solitary and distal, and excision biopsy therefore constitutes overtreatment[93]. Secondly, regardless of the extent of the bowel imaged, white light endoscopy is imperfect, and around a fifth of adenomas are not identified[94], especially if flat, depressed, or less than 1cm in size. Various endoscopic technologies can act as "red-flag" techniques, and are more commonly used for higher risk patients such as those with ulcerative colitis or Lynch syndrome[95]. These techniques include autofluorescence endoscopy, narrow band imaging (to interrogate the Kudo pit pattern), Fujinon intelligent colour enhancement (FICE), or chromoendoscopy using indigo carmine or methylene blue combined with magnification colonoscopy. The mucosal pit patterns can then be zoomed in on to provide clues[96]. But whilst these technologies can survey the entire lumen, and define regions of interest for closer inspection, they have inadequate positive predictive value to obviate the need for biopsy or polypectomy with their attendant risks, costs and delays to the management pathway[97]. More accurate real time diagnosis of abnormal colorectal mucosa could therefore a) improve the yield of any biopsies of

suspicious areas, leading towards the paradigm of “smart biopsies”; b) reduce both pathology laboratory costs and iatrogenic harm by eliminating the need for biopsy/overtreatment of benign polyps (the absolute risk of perforation and bleeding with polypectomy is small but the procedure substantially increases the relative risk during endoscopy[98]), and even eliminate the need for post-removal histopathological assessment of low grade tubular adenomas; c) if sufficiently accurate, allow endoscopic resection forthwith of many larger neoplastic lesions that normally require the histological report prior to definitive management; and d) confirm the adequacy of excision.

To understand how these ambitions have been explored with confocal endomicroscopy it is necessary to have an overview of the microanatomy of the colonic mucosa (Figure 2.3). The mucosal layer lines the colon and is adherent to the submucosa, muscularis propria and serosa; the submucosa and muscle provide the mural bulk and strength. The mucosa comprises the monolayer of epithelium, and the lamina propria; these sandwich a thin basement membrane. The lamina propria consists of loose collagenous connective tissue containing inflammatory cells and blood vessels. The epithelium invaginates into the lamina propria to form straight tubular glands, which form crypts (of lieberkühn) that open onto the mucosal surface. The epithelium consists of absorptive columnar enterocytes, and mucin excreting goblet cells, all tightly bound to one another. Each gland is wrapped with a network of blood vessels embedded into the lamina propria that transport absorbed fluid and solutes.

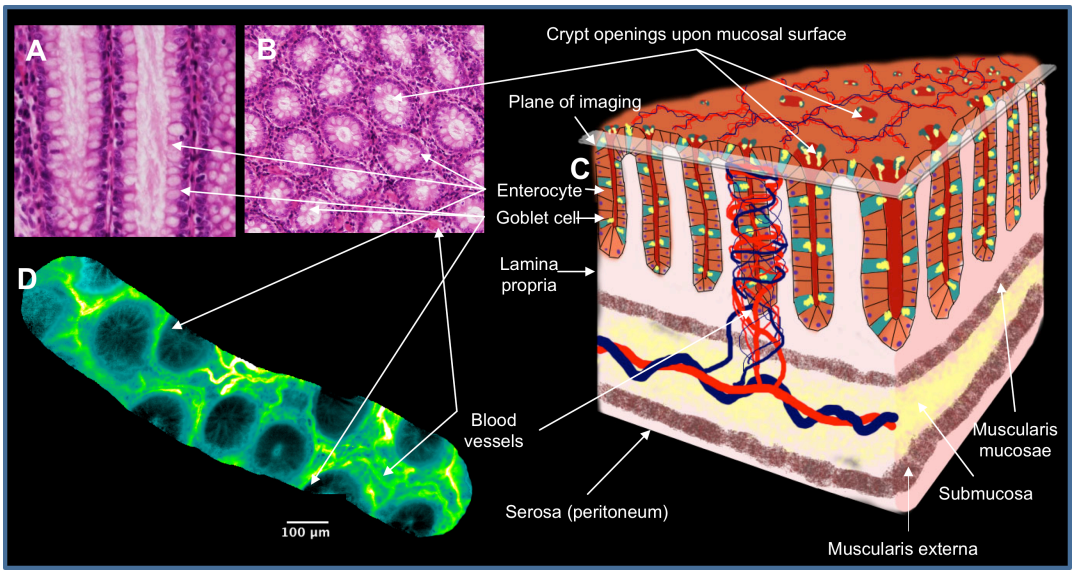


Figure 2.3 The histopathological features of colonic mucosa demonstrable with conventional haemotoxylin and eosin sections both vertically (A) and en-face (B) are illustrated in a schematic (C) and shown in a colour enhanced pCLE mosaic (D).

Several histopathological features of the mucosa that were first described with reflectance confocal microscopy on ex vivo samples[45], remain clearly demonstrable with confocal endomicroscopy. With colonic pCLE the image is obtained from a fixed plane depth of 150µm. This contrasts with eCLE, where the plane of imaging can be varied from 0-250µm below the surface. With both technologies, topical contrast agents that penetrate the cellular wall have the theoretical advantage of highlighting nuclear structure. These compounds include acriflavine hydrochloride, cresyl violet, and acridine orange. Whilst they provide strong superficial contrast, intravenous fluorescein sodium is more widely used owing to its ability to delineate the fine blood vessel network embedded within the lamina propria, with individual dark erythrocytes squeezing through the vessels. At the 150µm depth of pCLE images, the blood vessels are seen to weave between the glands, each of which has a central crypt surrounded by fluorescent enterocytes and darker goblet cells. Kiesslich et al. presented the Mainz criteria in 2004 to illustrate how the confocal image changes with mucosal pathology[55]. The subsequent Miami classification is very similar and validated for high-definition pCLE[99]. In summary, the crypt openings become fused together or star shaped in hyperplastic/regenerative mucosa, with a reduced proportion of goblet cells. This is contrasted with neoplastic mucosa where crypts are so distorted as to become unrecognisable, and long irregular villous epithelial ridges surround dilated, distorted and leaky neo-vessels (Figure 2.4).

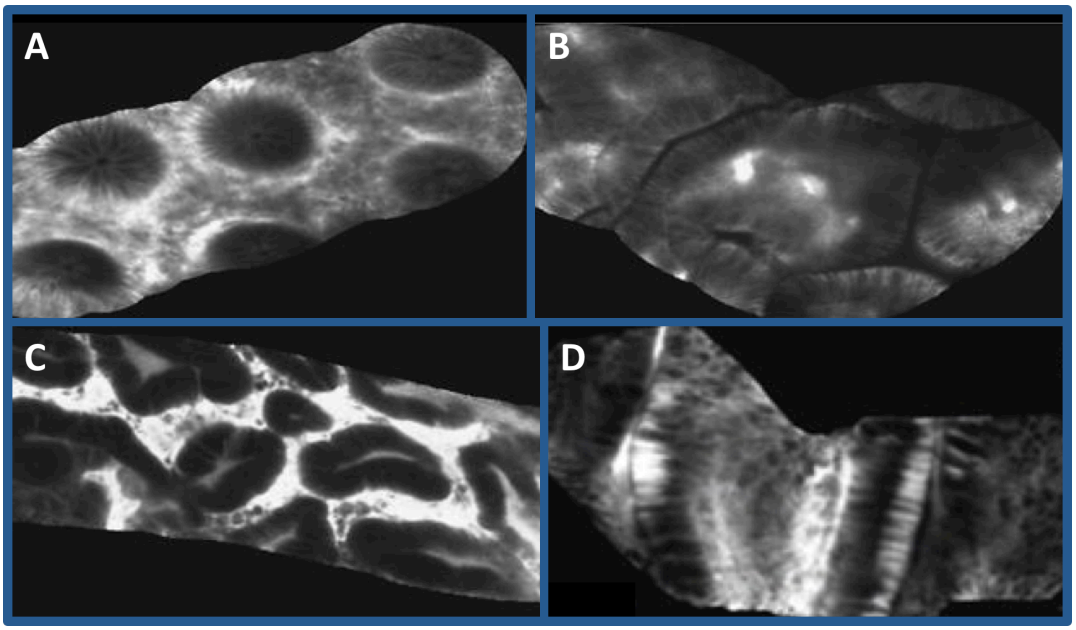


Figure 2.4 High-resolution pCLE mosaics showing normal (A) [100], hyperplastic (B)[100], and adenomatous mucosa (C)[100], with the typical morphological disorganisation of adenocarcinoma (D)[101].

The initial results with the Mainz criteria were extremely promising with a sensitivity and specificity for detection of neoplasia of 97.4% and 99.4% respectively. There are now many studies assessing CLE accuracy for colorectal polyps; they display a large variation in terms of accuracy (Table 2.2).

Author	Sensitivity	Specificity	PPV	NPV	System	Contrast Agent	Cohort	Criteria Used	Screening Method	Comments
Shahid 2012 [100]	86	78	76	88	pCLE	IVF	Screening and surveillance	Miami	High definition colonoscopy	Only polyps <10mm
Kuiper 2011[102]	66	83	n/a	n/a	pCLE	IVF		Novel (3 vessel and 7 crypt categories)		
Hlavaty 2011[103]	100	98.4	66.7	100	eCLE	TI	IBD	Mainz	WLE +/- CE	Only 12 neoplastic lesions
Günther 2011[104]	n/a	n/a	n/a	n/a	eCLE	IVF	IBD	Mainz	WLE	Improved biopsy yield during IBD screening
Buchner 2011 [66]	81-96	34-67	n/a	n/a	pCLE	IVF	Screening and surveillance	Mainz	n/a	Accuracy improved with learning
Xie 2011 [105]	93.9	95.9	96.9	92.2	eCLE	IVF	Polyps	Bespoke	WLE	
van den Broek 2011 [106]	65	82	n/a	n/a	pCLE	IVF	IBD	?	NBI and HD endoscopy	NBI with HD endoscopy more accurate
De Palma 2010[101]	100	84.6	90.5	100	pCLE	IVF	Known superficial lesions	Mainz	WLE	Small study
Sanduleanu 2009[107]	97.3	92.8	n/a	n/a	pCLE	IVF & TA	Screening and symptomatic	Bespoke	Chromoendoscopy	Designed to differentiate grades of dysplasia (97% accuracy)
Gomez 2010[108]	76	72	n/a	n/a	pCLE	IVF	Screening and surveillance	Mainz	WLE	
Buchner 2009[109]	91	76	89	81	pCLE	IVF	Diverse mixture	Mainz	WLE (+FICE or NBI)	Less experienced group
Hurlstone 2008[110]	97.4	99.3	94.6	99.7	eCLE	IVF	Screening and surveillance	Mainz	Chromoendoscopy	
Kiesslich 2007[42]	94.7	98.3	n/a	n/a	eCLE	IVF	Screening UC	Mainz	Chromoendoscopy	
Kiesslich 2004[55]	97.4	99.4	n/a	n/a	eCLE	IVF	Screening	Mainz	Chromoendoscopy and WLE	

Table 2.2: Studies assessing accuracy of pCLE for the diagnosis of colorectal polyps. IVF = intravenous fluorescein; TA = topical acriflavin; TI = topical indigocarmine

Whilst very encouraging, the results in Table 2.2 are mostly from interpretation of the images *after* the procedure, in tertiary centres, by experts in the field. However, in a pCLE study differentiating 80 neoplastic from 74 non-neoplastic polyps at colonoscopy, off-line interpretation only improved the overall accuracy from 79% to 83%[111]. Similarly, in a study that looked at pCLE diagnosis of gastric intestinal metaplasia, the accuracy of realtime interpretation was 88% versus 95% for subsequent blinded off-line review[112]. In a recent colorectal polyp metanalysis it has been suggested that real-time interpretation, aided by the unblinding effect of having the white light appearance available to view together with the optical biopsy, produces a favourable sensitivity and specificity[113]. Of note, this analysis sided with eCLE over pCLE in terms of overall

sensitivity (96% versus 89%) and specificity (99% versus 82%). There is also evidence that interpretation is easily learnt: eleven pCLE naive endoscopists were given a two hour tutorial on the Mainz criteria and then in a formative assessment of their understanding, improved their mean accuracy of dichotomising 76 colorectal lesions into neoplastic versus benign from 63% (lesions 1-20) to 86% (lesions 61-76)[66]. In a similar study for eCLE, but with only three endoscopists, Kuiper et al. described no significant learning curve across three slightly larger sequential groups of 30 lesions, with an overall accuracy of 91%[64]. If interpretation can be performed straight away and is relatively straightforward, perhaps automated classification software may in the future serve as an adjunct for the endoscopist; recently, the computer vision "bag of visual words" technique was used to match 135 pCLE video sequences to a training set, showing, compared to histology, an identical 89.6% accuracy to two expert endoscopists[114].

If the main attraction of colorectal CLE is the prospect of eliminating the current mandatory biopsy/polypectomy of *every* polyp[115], by identifying inflammatory polyps or even low grade adenomas[116], great confidence must be invested in the technology; indeed, gastroenterologists would require a consistent negative predictive value of 95-99% to leave a polyp in situ[117]. Therefore several strategies have been trialled to boost its accuracy toward this "diagnose and discard" strategy:

- Expanding the role of the "red-flag" multimodality imaging, Shahid et al. found that a neoplasia diagnosis in small polyps was much more accurate (95%) when there was agreement between the higher specificity of NBI allied with the higher sensitivity of pCLE[100].

- Wang et al. used quantitative measurements during pCLE with topical fluorescein to discriminate between benign and adenomatous polyps with an accuracy of 96% (Figure 2.5A). During the first 5 seconds after application, fluorescein passes through adenomatous mucosa much slower than it travels through healthy crypts; and after 5 seconds the contrast ratio between lamina propria and crypt was shown to be less for diseased mucosa[118].

- Whilst the characteristics of a cell's nucleus (size, heterogeneity, and chromatin arrangement) confer vital information to the histopathologist, fluorescein-based CLE is devoid of such information. Several topical contrast agents such as acriflavine[55] and cresyl violet[119] (Figure 2.5B) stain the nuclei, but raise theoretical risks about mutogenicity, (although epidemiological studies have

found no evidence for this[120]), and because they provide less definition elsewhere in the image, and fail to delineate blood vessels they have not improved diagnostic accuracy. A longer wavelength (685nm) prototype reflectance confocal microscope can visualise the irregular nuclei of ex vivo neoplastic tissue without contrast agent; but obviously requires miniaturisation[121].

- Great potential exists for molecular imaging with confocal endomicroscopy to provide functional information about cellular expression. It was first demonstrated in athymic mice, where, having bound to subsurface melanoma deposits, fluorescein-labelled antibodies were detected by a confocal probe[122]. Most colorectal cancers overexpress epidermal growth factor receptor (EGFR)[123], levels of which appear to correlate with poor outcome. EGFR monoclonal antibody therapies such as Cetuximab have a proven role in metastatic colorectal cancer treatment. Fluorescent labelled EGFR antibodies have therefore been trialled as molecular contrast agents to selectively stain colorectal cancer cells both in mice models and on ex vivo human tissue[124] (Figure 2.5D). More recently, Liu et al. used similar anti-EGFR molecular probes with CLE in patients with known neoplastic lesions, to demonstrate fluorescence in 18 out of 19 colorectal cancers, and 12 out of 18 adenomas, with substantial concordance with immunohistochemistry, and only slight background fluorescence of healthy mucosa[125]. Hsiung et al. also translated this theme into patients using pCLE to detect a topically applied fluorescein-conjugated heptapeptide that was found pre-clinically to have high affinity toward colonic adenomas. The best sensitivity and specificity obtainable was 81% and 82% respectively[126] (Figure 2.5C). To control for factors such as the contact pressure of the probe affecting the results of this study, it was necessary to image the exact junction between polyp and normal mucosa (fiddly and very challenging).

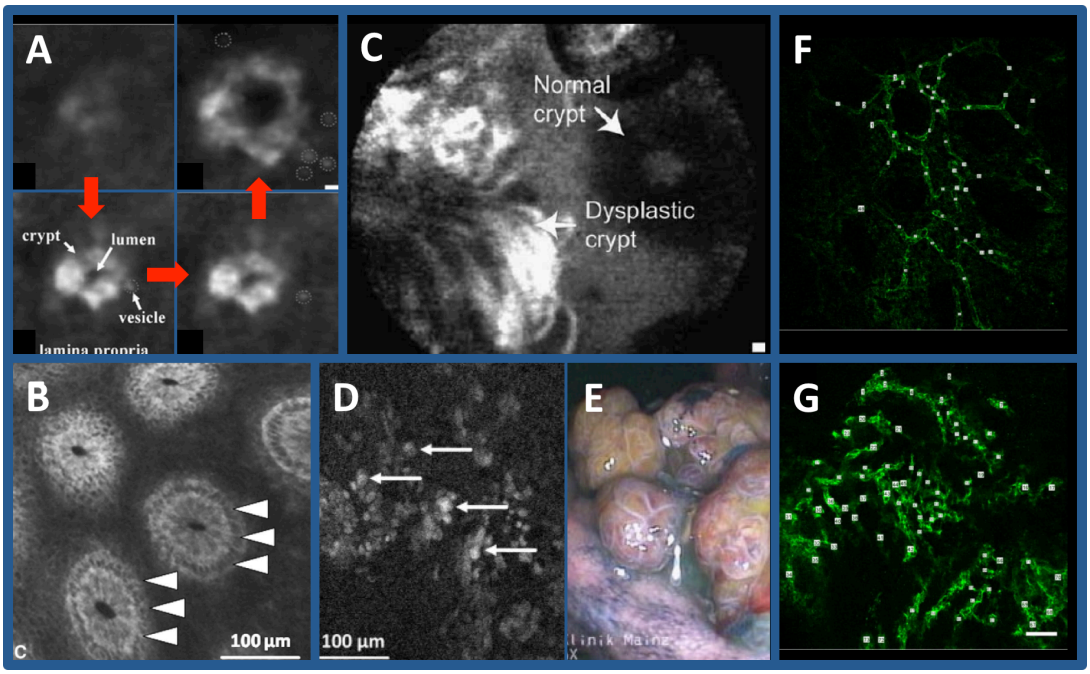


Figure 2.5 Attempts to improve diagnostic accuracy include measurement of the speed of absorption of topical fluorescein (A)[118], and the use of nuclear staining topical contrast agents like cresyl violet (B)[119]. Fluorescent molecular markers include heptapeptides (C)[126], and anti-EGFR antibodies (D) applied topically to the tumour (E) [124]. Fluorescent labelled anti-endothelial antibodies under colour enhanced eCLE imaging ex vivo illustrate a thinner more regularly hexagonal microvascular structure in normal colonic biopsies (F) versus colorectal tumour biopsies (G)[127].

Other diagnostic possibilities abound with transanal CLE. It may have a role in the assessment of EMR scars by detecting residual or recurrent areas of dysplasia following EMR of colonic adenomas[128]. CLE has been used in inflammatory bowel disease in an attempt not only to improve the yield of the approximately 32 random and targeted colonoscopic biopsies required for surveillance (time-consuming and of doubtful efficiency), but to assess inflammatory activity in ulcerative colitis based around changes to crypt and microvascular architecture[129]. With care, the terminal ileum can be cannulated with a pCLE probe and occasional epithelial gaps are evident through which fluorescein leaks into the lumen; increased shedding of epithelial cells appears to increase the density of these gaps in inflammatory bowel disease patients[130], and increased epithelial shedding with resulting intravenous fluorescein efflux appears to be a predictive marker for disease relapse[131, 132]. With time, CLE differentiation between ulcerative colitis and Crohn's disease is likely[133]. Another diagnostic application is acute graft-versus-host disease (GvHD); a frequent and severe complication of stem cell or bone marrow transplantation which often entails significant tissue destruction within the

gastrointestinal tract, necessitating an immediate increase in therapeutic immunosuppresion. Diagnosis currently requires endoscopic biopsy, often in thrombocytopaenic patients. In Bojarski et al.'s pilot study eCLE displayed specific morphological changes (crypt dropout and apoptotic cells) in 14 out of 19 patients with rectal GvHD out of 35 patients who were referred with diarrhoea after stem cell transplantation[134]. Similar crypt necrosis appears to be evident with eCLE for GvHD of the stomach[135].

It is worth highlighting that not all bowel diseases include mucosal changes, and by creating a breach in the mucosa it is possible to insert a pCLE probe to abut the submucosa and muscularis externa. Early work has concluded that the enteric neural network is particularly fluorescent with acriflavine; a finding that might have relevance to the understanding of functional and motility disorders[136, 137].

2.9.2 Imaging the biliary tree with pCLE

Early diagnosis of malignant biliary strictures remains imperative, especially in those patients who are fit enough for surgical resection. A false negative or delayed diagnosis may result in the window of operability being missed; conversely, incorrectly labelling a stricture as neoplastic may inappropriately subject a patient to a potentially highly morbid operation. However, it is often a challenge to differentiate malignant from benign strictures. Even when three intraductal methods of tissue biopsy are employed during endoscopic retrograde cholangiopancreatography (ERCP), (cytological brush biopsy, forceps biopsy, and fine needle aspiration) the sensitivity and specificity for detecting high grade atypia and malignancy is only 62% and 90% respectively[138], due to tumour either not invading the portion sampled (often because cholangiocarcinoma spreads up and down the duct mucosa rather creating a circumferential mass) or a desmoplastic reaction enveloping the tumour. More sophisticated processing of cytology using characterisation of DNA content with digital image analysis[139] and fluorescent in-situ hybridization[140] may only moderately improve sensitivity. In 2008, Meining et al. described, with a sensitivity of 83%, the appearance of irregular vessels and a reduced signal to noise ratio in the pCLE images from malignant strictures[141]. Benign epithelium featured a fine reticular pattern of narrow dark bands; ex vivo research suggests this reflects healthy lymphatics[142]. Other small studies have had similar findings (Figure 2.6) [143, 144]. The "Miami classification" has suggested that where two

or more suspicious features are present: thick white bands (tortuous vessels >20μM), thick dark bands >40μM, dark clumps, or epithelial structures, there is an improved sensitivity of 97%, but with a trade off in specificity at 33% due to false-positive cases from benign inflammatory strictures[145]. A recent attempt has been made to characterise those pCLE image abnormalities that are caused by benign strictures, in an attempt to improve specificity[146]. This study identified three factors which may contribute to false positives: a) a malignant looking ERCP clouding pCLE interpretation – during protocols entailing on-line pCLE interpretation, b) poor quality videos and c) recent dilatation or stenting of the ductal lesion in question causing fluorescein leakage.

The only work has so far to have been done on pCLE examination of ampullary lesions of the distal bile duct suggests that pCLE endoscopists struggle to agree on the image interpretation[147], a theme which is common to indeterminate biliary strictures elsewhere, with interobserver kappa agreements regarding the "Miami classification" ranging from poor to fair[148].

Future work is needed to correlate somewhat vague image findings with known histology.

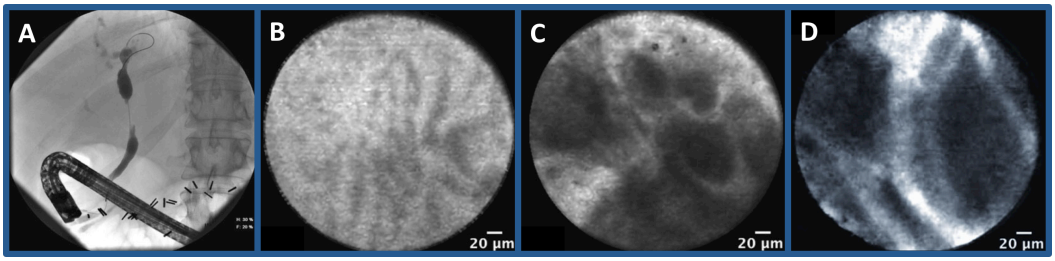


Figure 2.6 A stricture within the common bile duct is demonstrated using ERCP (A). pCLE images of healthy bile duct show thin dark bands (B), whereas large black cells and tortuous fluorescent vessels are evident in malignant areas (C and D)[143, 144].

2.9.3 Barrett's oesophagus and pCLE

The incidence of oesophageal cancer is rapidly increasing in the developed world. In the United Kingdom in 2008, 8170 people were diagnosed with it, rendering it the 9th most common cancer[76]. Mainly due to its often advanced stage at presentation, it has a dismal prognosis: the 5 year survival is less than 10%[149, 150] overall, but in those with early stage cancer it has been reported as high as 81%[151]. Early diagnosis is therefore essential, and as the main risk factor is Barrett's oesophagus (chronic acid reflux causing metaplastic transformation of the normal stratified squamous epithelium of the distal oesophagus into the secretory columnar epithelium typically seen lining the intestines),

Barrett's patients need identifying, in order to be offered screening endoscopy to identify areas of neoplastic transformation. Standard surveillance includes four quadrant pinch biopsy at 1-2cm intervals for the length of the Barrett'segment[152]. High grade dysplasia is treated with more intensive surveillance, radiofrequency ablation, submucosal endoscopic removal or surgery, whereas invasive cancer usually requires surgical resection. However, rigorous biopsy protocols have the dual problem of low yields, that still manage to miss high grade dysplasia owing to high grade dysplasia and early cancer frequently looking macroscopically normal[153]. To improve both the accuracy of surveillance, and the yield of biopsy, high resolution endoscopy, chromoendoscopy, autofluorescence endoscopy, narrow band endoscopy and optical coherence tomography have all been suggested.

In 2006, Kiesslich et al. showed that the goblet cells of Barrett's oesophagus were easily identifiable on eCLE, and trialled its use for eCLE detection of Barrett's neoplasia, thereby using analysis of vessel and cellular architecture to formulate the Mainz criteria[154]. In the Mainz criteria, neoplasia is revealed by irregular capillaries that leak fluorescein into the lamina propria, contrasting against prominent dark cells that have irregular shapes and borders (Figure 2.7). In this initial study, using blinded retrospective reporting of the images, neoplasia was diagnosed with 93% sensitivity and 98% specificity. A subsequent small prospective crossover study suggested that in patients with Barrett's associated neoplasia, suspected (but unlocalised) during prior white light endoscopy, the yield of neoplasia with a standard four-quadrant protocol every centimetre was 17%, but this doubled to 34% when mucosal biopsies were only taken from areas indicated as suspicious on eCLE; furthermore, 59% fewer biopsies were required for the diagnosis with the more selective approach[155].

Barrett's is relatively easily diagnosed with pCLE also[156], and therefore the Mainz criteria have been variously modified, generally requiring the presence of two of five or six parameters to denote neoplasia: an inhomogeneous gland lining, irregular epithelial lining width, presence of "dark areas" on the epithelial border, fusion of villi and glands, an irregular vascular pattern and absence of obvious goblet cells[157-159]. Pohl et al. showed that two independent endoscopists experienced in pCLE provided a 75-89% sensitivity and 75-91% specificity to detect high grade neoplasia/early cancer at retrospective image review[157]. By briefly training and then testing eleven experienced gastroenterologists, Wallace et al. suggested an overall sensitivity of 88% and specificity of 96% was achievable for neoplasia detection using the more recent high definition

pCLE probe with improved resolution, and also showed that the doctors who were previously acquainted with pCLE performed better[158]. Prior experience seemed to offer no advantage in the study of Gaddam et al. who, after systematically assessing the individual prognostic power of 9 image features, were unable to create a significantly improved classification system, with a sensitivity of 76% and specificity of 85% for diagnosing neoplasia[159]. Of note, this study showed that if the endoscopist was confident of the diagnosis, the accuracy was 98%, highlighting the importance of providing clear video sequences, and raising the possibility that in the future only those areas where the pCLE diagnosis is not clear need pinch biopsying.

Whilst investigators used blinded offline image evaluation in the above evaluations of pCLE in Barrett's, an obvious attraction of optical biopsy is real-time diagnosis. Spot diagnosis in vivo has inherent time pressures which could negate the potential advantages of being able to interpret the pCLE video sequence in the context of the patient and the mucosal white light image. In a prospective multicentre study enrolling 68 patients with Barrett's, the sensitivity for realtime detection of neoplasia per biopsy was a disappointing 12%, with a specificity of 95%[160]. Post-procedure image review only improved these figures to 28% and 97%. High grade dysplasia or cancer was only present in 8.3% of the patients studied, but in reality this is a more realistic prevalence for a Barrett's surveillance population. It was particularly salient in this study that this prevalence mirrored the seemingly high negative predictive value of 92%; which is essentially the same as the pre-test likelihood of absence of neoplasia. Also, the specificity of predicting neoplasia on a per-patient basis, fell from a respectable 95% to 59% when the investigators were blinded to the endoscopic findings, supporting the French philosopher Henri-Louis Bergson's quote that, "The eye sees only what the mind is prepared to comprehend"; in the context of mucosa with a macroscopically healthy appearance, an endoscopist may easily dismiss a few slightly abnormal video frames as spurious rather than score them as reflecting dysplasia.

The only randomised controlled trial to date has suggested that with an "enriched" study population (31% had high grade dysplasia or cancer), when pCLE is combined with high definition white light endoscopy, it has a sensitivity of 62.5% and specificity of 92.7%[161]. Though this significantly improved the biopsy yield, the sensitivity is still inadequate to obviate the need for conventional biopsy.

The classification systems described are obviously somewhat subjective, and a more quantified approach to the assessment of morphological differences may aid

interpretation. For example, computational analysis of pCLE frames has shown that whilst the mean vessel diameter remains similar, dysplastic Barrett's has a significantly greater mean vessel density than its non-dysplastic counterpart (24% versus 14%)[162]. Iguchi et al. demonstrated an 85% accuracy for observers to use specific microvascular pattern recognition to differentiate between Barrett's oesophagus, high grade dysplasia/intramucosal cancer, and more deeply invading cancer on eCLE[163]. They also showed in a more quantified fashion that the mean microvessel diameters increased: 11.4μm, 17.8μm, and 20.7μm respectively for the three groups (non significantly between the last two groups but there were only 15 patients in the study).

As with colorectal polyp imaging, in Barrett's, efforts have been made to interrogate cellular metabolism and function with confocal microscopic imaging. Following on from the paradigm of injecting radioactively labelled glucose analogues to screen for metastatic foci with positron emission tomography (PET), if ex vivo oesophageal mucosa biopsies are incubated in a fluorescently labelled deoxyglucose such as 2-NBDG, the uptake within the glandular epithelium, as determined by mean fluorescence intensity, is greater where high grade dysplasia or invasive cancer are present[164]. Similar results are seen with ex vivo EMR specimens[165]. Similar to that described for the colon, future developments will undoubtedly include fluorescently labelled peptides or antibodies that selectively bind proteins such as EGF-R, survivin (involved in mucosal protection)[166], and antigens that are expressed in neoplastic transformation[167, 168].

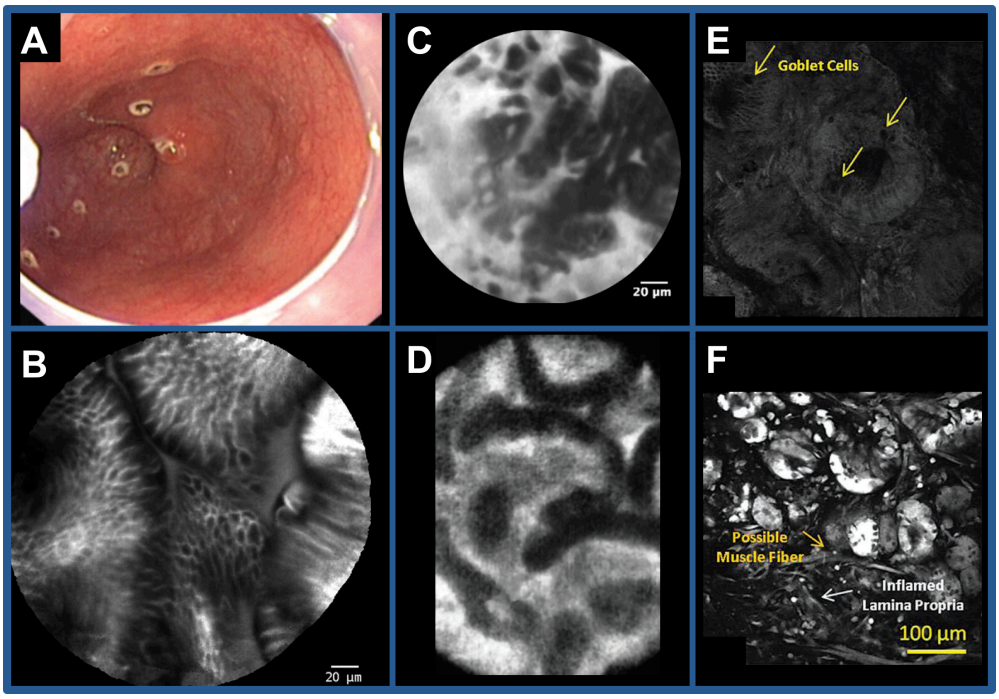


Figure 2.7 In (A), argon plasma coagulation marks the Barrett's segment of the distal oesophagus to enable optical and pinch biopsies to be obtained from the same site, immediately above the burn marks. On the end of the endoscope, the transparent mucosectomy cap is visible to enable suction stabilisation[157]. The pCLE appearance of regular columnar epithelium in non-dysplastic Barrett's mucosa, interspersed with mucin filled goblet cells is shown in B[158]. Features of dysplasia or cancer include epithelial inhomogeneity with large dark cells, and fluorescein leakage (C&D) [157, 160]. Desktop confocal microscopy images of non-dysplastic (E) and, as denoted by hyperfluorescent glands, high grade dysplastic oesophageal pinch biopsies (F) incubated in 2-NBDG[164].

Gastroenterologists generally agree that whilst larger studies in non-selected patients are required, the diagnostic power of neither confocal endomicroscopy system is adequate at present to replace the classic Seattle pinch biopsy protocol. Clearly a thorough Barrett's surveillance with CLE ultimately needs to 1) identify virtually all neoplastic areas with a level of certainty to allow immediate therapy, 2) be able to diminish the risk of neoplasia to a clinically acceptable level (from < 10% pretest to perhaps < 1% after a negative examination, and 3) identify low-grade dysplasia to enhance risk stratification and guide follow-up endoscopy frequency[169].

Ablative therapies such as photodynamic therapy, radiofrequency ablation (using devices such as the HALO system), or cryotherapy, as well as local endoscopic removal, known as mucosal (or submucosal) resection (EMR), are now being offered as far less invasive and morbid alternatives to oesophagectomy in cases of high-grade dysplasia and early cancer (suggested on biopsy and endoscopic ultrasound to be only stage $T1_{a\ LPM\ or\ MM}$;

intramucosal, thus breaching basement membrane but still confined to lamina propria or muscularis mucosa)[170]. The advantage of local resection is that the histopathologist can provide staging information on the extent of invasion, and confirm that more aggressive treatment is not required, but the larger the area of tissue removed, the greater the chances of perforation or oesophageal stricturing. An obvious niche for confocal endomicroscopy is therefore to delineate the extent and margins of disease during these procedures, and to confirm the lateral adequacy of resection/treatment. Furthermore, in theory, if all areas requiring treatment are identified and dealt with at the same sitting, there is less chance for the unavoidable resulting fibrosis to hamper subsequent local resection, and similarly if biopsies are avoided, it has been suggested that subsequent EMR is easier[163].

The feasibility of using confocal endomicroscopy to identify the exact location of high grade dysplasia as identified on previous biopsy, during the EMR procedure has been demonstrated with eCLE[171]. In the Dunbar et al. paper previously described, two patients underwent immediate EMR solely on the basis of eCLE suspicion[155]. In a retrospective series of seven patients with Barrett's neoplasia undergoing EMR with narrow band imaging and pCLE, the area resected was frequently adjusted owing to the pCLE findings[172]; clearly larger prospective studies are required to assess whether it is useful in this context.

2.10 Assessment of the Urological Tract with pCLE

Perhaps the most necessary function of an optical biopsy probe in the urological tract is to differentiate non-papillary neoplasia from inflammatory regions of bladder epithelium (urothelium) during white light cystoscopy, and to delineate the boundaries of these lesions for transurethral resection. White light cystoscopy only has moderate sensitivity and specificity for identifying early lesions, so along with narrow band imaging, ramon spectroscopy, photodynamic diagnosis with hexylaminolevulinate (HAL) fluorescence imaging, and optical coherence tomography, pCLE has been licenced for this purpose. Using intravenous or intravesical fluorescein, Wu et al. have proposed a representative image library from 66 patients, intended to enable differentiation between normal urothelium, inflamed urothelium, and low/high grade urothelial cancer (Figure 2.8)[59]; as well as to suggest typical images of prostate and urethral mucosa and (ex vivo) the upper urological tract. This, and a similar feasibility study[51] interestingly noted that blood flow was discernible even with topical/intravesical fluorescein administration; a

finding not replicated in other tissues. Chang et al. showed that after a two hour tutorial, there was substantial interobserver agreement regarding four out of six imaging features in a heterogeneous set of 31 fluorescein pCLE videos of bladder regions[173]. Non-clinical CLE novices picked up the technology as quickly with similar agreement. However, translating these observations into a diagnosis, only produced an accuracy for identifying cancer similar to that of white light cystoscopy. Clearly, more rigorous clinical trials are required to establish if cellular crowding, pleomorphism and distortion can be interpreted with sufficient consistency to provide adequate sensitivity and specificity to clinch a diagnosis of neoplasia. Similar to an endoscopic workflow of chromoendoscopy before CLE of the colorectum, pCLE may have a role after a technique such as HAL photodynamic diagnosis has provided regions of interest (HAL is an ester dye that accumulates preferentially in tissues with high metabolic rates, such as areas of neoplasia, and fluoresces red under blue light, though HAL fluorescence with the 488nm light of pCLE only highlights cytoplasm; fluorescein pCLE appears to correlate better with histology)[174].

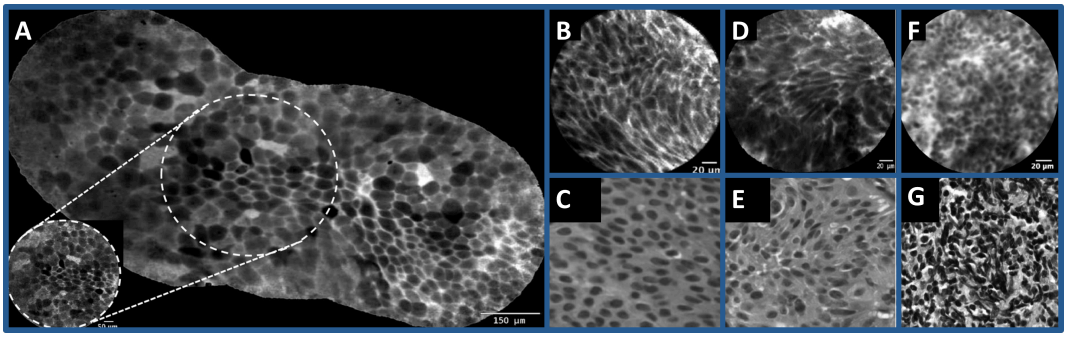


Figure 2.8 Healthy urothelium is shown in (A) in the form of a single pCLE image, also expanded into a panoramic mosaic. These "umbrella" cells appear more crowded in low-grade carcinoma (B), and display increasing pleomorphism in (D) which is taken from high-grade carcinoma. In (F), taken from chronically inflamed urothelium, there are small monomorphic cells. (C), (E) & (G) are the equivalent haemotoxylin and eosin stained histology images. Adapted from Wu et al. 2011[59].

2.11 Gynaecological Targets for pCLE

Early ovarian cancer is highly curable but notoriously difficult to diagnose; unfortunately, most women present with stage III or IV disease which has a 5 year survival of around 20%. This forms the justification for the development of a confocal microlaparoscope which has been used to image the surface of ovary in vitro and in vivo (Figure 2.9)[175].

Tanbakuchi et al. are yet to quantify the accuracy of interpretation of its images in vivo, but using topical fluorescein and then the topical nuclear contrast agent acridine orange, the size and distribution of the distinct epithelial nuclei became more heterogeneous in adenocarcinoma. Apart from the obvious concern that many tumours will develop from epithelium within the body of the ovary and thus remain inaccessible to the microlaparoscope, (images of the ovarian parenchyma have been obtained with a needle confocal which is subsequently discussed[67]),there are three challenges highlighted by their study:

- The issue of ideal contrast agent is present; only by using topical acridine orange were distinct images possible, but owing to the theoretical risk of mutagenesis it is unlikely that this could ever be used where stained tissue could be left in the body (oophorectomy was being performed immediately afterwards in this study).

- The epithelial coating of the ovary is fragile and easily denuded where manipulation of the organ and pressure of the thin imaging probe is difficult to control.

- In vivo, awkward ergonomics renders consistent pressure tricky, and dark areas on the image represent partial loss of contact.

Computer aided identification has been explored in many biomedical spheres. Early work by Srivastava et al. on images from the same group has suggested that it may improve accuracy and even outperform humans in terms of accuracy of detecting neoplastic ovarian tissue in CLE images, with a sensitivity of 98% and a specificity of 90%. Computational analysis of the subpatterns within the image (texture analysis) was employed using a) standard statistics from the normalised histogram of the image, b) spatial gray-level matrices, and c) spatial frequency based features[176]. Better accuracy was especially evident when compared against gynaecologists with little experience of CLE image interpretation.

The other obvious gynaecological target is the uterine cervix where the commonly performed Pap smear can miss lesions during screening but more often overcalls lesions, resulting in unnecessary colposcopy which often requires multiple tissue biopsies to exclude disease. A rigid handheld CLE probe with topical acriflavine has been used to detect cervical intraepithelial neoplasia (CIN) with a sensitivity of 97%, though differentiating the different grades (1-3) was more challenging[177].

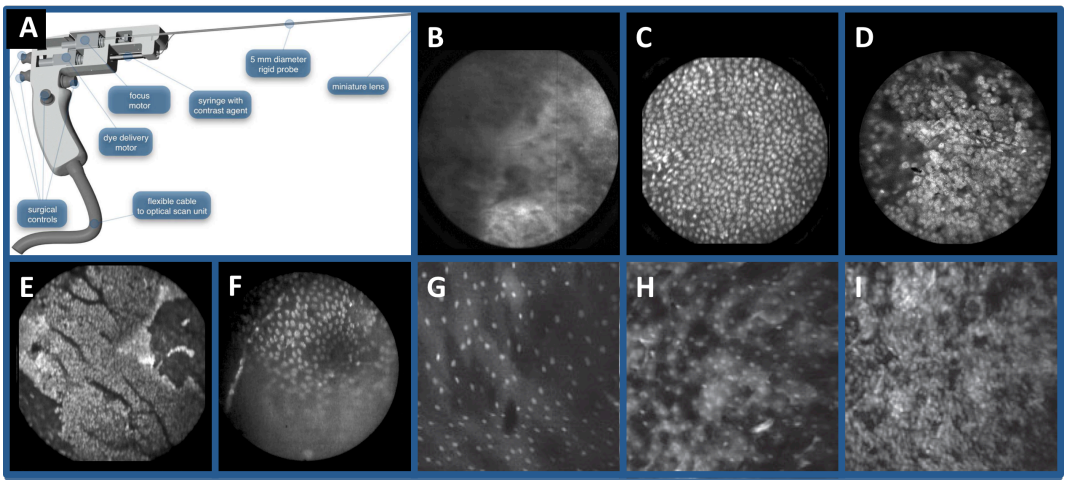


Figure 2.9 A schematic showing a novel device for confocal image acquisition during laparoscopy is shown in (A). Ovarian images obtained using this microlaparoscope were superior using topical acridine orange (C-F) compared to topical fluorescein (B). The distribution and size of nuclei are more heterogeneous in adenocarcinoma (D) than in healthy epithelium (C). Epithelium can be easily denuded with accidental mechanical scraping during imaging (E) and when the device is used in vivo, uniform contact is more difficult to achieve (F). Cervical CLE with topical acriflavine can easily differentiate healthy epithelium (G) from CIN3 (I) on the basis of nuclear density, but distinguishing CIN1 (H) from healthy epithelium is more problematic. Adapted from[175] and [177].

2.12 A role for pCLE in the Respiratory Tract?

2.12.1 Recent biophotonic developments in bronchoscopy

White light videobronchoscopy is commonly used for rapid macroscopic examination of the large and medium airways, but has a low sensitivity for the detection of small superficial mucosal abnormalities and areas of intraepithelial neoplasia[178]. This has led to the development of modalities such as autofluorescence bronchoscopy (AFB)[14-16], narrow band imaging (NBI)[11, 12], high magnification bronchoscopy[17], optical spectroscopy[179], and optical coherence tomography[27], which are being studied as adjuncts to white-light bronchoscopic imaging and tissue biopsy. Endobronchial Ultrasound (EBUS) is an increasingly utilised tool for imaging beyond the mucosal surface. High frequency (20MHz) radial ultrasound probes have a resolution of <1mm and can distinguish certain histological characteristics of the airway wall[180] and of peripheral lesions[26, 181], but even at this resolution biopsies are still required for a firm diagnosis to be made.

In general these modalities can improve the sensitivity for highlighting disease, but their specificity to differentiate neoplasia from inflammation or dysplasia is insufficient to obviate the need for tissue biopsy. Furthermore, they are unable to image beyond the larger airways to add diagnostic information during the investigation of parenchyal lung diseases (PLDs); even the thinnest commercially available bronchoscope is the Pentax FB-8V® with a diameter of 2.7mm[182].

To accurately diagnose many PLDs or solitary peripheral lung nodules, a multidisciplinary assessment is required[183]. This combines information from the clinical presentation, interpretation of the high resolution computed tomography (HRCT) images, and microbiological, cytological, and histopathological clues provided by bronchoscopy. Microscopic examination of cells from bronchoalveolar lavage (BAL) can cause dyspnoea, pleuritic pain[184] and fever/flu-like symptoms[185]. Histopathological analysis has the greatest influence upon establishing a diagnosis[186], but it does not always provide a definitive answer[187], sometimes requires biopsies from several bronchopulmonary segments[188], and is not free from risk. Indeed, a blind transbronchial biopsy (TBB) carries a 1-12% risk of pneumothorax[189-192], and a 2-9% risk of bleeding[190, 193, 194]. Consequently, despite many parenchymal diseases progressing histopathologically (as well as clinically and radiologically) over time[195], repeated biopsies require good justification. For lesions that are inaccessible to TBB, the risks of percutaneous or video assisted thoracoscopic biopsies are greater still[187, 196].

2.12.2 Adaptation of pCLE for the lung

pCLE has been used for bronchoscopy; the only commercial system being the Cellvizio-Lung® (Mauna Kea Technologies, France). It can image both the airways and the peripheral lung/lobule. In peripheral pCLE the probe is inserted blindly beyond the videobronchoscopic view until it is lodged and a relatively fixed alveolar image is obtained. The potential for tissue mosaicing is greater in the less constraining central airways, but the gentle and smooth manipulation which is required remains ergonomically challenging, due to cardiorespiratory and patient movement, and similar to what has been described in the gastrointestinal tract, the understanding that good imaging requires the sometimes awkward task of perpendicular probe abutment with the tissue.

For all CLE target organs described thus far, topical or intravenous administration of exogenous fluorescent contrast agents is required. However, elastin acts as an endogenous fluorophore when excited with a 488nm confocal laser beam, and elastin is abundant both within the basement membrane of the bronchial tree (Figure 2.10), and as a structural connective tissue component of the alveolar walls. Analysis of the spectral emission shape has demonstrated that these structures are responsible for the images created by pCLE without exogenous contrast during bronchoscopy[47].

2.12.3 pCLE of the upper airways

In 2007, by imaging healthy, premalignant and malignant bronchial mucosa in 29 patients and healthy ex vivo bronchus, Thiberville et al. described five apparently distinct lattice arrangements of the predominantly longitudinally orientated connective tissue fibres of the subepithelial lamina reticularis (deeper layer of the basement membrane) in separate areas of the bronchial tree, with small round/oval openings (up to 400μm in diameter) present down to the lobar divisions, representing bronchial gland openings [47]. These regular structures tended to become disorganised, and the spectral intensity of the fluorescing signal diminished (the probe used was actually a prototype combining imaging and spectroscopy) when overlying malignant, pre-malignant or even metaplastic epithelium was present. It was also suggested that non-malignant disease may affect the basement membrane appearance during pCLE; for example, the bronchial carina of a patient with sarcoidosis produced a granulomatosis like image, and a patient with Mounier-Kühn syndrome (atrophy of the airway smooth muscles and elastin causing infections and tracheobronchomegaly) displayed no pCLE autofluorescence. These alterations to the basement membrane appearance may be due to disease states altering the epithelial thickness, preventing the basement membrane falling in the plane of imaging, or may be due to damage to the membrane itself. Examples of Thiberville's descriptive conclusions are shown in Figure 2.10, and illustrate the need for rigorous future study to determine accuracy and agreement amongst observers.

Recently, Yick et al. in a very small study compared the pCLE appearances of the basement membrane at the bronchial carina between seven asthmatics and seven control subjects[197]. All pCLE images and histological slides were categorised into either "lamellar", "whispy", or "mixed". There was close agreement between pCLE and histological category, and surprisingly, whilst there was no association between asthma

and any one particular category, those with a "laminar" pattern had a significantly poorer lung function (forced expiratory volume over 1 second post inhaled bronchodilator).

To image the respiratory epithelium overlying the basement membrane, a contrast agent must be used: early work suggests that bronchial mucosa sprayed with physiologically pH buffered cresyl violet and imaged with a modified Cellvizio-Lung pCLE employing a 561nm yellow laser[198], penetrates cytoplasm and demonstrates the cell nucleus, and therefore provides better resolution than 488nm excitation and intravenous fluorescein[199]. Standard cresyl violet has been used for pCLE imaging of the bowel[63] but its high natural acidity could be enough to provoke dangerous inflammation in the lung. However, whilst limited in vivo study suggests that it is possible to discern differences between dysplastic and normal (pseudostratified columnar) epithelium (based around homogeneity and seemingly cellular discernibility), categorising degree of disease (mild, moderate or severe dysplasia) is impossible[198] (Figure 2.10 J, K & L). At 660nm, topical methylene blue has also been tried as an alternative agent for imaging bronchial epithelium[200].

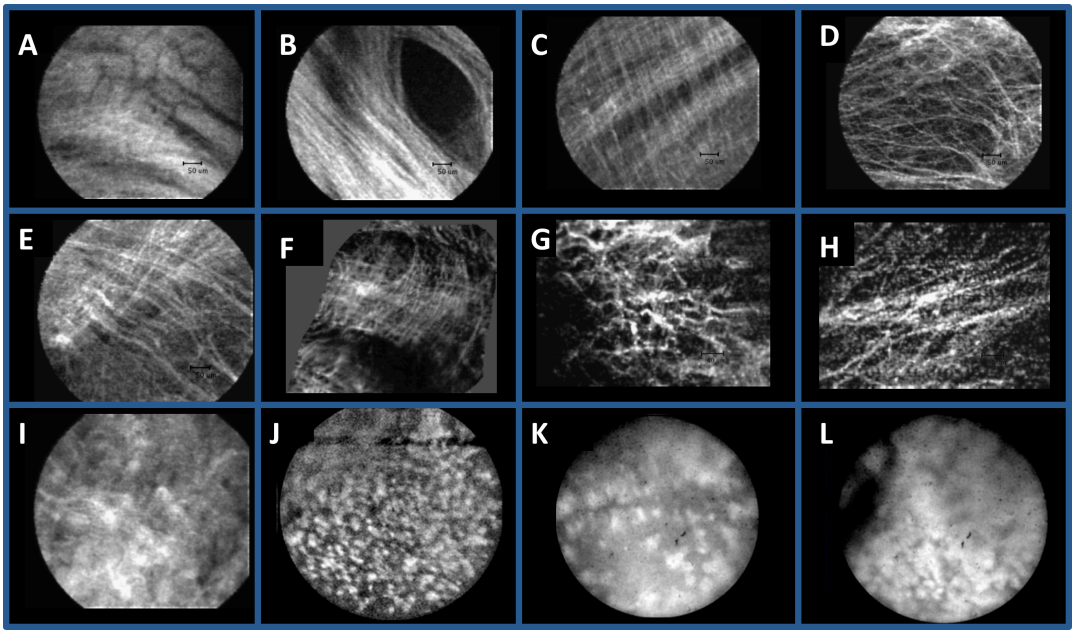


Figure 2.10 The arrangement of the elastin network beneath the airway epithelium autofluoresces and, it has been suggested, characteristically in different areas; dense, homogeneous without crosshatching in the anterior trachea (A), compact cross hatchings close to bronchial gland openings near lobar carinae (B), increasingly loose cross-hatchings of membranous trachea (C), and distal airways (D and E), and a "ringlike" appearance to noncartilagionous bronchioles (F). Disrupted basement membrane appearance is shown with carcinoma-in-situ (G), metaplasia (H) and sarcoidosis (I). Using topically applied cresyl violet in vivo at 561nm, it is possible to differentiate between normal epithelium (J) and dysplasia (K&L), but not between grades of dysplasia; mild (K), and severe (L). Adapted from [47] and [198].

A “distal scanning” bronchoscopic 488nm confocal endomicroscope prototype was recently constructed[201]. At 6.2mm diameter without facility for white light imaging it requires rigid bronchoscopy under general anaesthetic but has been used to image endobronchial mucosal abnormalities of larger airways using intravenous fluorescein. As previously described, a major advantage of distal scanning devices over pCLE is that the distal optics allow the Z-depth of imaging to be altered during the procedure; in this case 0-200µm below the surface, from individual ciliated epithelial cells down to submucosal smooth muscle and microvessels.

2.12.4 pCLE of the peripheral lung

As has been shown in the biliary tree, a key advantage of pCLE over eCLE, is size; a 1.4mm diameter stiff pCLE probe can be deployed to the periphery of the lung to microimage small blood vessels and the fluorescent elastin scaffold of the lobule, creating a realtime image of the arching elastic fibres forming the backbone of alveoli.

In 2009, Thiberville et al. performed pCLE bronchoscopy, using topical anaesthesia without sedation, in up to eight bronchoalveolar areas of 41 healthy subjects; there were no complications (chest radiographs were performed before and after all procedures to exclude pneumothorax) although there was transient pain when the probe tip was close to the pleura[48]. All bronchopulmonary segments were accessible except for the apical and posterior segment of both upper lobes (B1 and B2[202]) due to the stiff probe impairing the ability of the bronchoscope to flex adequately. Lobular microanatomy could not be identified in only 23 out of the 215 bronchial segments cannulated with the probe. Whilst the published images do not provide entirely convincing evidence that consistent geometric and structural measurements can be obtained for each image, post-procedure the authors measured the mean alveolar mouth diameters as 278±53µm, the mean elastic fibres forming the lobular scaffold as 10.05±2.71µm, and the mean extra-alveolar microvessels as 104±48µm (Figure 2.11). Only the latter measurement was not normally distributed owing to positive skew from occasional large vessels. Cyclical changes in the size and shape of the structures during the breathing cycle were evident. Alveolar autofluorescence increased with age of subject. The presence of highly fluorescent macrophages during pCLE examination was also relatively specific to the 17 smokers in the study, creating greater overall fluorescence intensity within the alveoli of smokers. There was also a positive correlation between number of cigarettes smoked per day and,

a) mean macrophages of size >30μm present per field of view and b) presence of mobile macrophages. Absorption of tar by the macrophages is the likely cause of the fluorescence[203]. For the many current smokers who undergo bronchoscopy, these bright macrophages potentially act as an additional endogenous fluorophore.

Thiberville observed that the probe could create alveolar distortion through the exertion of a pressure effect on the lobular geometry, and therefore only performed morphometric examination of those images which were recorded immediately prior to a loss of contact as the probe was gently withdrawn after finding its initial destination. In particular, if the probe was deemed to be entering the lobule down the axis of the alveolar duct, axial pressure upon the elastin structures created the illusion of increasing the working distance by compressing the first plane of focus against the backplanes.

If adjacent images can be readily tracked during steady probe translation, the field of view (FOV) can, in theory, be increased using the device's "mosaicing" software[57, 58].

So far, there are few reports of pCLE imaging parenchymal disease. A case study suggested that the globular lipoproteinaceous material that formed within the alveoli of a smoker with the rare condition pulmonary alveolar proteinosis (PAP) was visible and distinct from alveolar elastin and macrophages[204]. Short abstracts have suggested that a) pCLE at 660nm will provide intracellular resolution if methylene blue is squirted down an extended working channel to coat the lobular structures beforehand[205], b) there are "specific alterations" such as thickening of alveolar walls and structural disorganisation in patients with diffuse or focal interstitial lung diseases[206], and c) in a small study of patients either awaiting or having received lung transplant[207], the mean alveolar diameter of the 5 patients with end-stage emphysema was 389±127μm with alveolar wall thickness of 22±21μm; for the 5 with idiopathic pulmonary fibrosis, the mean alveolar diameter was 190±71μm, with alveolar wall thickness of 16±7μm; the same dimensions within the 10 transplanted lungs were comparable to Thiberville's results in healthy subjects. Recently, Thiberville's group have suggested that amiodarone-induced lung toxicity can be differentiated from other interstitial lung diseases by the presence of large (>20μm), aggregating, strongly fluorescent cells within the acini[208]. These are presumed to be macrophages, and therefore as a diagnostic imaging test this could only be specific in non-smokers, although the addition of pCLE in-situ fluorescence spectroscopy appears to enable differentiation between fluorescent macrophages created by tar from smoking, and from amiodarone related pneumonia. 100μm diameter round highly fluorescent opacities have been described in the alveoli of two non-smoking

Belgian sisters with pulmonary alveolar microlithiasis; a rare form of parenchymal calcification[209].

pCLE was inserted through transthoracic catheters to abut the pleura in a porcine model of acute lung injury (ALI), created by repeated surfactant washout, to evaluate the volume air index (VAI) as a computed parameter of alveolar recruitment[210]. VAI decreased following the induction of ALI, and only in the lower lobes could this be attenuated by increasing the positive end expiratory pressure. Intravenous fluoroscein was required for this, along with a similar transthoracic computational airspace analysis in mice[211]. Whilst the transthoracic approach is unlikely to have relevance in the clinical setting of ALI, if similar results could ever be obtained with bronchoscopy, it could be a useful tool in the critical care environment. Ultimately, as proposed for the gastrointestinal tract, and assuming safety concerns have been addressed, it may be feasible to use functional fluorescent markers to evaluate processes occurring during ALI. Chagnon et al. used the Five-1 (Optiscan, Notting Hill, Australia), a rigid handheld pen-like distal scanning CLE, to compare transthoracic parenchymal images from healthy rats, to those from which ALI had been induced by bleomycin or hyperoxia[212]. Amongst the contrast agents used, fluorescent labelled ricinus communis agglutinin (RCA-1) binds galactose residues on type 1 epithelial cells, and, administered via the trachea, it demonstrated that ALI rats had increased parenchymal thickness. In other rats, neutrophils were harvested and labelled with green fluorescent PKH2 and then tracked. There was a 28-fold increase in the number of labelled neutrophils sequestered into airspaces pre-treated with bleomycin. Intratracheal or intravenous administration of the fluorescent molecular marker YO-PRO-1 demonstrated increased apoptosis in ALI lungs. Finally, by imaging 5 minutes after the intravenous injection of fluorescent labelled dextran (at 77kDa it tends to stay intravascularly) it was possible to show the increased microvessel leakiness brought on by hyperoxia induced ALI.

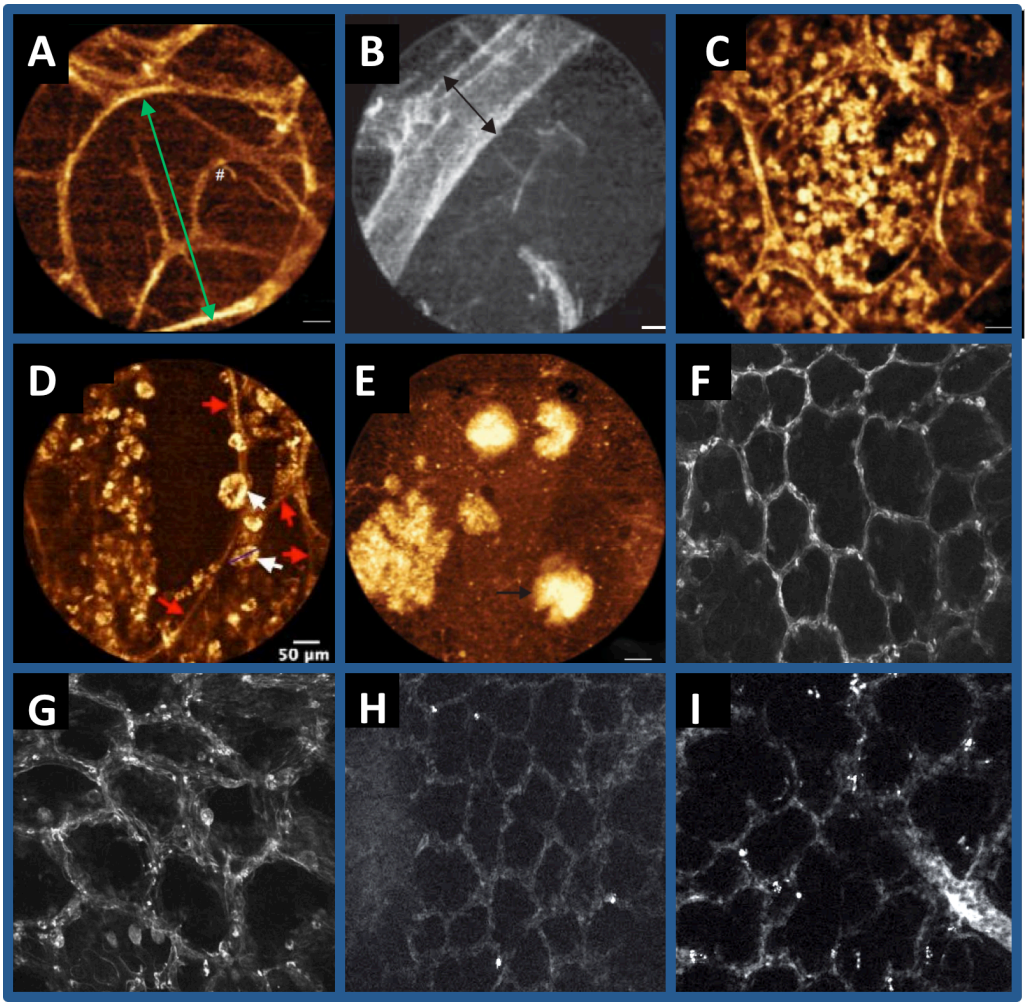


Figure 2.11 Confocal alveoscopy in a non-smoker demonstrates (a) the elastin scaffold of the lobule with a green arrow showing the alveolar mouth diameter, and (b) a microvessel. The alveolus is stuffed with autofluorescent macrophages in healthy smokers (c), and in amiodarone-induced interstitial lung disease (d). In PAP 100-300µm lipoproteinaceous globules are present (e). In rat models of bleomycin induced ALI, the parenchymal walls are thickened, as illustrated by type 1 epithelial cell fluorescent labelling in normal lung (f) and bleomycin induced ALI (g). Fluorescent labelled neutrophils are also drawn into the peripheral lung in ALI; healthy (h) and ALI (i). Adapted from [48, 204, 208, 212]

In another rodent transthoracic study, the diagnosis of pulmonary aspergillosis (fungal pneumonia secondary to *aspergillus fumigatus*) was addressed with immunoendoscopy (Figure 2.12). A timely diagnosis is of critical clinical importance in these often immunocompromised patients, but it is often unfortunately delayed. FITC (fluorescein-isothiocyanate) labelled peptides that relatively specifically bind to *a. fumigatus* were injected intravenously into immunodeficient rats previously inoculated with the organism, and pCLE images over aspergillosis foci on the lung surface showed a diffuse stromal

fluorescence, and with a sensitivity and specificity of nearly 95%, approximately 80% greater fluorescence intensity than that recorded without the peptide or with other fungal microabscesses or chronically inflamed areas[213]. It is possible that peptides for the targeting of other disease antigens could be used, but in vivo in situ translation into patients would require many things including proven safety of the peptides, and the transbronchial approach to be as accurate (it would be necessary to differentiate between the fluorescence created by acinar elastin and and the fluorescence from the label on the peptide; switching from 488nm to 660nm would be a possible solution).

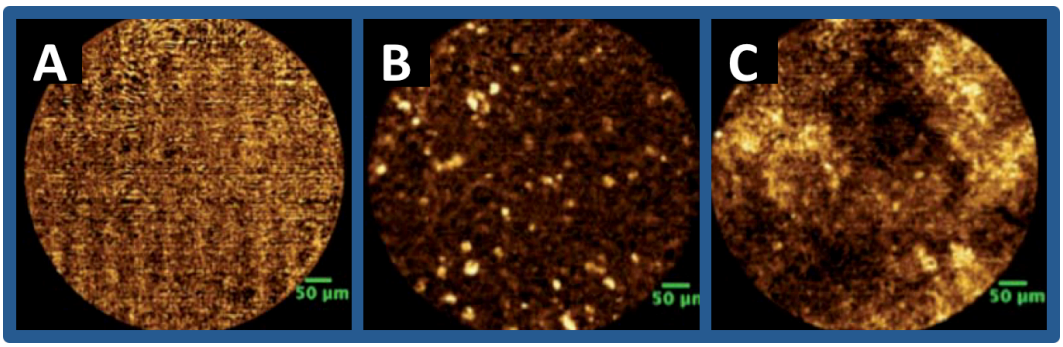


Figure 2.12 Transthoracic pCLE signal in rats showing no discernible fluorescence over a healthy area even after peptide injection (A). When imaging an aspergillus microabscess small specks were evident before peptide injection (B), becoming larger fluorescent patches after peptide injection (C). A similar appearance to (B) was seen overlying inflammatory areas, and *Geosmithia argillacea* microabscesses before and after peptide injection[213].

2.13 The Peritoneal Cavity and pCLE

2.13.1 The evolution of peritoneoscopy

The rigid laparoscope has become an essential diagnostic tool in minimally invasive surgery. Laparoscopy of the peritoneal cavity is widely used for diagnosis (and potential treatment) of endometriosis[214], chronic abdominal pain[215], unexplained sepsis in critical care[216], and it is employed as a vital staging procedure prior to resection of upper gastrointestinal or pancreaticobiliary malignancies[217]. Though the abdominal scars and physical trauma created by diagnostic laparoscopy are smaller than those of open surgical exploration, recent technological advances in the form of Single Incision

Laparoscopic Surgery (SILS), or flexible endoscopic approaches such as natural orifice transluminal endoscopic surgery (NOTES) aim to further reduce the physical and psychological burden, and reduce peri-operative mobidity and analgesic requirements. Indeed, NOTES peritoneoscopy has been explored clinically as an alternative to diagnostic laparoscopy[218-221].

2.13.2 The integration of optical biopsy into peritoneoscopy

Concominant with the evolution of these minimally invasive approaches to examine, biopsy and potentially operate on the intraabdominal viscera, several of the probe based imaging technologies outlined in chapter 1 have been developed and experimentally integrated into the laparoscopic/endoscopic workflow. These include near infrared fluorescence[222], optical coherence tomography[223], and endocytoscopy[224]. These are particularly relevant in the context that staging laparoscopy can only prevent up to half of unresectable gastrointestinal malignancies, initially thought to be resectable on CT, undergoing fruitless laparatomy[225]. Von Delius et al. showed that pCLE provides interpretable images of the surface of the peritoneum and liver during porcine transgastric NOTES peritoneoscopy using intravenous fluorescein [52]. Splenic surface images only showed a few non-specific vessels. The 10μm depth "s" miniprobe was used for peritoneum, and the 100μm depth "z" miniprobe for the liver and spleen. Challenges highlighted included a) inaccessibility of particular areas of the peritoneal cavity with spatial disorientation; themes common to all NOTES research, b) movement artefact created from the pig breathing, although this was reduced by tilting the pig head down, and c) an inability to delineate nuclei with fluorescein; a feature which may be vital in identifying malignant deposits within the peritoneal cavity.

2.14 Confocal Endomicroscopy of Solid Viscera

To image slightly deeper, alternative fluorophores can be employed, which require excitation by a longer, and thus more penetrative, wavelength of confocal laser beam. For example, during liver laparoscopy of 22 patients under conscious sedation, fibrosis and steatosis were predicted correctly in 90% and 81% respectively using a prototype rigid eCLE, imaging to a depth of 350μm with 780nm light (near infrared) with intravenous indocyanine green[226]. Nevertheless, in contrast with the gastrointestinal lumen or bladder, solid abdominopelvic viscera may contain deeper areas of suspicion still that a

CLE probe merely abutting the surface could never interrogate. Needle based CLE (nCLE) has been proposed as a solution: a hollow 19 or 22-gauge endoscopic needle is first inserted into the organ of interest, through which a probe similar to the 0.85mm diameter cholangioflex used for biliary pCLE is passed. Via either a transgastric/transigmoid NOTES approach, or through the gastric wall with endoscopic ultrasound (EUS), Becker et al. were able to produce images of variable interpretability of the deep parenchyma of liver, spleen, abdominal musculature, and ovary in ten pigs[67] (Figure 2.13). Whilst there was no bleeding of clinical significance, bleeding tended to impair imaging by absorbing light or extravasating fluorescein requiring probe repositioning. Sentinel lymph node imaging within the bowel mesentery (using patent blue dye for identification) was also feasible; a potentially useful tool for cancer staging, though the images were not especially convincing. Via the transigmoid or EUS approach, in 8/10 pigs it was even possible to access the pancreas with the nCLE, though owing to instability of the probe or perhaps insufficiently identifiable morphology, only 40% of the pancreatic image sequences could be evaluated. Konda et al. performed EUS FNA with nCLE in 18 patients (16 cystic and 2 solid lesions)[227]. On a Likert scale, only 10/17 image sequences were graded as very good or good. Blood vessels were visible in 6 lesions, papillary proliferations were observed in 3 out of 7 cases of intraductal papillary mucinous neoplasia (IPMN), and 3 cases showed a reticular network similar to that observed in ERCP pCLE of ductal epithelium. Otherwise, non-specific cellular structures were speculated upon. With around 10% of EUS FNA/core needle biopsies failing to provide a diagnosis in patients with indeterminate pancreatic cystic lesions[228] and difficulty arising from the differentiation between chronic pancreatitis and malignancy[229], pancreatic nCLE could clearly have a niche if the ergonomics and imaging quality were adequate. It could also enhance safety by reducing the number of traumatic passes into the pancreas to achieve a diagnosis and even allow single stage diagnosis and treatment, such as chemoradiotherapeutic ablation of cystic neoplasms[230].

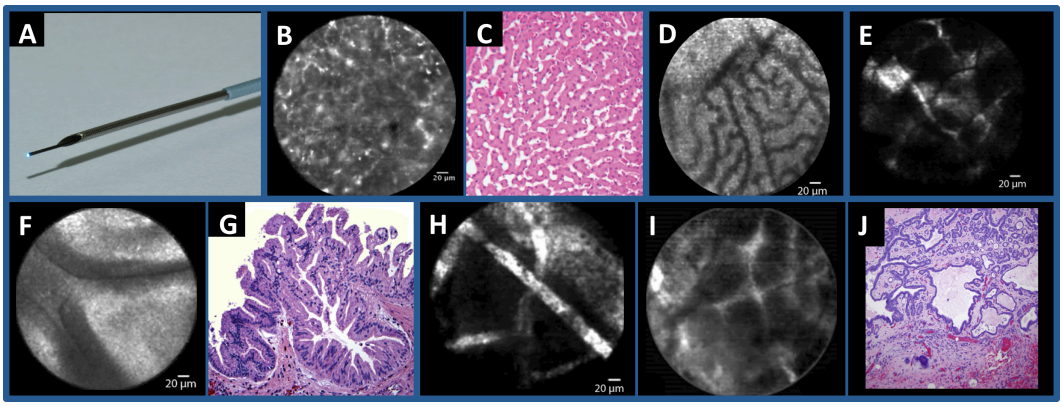


Figure 2.13 The nCLE consists of a probe similar to a cholangioflex deployed through a 19 or 22 gauge needle (A). nCLE images of porcine liver (B), appear to delineate sinusoids shown with H&E staining in (C). nCLE of the pancreas after EUS sometimes shows a reticular pattern similar to that found with biliary pCLE, suggesting the pancreatic duct has been abutted (D). A non-mucinous pancreatic neoplasm (E), and an intraductal papillary mucinous neoplasm showing papillary proliferation (F&G) are shown. The highly vascular histology of a mixed serous/acinar cell pancreatic cystadenoma is shown in (J) with corresponding blood vessels (H) and acinar cells (I) demonstrated on nCLE. Adapted from [67] and [227].

2.15 CLE for the Assessment of Vasculature

The potential utility of CLE to provide dynamic images of blood vessels and flowing blood within them cannot be overemphasised. Microvascular assessment frequently features in the classification systems here described for CLE of many organs, because neoangiogenesis with irregular leaky vessels is such a key component of the development of most cancers; indeed for a tumour to exceed 1-2mm in size, it must produce vascular endothelial growth factor (VEGF) and induce "angiogenic switch" to acquire enough new vessels for an adequate nutrient supply[231]. VEGF expression is also positively correlated with tumour progression and negatively with prognosis. VEGF is therefore another in vivo immunohistochemical imaging target. Foersch et al. used anti-VEGF antibodies labelled with AF488 (a similar fluorophore to fluorescein) with the FIVE-1 (Optiscan) (a rigid handheld version of the CLE) to delineate colorectal tumours in vivo in both mouse models of colorectal cancer (both genetic knockout and human xenograft), and in ex vivo surgical specimens[232]. Antibodies were injected into the mouse tail vein or applied topically onto the surgical specimens. Computed fluorescent intensity and VEGF positive cell counts significantly increased in regions of interest (ROI) representing colorectal cancer, indicating relatively specific binding (mostly within the

cytoplasm). In the surgical specimens VEGF labelled cell counts were positively correlated with histological grade.

Assuming the anti-VEGF antibodies could be safely used in humans there may be potential for improving colonosocopy (immunoendoscopy). Alternatively, Bevacizumab (Avastin®) is an expensive monoclonal antibody which inhibits VEGF, now licensed for use in metastatic colorectal cancer. However, only half of patients respond to it, it has side-effects, and its enormous expense has provoked controversy. Therefore, if CLE could quantify tumour VEGF expression at baseline and during treatment it may identify the cohort of patients that may benefit from this and other drugs. Alternatively, it may be preferable to quantify microvascular architectural changes before or during treatment with chemotherapeutic/antiangiogenic agents directly either with a conventional intravenous fluorophore, or with something that binds more selectively to endothelium. This has recently been done with eCLE (ex vivo) using AF488 labelled anti-PECAM-1 antibodies, showing that tumour blood vessels were subjectively more tortuous and when measured were quantitatively wider than their healthy mucosal counterparts (13.5 ± 0.7μm versus 8.5 ± 0.9μm) (Figure 2.5 F&G)[127].

Other interesting microvasculature discoveries courtesy of CLE include:

- In a mouse cremaster muscle model there is excellent agreement between diameter of microvessels measured by intravital (in vivo) microscopy and by pCLE. Using FITC labelled albumin pCLE reliably picks up calibre changes courtesy of topically applied vasomotor compounds, and by injecting a fluorescent labelled macromolecule (FITC-dextran) and computing the changing mean gray level in the extravascular area, vessel leakiness can be assessed[233].

- pCLE has been shown to identify rogue blood vessels responsible for anaemia in angiodysplasia of the stomach[234].

- After subcutaneous injection of colorectal cancer cell lines into mice, pCLE has shown that the resulting xenografts feature an increasing proportion of grossly dilated chaotic vessels as they grow with decreasing permeation of the FITC-dextrans fluorescent tracer[235].

- In a p53 knockout carcinogen exposed mouse model, the development from healthy colonic mucosa to adenoma to carcinoma is associated with increased

length and area of blood vessels. This change is partially reversed when the antiangiogenic agent sunitinib is used[236].

- In the lamina propria of the colon, the capillary density decreases distally, which corresponds with the physiology of water absorption within the colon[237].

2.16 The Ergonomics of pCLE

Regardless of the target organ, or the particular imaging device employed to manipulate high magnification optical biopsy probes such as pCLE, there are significant ergonomic hurdles[52, 226]. For example, using an endoscope intraluminally to create a panoramic pCLE mosaic or representative video sequence of a gastrointestinal mucosal lesion requires gentle and steady perpendicular probe contact, followed by slow and controlled translation over a few millimetres, created by twisting the endoscope or turning its wheels: a difficult task further hampered by bowel flacidity, peristalsis, cardiorespiratory movement, and in the case of pedunculated colonic polyps, a high degree of mobility. Patient agitation or poor compliance also hampers image acquisition with some evidence that different sedation regimens can affect the quality of the optical biopsies obtained[238]. The delivery of pCLE via a rigid probe makes perpendicular probe abutment difficult, as is observed with rigid cystoscopy, particularly of the anterior bladder wall[51].

In the seminal colonic polyp CLE paper by Kiesslich et al., movement artefact rendered 30% of acquired images less than satisfactory[55]. More recently, in Hlavaty et al.'s eCLE trial in inflammatory bowel disease patients[103], there was disappointment regarding the ability to adequately anchor mucosal irregularities to obtain stable video sequence. Experience may play a role, and other series have included fewer raised lesions but the main issue in this study was that pedunculated polyps tended to flip over the tip of the endoscope, resulting in 2/30 flat and 30/70 pedunculated lesions not being amenable to eCLE imaging. Iguchi et al. found that 4/15 invasive oesophageal cancers could not be imaged with eCLE due to an inability to accurately negotiate the awkwardly placed viewing window of the stiff endoscope tip onto the centre of the curved lesion, especially if they were small and situated in the upper oesophagus[163]. Using pCLE, Van den Broek et al. were similarly hampered by mobile lesions[106], and it appears that video mosaic quality may be hindered by imperfect ergonomics that contribute to movement

artefact[101]. Movement artefact from instability is certainly exacerbated by flaccidity in the bowel, and by cardiorespiratory movement in the distal oesophagus[239]; a particularly problem for eCLE with its slower frame rate of 1.4 frames/second.

In the distal oesophagus, even with 30-60 seconds of pCLE imaging per target, Pohl et al. found that between 6% and 18% of sequences were so poor as to be uninterpretable[157]; it is likely that awkward ergonomics contributed to this. Prior to attempting a retrospective diagnosis with each pCLE video sequence, Gaddam et al. asked subjects to rate video quality; less than a third were rated as "high quality", and importantly subjects were 20% more accurate with these sequences, demonstrating a far superior interobserver agreement[159].

It is a self-evident and frequent observation that clear images and videos yield better diagnostic accuracy and interobserver agreement[108], and greater challenges with tissue/probe abutment may be a reason why diagnostic accuracy was reduced in a study with smaller polyps where only 72% of the pCLE videos were deemed to be "high quality"[100].

Such awkward manipulation is also a likely contributing factor to endoscopic procedures being far slower when confocal endomicroscopy is incorporated: by adding targeted pinch biopsies to the conventional random quadrant biopsy screening colonoscopies of patients with inflammatory bowel disease, Günther et al. found 10 minutes was added when chromoendoscopy was used for targeting, versus 25 minutes when eCLE was employed[104]. Similarly, in the oesophagus, Dunbar et al. found that eCLE for Barrett's surveillance took a median of 18 minutes: twice as long as conventional four quadrant biopsies[155]. This clearly poses issues for both cost and patient comfort.

Some endoscopists find that for both ends of the gastrointestinal tract [100, 157] a transparent mucusectomy cap fitted over the distal end of the endoscope enables the mucosa to be anchored under suction prior to deployment of the pCLE probe; however the cap's benefits may be limited[240]. This stabilises the surface, and creates a more tangential angle of approach for the probe; if the intention is to create mosaics, it enables controlled translation between tip and tissue. An intravenous bolus of hyoscine-N-butyl-bromide (buscopan) can also limit peristaltic artefact[101].

With endobronchial pCLE, the optimum images of the fairly stiff bronchial wall are certainly obtained with perpendicular probe contact; this is not always straightforward, particularly with cardiorespiratory movement[198]. With the slower scan rate of

endobronchial eCLE (0.7-1.2 frames/sec), even under general anaesthetic 60% of images were impaired by motion artefact[201]. Even when the lesions of interest are in the pharynx and being inspected with a rigid eCLE probe, movement artefact from instability and respiration is troublesome[241].

Where an endoscope is used to manipulate a pCLE probe outside of the constraining boundaries of the gastrointestinal tract lumen, during diagnostic inspection of the peritoneal or thoracic cavities for example, there are further ergonomic hurdles to overcome. Here, the endoscope is beset with the issues of instability, counterintuitive movement and disorientation that the NOTES community has been keen to overcome with robotic devices. The potential advantages of precision robotic actuation of optical biopsy both intraluminally and especially extraluminally over the awkward, somewhat crude control, provided by flexible endoscopes is clear when considering that maintaining steady probe apposition with consistent pressure is even problematic with close handheld manipulation of a confocal probe during open surgery[242]. Furthermore, robotic actuation may avoid variations in the contact force between tissue and optical biopsy probe. This may have implications for safety, as well as for maintaining the consistency of the images acquired and the information gleaned during optical biopsy[243-245].

If the interpretation of CLE imaging is hampered by excessive instability and movement causing flitting of the video frames, mosaicing can create a smooth panorama, and improve the ability to identify important regions of interest[59]. However, at present, this is a task that is currently optimally performed offline post-procedure; this is inadequate for intraprocedure diagnosis and decision making, but might become realtime with more stability and precise translation. Mosaicing is significantly impaired by tissue deformations during translation, and a recent study has understandably demonstrated better mosaics on a tissue phantom with a precise industrial robot than with a prototype handheld actuator, but that the handheld actuator can produce mosaics of up to 1600 images blended together by employing “visual servoing”[246].

The ergonomic clumsiness of confocal endomicroscopy may also have relevance to its safety, in the sense that repeated inelegant manipulation of a stiff narrow tipped probe may create damage; indeed the requirement for multiple imprecise deployments, manoeuvrings and extractions of the nCLE probe into pancreatic lesions to achieve satisfactory imaging is a possible reason for 2 out of Konda et al.’s series of 18 patients suffering from post-procedure acute pancreatitis[227].

2.17 Tracking the pCLE Probe's Tip

In the peripheral lung, the blind insertion of a pCLE probe beyond the tertiary bronchiole enjoys no better manoeuvrability or targeting accuracy than that of a peripheral bronchoscopic forceps biopsy. The bronchoscopist can only estimate the location of the probe tip from the angle of deployment beyond the tip of the bronchoscope, the distance it passes, a knowledge of bronchial tree anatomy and any cross sectional imaging available for the patient.

As CLE leaves no trace on the tissue, it is difficult to know exactly from where its images have been obtained. This poses a problem in several situations:

1. If CLE is used to direct simultaneous tissue sampling, it is difficult to ensure that optical and pinch biopsies are obtained from exactly the same area; this is clearly a more significant problem in heterogeneous tissue. As an approximation, with pCLE, argon plasma coagulation can mark adjacent to the target. For eCLE, an approximation can be made by pinch biopsying to the left of the suction polyp created during stabilised confocal image acquisition[155], as the suction and confocal channels lie adjacent to one another.

2. The endoscopist may be keen to perform all CLE within the colon or oesophagus prior to any therapeutic intervention (or pinch biopsy), because intravenous contrast agent decays with time, and constantly inserting and removing the probe is cumbersome and time-consuming. Unless each optical biopsy has been taken from a small lesion with a unique appearance, it may be difficult to relocate the correct target. In the oesophagus, a note of the circumferential position and distance from the incisors may be of help. With the deformability of the colon, this is a strategy that cannot be readily employed.

3. Similarly, unless the diseased area is obvious, if diagnosis and therapy happen on different endoscopy sessions, relocation may be difficult.

4. In the treatment of flat, macroscopically normal lesions, such as EMR/ablation for areas of Barrett's dysplasia, or transurethral resections of non-pedunculated bladder tumours, in theory, CLE could precisely identify the transitions between normal and abnormal tissue and therefore map out the troublesome area for treatment[172]. Nevertheless, there is no guarantee of similarity between this, and

both the mental map that the endoscopist creates, and the resultant mucosal specimen removed.

2.18 Conclusion

The obvious potential of pCLE creates considerable academic drive to enhance it and identify its best applications. There were 200 participants from 17 countries at the 5th International Conference of Cellvizio Users in 2013. However, as discussed in this chapter, there are many reasons why it has not yet become a mainstream device.

2.18.1 Enhancing the F.A.T.E. of pCLE

This thesis will concentrate on four important challenges to pCLEs more widespread uptake and utilisation: force, accuracy, tracking and ergonomics.

1. **Contact Force**

   Pressure induced changes to the diffuse reflectance spectra and the intensity of the fluorescence spectra occur when spectroscopy is the biophotonic technique employed, probably due to alterations to blood perfusion[244]. However, apart from the observation that probe pressure can distort the lobule of the peripheral lung[48], little is known about the effect of contact force on pCLE images. Contact force may affect the level of imaging, which has obvious implications when imaging epithelial surfaces that consist of cells that mature and change morphologically as they migrate away from the basement membrane. However, the way in which the images change with force may also provide diagnostic information.

2. **Insufficient Diagnostic Accuracy**

   Despite high resolution probes, detailed classification systems, and optimisation of contrast agent protocol, pCLE is diagnostically inferior to pinch biopsy. Essentially, its ability to confidently identify worrisome pathology, and to

provide reassurance elsewhere, is inadequate. It cannot allow the operator to avoid pinch biopsying *any* colonic polyps, nor can it make four quadrant biopsy of Barrett's oesophagus redundant. Perhaps the *Ultimate Selling Points* of pCLE require more exploitation. As examples, a) pCLE's assessment of in vivo vascular structure and function is a concept unavailable to the world of conventional histology, and b) pCLE's thin cross section allows examination of otherwise inaccessible regions of the body – in the biliary tree it is showing great promise, perhaps pathology within the peripheral lung could be as accurately identified.

3. Probe Tracking

As with other point-based biophotonic probes, pCLE probes image only small areas which may not be representative of the neighbouring tissue, do not create much visible trauma, and are often blindly deployed into narrow lumen. It is therefore important to know where the probe has been, and what it has been in contact with, to allow correlation between pCLE images and corresponding white light images, cross-sectional imaging and pinch biopsies, and allow sequential pCLE surveillance endoscopies to image the same area each time. Whilst partial solutions have been described with OGD eCLE in the form of transient suction polyps or argon laser marking, these approaches are limited. Scene recognition/clustering methods have been described[247], and the concept of augmenting the endoscopic view with labels indicating the sites that have undergone optical biopsy has been shown using a phantom model[248]. However, it remains to be seen whether this is feasible in a more chaotic in vivo situation.

4. Awkward Ergonomics

Minimal ergonomic evolution of the endoscope has occurred since Hopkins' flexible fiberscope of the 1950s, a device which was not designed to manipulate cellular resolution optical biopsy devices. Elaboration of this problem, and solutions will be explored.

Chapter 3 In Vivo Experimental Assessment of the Challenges Facing pCLE

3.1 Introduction to Both Studies

In chapter 2, four major challenges to pCLE use were identified within the literature. The aim of chapter 3 was to experimentally assess the ubiquity of these and any other hurdles, through in vivo human pCLE examination of two different mucosal surfaces: 1) healthy and diseased endobronchium, and 2) healthy and diseased rectum. These hurdles may be partly illustrated by creating a small library of images for each organ.

The discussion section at the end of this chapter places the findings of both studies in the context of the four challenges highlighted in the previous chapter.

3.2 Introduction to pCLE for Endobronchial Disease Study

The endobronchial pCLE knowledge base described in chapter 2 is thus far limited to a few papers, but no further justification is required for this work with a) endobronchial basement membrane elastin autofluorescence potentially obviating the need for exogenous contrast agents, b) lung cancer being the most common worldwide cancer and growing in incidence particularly in low income countries (and its outcome less bleak if diagnosed early), c) and epithelial induced basement changes being a key feature of several benign lung diseases[249].

3.3 Methods for Endobronchial Study

A single expert interventional bronchoscopist performed pCLE bronchoscopy in 16 patients at the Royal Brompton Hospital immediately after performing diagnostic bronchoscopy for varied clinical reasons. All subjects were given verbal and written information about the study and gave prior written informed consent. The study was

approved by the Brompton, Harefield & NHLI Research Ethics Committee (09/H0708/18).

3.3.1 Bronchoscopy

Subjects had topical local anaesthesia applied to the back of the throat and were given conscious sedation if required (1-5mg intravenous midazolam). They were given 2 litres/minute oxygen via nasal prongs and monitored with pulse oxymetry. The pCLE laser unit and probes were standard and commercially available (Alveoflex®, Cellvizio®, Mauna Kea Technologies, France; specification tabulated in chapter 2). Subjects were reclined at 45 degrees. As per the manufacturer's recommendation, the laser unit was switched on for 15 minutes before recalibration, and the auto-power setting used. An Olympus 1T260 bronchoscope was used to perform the initial bronchoscopy; transbrochial biopsies and bronchoalveolar lavage were performed if required according to the situation. The central airways were then systematically evaluated with white light imaging, and then the probe was gently advanced through the bronchoscope beyond the distal opening of the working channel until it abutted the endobronchial wall. During normal respiration, 1-3 pCLE video loops were acquired of macroscopically healthy endobronchial regions (trachea or main bronchi), as well as abnormal regions, and where clinically justified, endobronchial biopsies were obtained. These biopsies were fixed in formalin, embedded in wax, and slides cut. Standard stains were used by an expert pathologist to provide a histopathological diagnosis.

pCLE Video Assessment: Each dynamic video sequence was examined and a representative selection of the most clear and distinct frames selected for further inspection and subsequent illustration.

3.4 Results of Endobronchial Study

It was straightforward to touch normal and abnormal endobronchial targets with the pCLE probe. This was only perpendicular at the carinas, but the angle was usually sufficient to enable tissue abutment and the capture of autofluorescence sequences. There were no complications. 20 pCLE sequences were acquired during the bronchoscopies of

16 subjects; 12 from healthy endobronchial surfaces and 8 from diseased areas (Table 3.1).

Biopsy Number	Likely Diagnosis of Endobronchial Area	Bronchoscopic Appearance of Endobronchium	Endobronch. biopsy Diagnosis	Reason for Bronchoscopy/ other relevant pathology	pCLE video/images	
					Reticular Pattern	Bronchial Glands
1	Normal	Normal	N/A	Parenchymal infiltrates	++	+
2	Normal	Normal	N/A	COPD	++	++
3	Normal	Normal	N/A	Fungal pneumonia	+	+
4	Normal	Normal	N/A	COPD	++	+
5	Normal	Normal	N/A	COPD	++	++
6	Normal	Normal	N/A	COPD	+	-
7	Normal	Normal	N/A	COPD	+	++
8	Normal	Normal	N/A	COPD	++	++
9	Normal	Normal	N/A	Peripheral sarcoma metastasis	+/-	+/-
10a	Normal	Normal	N/A		+	+
10b	Carcinoma-in-situ	Inflamed	Squamous cell carcinoma-in-situ	CIS	-	-
11a	Normal	Normal	N/A		++	++
11b	Mucus hypertrophy/ inflammation	Inflamed mucosa adjacent to lesion	N/A	COPD with endobronchial lesion on CT	+	++
11c	Small cell lung cancer	Nodular lesion right main bronchus	Small cell lung cancer		+/-	+/-
12a	Normal	Unaffected right main bronchus	N/A	Haemoptysis	++	+
12b	Tracheobronchial amyloidosis	Nodularity	Squamous metaplasia and amyloid	Haemoptysis	"cotton-wool" like appearance	
13	Mild dysplasia	Mildly reduced autofluoresence	Mild dysplasia	Screening bronchoscopy	+	+
14	Mild dysplasia	Slightly inflamed on fluorescence	Mild dysplasia & focal squamous metaplasia	Screening bronchoscopy	+	+/-
15	Shrinking inflammatory nodules	Small bronchial nodules	Neutrophilic infiltrate (biopsy performed previously)	Ulcerative colitis & bronchial nodules	+/-	-
16	Tracheobroncho-pathia osteochondro-plastica	Anterolateral wall nodularity and plaques	Dystrophic calcification with chronic active inflammation	Haemoptysis, dypsnoea & weight loss	"cotton-wool" like appearance	

Table 3.1 pCLE image description and interpretation of 20 different endobronchial surfaces.

3.4.1 Healthy endobronchium

Trachea or main bronchus with a normal appearance under white light bronchoscopy was optically biopsied with pCLE in 12 subjects (Figure 3.1). With retrospective analysis, every sequence included at least some frames displaying thin fibres, presumed to be

elastin, and apart from sequence 6, there was ubiquitous evidence of bronchial gland entrances. Nevertheless, obtaining recognisable morphology was not always immediately possible: for example, initial imaging in the trachea of sequences 4 and 9 provided poor and negligible autofluroescence respectively, requiring distal repositioning of the probe. Of note, the elastin fibres varied in their distinctiveness or discreteness (compare subject 7 with subject 8), and during sequences there was variation in the visible appearance of the fibre orientation. This is illustrated in subject 8 which displays cross-hatched fibres at the beginning, and parallel fibres towards the end.

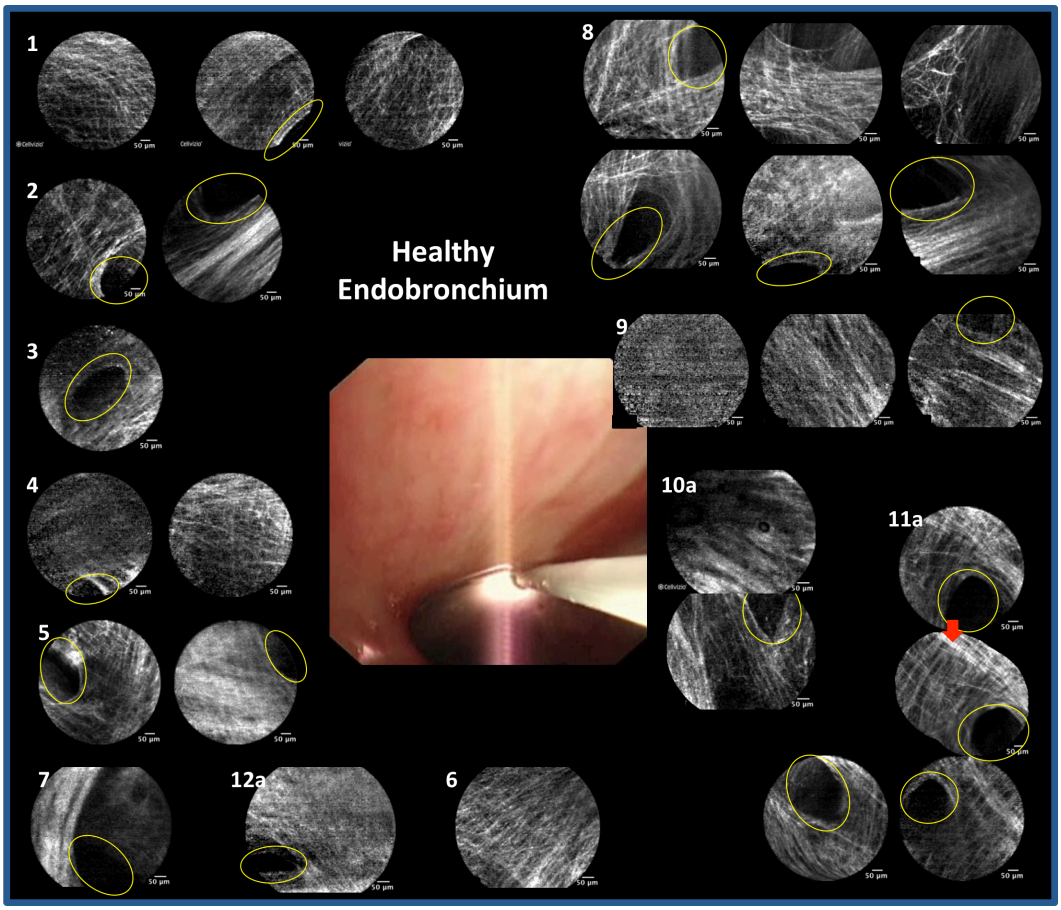


Figure 3.1 Representative still images from pCLE video sequences in 12 subjects; all taken from endobronchium that appears normal during white light bronchoscopy. The yellow ovals indicate where bronchial gland ducts penetrate the elastin rich basement membrane. Sequence 11a demonstrates a short mosaic.

3.4.2 Inflammatory endobronchium

Mucosal surfaces affected by four different inflammatory pathologies were imaged using pCLE (Figure 3.2). The most consistent images were obtained from two very rare conditions of endobronchial nodularity worthy of elaboration: tracheobronchopathia osteochondroplastica[250] (TBOP) and tracheobronchial amyloidosis[251] (TBA). The TBOP patient had sessile submucosal nodules with a cartilaginous/bony appearance protruding into the lumina of the anterior and lateral walls of his lower trachea and upper main bronchi. The posterior membranous portion of the trachea was characteristically[252] spared; this was evident with white light imaging as well as with pCLE. EBB confirmed active chronic inflammation of the affected areas with an eosinophilic infiltrate and dystrophic calcification. Whilst TBOP seldom requires much treatment, the patient with TBA has a much poorer prognosis, displaying characteristic *circumferential* nodular thickening and plaques on bronchoscopy which require debulking treatment. The TBA biopsies showed squamous metaplasia of the mucosal epithelium overlying extensive amyloid fibrosis containing scattered foreign body type giant cells. Congo red staining demonstrated extensive amorphous material displaying apple-green birefringence when viewed under high intensity cross-polarised light; the classical histochemical sign of amyloid[253]. pCLE imaging of the nodular excrescences in both patients (sequences 12b and 16) demonstrated a mottled “cotton-wool like” appearance, from autofluorescent calcifications and amyloid respectively causing disruption to the basement membrane.

Two other inflammatory sites were examined: an area of mild inflammation and mucous hypertrophy close to a neoplastic lesion (sequence 11b), and an inflammatory nodular area as a very rare systemic manifestation[254] of ulcerative colitis (sequence 15). There was more heterogeneity exhibited within these pCLE sequences, and the fibres were not as clear or as consistent as those seen within the healthy sequences, but at least in part, elastin basement membrane fibres and bronchial glands were present.

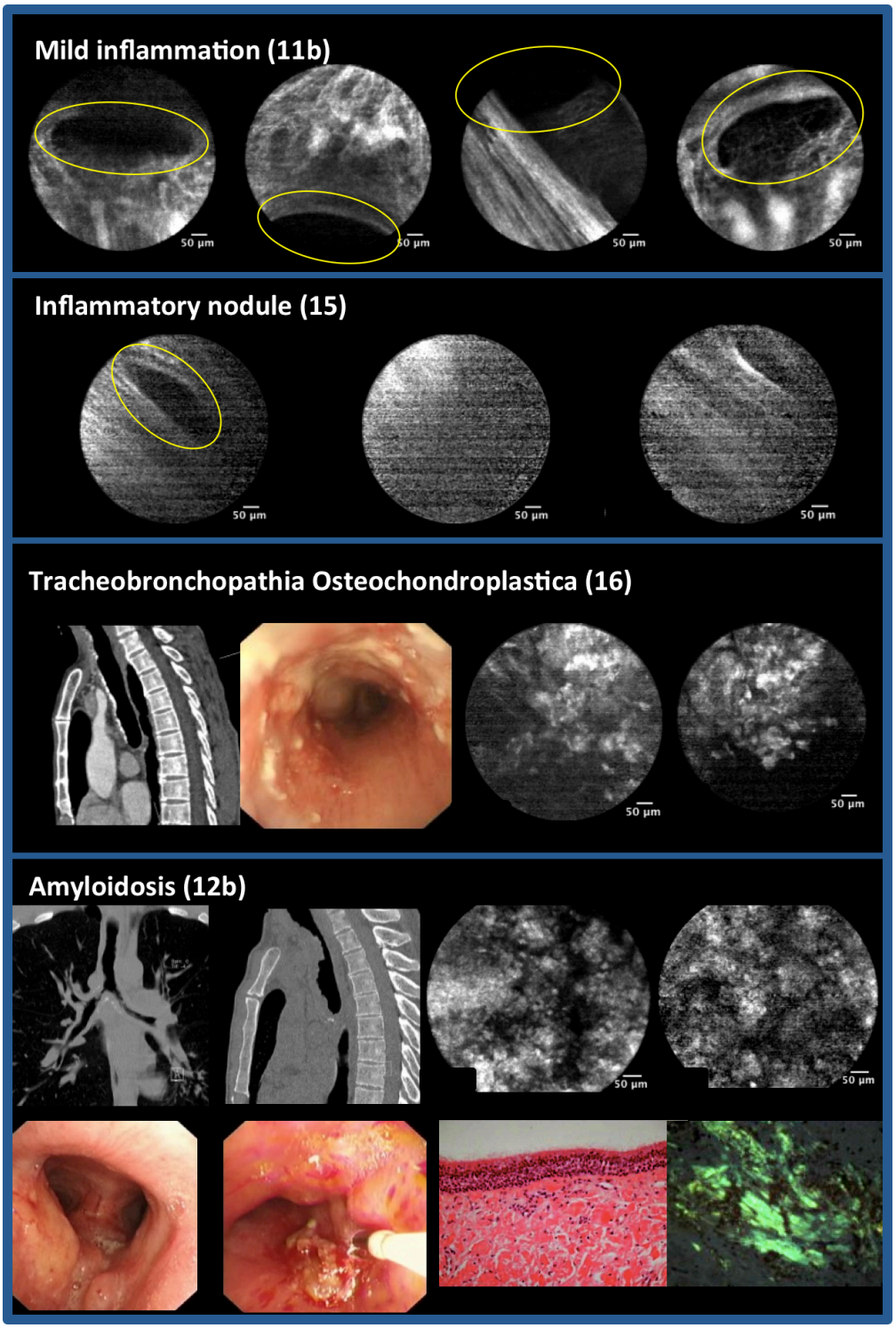


Figure 3.2 pCLE images of inflammatory endobronchium. Yellow ovals once again highlight bronchial glands. The reticular elastin pattern appears to be at least partly preserved in mild inflammation or nodularity, but a "cotton wool" appearance is seen in the more dramatic nodularity of tracheobronchopathia osteochondroplastica and tracheobronchial amyloidosis. These conditions are illustrated in the CT scans and bronchoscopic images. Endobronchial biopsies of the mucosa affected by amyloid show acellular pink material underlying the respiratory epithelium after haemotoxylin and eosin staining; viewing this material with polarised light after congo red staining demonstrated apple-green birefringence.

3.4.3 Neoplastic endobronchium

A long sequence imaging over the small cell lung cancer (SCLC) was mostly devoid of any recognisable autofluorescence (sequence 11c), though there was a brief normal reticular portion with bronchial glands (Figure 3.3). The autofluorescence was negligible in CIS (sequence 10b), but the reticular pattern was evident in the mild dysplasia sequences, though partially disrupted in sequence 14.

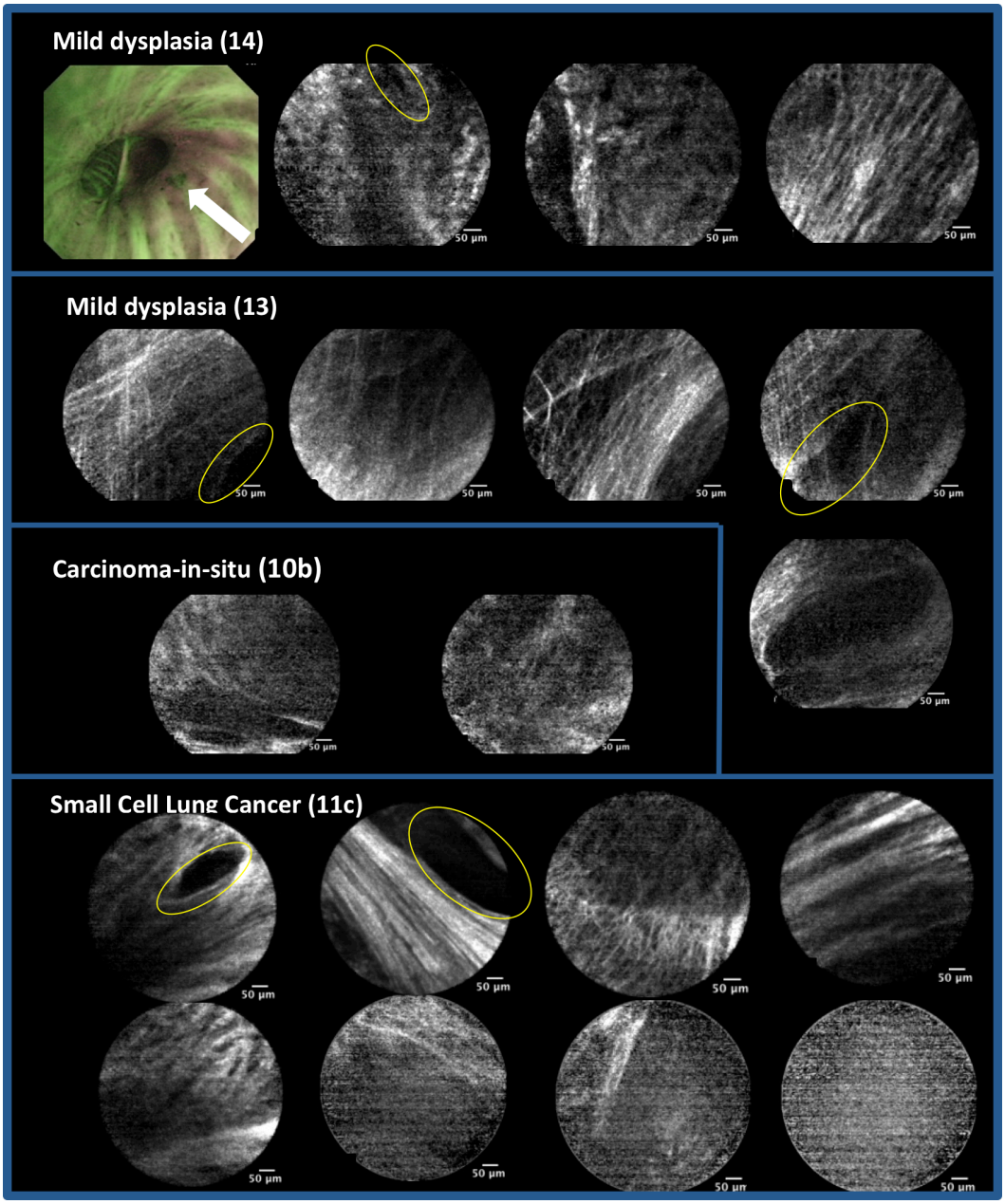


Figure 3.3 pCLE images of endobronchium affected by dysplasia and neoplasia. To highlight the subtlety of these lesions sometimes, the arrow within the autofluorescence bronchoscopy image points to an area of mild dysplasia.

3.5 Introduction to Rectal Cancer Study - can pCLE identify Effects of Chemoradiotherapy?

3.5.1 A background to predicting tumour response

With recent developments in cross-sectional imaging, tumour characteristics such as size and shape, vascularity, and metabolic activity can be tracked during systemic treatments. It would be of enormous benefit if these highly variable responses could be predicted before treatment commences or early in the course of treatment. For example, it has been shown that the likely response to neoadjuvant chemotherapy in locally advanced breast cancer can be predicted using magnetic resonance spectroscopic imaging before and straight after the first dose of chemotherapy[255]. In locally advanced rectal cancer, neoadjuvant chemoradiotherapy is the standard of care as it improves resectability and disease free survival. However, whilst a complete pathological response (CPR) to neoadjuvant treatment (no viable tumour cells in the specimen) is associated with an improved outcome, this only occurs in 10-30% of patients with rectal cancer[256]; remaining patients have either some or no response, and therefore many will incur net harm from neoadjuvant therapy through delays to surgery and direct side-effects and unpleasantness of chemoradiotherapy. The ability to accurately identify responsive tumours during neoadjuvant therapy might lead to targeted treatments for patients. This might entail an adjustment of dose, or proceeding straight to surgery in those patients that are not predicted to respond. If it was possible to accurately predict or diagnose patients with a CPR without providing the surgical specimen, an option may then be for some patients to avoid significant surgical morbidity by having endoscopic resection, or simply attending for regular surveillance under the "watch and wait" strategy[257]. This is a management option that many feel is dangerous because of inadequate methods of proving complete disappearance of tumour[258].

MRI alone can struggle to differentiate between active tumour and radiotherapy induced fibrosis, and the predictive value of changing tumour marker titres seems inadequate at present [259]. Unlike in breast cancer, current gene expression profiling cannot accurately predict responders[260]. At the conclusion of neoadjuvant treatment 18-fluorodeoxygluocose FDG PET/CT can identify good responders[261], and several studies have suggested that some predictive information may be gleaned by performing the scan in the first or second week[262] when there is the potential for modification or interruption of the treatment offered. If PET/CT or optical biopsy techniques such as CLE

could provide adequate realtime virtual histopathological tissue assessment, this could stimulate a paradigm shift in colorectal cancer management.

3.5.2 Pelvic radiotherapy side effects

In the UK, approximately 17000 patients each year are treated with radiotherapy for a pelvic malignancy of the prostate, cervix, uterus and rectum, mostly with curative intent. Radiotherapy regimes are increasingly successful, but damage surrounding tissues. The oncologist's aim is to treat the target organ with the maximum effective dose whilst simultaneously providing the greatest protection for adjacent tissue. This has resulted in evolutions of radiotherapy technology. For example, intensity-modulated radiotherapy (IMRT) is designed to make the treatment more selective for the prostate than conventional 3D conformal radiotherapy[263, 264]. Pelvic radiotherapy can exacerbate pre-existing conditions, it can damage neurological, enzyme-based and muscular functions within the region, but most obviously it causes proctopathy. These gastrointestinal injuries cause significant impairment in quality of life[265]. Prospective follow up data from 77% of survivors for more than 5 years in the Swedish Rectal Cancer Trial using preoperative high-dose (5x5 Gy) radiotherapy showed that 30% of the irradiated group had a significantly impaired social life because of bowel dysfunction, compared with 10% of the surgery-alone group[266].

Based on clinical and pathological distinctions, this damage is divided into acute and chronic injury.

3.5.3 Acute radiation proctopathy

Acute radiation proctopathy occurs during the 5-6 week treatment regimen and usually subsides during the few weeks after treatment. Diarrhoea, abdominal cramps, tenesmus and less commonly bleeding are the main features. Sigmoidoscopy reveals an oedematous, granular, inflamed and friable rectal mucosa; the pathological changes are usually limited to the rapidly dividing cells of the superficial mucosa. Histopathologically there is cryptitis, crypt distortion and abscesses, a presence of inflammatory cells, a loss of superficial cell height, and a reduction in lamina propria lymphocytes[267-269]. Despite symptoms worsening throughout radiotherapy, histological changes are worst after the first two weeks of a 6 week course[268].

3.5.4 Chronic radiation proctopathy

Chronic radiation induced proctopathy occurs months or years after treatment; many authors define the earliest point at which it can be differentiated from acute radiation proctopathy is at 90 days[270]. Up to 80% of treated patients describe a permanent change in their bowel behaviour after radiotherapy[271], and a smaller number will endure serious complications of sepsis, fistulation, stenosis and severe bleeding. These gastrointestinal injuries cause significant impairment in quality of life[265]. The pathophysiology of chronic radiation proctopathy and the histological changes observed are thus far very poorly characterised. Endothelial cells are highly radiosensitive[272], and the mucosa and submucosa display vascular abnormalities such as focal distortion and destruction of small arteries and arterioles; those vessels that remain display fibrosis of the tunica intima, thickening of the tunica media, and fibrin thrombi[273]. This chronic obliterative endarteritis leads to reduced vascularity of the entire bowel wall and associated mesenteries creating secondary ischaemic changes including fibrosis of the lamina propria[274], submucosal hyalinization/fibrosis, crypt distortion and focal mucosal ulceration[275]. Neovascularisation is a resultant feature of the ischaemia and is evident with congested dilated mucosal capillaries on histology and at endoscopy in the form of superficial telangiectatic vessels[274] which are the likely source of bleeding per rectum in these patients. Changes, not necessarily resulting from vascular damage, include changes to villi and goblet cells[273].

3.5.5 pCLE and acute radiation proctopathy

It would be a clinically important development to be able to predict at an early stage during or after radiotherapy treatment which patients will develop significant acute and chronic gastrointestinal toxicity. With no mainstream serum markers or metabonomic assays[276], a tolerated optical biopsy method of risk stratifying and diagnosing these problems would be invaluable. If patients at high-risk of fibrosis and chronic gastrointestinal problems could be defined accurately at an early stage during treatment, this would allow the radiotherapy prescription to be reconsidered. If those at high risk of significant fibrosis were known soon after the end of treatment, it could allow early initiation of anti-fibrotic therapies.

3.5.6 Aims of rectal cancer study

This was (owing to enormous recruitment difficulty) a single patient feasibility study to assess whether flexible endoscopic pCLE examination before, during and after neoadjuvant chemoradiotherapy for rectal cancer,

1. may have a role in identifying chemoradiotherapy induced endomicroscopic changes to both the tumour and the healthy mucosa falling within the radiation field, and,

2. is potentially acceptable to patients.

3.6 Methods for Rectal Cancer Study

In accordance with the ethical approval obtained from the NHS Regional Ethics Committee (Riverside: 10/H0706/6), the chosen volunteer was a 57 year old male with a T4N0M0 adenocarcinoma invading 3.2cm into the right seminal vesicle on pelvic MRI. The tumour covered 9cm in length of the right anterolateral wall of the rectum, from 4cm above the anal verge. He had presented with rectal bleeding, but had no other past medical history except for the endoscopic removal 7 years previously of a highly dysplastic rectal adenoma.

The patient attended five endoscopy sessions: 1) at baseline, the week before the 6 week course of chemoradiotherapy commenced, 2) after one week of treatment, 3) after two weeks of treatment, 4) 5 weeks after the conclusion of treatment, and 5) 11 weeks after the conclusion of treatment during the week prior to definitive surgery. The large gap between sessions 3 and 4 was considered necessary to avoid unnecessary discomfort during the latter stages of radiotherapy. Standard “time to surgery” is 6 weeks; however the volunteer had been randomised to 12 weeks in a concurrent clinical trial.

Chemotherapy entailed 6 weeks of oral capecitabine 825 mg/m^2 twice daily, 5 days a week, with intravenous oxaliplatin 50 mg/m^2 once a week. The patient also received concomitant radiation therapy to a dose of 50.4 Gray in 28 fractions.

Prior to each of the 5 endoscopy sessions, a phosphate enema was administered to evacuate the rectum, and the patient was put into the left lateral position. Three sites were examined each time: the tumour itself, the healthy mucosa opposite the tumour within the radiation field, and mucosa outside of the radiation field above the rectosigmoid junction

at 20cm from the anal verge. After white light videoendoscopy footage had been recorded, 2.5ml boluses of 10% intravenous sodium fluorescein (Martindales, UK) were administered. pCLE videos of each site were then obtained using the Cellvizio-Coloflex HD (Mauna Kea Technologies, Paris, France) through the colonoscope; representative still frames were recorded and analysed.

Four radiation toxicity scales were used to quantify proctopathy symptom severity for potential correlation to pCLE images. The endoscopist completed the simple but somewhat blunt EORTC/RTOG (Radiation Therapy Oncology Group) late proctitis score for the patient[277], and for greater insight[278] the patient completed a Vaizey Incontinence Score and a modified Inflammatory Bowel Disease Questionnaire (modified IBDQ) prior to their endoscopy session. The modified IBDQ is the Inflammatory Bowel Disease Questionnaire which has been developed for use in monitoring disease activity in Ulcerative Colitis and Crohn's Disease[279], and 10 of its 32 questions provide an IBDQ-B (bowel specific) score. The day after the procedure the patient completed a brief questionnaire using a Likert scale, covering acceptability and side effects.

3.7 Results of Rectal Cancer Study

3.7.1 Symptom severity and endoscopy procedure acceptability

As expected, the patient's gastrointestinal symptoms worsened during treatment being worst after 2 weeks of chemoradiotherapy, and generally eased afterwards (Table 3.2). According to the completed visual analogue scales the procedure was never even considered "uncomfortable" (Table 3.2).

Timepoint	Toxicity Scale				Acceptability (V.A.S.)
	RTOG 0=asymptomatic 5=death from DXT morbidity	**Vaizey** 0=perfect continence 24=total incontinence	**IBDQ** 224= asymptomatic 32=severely symptomatic	**IBDQ-B** 70=no bowel symptoms 10=severe bowel symptoms	**"How was today's endoscopic procedure (1-7)?"** 1=very comfortable 4=uncomfortable 7=very painful
Baseline	1	1	209	64	3
Week 1	1	6	204	62	3
Week 2	3	8 (eg. wearing pad)	193	57	2
5 weeks post DXT	2	6	205	63	3
11 weeks post DXT	1	5	200	61	1

Table 3.2 Radiation induced side-effects during the study were most severe at week 2, but no endoscopy sessions were considered particularly uncomfortable by the patient.

The patient's urine was discoloured for a maximum of 24 hours after the procedure which he considered to be at most mildly inconvenient. Nausea was experienced on two of the five sessions but was only ever considered mild and lasted less than 3 hours.

3.7.2 Serial endoscopies

Over the 17 week period, the tumour macroscopically shrunk until it was a small recessed ulcer (Figure 3.4). To the unblinded observer, there was only very mild oedema of the posterior wall on the two endoscopy sessions at the start of treatment (less than even grade 1 on the Hanauer scale used for ulcerative colitis[280]). On each occasion, it was relatively straightforward to acquire pCLE videos of all three regions, although slight difficulty with endoscope advancement after 2 weeks of treatment meant the most proximal pCLE footage (outside the radiation field) was just above the rectosigmoid junction. 2.5mls of intravenous 10% fluorescein provided adequate fluorescence for image acquisition; a further 2.5mls towards the end of the procedure arguably made the glands more obvious.

3.7.3 pCLE image interpretation

Tumour: As expected, at baseline the tumour produced a heterogeneous collection of images containing long irregular epithelial ridges combined with amorphous areas. More normal morphology was seldom present, mostly at the tumour periphery, containing

recognisable circular glands and some distinct blood vessels. The endoscopy after 2 weeks of treatment potentially demonstrated greater vessel leakiness/fluorescein spillage, but otherwise there were no clear changes during the study (Figure 3.4). Preoperative pCLE images of the contracted tumour still showed similar disorganisation to that of baseline.

Healthy mucosa above and within radiation field: Throughout the study, good definition videos/images were acquired from both regions (Figure 3.5 and Figure 3.6). Post-processing enabled mosaics up to 2.5mm in length to be created where gradual probe translation had been used. Glands of 70-90µm diameter were consistently observed, with 10µm vessels filled with moving erthyroctyes. Specific to the radiation zone, there was the unblinded observation of some thicker blood vessels, around 20µm, in the last three endoscopies. Irrespective of area, it was also apparent that despite selecting settings which varied the power to maintain relatively constant brightness, parts of video loops would vary between showing an excessively fluorescent lamina propria with good glandular contrast, or black glands with better lamina propria/vessel contast.

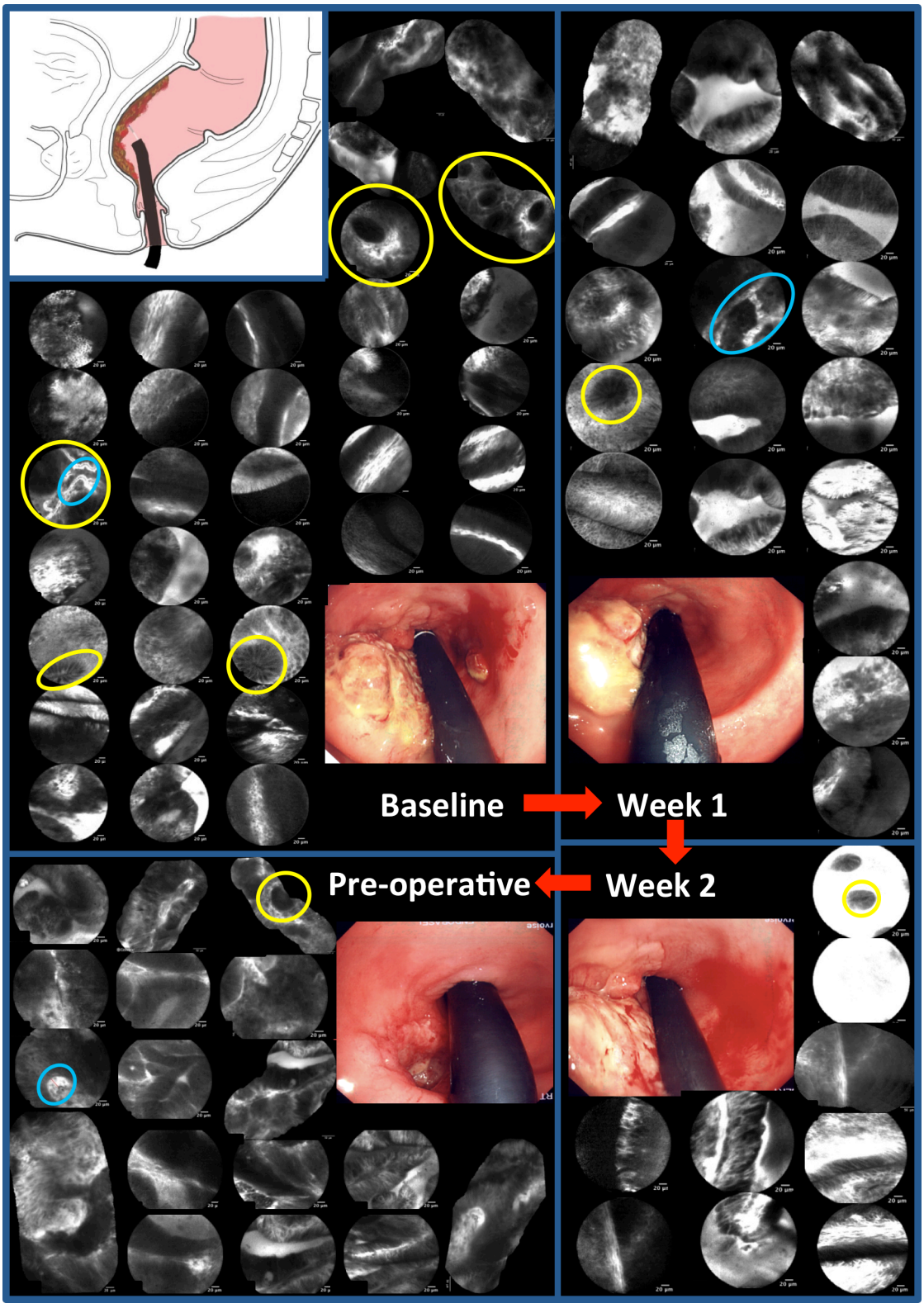


Figure 3.4 Representative pCLE still images and mosaics of the tumour during treatment demonstrating mostly disorganisation and loss of recognisable structure. Yellow and blue ellipses respectively highlight frames which include recognisable glands, and those containing vessels with flowing blood. The white light endoscopy images are taken with the endoscope retroflexed, and

show the tumour shrinking during treatment. (For simplicity, images from the fourth endoscopy session have been omitted).

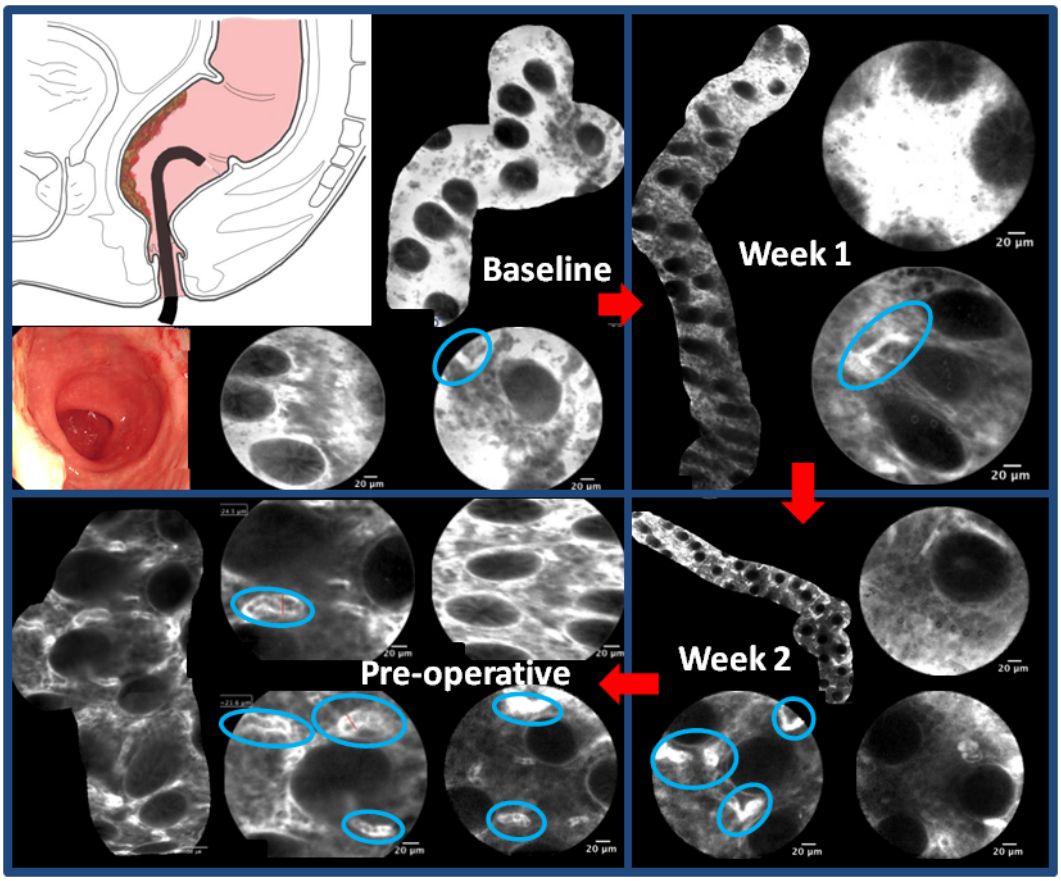


Figure 3.5 pCLE images of the posterior wall of the rectum during treatment. Blue ellipses highlight vessels; these are usually approximately10µm , but larger diameter ones are present after a couple of weeks of radiotherapy (20µm).

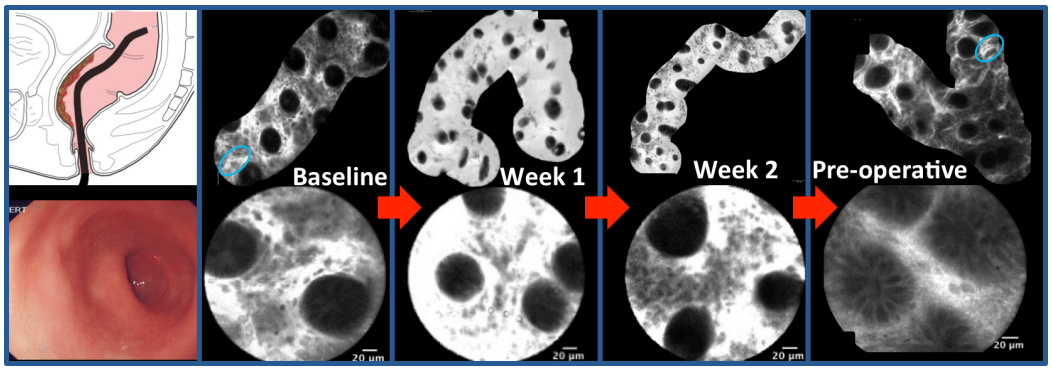


Figure 3.6: The glandular and vascular morphology of descending colonic mucosa (control) imaged with pCLE during neoadjuvant treatment did not seem to alter significantly. Blue ellipses once again highlight vessels.

3.8 Conclusion

These two short studies support previous declarations that pCLE within the upper respiratory tract and colorectum is well tolerated (even with marked inflammatory symptoms from local radiotherapy), and that fluorescein is well tolerated. Whilst the conclusions that can be drawn are limited by the size of both studies, they have examined the challenges that face pCLE:

3.8.1 Force

The manipulation, often up to a metre from its tip, of a flexible fine probe, which lies restrained within the narrow operating channel of an endoscope, would appear liable to create unpredictable variations in contact force. Greater probe resistance, and therefore even less probe control seemed available when the endoscope was contorted in the lungs or retroflexed within the rectum. In an in vivo situation, it is difficult to establish whether or how contact force variations affect the images acquired, perhaps through tissue deformation, imaging in different confocal planes, or the alteration of dynamic processes such as compression of microvasculature blood flow. It is possible that force variation is responsible for some of the heterogeneity within the videos; for example during imaging of a) healthy rectal mucosa, the unpredictable switch in maximum contrast between lamina propria and glands, or b) transient amorphous frames prior to characteristic reticular basement patterns in some healthy endobronchial areas (it is nevertheless appreciated that many of the "healthy" endobronchial regions were not confirmed on tissue biopsy and were not from otherwise healthy lifetime non-smokers; the endobronchial histopathological features of COPD include epithelial, goblet cell, and

bronchial gland hyperplasia creating mucus hypersecretion on a background of a thickened basement membrane, thus creating a significant likelihood of changes to the endobronchial pCLE morphology[249]). The implications of variable contact force on image acquisition are addressed in Chapter 5.

3.8.2 Diagnostic accuracy

Both studies corroborate published work attesting that pCLE can generate high resolution virtual histopathology of varied mucosal surfaces, enabling a reasonable degree of tissue phenotype differentiation between firstly endobronchial basement membrane whilst in health, affected by endobronchial nodularity, or affected by carcinoma/carcinoma-in-situ, and secondly healthy rectal mucosa, and that affected by invasive carcinoma. However, there are limits with pCLE's specificity: the endobronchial diseases TBOP and TBA seem indistinguishable on pCLE; and with dysplasia, carcinoma-in-situ, and small cell lung cancer all displaying significantly reduced or negligible autofluorescence, this troublesome distinction between grades of neoplasia matches other work[198].

The rectal cancer patient studied had more severe acute symptoms than average: Khalid et al.[278] described milder median toxicity scores (RTOG of 1, Vaizey of 5, IBDQ of 199, and IBDQ-B of 60), after pelvic radiotherapy for gastrointestinal cancers (after 5 weeks of treatment - when symptoms would be expected to be worse[268]). Therefore, it would appear that any microanatomical changes created by the chemoradiotherapy are likely to be subtle, and would clearly need to be more thoroughly investigated with a larger study. This was essentially a hypothesis generating study and it was hinted that within tumour, a greater degree of fluorescein leakage occurred following 2 weeks of treatment, and within the otherwise healthy radiation zone microvessel calibre increased after treatment.

3.8.3 Tracking

Despite the exclusion of all segments of endoscopic pCLE sequences which had been noted to include acquisitions from when the probe unintentionally tracked across more than one tissue type, there was marked heterogeneity in many videos, such as a few frames resembling healthy microanatomy within the typically significantly disrupted morphologies of both small cell lung cancer and rectal cancer. This might reflect the probe coursing the margin of the diseased area, or genuine microarchitectural

heterogeneity within the diseased region of tissue. The facility to accurately track, record and after the procedure display the path of the probe with corresponding pCLE footage would therefore be of major benefit. This would also make the longitudinal assessment (for the purposes of studying natural history or effects of treatment) of specific tissue regions using pCLE more accurate; for example, areas affected by radiation proctopathy or endobronchial dysplasia could be accurately followed-up.

3.8.4 Ergonomics

Obtaining videos and images is not difficult for a reasonably experienced endoscopist. Nevertheless, it is not clear how important perpendicular pCLE probe abutment with constant force is, and to what extent it might influence the heterogeneity in some video loops previously mentioned. In certain luminal areas such as during retroflexion within the lower rectum or within narrow bronchi this seemed more awkward.

Currently there is no evidence to support the benefit of mosaics over individual frames or videos for pCLE interpretation. However, it can be expected that any pCLE role is likely to be enhanced by the facility for creating large mosaics. The post-procedure Cellvizio-Viewer software was certainly able to create much longer mosaics of the roomier colorectum compared to the endobronchium, probably due to easier and less confined manipulation facilitating easier probe translation.

Chapter 4 Imaging Parenchymal Lung Diseases with pCLE

4.1 Introduction

A striking advantage of pCLE probes, over many other optical imaging devices is their potentially tiny cross section. This allows imaging within anatomical areas that are otherwise relatively inaccessible, including the biliary tree and cystic lesions of the pancreas, using the sub millimetre cholangioflex and nCLE, respectively.

The peripheral lung is similarly isolated from conventional white light inspection, and with parenchymal lung diseases having greater prevalence than biliary strictures or indeterminate cystic lesions of the pancreas, chapter 4 seeks to explore a potential role for pCLE in diagnosing parenchymal lung diseases (PLDs). As described in Chapter 2, prior to this study, for pCLE of the peripheral lung, there has been little more than a description of the images and safety profile in 41 otherwise healthy smokers and non-smokers[48].

4.1.1 Hypotheses - assessing and maximising the accuracy of a new niche for pCLE

1. The first hypothesis was that pCLE would detect morphological changes evident in specific PLDs.

2. As previously discussed, unlike in the elastin rich lung, the gastrointestinal tract requires exogenous fluorescent contrast agents for imaging to delineate the cellular architecture of the glands embedded within the epithelium, and demonstrate dynamic in vivo blood flow. Therefore, the second hypothesis was that intravenous fluorescein would provide additional in vivo information in pCLE imaging of peripheral lung in health and disease. Despite some evidence from the literature, that topical agents which can penetrate the cellular membrane, such as acridine orange or acriflavine delineate microanatomy better, intravenous

fluorescein was used owing to its proven safety profile in the GI tract, and in an attempt to delineate microvessels prior to contrast extravasation.

3. The third and final hypothesis was that pCLE would be safe in PLD patients.

4.2 Methods

4.2.1 Subjects

pCLE was performed in 1) healthy non-smoker volunteers, 2) patients with chronic obstructive pulmonary disease (COPD) undergoing lung cancer screening bronchoscopy or endobronchial valve insertion for lung volume reduction, and 3) patients with PLD during their diagnostic bronchoscopy. The healthy subjects had no significant cardiorespiratory disease or bleeding diathesis. All COPD and other PLD patients had undergone HRCT scanning prior to bronchoscopy. Emphysema severity for each bronchopulmonary segement imaged with pCLE was ascertained from the HRCT scan closest to the investigation bronchoscopy by grading 0-4 (Table 4.1) [281] by an expert radiologist who was aware that emphysema was a likely component of many of the scans but was blinded to other clinical data.

Grade	Radiological Severity (percentage of lung affected)
0	None/Trivial (<5%)
1	Mild (5-25%)
2	Moderate (26-50%)
3	Marked (51-75%)
4	Severe (>75%)

Table 4.1: Quantification of percentage of lung affected by emphysema on HRCT

All subjects gave prior written informed consent. The study was approved by the Brompton, Harefield & NHLI Research Ethics Committee (09/H0708/18).

4.2.2 Bronchoscopy

Similar to the endobronchial study in chapter 3, subjects had topical local anaesthesia applied and were given conscious sedation if required (1-5mg midazolam). They were given 2 litres/minute oxygen via nasal prongs and monitored with pulse oxymetry. The pCLE laser unit and probes were standard and commercially available (Cellvizio®-Lung, Mauna Kea Technologies, France) producing a 600µm diameter FOV at 12 frames per second, imaging to a Z-depth of up to 50µm. Subjects were reclined at 45 degrees. The laser unit was warmed up for 15 minutes before recalibration, and the auto-power setting used. An Olympus 1T260 bronchoscope was used to evaluate the central airways and then advanced into the most distally accessible bronchi, whereupon the probe was gently advanced beyond the distal opening of the working channel until recognisable images were obtained of the acinus. During normal respiration, successive pCLE video loops were acquired of up to six bronchopulmonary segments (BPSs) named according to international nomenclature[202]. In each PLD patient, an attempt was made to optically biopsy areas of both maximal and minimal disease. Where clinically indicated, bronchoalveolar lavage (BAL) was performed using 100mls of 0.9% saline, and TBB was performed with Olympus EndoJaw disposable biopsy forceps (Model FB-211D). Diagnosis in two patients required subsequent CT-guided percutaneous biopsy. All patients undergoing transbronchial biopsies had post-procedure erect chest radiographs performed.

For the first 5 patients who underwent BAL/TBB correlation, an extended working channel (outer sheath) was initially deployed through the working channel and blindly wedged distally in an attempt to improve the likelihood that pCLE, BAL and TBB were all obtained from the same location.

Incremental doses of intravenous fluorescein (0.1ml-20ml of 1%) (Martindales, UK) with a saline flush were injected through a peripheral cannula towards the end of the procedure in five bronchoscopies during video acquisition. The same BPSs were then reimaged.

4.2.3 BAL/TBB analysis and definitive diagnosis

Differential cell separation, cytopathological examination, and microbiological culture were performed on all BAL fluid samples. Where there was spare BAL fluid, constituent cells were differentially separated, resuspended, and ex vivo pCLE imaging performed.

TBB samples were fixed in formalin, embedded in wax and 5µm sections were examined by an expert pathologist. In accordance with current guidelines[183], all available data was discussed at a multidisciplinary team meeting to reach a diagnostic consensus.

4.2.4 pCLE image acquisition, processing and interpretation

pCLE video loops were recorded for up to 30 seconds in each BPS until a consistent image had been obtained. At least five representative stills were created for each video, for subsequent qualitative appraisal by two observers (RN & PS) using Cellvizio Viewer® software (Mauna Kea technologies, France), including an assessment of the septal walls and vessels (autofluorescence intensity, regularity of structure) and any fluorescent cellular infiltrate. The Cellvizio Viewer® software's mosaicing function was used to create automated mosaics. For each video sequence that enabled mosaic construction, the longest individual mosaic axis was recorded as a quantification of how well the FOV could be retrospectively increased. SPSS version 17 was used for statistical analysis.

4.3 Results

4.3.1 Subjects

Bronchoscopic pCLE videos and still images were obtained from 4 control volunteers and 1 lung-disease free patient (normal HRCT but cutaneous erythema nodosum) (mean age 34.8 ± 9.7) (Figure 4.1 A-C), together with 37 patients (mean age 54.9 ± 11.8). TBB and BAL were performed in 21 and 23 patients respectively. Final diagnoses were COPD (13 patients mean age 61.7 ± 6.8), or other PLD (24 patients mean age 48.9 ± 13.6) (Table 4.2). The only two current smokers were PLD patients (sarcoid and respiratory bronchiolitis). The single chronic bronchitis patient had smoked until 2 weeks before bronchoscopy. RB1 and LB1/2 were the only BPSs that were not always possible to cannulate, but this occurred only during 4 bronchoscopies. Previously, cannulation of these BPSs has been regarded as impossible due to probe stiffness[48]. Each subject had 1-6 BPSs optically biopsied creating 116 pCLE videos for analysis.

	Number of subjects (main diagnosis)	Overall number of affected BPSs imaged
Healthy		
Volunteers	4	19
Nil abnormal on CT, TBB & BAL, or remote from diseased area	1	8
Subtotal	*5*	*27*
COPD		
Grade 1 emphysema	2	2
Grade 1 emphysema with partial collapse	1	1
Grade 2 emphysema	0	3
Grade 2 emphysema with mild infection	0	1
Grade 3 emphysema	0	3
Grade 3 emphysema with mild infection	1	1
Grade 4 emphysema	8	15
Chronic bronchitis	1	3
Subtotal	*13*	*29*
Other parenchymal lung diseases		
Respiratory bronchiolitis	1	5
Pulmonary sarcoidosis	4	12
Mild radiotherapy damage	1	1
Tuberculosis	1	4
Pulmonary fibrosis with infection	1	1
Drug-induced pneumonitis	2	3
Peri-chemotherapy pneumonia	7	19
Amyloidosis	1	2
Peripheral non small cell lung cancer	1	1
Bronchioloalveolar carcinoma	1	5
Metastatic cancer (breast, endometrial or fibrosarcoma)	4	7
Subtotal	*24*	*60*
Total	42	116

Table 4.2: The main diagnosis of the 42 subjects bronchoscoped, providing the 116 BPSs that were imaged.

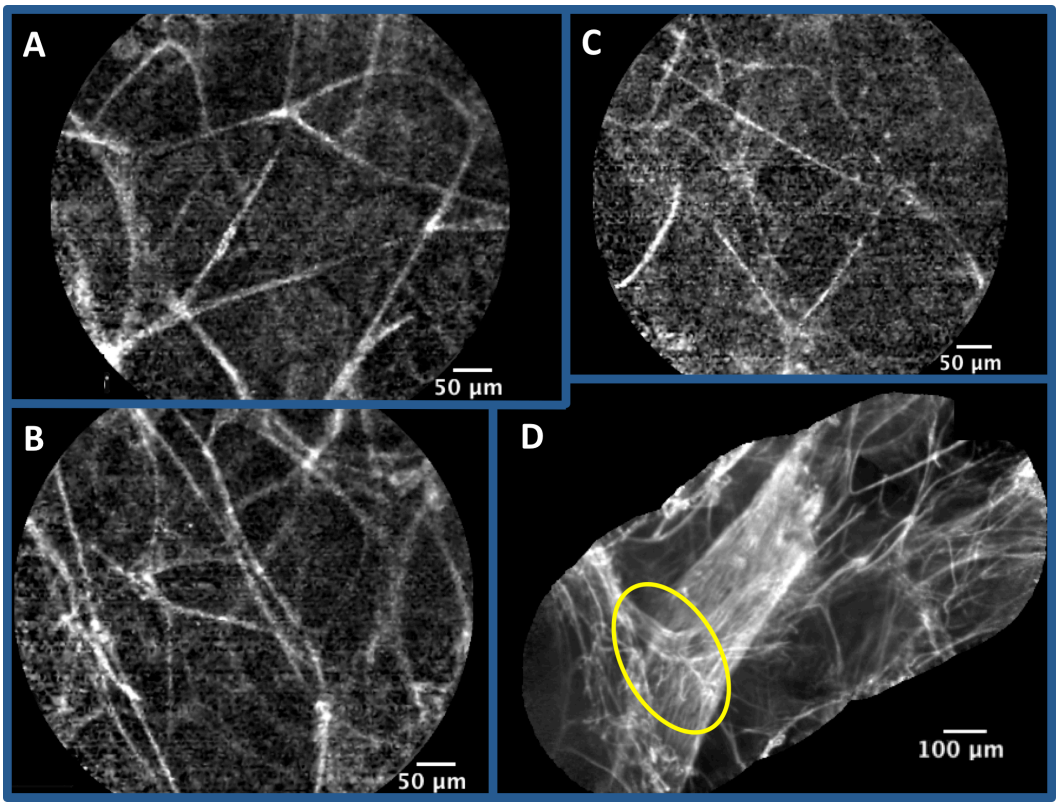


Figure 4.1 Still pCLE images in A,B & C are from healthy BPSs and show fine undistorted septal wall elastin architecture (<10µm thickness), though age seems to play a role in the septal wall fluorescence intensity (A and B are from a 52 year old patient; C was aged 29). Mosaicing was able to increase the FOV in 64/116 BPSs: D shows the longest mosaic created (1268µm); the oval highlights a 150µm microvessel with a small branch (from a BPS with grade 1 emphysema).

4.3.2 Safety and acceptability

pCLE adds between 1 and 5 minutes to the bronchoscopy procedure depending on the number of BPSs being optically biopsied. Blood originating beyond the bronchoscope tip, along the path of the probe toward the lobule, was significant enough to spill proximally and impair the bronchoscopic or pCLE views in 3 patients before TBB. However, one of these patients had a clotting abnormality (prothrombin time of 19 seconds), and within the probed BPS of another patient was a metastatic breast tumour displaying microvessel invasion. Nevertheless, there was clear observation of a microvessel being snapped in vivo by the probe in three separate BPSs (Figure 4.2E). The probe causes some pleuritic pain during image acquisition, but there were no pneumothoraces. The largest fluorescein dose injected caused retching during the procedure in one healthy subject. Seemingly snapped elastic fibres of the septal walls flapped around on the video loops of 28 BPSs

(Figure 4.2A-D). This may be sometimes related to pre-existing disease; it was indeed more commonly observed in COPD BPSs than in areas that were affected by other PLDs or healthy lung. Nevertheless, direct damage from the probe was witnessed in 6 BPSs as septal walls snapped during image acquisition (Figure 4.2D).

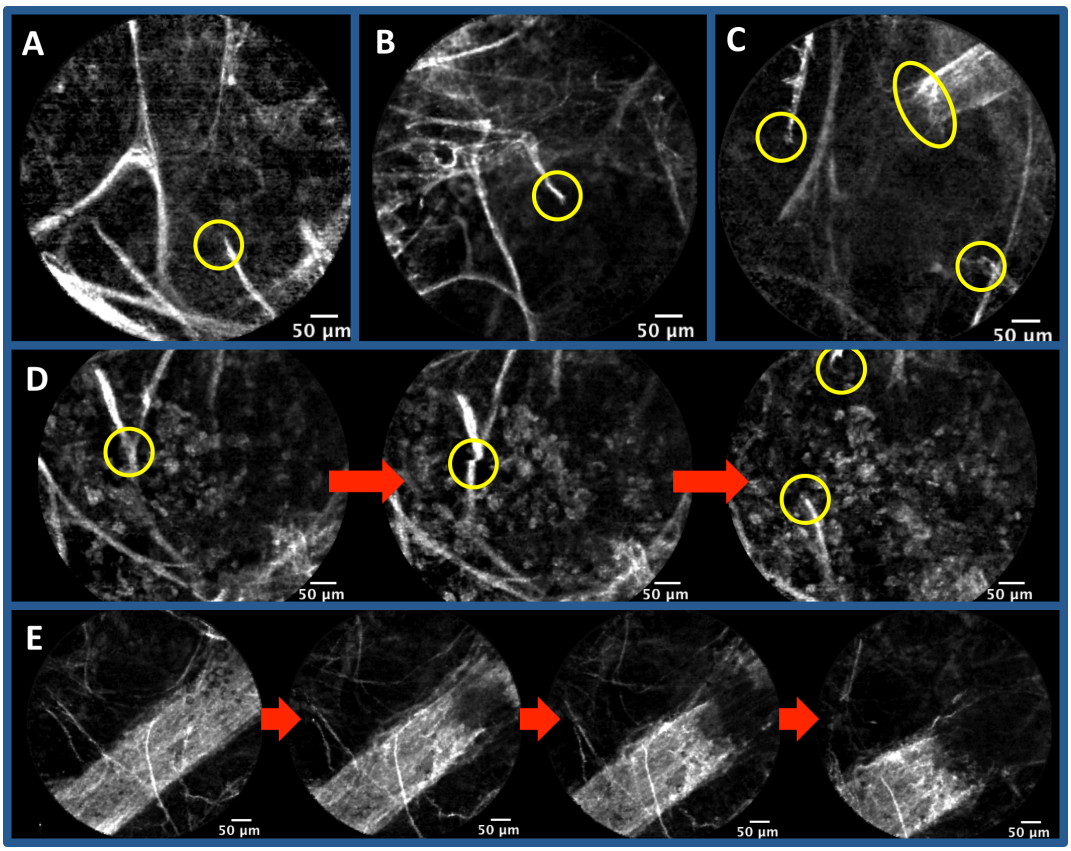


Figure 4.2: Free ends of septal walls, observed on video loops to flutter loosely, were apparent in 28/116 BPSs (highlighted with circles in A, B, C and D). This phenomenon could be partly illustrative of the primary disease, however, in 6 BPSs, individual septal walls were observed to fracture, separate and then their blind ends swing freely, presumably from the axial pressure of the probe (demonstrated in C, and in D across 3 sequential frames; each separated by 83ms). Microvessels were also observed to snap under axial pressure in 4 BPSs (highlighted by an oval in C, and sequential frames shown in E). A is from a grade 1 emphysema BPS, B, C and E are from different grade 3 and 4 BPSs, and D is from a patient with respiratory bronchiolitis.

4.3.3 Mosaic function

The automated mosaic function was used on the Cellvizio Viewer® software. Mosaics were creatable for 64/116 video loops, but the mean maximum mosaic length was a modest 760± 124μm. Video loops with bright distinct images, where there was some controlled movement of the probe tip tended to yield longer mosaics (Figure 4.1D).

4.3.4 Basic analysis of emphysema

It is evident from studying the 116 video loops and representative stills, that the appearance of copious, regular, 10μm elastic fibres within the alveolar septal wall structure previously described in healthy subjects[48], and illustrated in Figure 2.11, becomes variably disorganised in peripheral disease (Table 4.3). For example, pCLE highlights some of the morphological alterations in severe emphysema, the main one being a loss of the number of septal walls (Figure 4.3). In many cases there is distortion of the remaining septal walls, or thickening that leads to an inability to distinguish septal wall from microvessel (Figure 4.3G & Figure 4.5). In two emphysematous BPSs containing large bullae, a sudden black image was followed by a fine reticular pattern, suggesting the possibility that the inner surface of the visceral pleura had been reached via a bulla (Figure 4.3 I&J).

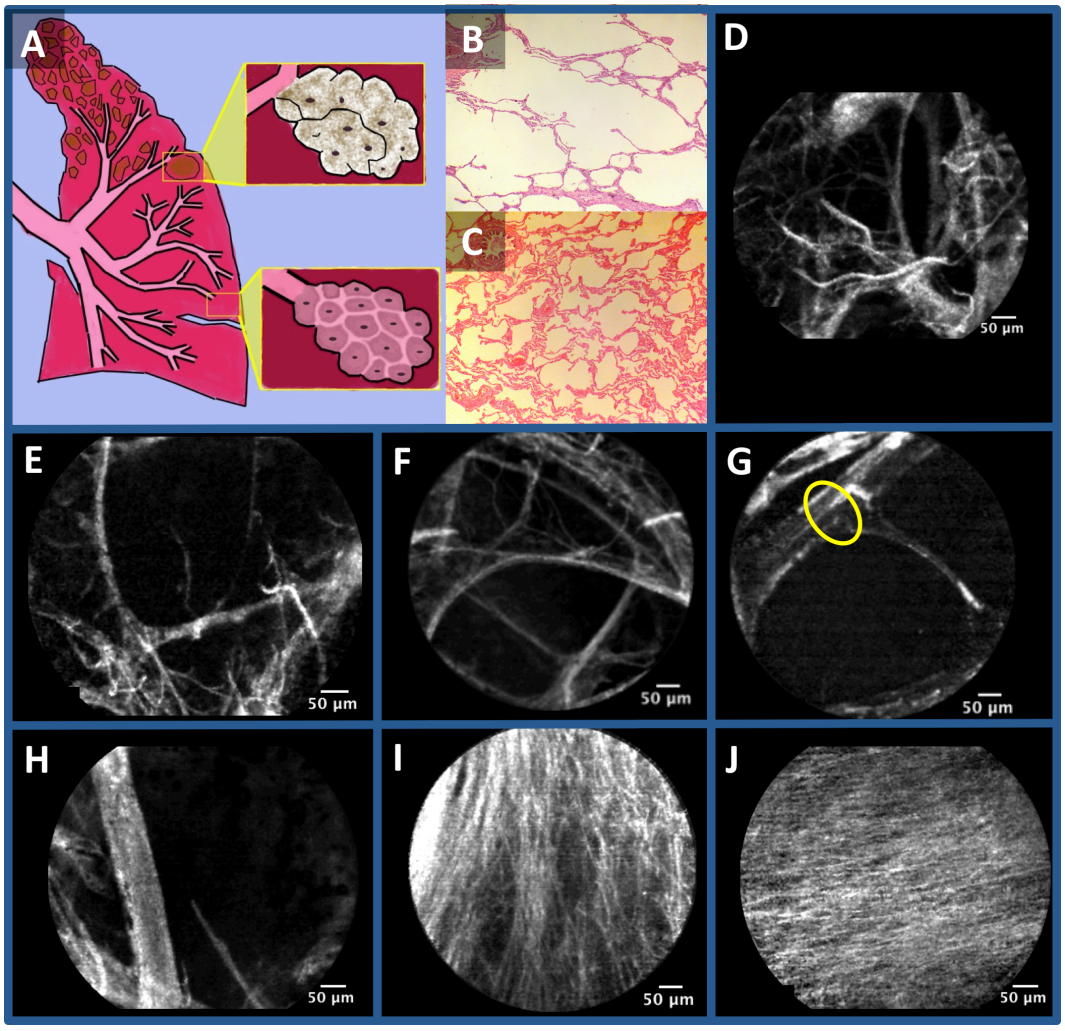


Figure 4.3: A schematic (A) shows the loss of of alveolar septal wall density in emphysema, often in the apices. White light microscopic images of emphysematous (B) and healthy (C) transbronchial lung biopsies are shown. The number of visible septal walls on pCLE tends to reduce as emphysema worsens: grade 1 emphysema (D&E), grade 4 (F). G and H are images near large bullae. The ellipse in G highlights probable distorted thickened septal wall that on discrimination by thickness could be confused with a microvessel. H shows a probable vessel but minimal septal wall. I and J are images of pleura beyond bullae.

4.3.5 pCLE images of PLD

In most parenchymal lung diseases other than emphysema, the pCLE architecture becomes unrecognisable (Figure 4.4 and Figure 4.5F). The autofluorescence is reduced and the images become indistinct and noisy. The most radiologically affected areas tend to display the most disruption and loss of autofluoresence in their corresponding pCLE images. However, whilst BPSs exclusively affected by emphysema have a smaller number of septal walls per FOV, creating the appearance of "holes", they do not appear to

lose autofluorescence intensity, and the elastin scaffold of the lobule tends to retain its distinctiveness even in severe disease, even if sometimes vessels become indistinguishable from septal wall.

Whilst the septal wall structure was more distinct in healthy volunteers than in subjects with marked disease, the autofluorescence was generally weaker than healthy or emphysematous areas of older patients. This effect of age on autofluorescence has previously been described[48].

Observation	**Healthy/Normal (N=27)**	**COPD (N=29)**	**Other PLD (N=60)**
↓ autofluorescence of individual elastic structures [S]	12/27= 44.4%	1/29 = 3.4%	19/60 = 31.7%
Unrecognisable structure & ↓ distinctiveness [NS]	7/27 = 25.9%	5/29 = 17.2%	45/60 = 75%
Distorted septal wall morphology [S]	1/27 = 3.7%	22/29 = 75.9%	35/60 = 58.3%
Snapped septal walls or vessels [S]	2/27 = 7.4%	15/29 = 51.7%	11/60 = 18.3%
Autofluorescent macrophages (15-30µm & mobile) [S]	0/27 = 0%	3/29 = 10.3% [b]	10/60 = 16.7% [a]
Mucus globules/bubbles[NS]	9/27 = 33.3%	11/29 = 37.9%	21/60 = 35%
3µm specks[NS]	6/27 = 22.2%	8/29 = 27.6%	26/60 = 43.3%
Are mosaics creatable?[S]	6/27 = 22.2%	26/29 = 89.7%	32/60 = 53.3%
Mean maximum mosaic length (µm) [NS]	709 ± 78	811 ± 134	800 ± 90

Table 4.3: A summary of the observations and measurements from the 116 BPSs analysed. Whilst the elastin scaffold morphology with emphysema is most likely to appear distorted, structures tend to be vivid and brightly autofluorescent. Diminution of both autofluorescence and recognisable distinct structure is common in other PLDs. The few BPSs displaying autofluorescent macrophages were from the only two current smokers in the study, both with PLDs [a], and a COPD patient who had only quit smoking 2 weeks previously[b]. (Using ANOVA for mosaic length, and 2-sided chi-square tests for the other observations $p<0.05^{S}$, $p\geq0.05^{NS}$)

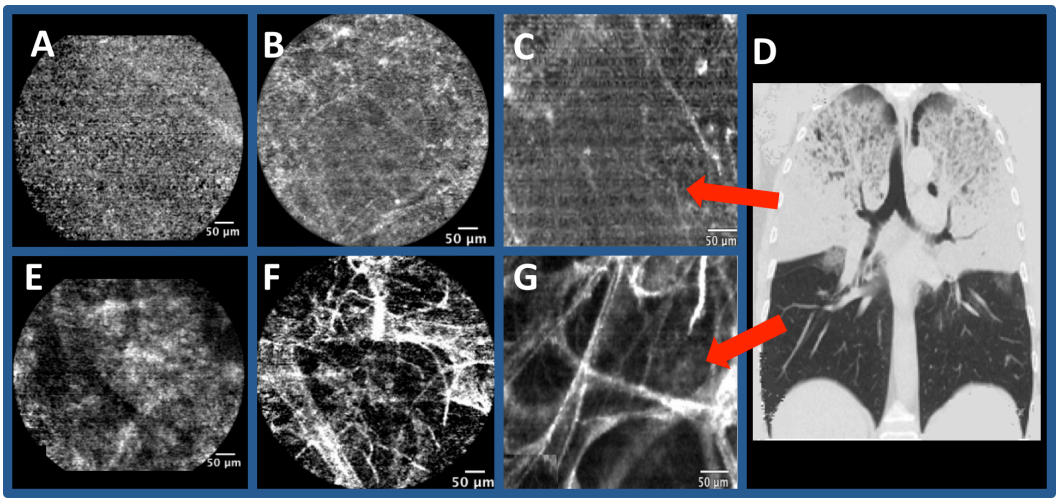


Figure 4.4: Many PLDs cause a non-specific loss of fluorescence and distinctiveness. This is demonstrated with a peripheral metastatic fibrosarcoma deposit (A), an organising pneumonia (B), and an area of lung affected by a lymphocytic infiltration secondary to a peri-chemotherapy pneumonia (F). In a patient with bronchioloalveolar carcinoma, HRCT showed severely affected upper lobes (D), and pCLE provided virtually no recognisable autofluorescence within the right upper lobe (C) whereas the spared right lower lobe showed distinct alveolar structures with greater autofluorescence (G). E was acquired from maximal distal cannulation of LB6 in a patient with tracheobronchial amyloidosis: the "cotton wool like" autofluorescence was similar to that observed in pCLE of endobronchial amyloid deposits[282].

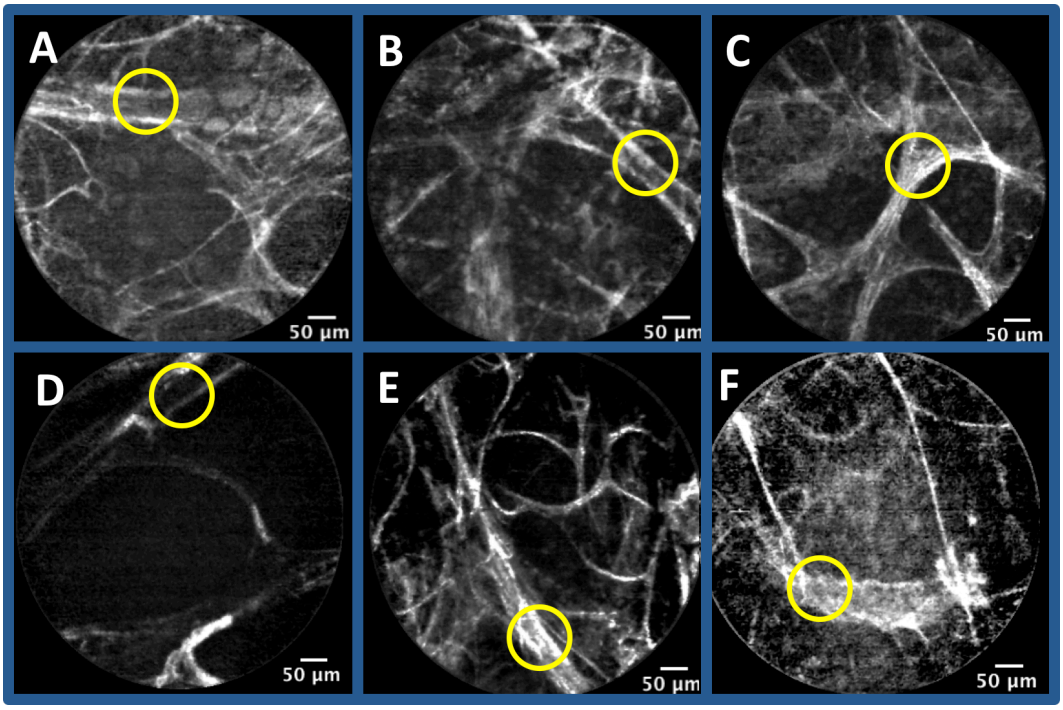


Figure 4.5: In health, differentiation between microvessels and septal walls (Figure 2.11A&B) is done on diameter and shape characteristics[48]. This is not as straightforward in diseased BPSs, and here the circles show indeterminate structures from diseased BPSs which cannot be identified as either structure on the basis of their shape or intermediate calibre. A-E are from emphysematous BPSs (grades 2, 3, 3, 4, and 4 respectively) and F is from a BPS with drug-induced pneumonitis.

4.3.6 Inflammatory cells

The appearance of undetermined 3µm specks (particularly on approach to the acinus), mucus globules/bubbles or even faint inflammatory cells is a non-specific finding to healthy and diseased areas (Figure 4.6). However, brightly autofluorescing 15-30µm cellular infiltrates were exclusively observed in the BPSs of the only 2 current smokers in the study (respiratory bronchiolitis and sarcoid), as well as one recently ex-smoker with chronic bronchitis. The 3 other sarcoidosis patients were non smokers and their in vivo pCLE and ex vivo BAL pCLE images had no visible inflammatory cell infiltrate. Differential cell separation of the 2 current smokers' BAL fluid demonstrated that the responsible cells were autofluorescent macrophages. The subject with chronic bronchitis had endobronchial washings only, which displayed no ex vivo fluorescent cells.

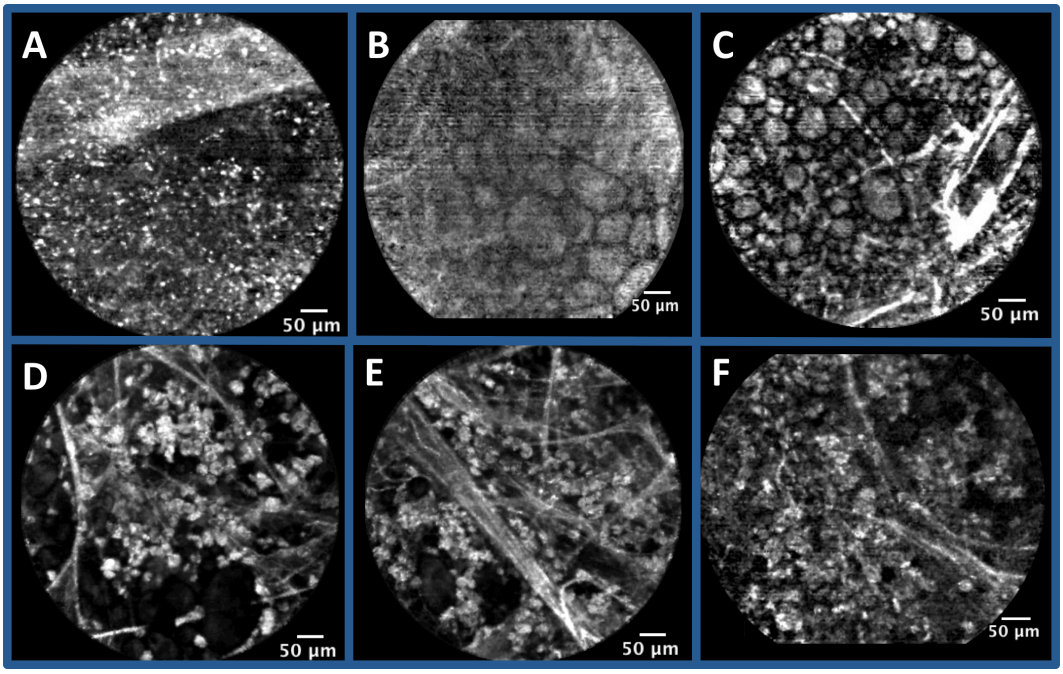


Figure 4.6: Bright indeterminate 3µm specks are common on approach to the acinus regardless of smoking status (A is from a patient with pneumonia). Apparent mucus blobs or bubbles are non-specific (B is from a resolving pneumonia, and C is from a BPS with grade 3 emphysema). Whilst some very faint cells are suggested even in non-smokers, brightly autofluorescing alveolar macrophages are exclusive to smokers (or those with a recent smoking history) regardless of disease (D&E are from RB4 and RB6 of a recently quit heavy ex-smoker with chronic bronchitis). F shows that these macrophages sometimes "drown out" the alveolar walls (respiratory bronchiolitis).

4.3.7 Intravenous fluorescein

Incremental doses of 1% fluorescein were administered intravenously in 3 healthy volunteers and 2 patients with emphysema. 0.25mls was the minimum required to observe a change. This change consists of a hyperfluorescent foreground containing non-fluorescent bubbles; it appears within a few seconds of drug administration and is not initially confined to the microvessels (as might be expected) (Figure 4.7). Therefore, there is no discernible increase in the autofluoresence of the septal walls, microvessels or cells during incremental administration of the drug.

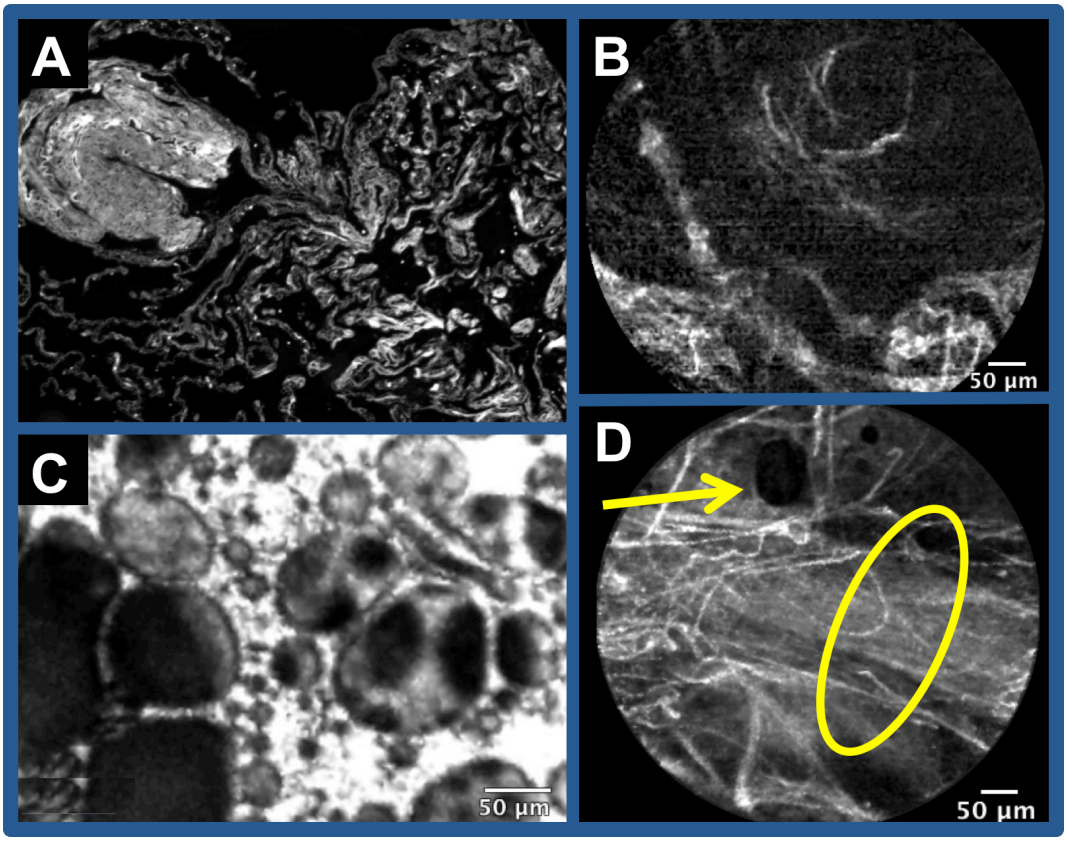


Figure 4.7: Compared to standard biopsy, there is reduced resolution/diagnostic information with conventional elastin autofluorescence pCLE: from the same sarcoid BPS, compare the H&E stained TBB (autofluorescent microscopy x200) (A) of a pathognomonic non-necrotising granuloma to the non-specific disruption seen with pCLE (B). Could the administration of intravenous fluorescein help? It causes a general white appearance of the mucus/surfactant (C shows a healthy BPS following injection of 5ml of 1%) with bubbles displacing the contrast agent. All other acinar structures are disguised. Even when tiny quantities are used (such as 0.4ml of 1% in D), the microvessels (marked by the ellipse) are no more distinct, but bubbles are still evident where the newly fluorescing mucus is being disturbed.

4.4 Conclusion

A previous study has demonstrated that pCLE accurately displays the morphology of the elastin microskeleton within the healthy acinus[48], which has led to speculation that pCLE may provide diagnostic clues in peripheral lung diseases[199, 205, 283]. This study has described the feasibility and findings of pCLE imaging in a group of patients with varied diseases.

4.4.1 Contact force and safety

It suggests that in this context, pCLE is safe for patients not suffering from bleeding diatheses. Whilst the probe causes pleuritic pain, no pneumothoraces were identified during the study. However, damage to the delicate pulmonary lobule cannot be excluded. For example, the terminal and respiratory bronchioles are substantially narrower than the 1.4mm diameter probe[284]. Whilst grossly magnified, free ended swaying septal walls were observed in 28 BPSs. Sometimes, this may be the product of lung disease, (more were observed in the emphysematous BPSs) but the probe was shown to be the likely culprit in several videos where traumatic tearing of vessels and delicate septal walls was observed in real time. Whether this has any minor clinical significance remains to be established, but the trauma should still be less than for TBB.

4.4.2 Accuracy of pCLE

Regarding image interpretation and the diagnostic potential of pCLE, the best case scenario was that alterations to elastin would be specific to individual diseases and provide unique image features such that, for example, non-necrotising granulomas were visible in sarcoidosis[285], and the fibrotic zones of dense collagen found in pulmonary fibrosis were enough to specifically alter the elastin appearance[286]. However, the pathognomonic features of specific diseases, observed under standard haemotoxylin and eosin histopathological microscopy are unlikely to match the changes occurring to the elastin. Nevertheless, elastin structure and production is known to alter in lung disease[287-290], and the most salient image finding from this series is the degree to which many peripheral diseases (emphysema excluded) are able to create a non-specific attenuation of the stunning highly recognisable images of healthy acini. The observed loss

of distinctiveness and autofluorescence in the non-emphysematous diseases within this study may be due to elastin destruction, alveolar collapse or substances such as collagen, blood, inflammatory infiltrate or mucus impeding the incident laser light and emitted autofluorescence.

Predictably[48], the autofluorescence intensity of individual fibres was greater in the older subjects; the healthy volunteers were young and whilst their individual septal walls were generally distinct, they displayed consistently weaker autofluorescence than from older non-diseased BPSs, or those BPS only affected by emphysema.

It appears that severe emphysema is often evident on pCLE imaging with dark holes and a reduction in the number of septal walls visible in each frame. Residual elastin is often thickened or disrupted. This is perhaps logical, considering that a major feature of COPD is fragmentation and loss of alveolar elastin[291]. The next section of chapter 4 looks at the reliability of these diagnostic findings, and whether milder disease is adequately demonstrable. If so, pCLE could be employed to grade the severity of emphysema for trials, or to assess the efficacy of interventions. Currently, subclinical COPD in asymptomatic smokers is screened for using spirometry[292] but whilst much more invasive, pCLE could have an additional diagnostic role, particularly if it had greater sensitivity for detecting early morphological damage which was predictive for future symptomatology. However, centrilobular emphysema tends to be heterogeneous which will inevitably create sampling bias; a particular problem in alveolar pCLE where to image a new area, mural restraint of the probe necessitates blind reinsertion into the BPS in the hope of cannulating a different terminal bronchiole. Conversely, the homogeneity of panacinar emphysema in alpha-1-antitrypsin deficiency makes early diagnosis difficult using HRCT; this provides a possible niche for pCLE.

In this current study, it should also be highlighted that two patients with bullae inadvertently had what is likely to be the first described in vivo bronchoscopic imaging of the inner surface of the elastin rich visceral pleura[293].

Thiberville et. al. bronchoscoped 41 healthy volunteers and confidently measured the septal walls as being 10±2.7µm and the microvessels as 90±50µm[48]. However, in the diseased BPSs, discrimination between these two image components was often impossible. This is likely due to pathological disruption of the elastin architecture forming the septal walls and microvessels[294-296], along with in many BPSs, the disease related reduction of image distinctiveness and autofluorescence described.

Using the mosaicing software, the standard 600µm FOV could only be modestly increased in just over half of the BPS overall, and only two BPS yielded mosaics >1mm. Unlike pCLE in less constrained areas, such as the proximal endobronchium or the gastrointestinal lumen, the probe cannot easily be translated, and within the acinus gentle withdrawal or further advancement does not always provide adjacent images to stitch together. The mosaicing function was likely impaired by fainter septal walls in the younger subjects, and distinct feature loss in non-emphysematous disease.

Whilst this series included only three current or recently quit smokers, the previous finding in healthy subjects that bright autofluorescent macrophages are specific to smokers or ex-smokers[48], seems to remain true in disease. Whilst there was a suggestion of similarly sized faint cells in the acinae of several subjects, the inflammatory cells in the video loops from the current and recently quit smokers were very bright and clearly independently mobile and therefore distinct from the septal walls they were within. The smokers' BAL fluid uniquely demonstrated fluorescent cells (macrophages). The fluorescence imparted upon alveolar macrophages from cigarette smoking takes years to fully diminish[203] and there is in vitro evidence that air pollutants have a similar effect on macrophage fluorescence[297]. These factors could explain any less obvious fluorescent cellular infiltrates. Further work is needed to elucidate the identity of the mucus globules/bubbles and the bright 3µm specks.

4.4.3 The role of fluorescein

Intravenous fluorescein is the *modus operandi* for pCLE in the GI tract by highlighting the calibre, course and leakage of microvessels[239], as well as providing fluorescence of the epithelium and glands. For this study, it was postulated that intravenous fluorescein might facilitate the discrimination between microvessels and septal walls, and therefore might have a role in diagnosis. However, there was no concentration that provided a useful role in peripheral lung pCLE imaging as there is "white-out" of the image before delineation of any microvessels can take place. A recent small study using only a fixed dose of IV fluorescein has suggested there may be subtle differences in the dark bubbles in health and disease, though this was not our finding[199] (it also showed that imaging of the epithelium of central airways is hampered by intravenous fluorescein). In this current study, severe nausea and wretching was induced by the fluorescein in one patient, but this has been previously well described during gastrointestinal pCLE[70]. Whilst

fluorescein would not preferentially outline microvessels, additional information for acinar pCLE imaging may be gleaned in the future by using topical contrast agents as has been briefly described in the upper airways[198] and peripherally[205].

An in vivo instrument such as pCLE has theoretical advantages over conventional histology. We observed both cyclical movement related to respiration within the acinus, and mobile cells. There were no serious complications and there was no delay or alteration (from histological preparation) to the structure observed. However, with the exception of emphysema, there is significant diagnostic information lost with pCLE as compared with histopathology. Whilst this study provides a basis to develop pCLE for PLD imaging, further work is needed to realise the goal of providing accurate diagnosis without tissue biopsy. Safe topical contrast agents that penetrate the cell wall may have a role[205]. pCLE imaging of endogenous structures other than elastin may also be realised by employing combinations of confocal wavelengths to provoke simultaneous autofluorescence from multiple endogenous sources such as collagen[298], or by combining fluorescence lifetime imaging with confocal endomicroscopy[299].

4.4.4 Tracking

The prediction or retrospective estimation of probe destination remains an issue. Even in Thiberville et al.'s healthy cohort, over 10% of cannulated BPSs did not yield an alveolar image[48], presumably because of an inability to adequately deploy or position the probe beyond the respiratory bronchiole. In severely diseased BPSs it was difficult to ascertain if a reduction in image quality represented this incomplete deployment, or if the probe was imaging a bulla/diseased area. Similarly, it is not possible to confirm that the pCLE image was taken from exactly the same location as the diagnostic TBB and BAL. An extended working channel was used in the first five patients but this had to be abandoned owing to it impairing the ergonomics of the procedure. Whilst this should not be a concern in widespread homogenous disease, focal patchy disease may cause difficulty with reliable correlation.

4.5 Quantification of Emphysema Severity: the Accuracy of pCLE Compared to HRCT

4.5.1 Introduction

As discussed within the introduction, COPD is a significant worldwide health burden. In the United Kingdom alone there are estimated to be 3.7 million people with the disease[300] and 30,000 deaths per year are attributed to it[301]. Assessing lung function with spirometry remains the mainstay of diagnosis and longitudinal observation in the 900,000 who obtain a formal diagnosis[302]. Where indicated, HRCT provides fast, high resolution images of the anatomical destruction, hyperexpansion and bullae. However, with these modalities, early diagnosis is not always possible, and moreover with HRCT only providing a resolution of approximately 100μm[303] there is no means of providing imaging of individual alveolar walls. A method of providing in vivo images of individual alveoli could be useful for identifying early disease and evaluating any therapeutic modality for tissue regeneration[304].

Section 4.3.4 Basic analysis of emphysema) demonstrated that when severe emphysema is present, the pCLE images reflect this, with a destruction of the regular morphology and, in particular, areas where the elastic fibres are more scant in the FOV. However, it was not clear after lengthy unblinded inspection of the video loops and stills if this was a reliable feature (Figure 4.8), or perhaps more usefully, if the images could be used to predict the degree of emphysema in the less severe areas.

4.5.2 Objectives and hypothesis

This sub-study aimed to compare the accuracy, interassessor reliability and intraassessor reproducibility of trained assessors determining emphysema severity according to the modified NETT classification for HRCT (Table 4.1) using pCLE imaging presented in 3 different formats[281]. The hypothesis was that pCLE would accurately classify emphysema.

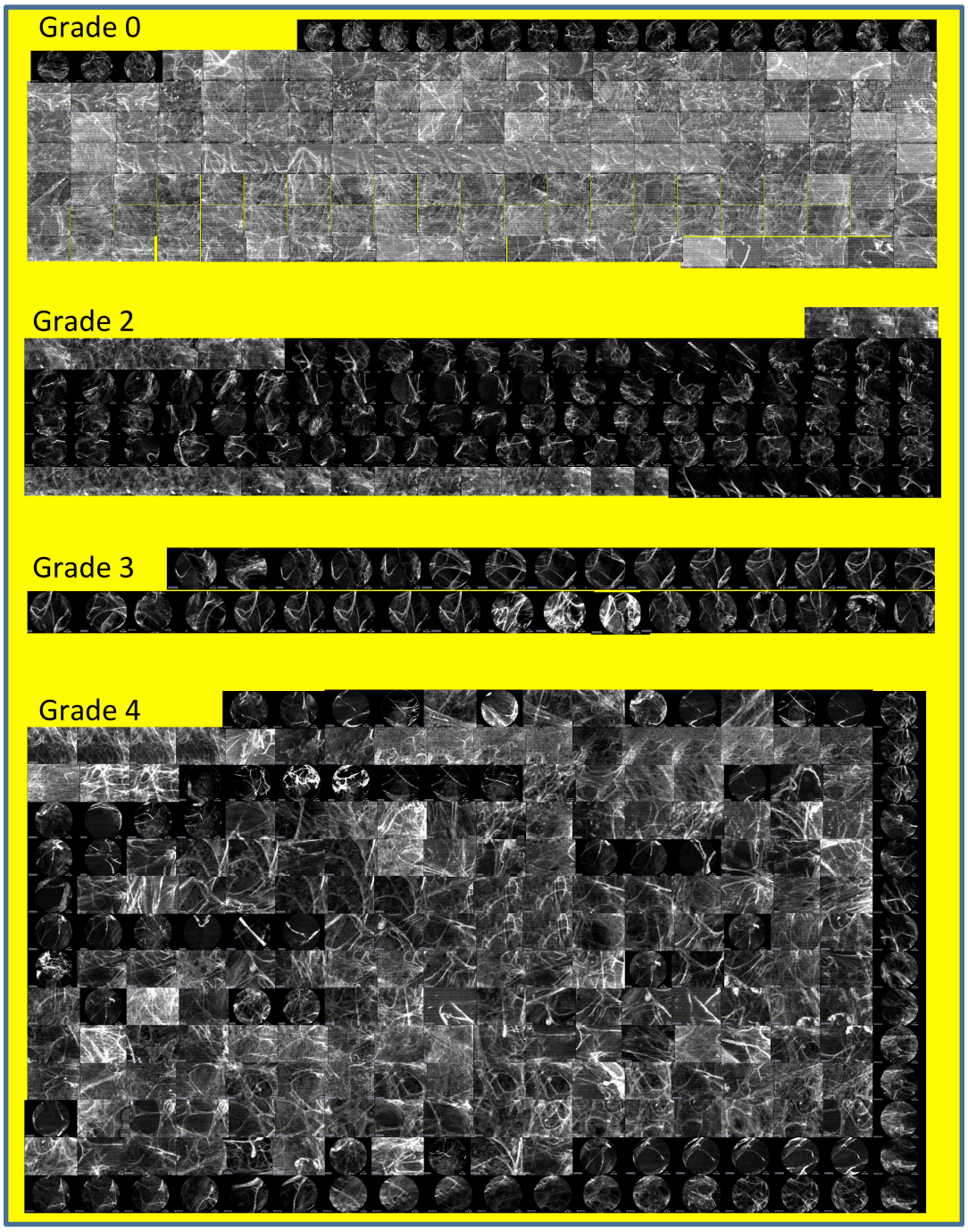


Figure 4.8 A few of the unenhanced collated still images (CSI) selected from the pCLE video loops of the BPSs of healthy and emphysematous BPS. Whilst it would appear that the most abnormal/destroyed lobules on pCLE fall within the worst two radiological classifications, there do seem to be multiple "false negative" grade 4 images that have good septal wall density compared to the destruction evident upon HRCT.

4.5.3 Methods

Using data from the first 15 subjects bronchoscoped in the last section, from 35 BPS, 35 representative sets were compiled of a) 20-30 second video sequences (VS), b) collated still images (CSI) and c) collated enhanced still images (CESI). CESI were produced by inputting CSI through brightness equalisation and a low pass filter to eliminate noise; the rationale for CESI was to improve the delineation of the septal walls within the FOV. Normal areas were obtained from 3 healthy volunteers and from radiologically unaffected areas of the first 12 patients with lung disease. As previously described, emphysematous areas were ascribed severities based around the modified NETT classification described in the last chapter. Overall, 18 BPS were grade 0 (normal parenchyma), 5 BPS were treated as grade 2 (26-50% of BPS being affected), 2 BPS grade 3 (51-75%) and 10 BPS grade 4 (>75% involvement) (Figure 4.10A). No grade 1 BPS were available/used at the time.

As many representative individual greyscale JPEG snapshots as possible were acquired from the pCLE video loops from each BPS selected for the analysis. The "shadow remove" function was used where offered and an attempt was made to avoid images with motion artefact, bubbles, inflammatory cells or microvessels. Snapshots from the same optical location were a minimum of 4 frames apart on the pCLE video loops to avoid repetition. No mosaics were used.

Using Microsoft PowerPoint, 5 assessors (4 clinicians and 1 image scientist) were each given an individual 10 minute tutorial on the basics of pCLE in the peripheral lung with an explanation of the elastin-containing structures that can be observed (septal walls and microvessels). One example of each of the 4 emphysema severities (0, 2, 3 & 4) was then provided in each of the three formats for training and for subsequent reference (Figure 4.9). The assessors (blinded to the prevalence of disease severities) were then asked to grade all the 31 remaining BPS, first in VS format, then all in CSI, and finally in CESI, presented in a different disarranged order for each format series. For the CSI and CESI formats, the individual frames from each BPS were presented on a single PowerPoint slide, similar to that seen with the training slides. To evaluate the stability of assessor classification, the same observers reclassified some of the VS (14) and CSI (13) one week later. The assessors were asked to provide their degree of confidence with each classification, and asked for feedback on the exercise.

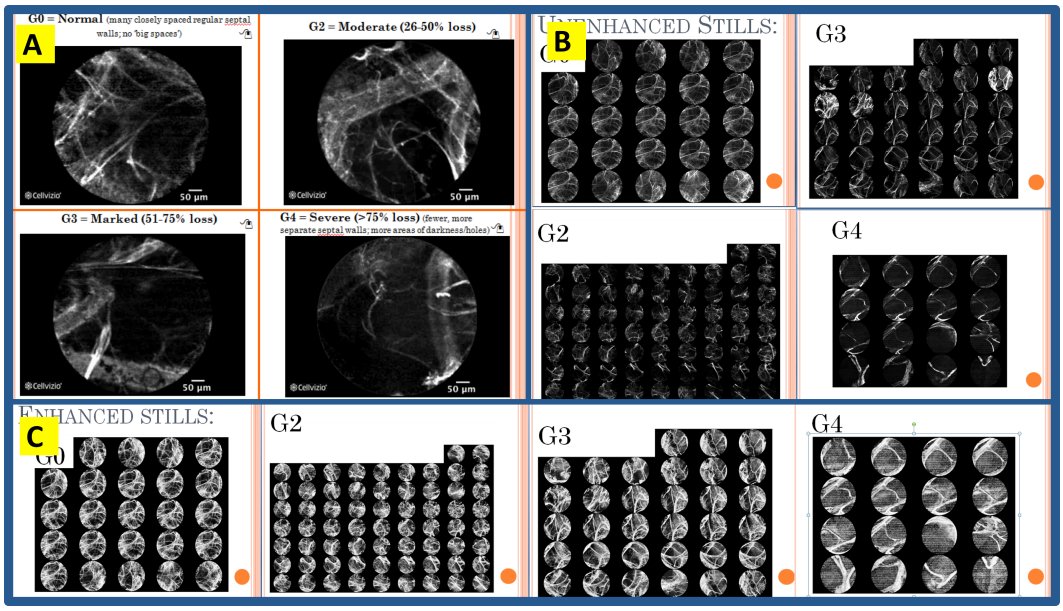


Figure 4.9: Prior to being asked to grade the BPS on each of the two occasions, each assessor was given general background information about the essence of emphysema and pCLE, and shown examples on slides of G0, G2, G3 and G4 emphysema in the form of VS (A), CSI (B) and CESI (C).

For the week 1 interobserver reproducibility and week 2 intraobserver reliability, Fleiss and Cohen's weighted Kappa coefficient for multiple observers and multiple classes was used [305] and interpretation was performed according to the guidelines of Landis and Koch[306]. Kappa values can range from -1 to +1 (perfect disagreement to perfect agreement), with a value of 0 equating to random agreement. Values of 0.81–1.00 indicate excellent agreement, 0.61–0.80 substantial agreement, 0.41–0.60 moderate agreement, 0.21–0.40 fair agreement, 0.00–0.20 poor agreement, and < 0 no agreement. SPSS Statistics (Version 17, Chicago, IL, USA) with the MKAPPASC.SPS macro was used together with an online kappa calculator[307]. Values were expressed with 95% confidence intervals.

4.5.4 Results

The assessors spent approximately10 minutes having instruction and studying the VS, CSI and CESI. The comprehensive week 1 assessment and interrogation of intraobserver reliability at week 2 took around 1 hour, and 30 minutes respectively. The accuracy for exactly classifying HRCT severity with pCLE was only 13.6% (9.04-19.8) when classification was demanded from the VS; 19.31% (13.7-26.5) for CSI; and 11.72%

(7.45-18.0) for CESI (Figure 4.11A). Whilst there were examples of both substantial underscoring and overscoring, every assessor on average overscored the severity with each imaging modality. For example, as shown in Figure 4.10B, the mean overscoring for VS was 0.73, 0.63 for CSI and 0.61 for CESI.

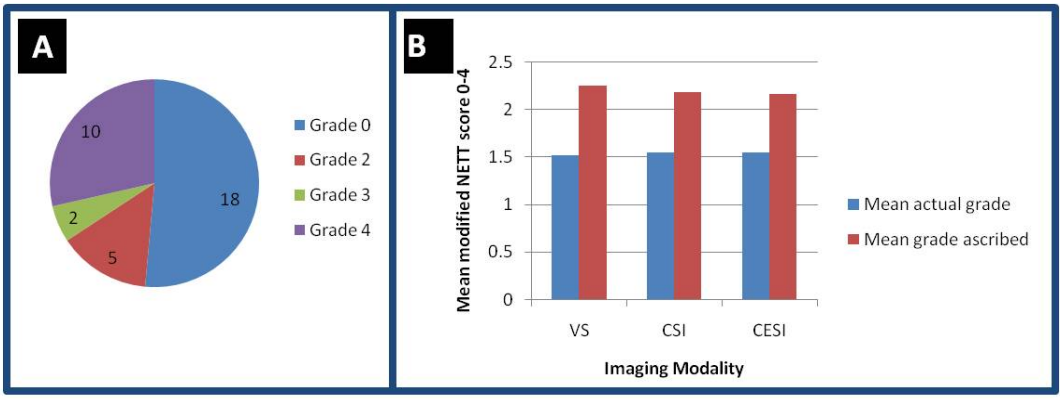


Figure 4.10 A shows the prevalence of BPSs identified for the study of each different NETT emphysema grade. Over half of the BPS were of normal density, perhaps contributing to the assessors overscoring them by a mean of 0.73, 0.63, and 0.61 grades for VS, CSI and CESI respectively (B).

According to the weighted Kappa coefficients, the interassessor agreement was fair for CESI (0.31), but poor for both VS (0.13) and CSI (0.19) (Figure 4.11). At the week 2 reassessment, the mean intraassessor reliability was judged as moderate for CSI (0.48) and fair for VS (0.21) (Figure 4.11).

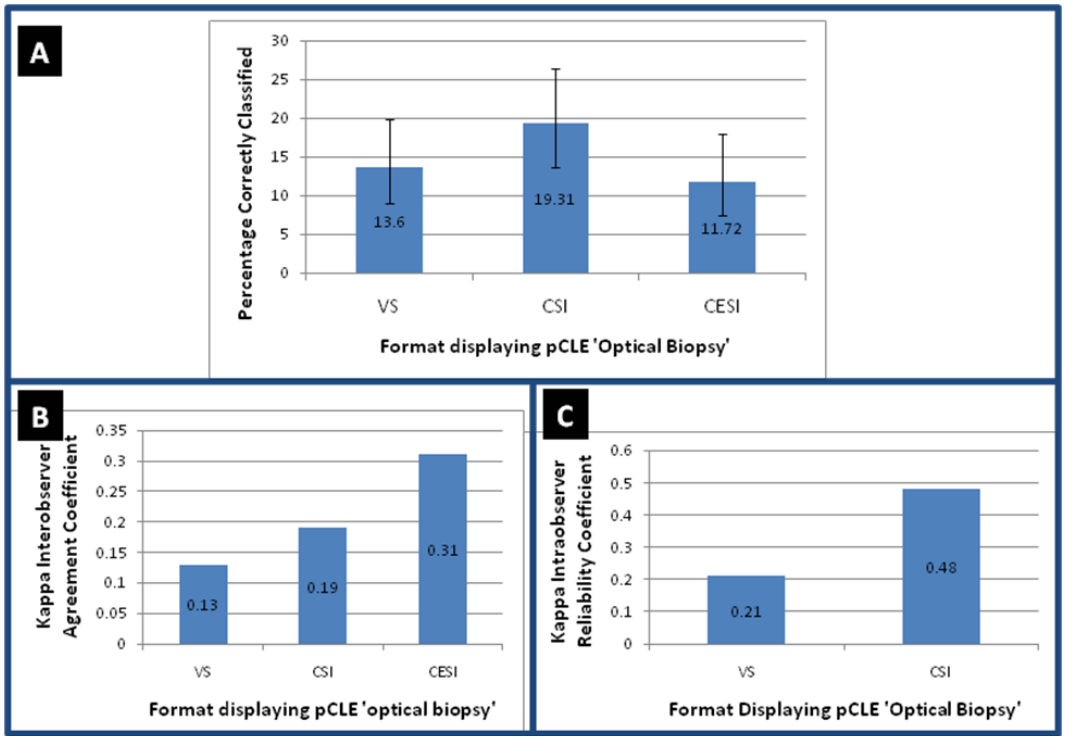


Figure 4.11: In each format there was a disappointing accuracy for the assessors correctly predicting the actual emphysema grade of the BPSs (A). B shows the interobserver agreement coefficient for each format, and C shows the intraobserver reliability.

4.5.5 Conclusion

With this limited data set, the ability of five previously pCLE naive assessors briefly trained with a very small training set to predict the emphysema severity as determined by HRCT was generally disappointing. There was a little intraassessor reliability (particularly for CSI) indicating slight stability for individual assessor's response. However, there was less interassessor agreement and none of the 3 formats enabled pCLE interpretation to accurately categorise emphysema severity. The "best" agreement was seen with intraassessor agreement for CSI and this was still only a "moderate" 0.48.

It is important to note that this level of agreement is very poor in comparison to levels that would ever be considered acceptable for a diagnostic investigation. Kripperndorf suggested more conservative cutoffs than Landis and Koch, with values <0.67 being being discountable, values between 0.67 and 0.8 requiring scepticism, and values >0.8 being required for firm agreement to be concluded[308].

In addition to the small number of training and data sets, and assessors, there are multiple limitations to this study. The training was brief, although with other organ targets the

learning curve for pCLE is short, with one or two sessions enabling proficiency[65, 66]. There is no pCLE classification available so the training was very basic and limited. 26/31 of the BPS for post-training categorisation by the assessors were either normal or severely diseased - grade 0 or grade 4: a more even spread, including some grade 1 emphysema would have been desirable. Many of the grade 0 subjects were younger and therefore known to display less autofluorescence and therefore more noise, and many of these "normal" BPS came from lungs with disease elsewhere; therefore mild non-emphysematous disease may have affected the results. Whilst it was hoped that one benefit of computational enhancement of the images might be to better delineate elastin, CESI images were not more accurately interpreted.

A recent study has shown that even in healthy lung transplant patients having similar pCLE bronchoscopies 3 months apart, there are only moderate coefficients of correlation for measurements of septal wall thickness and lobular diameter between the two bronchoscopies[309]. This likely relates to factors mentioned such as dynamic movement of the acinus, and the the subsegment of lung imaged on each occasion being slightly different geographically, but still not adequately representative of the region. Clearly if the data consistency is limited in clinically stable patients, it is likely to be worse in lung which is affected, often heterogeneously, by disease.

Tracking the Probe Location: It is possible that the heterogeneity of centrilobular emphysema often results in the pCLE probe advancing through micro-bullae until relatively normal elastin structure is reached, imaged and therefore inaccurately interpretated as normal lobule. Furthermore, a relatively blank screen could be a micro-bullous or the probe not having reached the lobule; without an understanding of the whereabouts of the probe at any one time this is difficult to establish when cropping videos or selecting stills for assessment.

Chapter 5 The Significance of Contact Force during pCLE Imaging

5.1 Introduction

Little is known about any effects that the optical biopsy technique may have upon the images acquired. The angle of approach of the device, the degree of spread of the tissue, and the contact pressure of the probe may all exert influence. Experience suggests that variations in angle of approach of the device seem to be countered to some degree by tissue deformation and accommodation of the probe. The degree to which an epithelial surface is contracted or stretched out will be affected firstly by multiple biological factors, and secondly by inflation pressures (for those targets which depend upon the insufflation of gas to create a working space, such as the peritoneal cavity and moreover the floppy gastrointestinal lumen). As discussed in chapter 2, the contact force of an imaging probe may also play a role; it certainly affects spectroscopic signals [244], and pCLE probe pressure can distort the lobule of the peripheral lung[48]. From pCLE imaging of the respiratory tree and colorectum in chapter 3, it appears that image quality and consistency is not always the same even in healthy tissue, and that small probe movements can rapidly alter the field of view or image; it is feasible that probe contact pressure could be partly attributable.

An example of the potential importance of geometry in the interpretation of confocal endomicroscopic images was highlighted by Li et al. who found that eCLE images of ulcerative colitis mucosa showed a quantifiably reduced number of crypts per image, with increased distances between crypts and enlarged crypt openings[129]. However, the accuracy of any potential assessment of colitis using a CLE device would be compromised if this geometry was unpredictably disturbed by tissue stretch or the angle or pressure of the probe itself. Early work into computer aided diagnosis has begun with “content-based image retrieval”, using automated detection and interrogation of simple glandular features to discrimate between eCLE images from colonic mucosal surfaces affected by different conditions[310]. By assessing (amongst other things) the compactness, roundness, border size and separation of glands and crypts of a particular image, it is possible to search a large library of optical biopsies that have been previously correlated with histopathology and provide similar images to aid the endoscopist. This is

known as content-based image retrieval; clearly its potential will be limited if probe contact pressure affects these simple parameters.

A very simple preliminary test is shown in Figure 5.1 to explicate the concept. A 2.5mm gastroflex pCLE probe was used manually, first with minimal contact force 10 times, and then with significant contact force (approximately 3N with a force torque sensor) 10 times to perpendicularly image four different materials. Topical 1% fluorescein was dropped onto lamb kidney and lamb liver; this was not required for the natural sea sponges as their collagenous fibres are autofluorescent at 488nm. 80 images were acquired; each from a new site. The firmer contact force upon both densities of sponge produced a more crowded cluster of filaments, perhaps as fluorescent fibres were squashed together into the plane of imaging. Any qualitative effects of contact force upon the kidney and liver images were very subtle; perhaps some spreading out of the tissues was observable. However, the force changes were crude, and subtle differences could easily be missed owing to the lack of distinctive features.

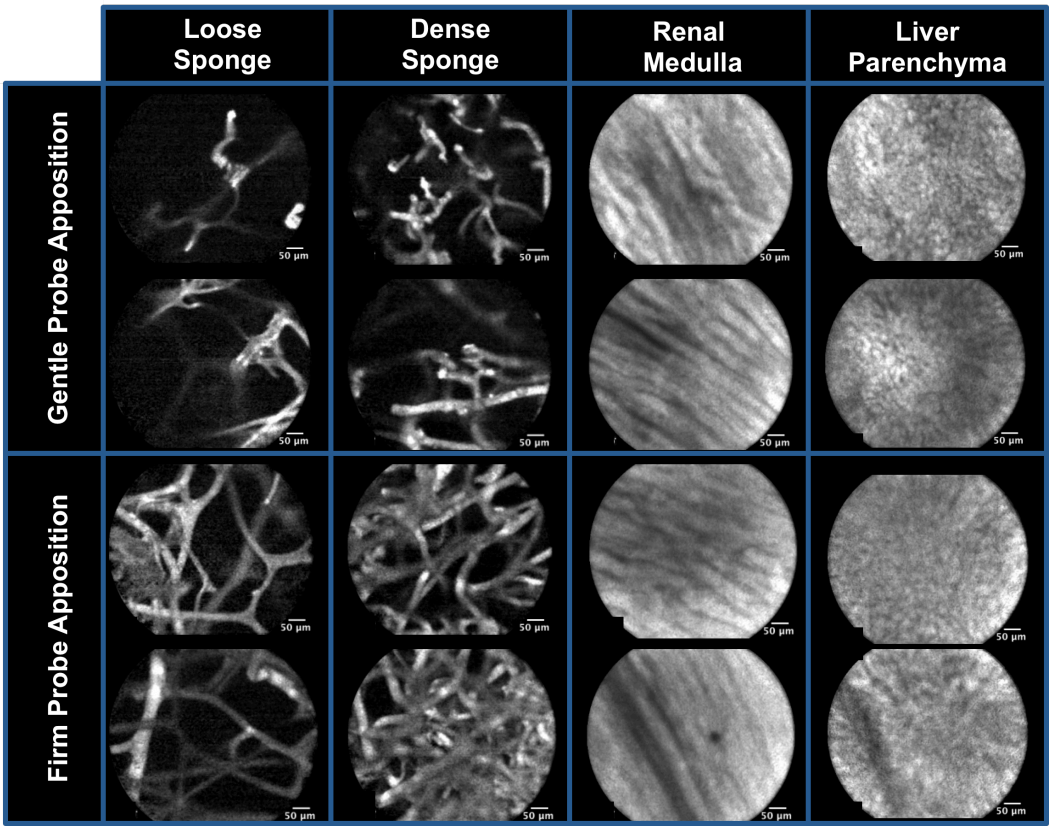


Figure 5.1: The effect of contact force alterations to pCLE images was mostly evident upon sea sponge.

5.1.1 Initial hypotheses

The first two hypotheses tested in this chapter were that the morphology of colonic glands would be influenced by two different ergonomic factors: the degree of inflation of the bowel, and variations in the static contact forces of the probe.

5.2 Methods

5.2.1 Colon inflation study

A 70kg landrace pig under general anaesthetic for an unrelated minimally invasive non-survival gynaecological experiment underwent midline laparotomy and bimanual evacuation of the rectum. 3.5mls of 10% fluorescein was injected intravenously. A 2.5mm diameter standard resolution gastroflex pCLE probe was immediately deployed through a gastroscope which was navigated above the peritoneal reflection into the colon. With the probe gently abutting the tissue and undergoing slow translational movement, 2 minute pCLE video sequences were recorded with the bowel a) collapsed, b) inflated to 4cm diameter, and c) hyperinflated to 6cm with the aid of an occluding doyen intestinal clamp (Figure 5.2D). From each video sequence 20 representative still images were extracted: the maximum diameter across each gland was measured using the Cellvizio Viewer software, and the number of complete glands per image was recorded (Figure 5.2E). The study was undertaken under Home office licence PPL 80/2297.

5.2.2 Static force study

A rigid aluminium board was bolted vertically to an optical breadboard. 4x4cm pieces of fresh full thickness distal large intestine from a contrast agent naive pig were irrigated with saline to remove mucus and faeculent residue. They were then suspended against the aluminium board, but separated and cushioned from its rigid surface by clamping a piece of full thickness porcine stomach in between (Figure 5.2B). The same gastroflex pCLE probe was used; its smooth distal tip consisted of flat glass constrained by an encircling metallic tube lying flush. The topical nuclear staining contrast agent 0.02% acriflavine was applied to each sample of colonic tissue immediately before imaging (as intravenous contrast was not feasible for this study, a nuclear staining contrast agent was found to offer better discrimination of mucosal morphology than topical fluorescein). The probe

was clamped 3cm from its tip into a force-sensitive linear servo mechanism that has been described in detail for a different application[311]. In summary, a bespoke LabVIEW programme (National Instruments, Texas) enables a DC motor to linearly drive a rack and pinion system attached to the clamped probe until a predetermined contact force between probe tip and tissue is achieved (Figure 5.2A).

The probe was driven perpendicularly into fresh tissue regions of healthy bowel only, until a contact force of 0.005N, 0.05N, 0.1N, or 0.5N was achieved. 0.005N was the minimum programmable contact force required to ensure contact, and the acquisition of an image. Twenty good quality still pCLE images were acquired and analysed for each force. As for the in vivo experiment, the number of complete glands per image was counted, and the maximum diameter was measured across each gland.

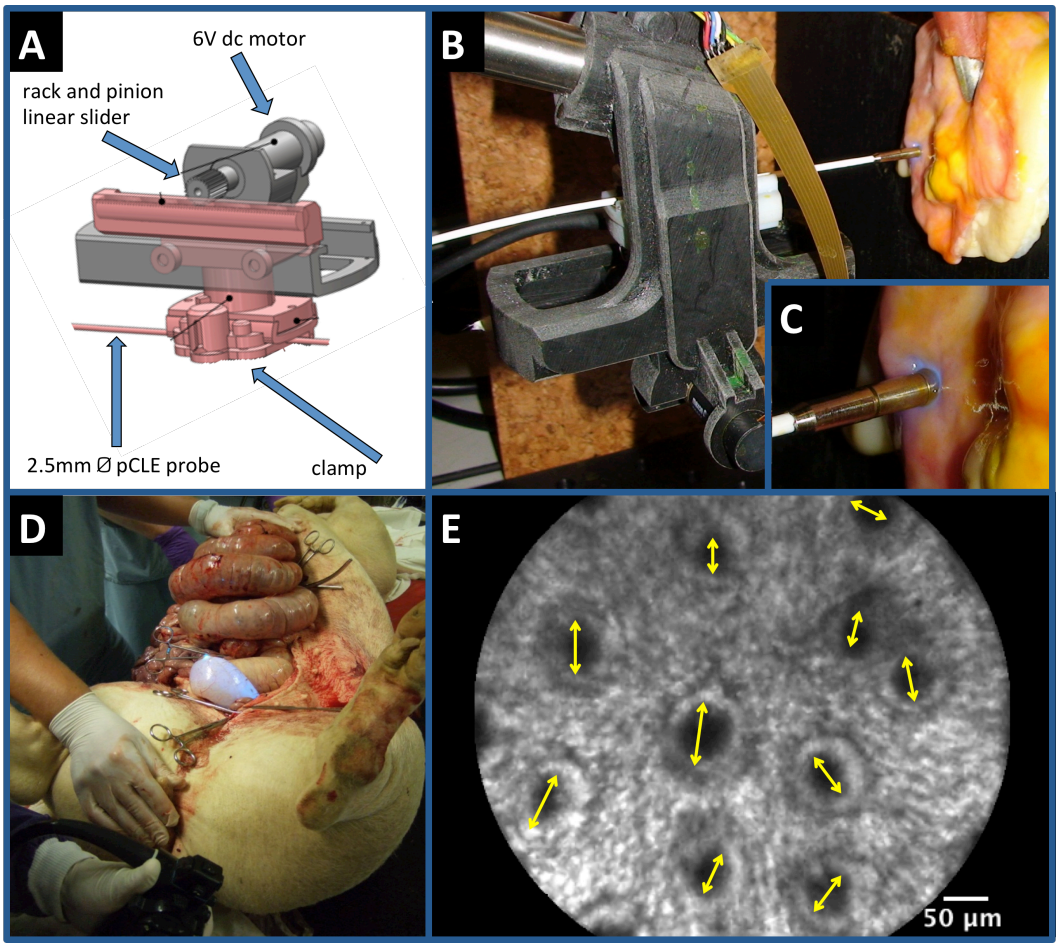


Figure 5.2: For each image, every gland was counted and its maximum diameter measured (E). Imaging conditions were altered in an ex vivo experiment by changing the contact force using a bespoke programmable actuator to drive the probe into porcine colon (A, B & C), and altered in an in vivo experiment by changing the colon diameter using occluded insufflation.

Statistics: Owing to gland number and diameter being slightly non-parametric, 2-tailed mann-whitney tests and Kruskal-Wallis analysis of variance tests were used.

5.3 Results

5.3.1 Colon inflation study

For collapsed, inflated, and hyperinflated distal colon respectively, the mean number of complete visible crypts per field of view decreased: 23.8 (±3.1), 14.0 ((±2.1), and 8.1 (± 0.7) ($p<0.0001$). Similarly, the mean crypt diameter increased: 65.4µm (± 2.2), 85µm (± 2.1) and 95.6µm (± 2.8) ($p<0.01$) (Figure 5.3). It was also apparent that in the collapsed bowel, fluorescence was obvious in the centre of the gland, appearing to pool in the crypt.

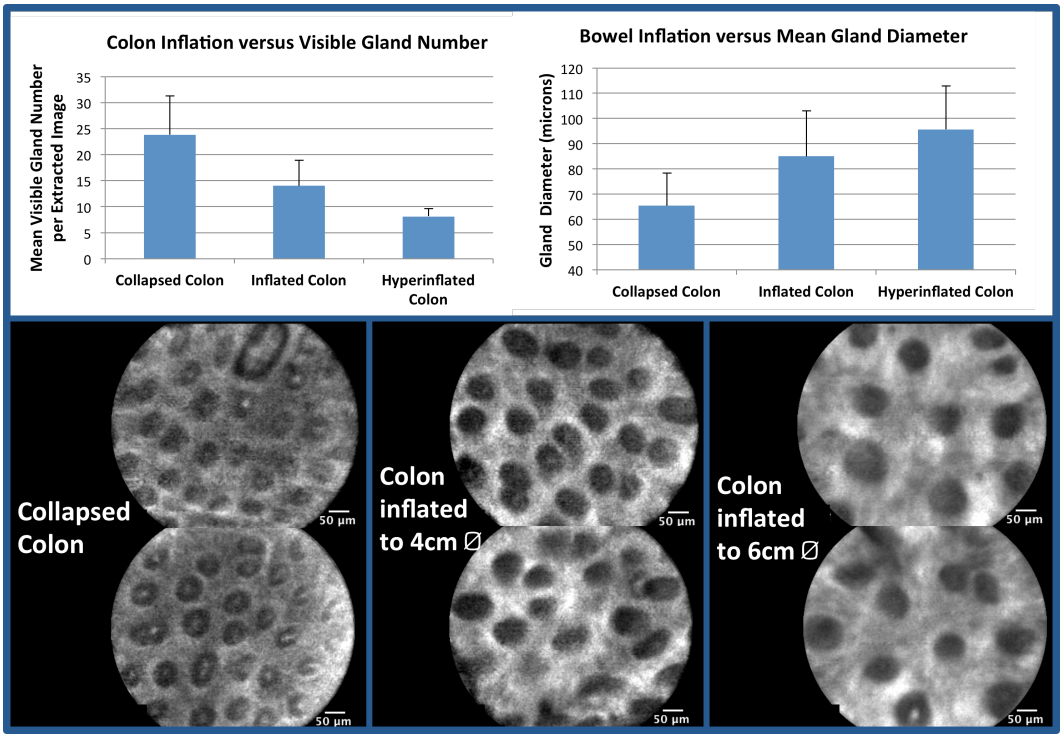


Figure 5.3: The result of colonic inflation on gland density and diameter.

5.3.2 Static force study

In total, 80 still pCLE images were acquired, at one of 4 pCLE probe contact forces (0.005N, 0.05N, 0.1N, or 0.5N). Only a few had to be repeated, either due to residual

mucus causing an unrecognisable image, or in the case of 0.005N images because of shadow artefact (Figure 5.4). Analysing the complete glands per field of view and maximum diameter across each gland was straightforward, though the gland boundaries were not always as distinct in 0.5N images (Figure 5.4).

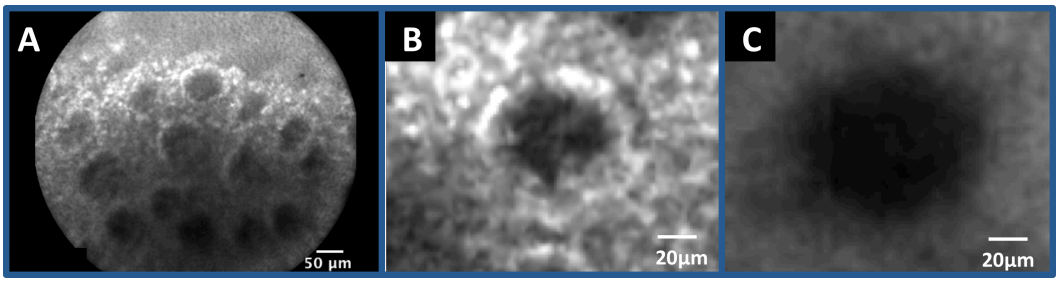


Figure 5.4 The number of glands and their maximum diameter was easily calculated for each image although a few of the 0.005N images had to be repeated due to shadows, perhaps due to incomplete contact (A). Some of the 0.5N glands had less distinct boundaries (C) than those observed at the smaller forces (B).

It was evident that greater contact forces produced images with fewer glands per field of view (Figure 5.5): 18.9 ± 2.6 at 0.005N, 10.3 ± 3.6 at 0.05N, 9.6 ± 1.6 at 0.1N, and 6.6 ± 1.6 at 0.5N ($p<0.01$ for all except 0.05N versus 0.1N). Similarly, the images acquired during firmer probe contact resulted in those fewer mucosal glands being wider across their maximum diameter: 44.6 ±10.5µm at 0.005N, 68.5 ± 25µm at 0.05N, 73.3 ± 21.6µm at 0.1N and 92.7 ± 35.8µm at 0.5N ($p<0.01$ for all except 0.05N versus 0.1N).

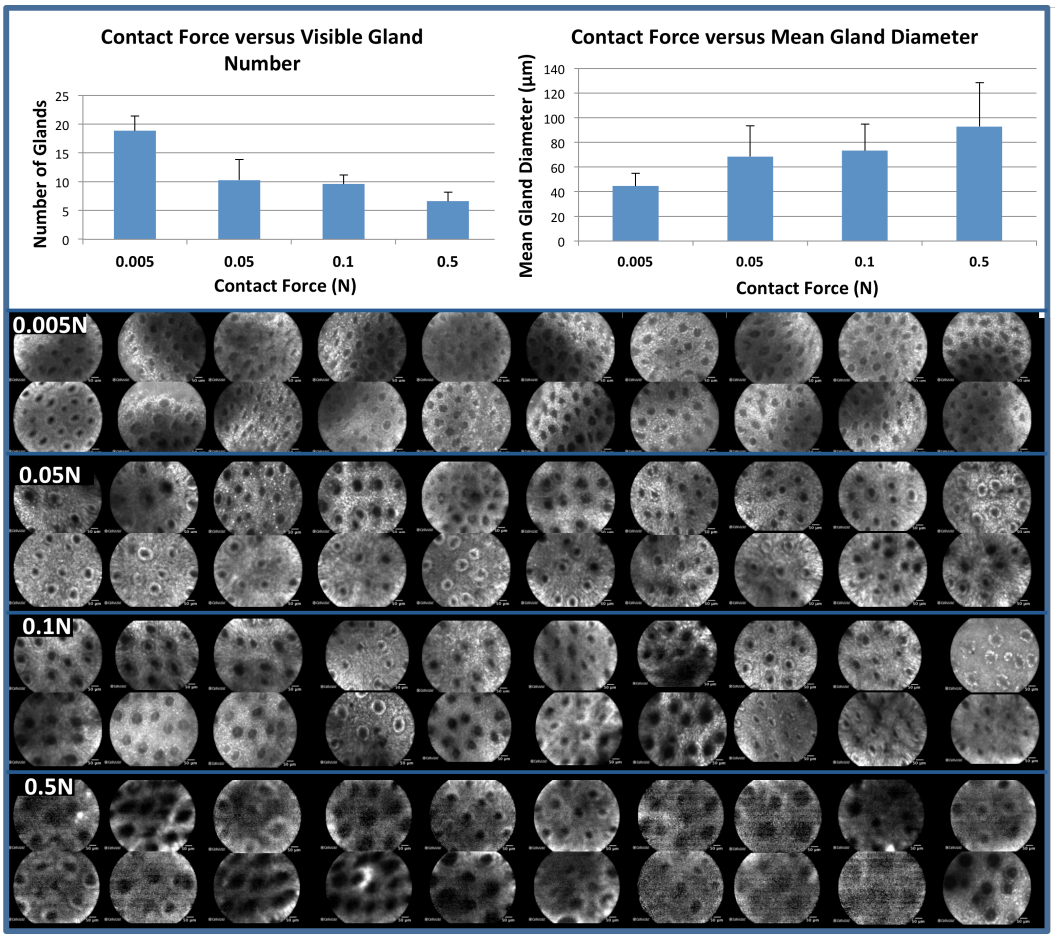


Figure 5.5: The effects of contact force on gland density and diameter in an ex vivo set-up.

5.4 Conclusion

These two studies have shown that bowel inflation and probe contact force are able to affect gland density and apparent diameter of the glands, at least in the extremes that were created in this experimental set-up. This may have important implications for standardising image acquisition protocol during endoscopic pCLE to ensure morphological alterations to crypts can be exclusively attributed to tissue differences.

In the in vivo study, the most striking observation was that in the collapsed bowel the number of glands per image was almost three times that of the hyperinflated bowel. The gland diameter was 46% greater in the hyperinflated bowel. During endoscopy, fully collapsed bowel would be challenging to image, and hyperinflated bowel would cause the patient severe pain; the endoscopist inflates a lumen such as the colon "just enough", and further work would need to be done to ascertain what the variation in colonic inflation is.

Having shown fluorescein in the crypt lumens of the collapsed colon, if intercryptal fluorescein remains a marker of disease[129] it may also be important to ensure bowel is adequately inflated. Future work would also have to find a way of maintaining a constant contact force independent of bowel dilatation, and be performed on more than one animal. Though imaging at all three inflations only took a few minutes, image quality begins to deteriorate 8 minutes after contrast injection[74], and therefore it would be important to alternate the order in which the sequences at different inflations are acquired.

In the static force experiment it was found that the mean gland diameter at 0.5N was over twice the value observed at a "just touching" value of 0.005N. At the higher force there were, on average, less than half as many observable glands per field of view. It is likely that the greater the contact force, the more the probe flattens the mucosa and stretches out the glands and epithelium; this creates wider glands and squeezes some of them out of the field of view. With gland and crypt morphology being an important part of pCLE disease classification and understanding[109, 129], this finding in itself may have clinical relevance, with contact force being difficult to accurately control endoscopically. With manual deployment through an endoscope, the pressure at which the pCLE probe abuts the tissue during clinical examination is likely to be between the extremes, but this would require further analysis. Our data (unpublished) suggested that, depending on position (from straight to retroflexed), between 0.1 and 0.6N respectively of axial force was required simply to overcome resistance through the working channel of a colonoscope in order to begin to advance the probe toward a tissue target. This suggests that the current ability to carefully control the contact pressure is probably limited. On the basis of this work, as a first step towards controlling the contact force distally, our laboratory has developed a handheld device incorporating force and position sensors with linear voice coil actuator to grasp a pCLE probe and ensure a consistent contact force with tissue[243].

Measurement was made harder by fuzzier edges at higher forces and greater inflation pressures; it is possible that a high definition probe may help in future, together with the arguable benefits of using intravenous fluorescein (in vivo) over topical acriflavine (ex vivo). As future force adjustment study translates into the in vivo environment, it will be interesting to see if blood flow through the microvessels is affected. If the mucosal capillary blood pressure between arteriole and venule is assumed to range between 1.3KPa and 4KPa respectively [312], a 2.5mm diameter probe would need to exert a force between 0.026N and 0.079N to obstruct the flow.

5.5 Introduction - a Study in Dynamic Force

5.5.1 Diagnosis through assessment of a tissue's mechanical phenotype

5000 years ago, the Ancient Egyptians described digital palpation to elicit information about aneurysmal blood vessels in the Edwin Smith papyrus[313]. Palpation remains an important clinical skill for assessing not only the shape and texture of tissues and organs but their hardness and springiness. As the fingers attempt to deform and displace the tissue, pressure receptors provide localised information about the stresses that the tissues are exerting on the pads of the fingers, and the temporal variation of these stresses as the tissue deforms. Indeed, the palpation of hard, irregular tethered masses over soft, well-circumscribed, mobile lesions *tends* to discriminate malignancy from benign processes in many organs such as during breast examination of a solitary lump, or during digital rectal examination of an enlarged prostate. Several technologies are able to more accurately extract similar information about the mechanical phenotype of a biological specimen, ultimately quantifying stiffness with Young's Modulus, which is a ratio of the stress applied (force per unit area) over the strain (fractional change in length of the object).

Perhaps the simplest method of comparing tissue stiffness in vivo was demonstrated by Carter et. al.[314] using a handheld compliance probe. Consisting of a fixed reference ring, surrounding a round tipped rod attached to a linear variable displacement transducer, it indented normal and less compliant cholestatic liver parenchyma to a maximum of 5mm. A similar device has shown that the soft tissues overlying the metatarsal heads of diabetics is stiffer than in controls[315]. By employing a 5-50Hz cyclical stress upon chippings of benign prostatic hypertrophic tissue, Phipps et al.[316] were able to demonstrate that the amplitude ratio between the excitation force and the resultant displacement was dependent upon the smooth muscle content; smooth muscle being fairly elastic. Equally, they found that the phase difference between the two waveforms, as a positively correlated marker of tissue viscosity, was smaller in chippings from malignant prostates[317]. For the assessment of skin turgor, the cutometer is a suction technique that measures the force required to raise a pre-defined amount of skin[318]; similarly shear modulus can be measured with a twisting device placed on the epidermis[319].

Assessment of mechanical phenotype can also incorporate modern imaging modalities such as "echopalpation" during B-mode ultrasonography; an area of interest is compressed either digitally or with the ultrasound transducer; in general, firm lesions (such as a thrombosed vein) move as a unit whereas soft lesions (such as a patent vein)

flatten. This effect is more elegantly displayed during *ultrasound elastography* where cross-correlation between pre-compression and post-compression radiofrequency waveforms enables the degree of tissue displacement to be calculated[320]. Derived from this are *localised strain values:* soft tissue has a high rate of change of displacement and is displayed brightly, whereas hard areas strain less and appear dark on the elastogram. A study of transrectal ultrasound elastography with a water-filled balloon to create the necessary tissue movement produced an area under the receiver operator curve of 0.97 for differentiating adenocarcinomas from their softer pre-malignant adenoma precursor[321].

On a nanotechnological scale, the atomic force microscope [322] can measure the stiffness of cells, with neoplastic cells invariably being more deformable[323, 324] owing to cytoskeleton changes. Of relevance to this current study however, tumours are generally hard, despite their constitutive cells being soft, owing to increased compression secondary to the rapidly expanding tumour mass[325], stiffening of the extracellular stroma from the desmoplastic fibrosis induced by the tumour[326], and increased interstitial pressure from damaged lymphatic drainage and leaky abnormal blood vessels[327].

5.5.2 Aims and hypothesis

The purpose of this section was to establish if pCLE can be used to assess the mechanical phenotype of tissue at a microscopic level, and whether the simulation of disease by prior chemical alteration of the tissues' physical properties, can be detected by the way in which the pCLE morphology responds to a dynamic force. As discussed, the most commonly studied morphological feature of pCLE images of the bowel thus far, which has been repeatedly integrated into diagnostic criteria, has been the colonic glands which, if healthy, are regularly spaced across the en face image, and comprise small circular crypts lined by mucin secreting goblet cells; therefore, as with the colon inflation and static force studies, the glandular microanatomy was studied.

The hypothesis was that the distortion observed during imaging with a cyclical force would be less in stiffened tissue than otherwise healthy ex vivo tissue.

5.6 Methods

The experimental set-up with rack and pinion linear slider was similar to the static contact force study. The axial contact force was measured at 500Hz by an embedded force-torque sensor. Actual force values were recorded for retrospective confirmation of achievement of the desired cyclical forces, and also for overlying with the image analysis traces.

The linear servoing mechanism was programmed so that the probe exerted a 0.43Hz sinusoidal contact force with a trough to peak amplitude of 0.07N (from the 0.005N required to ensure contact, to a maximum force of 0.075N). pCLE video sequences were recorded for nine healthy and seven stiffened pieces of tissue. Stiffened tissue, to mimic neoplastic transformation, was created by partial fixation of healthy full-thickness colon from the same pig (soaked for two hours in 10% formalin before rinsing in saline). For this study the analysis of the pCLE video sequences was more automated. Thus, for each video, the centre of every distinct gland was manually selected prior to the entire frame undergoing histogram equalisation and median filtering. This removed spurious noise, and improved the contrast between the poorly fluorescing boundaries of the glands and the fluorescent surrounding epithelium. A binary thresholding operation was applied to the filtered frame, with a threshold dependent on the intensity of the manually selected points and their immediate surroundings. Only connected regions containing the selected points were retained and their centroids calculated; this outlined the desired regions. For each frame, filtering and thresholding were automatically applied and the glands were temporally and spatially tracked by checking which connected regions contained the centroids computed at the previous frame. Under the assumption of smooth motion and medium to large crypt size, regions were tracked consistently and they were usually recovered from temporary occlusions. For each region tracked within the frame, information about its centroid, and average distance to the centroids of the other tracked regions was recorded. All glands that remained trackable for a minimum of three sinusoidal force cycles were included in the subsequent analysis for both mean gland surface area and mean intergland separation. Both these measurements were plotted as a moving average of the neighbouring three values, and overlain onto the waveform of contact force. For each gland analysed, the mean percentage change in area over two consecutive cycles was calculated (with the smaller area/trough used as the denominator). Data was taken from a trendline which averaged area and separation readings effectively over every quarter second. This method was also used for assessing the mean percentage change in separation between the centroids of the glands as the contact force varied.

Direct visual observation and the data from the static force study suggested that the greatest alteration to gland size and the number of glands per field of view/gland separation was occurring across forces less than 0.1N. This finding supported the choice of the minimum and maximum parts of the sinusoidal dynamic force as being 0.005N and 0.075N respectively.

5.7 Results

From the videos of the 9 healthy/fresh bowel specimens, 29 glands were tracked and analysed. 36 glands were tracked from the 7 specimens that had been partially fixed and stiffened by formalin to mimic disease. The morphological changes in response to a sinusoidal force appeared to also be approximately sinusoidal for healthy and pre-treated tissue (see healthy example in Figure 5.6). The mean surface area of the glands during minimum probe contact force (0.005N), which was effectively baseline, was greater for healthy bowel (712 pixels ± 297 SD) than it was for stiffened tissue (379 pixels ± 196 SD) ($p<0.01$).

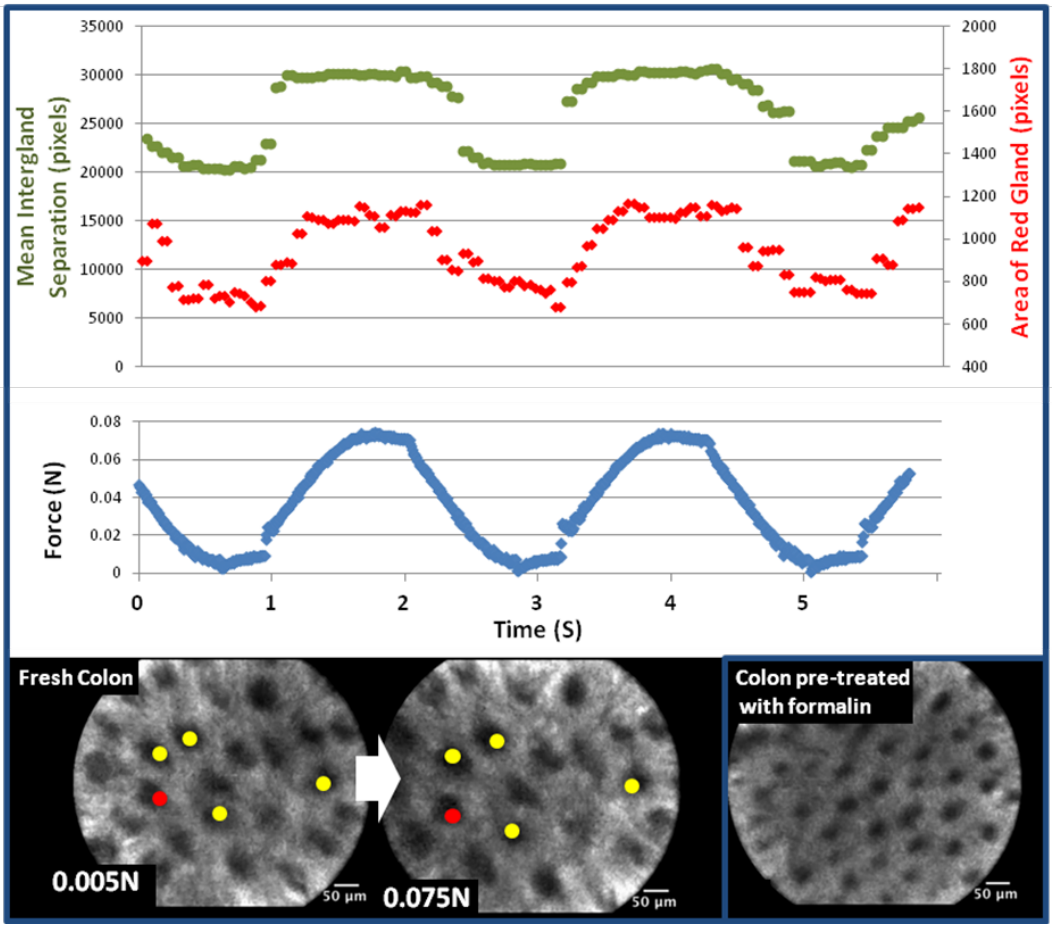


Figure 5.6: An example of the temporal effect of a sinusoidal force on the mean separation of five tracked glands in a fresh piece of colon with the corresponding area of one of the glands (marked in red). Formalin pre-treatment toughens the tissue and appears to condense more glands into the field of view (bottom right).

As the probe was pushed in and out of the mucosa to cyclically increase and decrease the contact force, the mean gland area rose and fell for both tissue types, but for the constant amplitude of force applied, the mean percentage change of mean gland area was greater for the healthy tissue compared to the less compliant stiffened tissue: 52.8% ± 47.4 SD versus 20.1% ± 14.2 SD ($p<0.01$).

Though the glands selected for analysis in each video were picked on their trackability and not on their spatial relationship with one another, probably due to the formalin treatment, the glands analysed within the videos of stiffened tissue were closer together during the minimum probe contact force within the force cycle (0.005N) than the healthy glands: the mean centroid separation at this force was 11.7 (± 5.07 SD) kilopixels versus 16.8 (± 7.61 SD) kilopixels ($p=0.028$).

As the probe was sinuisoidally driven in and out of the mucosa with the linear servo rig, it was evident that the glands in both tissue phenotypes were cyclically becoming more spread out before returning to their original position. Analysis of the percentage change in this intergland separation showed that the stiffened tissue contained glands which separated proportionally less than the healthy ones during the same cyclical force changes: the mean percentage change in intergland separation was 19.3% (± 23.3 SD) for healthy tissue versus 3.66% (± 2.12 SD) for stiffened tissue (p=0.045).

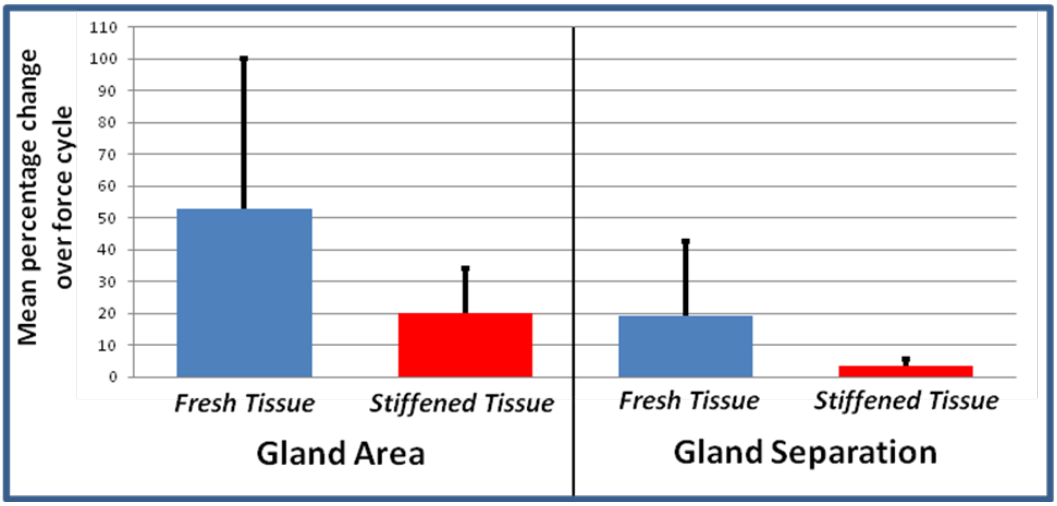


Figure 5.7: Columns demonstrating that for the same additional axial force, the pre-treated tissue's glands did not enlarge or separate to the same degree as the fresh tissue.

5.8 Conclusion

The ultimate aim for the multitude of in vivo optical imaging probes currently being trialled is to provide sufficient information for the clinician to safely make realtime accurate diagnoses and decisions about management without needing to biopsy, or at the very least to be able to take more focussed higher yield biopsies. To this end, pCLE has made enormous progress over the last decade, but in general, still only provides complementary information. For example, as discussed in chapter 2, screening for neoplasia in Barrett's oesophagus has been the focus of most of its clinical research, but the sensitivity was as low as 12% in a recent multi-centre study[160]. Similarly, during screening endoscopy of the lower gastrointestinal tract of asymptomatic patients[91] (a procedure which is likely to put enormous burden on pathology services in the next decade) pCLE would be an invaluable tool if it could obviate the need for biopsy of every

small benign appearing mucosal polyp, but a current sensitivity of 88% is inadequate to do this safely[109]. Current diagnostic criteria for pCLE are predominantly based around qualitative architectural abnormalities, and as such are highly subjective.

Therefore, the second part of this chapter aimed to establish whether the mucosal lining of the gastrointestinal tract provides other, more quantifiable clues as to its phenotype that could potentially be identified during elastographic assessment with pCLE. Computational analysis has shown that with the application of a sinuisoidal axial stress, the dark areas representing glands cyclically enlarge and shrink, but the proportional change in area of healthy glands is over double that of glands from stiffened tissue. The cyclical force also induces glandular dispersion and coalescence, and whilst this is minimal in the stiffened tissue, there is a 19.3% variation in interglandular separation over the force cycle in fresh tissue. It is interesting therefore that the stiffened tissue's glands appear to expand their own area with greater ease than which they disperse; this is partly explained because a change in area is being compared with a linear dimension, but it is possible that their orifices or goblet cells are less affected by the stiffening than the epithelium and lamina propria. The sinusoidal input force was a similar shape to the strains produced, suggesting that both tissues were behaving approximately elastically.

It is known that diseased cells and tissue present altered mechanical properties[314, 324], and that fibrotic or malignant tissue tends to be stiffer than its healthy precursor. Nevertheless, formalin immersion to create protein cross-linking and toughening is a relatively crude method of simulating the increased stiffness of neoplastic change within mucosal tissue, and indeed the baseline morphology is affected. Future work should aim to see if the elastographic response is affected by actual mucosal disease, and also to establish if the results demonstrated using topical contrast agent on flaccid mucosa with very gentle forces on a steady platform can be replicated endoscopically in vivo using intravenous fluorescein.

It is likely that if probe contact force is ever to be adequately controlled or expoited some kind of robotic actuation will be required. This is presented next, in Chapter 6.

Chapter 6 **Probe Manipulation – Improving the Ergonomics and Tracking of pCLE**

6.1 Introduction

In chapter 2 the multiple ergonomic challenges of pCLE were discussed and have been further described in the intervening chapters. Essentially, to adequately exploit its high magnification and fine resolution, the pCLE probe must remain completely still, or translate very gradually and predictably over the tissue to avoid movement artefact. It must abut the tissues near perpendicularly, and not be fazed by tissue deformation, cardiorespiratory movement or peristalsis.

The potential need for control of contact force has been highlighted, with extremes of axial force shown to alter the colonic gland diameter by a factor of two in chapter 5, with different elastographic responses obtained from stressing simulated diseased tissue. In chapter 4 it was shown that axial force may cause subclinical damage to delicate tissue, but back in chapter 3 it was observed that force control is not always straightforward with pCLE through a resistant endoscope working channel, especially if retroflexed.

It was apparent in chapter 3 that, occasionally, marked heterogeneity is apparent in the pCLE sequences analysed post-procedure from what was seemingly a specific lesion or macroscopically uniform area of colorectum or endobronchium. This underscores two requirements:

6.1.1 Probe manipulation for a larger optical biopsy

Using breast lesions as an example, the more tissue that a histopathologist is presented with, the higher the chance of a firm diagnosis: a surgical biopsy provides more

information than a core biopsy, which is itself more informative in most situations than fine needle aspiration cytology. Similarly, small areas sequenced by pCLE do not necessarily represent adjacent tissue characteristics and a more accurate impression should be gleaned if pCLE examines a larger area to illustrate the heterogeneity more accurately, with longer video sequences or preferably a large mosaic. Therefore if a larger area is to be scanned quickly and consistently, one solution could be to incorportate robotic actuation. This could ultimately enable mosaics to be constructed in a more structured way such as a raster pattern or outward spiral; along with the potential benefits of easier navigation of the pCLE probe to the optical biopsy target, and more controlled contact force.

6.1.2 Precise tracking of probe tip location

It is not realistic to assume microarchitectural homogeneity of all examples of endobronchial nodularity or rectal carcinoma, with distinct borders that the translating probe will never stray across. Nor is it possible to accurately identify the geographical target of a pCLE sequence acquired following blind deployment of a probe into perhaps the biliary tree or ureter, or more particularly the peripheral lung with its extensive branching. Chapter 4 illustrated the point that negligible autofluorescence on screen during peripheral lung pCLE may represent the probe having not yet reached the lobule, or be indicative of a large bullous. It is also difficult to guarantee that optical and pinch biopsies are taken from exactly the same target in the lung. Hence, for a diagnosis to be ever feasible from a pCLE image, the clinician must know the area from which it was taken.

In the peritoneal cavity or bowel lumen a macroscopic image can be saved of the specific point/s that the probe has touched, although precise co-registration of pCLE and white light endoscope imaging would be of great benefit for post-procedure analysis. If there are local features to put the site in context, it may be possible to revisit almost the same place for subsequent follow-up imaging or treatment, especially if a tissue biopsy has been performed and has not completely healed, as was found in the rectal cancer patient in chapter 3.

However, during peripheral lung bronchoscopy, accurately linking an individual pCLE video sequence with a site (essentially its corresponding CT image) is sometimes difficult due to the inherent problems of establishing where the tip of the probe has been blindly deployed to - without using fluoroscopy.

The bronchial tree comprises over 20 generations. When the bronchoscopist advances the probe blindly from beyond the bronschope tip, at perhaps the 3rd or 4th generation, into an area of peripheral lung, is it even possible to predict where the probe will travel to?

Perhaps, analogous to a locomotive following the path of least resistance determined by the setting of the points on the track, the physical constraints of the bronchial tree dictate that the probe can only ever end up in one place: factors like speed, angle of insertion, relationship within breathing cycle are irrelevant and the probe's destiny is pre-determined. This would lead to the exciting possibility of the CT scan or the resistance experienced during deployment of the probe providing sufficient information to predict where the probe's image is being acquired from without using fluoroscopy. It may also allow the MDT to establish if access to a lesion with pCLE (or indeed TBB) would ever be feasible bronchoscopically, or whether diagnosis would be expedited by a transthoracic approach from the outset.

However, this suggestion is contradicted by an individual case report taken from the peripheral lung pCLE imaging study in chapter 4. A 67 year old ex-smoker presented with a spiculated mass in the upper segment of the left lower lobe (LB6). Subsequently, transthoracic biopsy showed that it was a non-small cell lung carcinoma. During pCLE bronchoscopy, the bronchoscope was navigated as far distally as possible down the tapering bronchial tree before blind probe deployment distally into the opening of the corresponding segmental bronchus of the lesion. Initial insertion yielded a video sequence with surprisingly relatively normal density fluorescent septal wall appearance (Figure 6.1). Two subsequent deployments into the same bronchial orifice produced video images with attenuated autofluorescence and diminished structural distinctiveness. It was hypothesised that these sequences were from structurally dissimilar regions of the lung, and potentially identifiable variables in the workflow were responsible for the probe having more than one terminal destination.

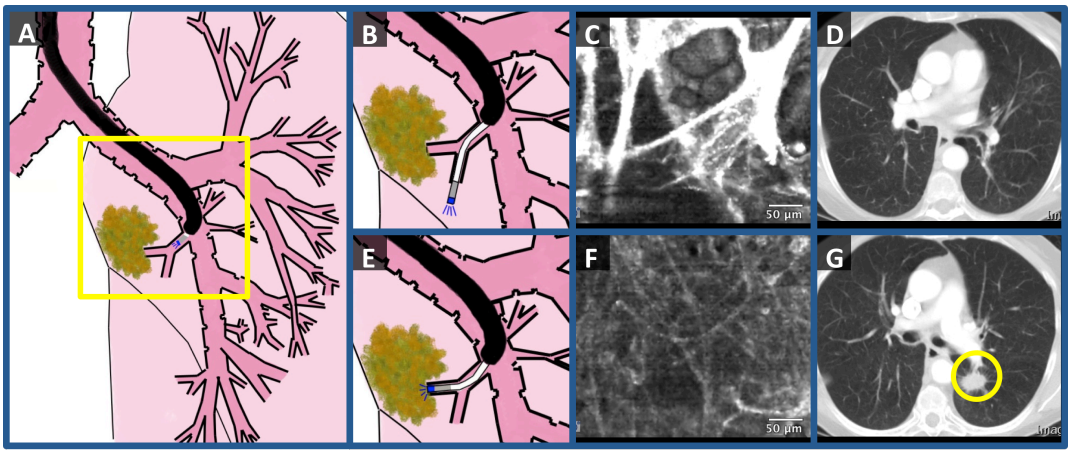


Figure 6.1: LB6 was cannulated with the probe (A), in an attempt to image the circled lesion on CT in (G). It is suspected that the probe was able to pass either inferiorly (B) and image relatively normal lung (C&D) or pass superiorly (E) to image abnormal parenchyma (F&G).

6.1.3 The aims and hypotheses of the robotic manipulation and tracking studies

Two studies were performed and are described in turn in the following sections, with an overall discussion at the end of the chapter.

1. The manipulation study looked at the feasibility of robotic actuation for pCLE optical biopsy. Considering the specific ergonomic and technical challenges posed by pCLE probe tip manipulation within the peritoneal cavity, with its lack of luminal restraint and irregular geometry, a projection was made of how a multi-articulated robotic endoscope would safely perform transvaginal pCLE peritoneoscopy, using an estimated workspace derived from patients' computed tomography (CT) scans. A porcine study was then performed to assess the feasibility of this ergonomically more sophisticated method of acquiring interpretable targeted pCLE optical biopsies.

2. The aim of the tracking study was to assess any predictability of probe tip destination in an ex vivo lung porcine model. The hypothesis was that for peripheral lung pCLE, as the probe tip is deployed beyond the starting point of the most distally visualised bronchial divisions, there are multiple potential terminal destinations.

6.2 Methods - Robotic Manipulation Study

6.2.1 Articulated robotic endoscope

The articulated robotic endoscope has been previously described[328, 329]. In summary, it provides seven independently controllable degrees-of-freedom from five serially connected segments attached to a rigid aluminium shaft. Proximal to the distal and middle segments are universal joints each providing ±45° pitch and ±45° yaw, whereas the proximal three joints provide ±45° yaw only. Combined, the endoscope's distal tip can pan ±90° vertically and ±225° horizontally. The 500mm length shaft, 44mm proximal and middle segments, and 36mm distal segment are all 12.5mm in diameter and therefore compatible with existing trocar ports. The device is insulated and protected by a bellowed latex sheath.

Each of the degrees-of-freedom is actuated by an embedded Ø4mm Brushless DC micromotor (Namiki Precision Jewel Ltd, SBL04-0829) with a 337:1 planetary gearbox. The rotary motion of the motor is converted to joint rotation via an internal mechanism. The device features three internal channels: a Ø1.8mm internal channel to pass power and signal lines for the motors; a Ø3mm channel to pass an IntroSpicioTM 115 Micro CCD video camera (Medigus Ltd, Israel); and a Ø3.5mm channel through which standard endoscopic instrumentation can be passed. In this study, the latter channel was used for the pCLE probe. The device is controlled via a thumbstick embedded within a handheld controller[329].

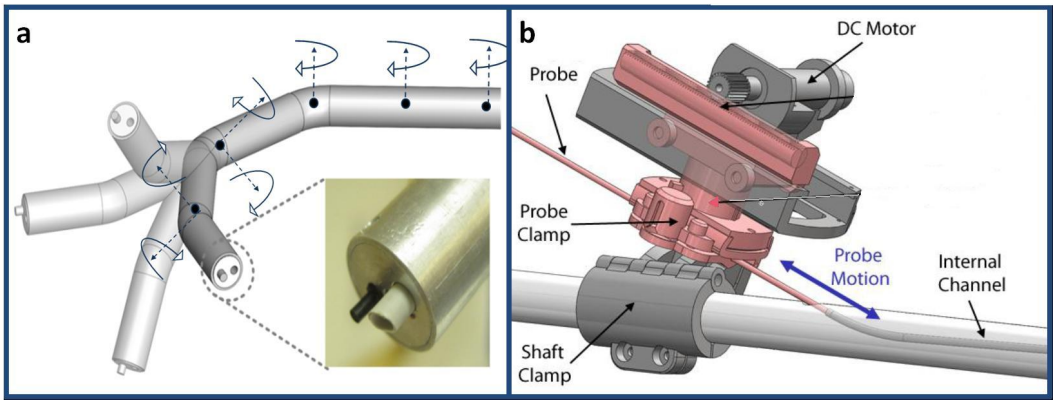


Figure 6.2 The 7 degrees-of-freedom robotic articulated endoscope (a) has two operating channels for the camera and interchangeable instruments (eg. pCLE probe). In the linear translation mechanism schematic (b), the components which translate to servo the probe (rack, slider, clamp and pCLE probe) are shaded in red.

6.2.2 Imaging probe and deployment

A standard 2.5mm diameter Gastroflex pCLE probe was inserted through the 3.5mm operating channel of the articulated endoscope.

To simplify the ergonomics of engaging the pCLE probe with target tissues, and to enable the operator to manually maintain effective contact between probe tip and tissue regardless of tissue movement and distal joint movement, a linear translation mechanism is attached to the proximal end of the robot's shaft (Figure 6.2). Where the probe exits the robot proximally, it is clamped into the translation mechanism which utilises a 6V brushed DC motor and a rack and pinion slider to manually advance or retract the probe at a fixed speed based on a switch on the handheld controller. Note that in chapter 5 the translation device produced a prescribed force; this was not feasible with the robot, as the probe tip was substantially further away from the transducer and the probe was variably contorted along the articulating endoscope shaft. Nevertheless, the aim of this mechatronically-assisted approach was to allow the operator to both steer the distal tip and engage the probe using a single hand, thus simplifying the overall deployment of the pCLE probe when compared to a conventional endoscope.

6.2.3 Estimation of clinical workspace

To predict how the robot would perform pCLE peritoneoscopy clinically, an estimated average pneumoperitoneum workspace was required. Whilst it is known that the diaphragm is raised 2-3cm caudally by a pneumoperitoneum[330, 331], and external elevation of the abdominal wall fascia prior to insufflation raises the umbilicus by approximately 8cm[332], there is a paucity of data on the shape and size of the pneumoperitoneum created for intraperitoneal procedures.

The shape of the workspace was therefore obtained from the CT scan of a patient with a pneumoperitoneum secondary to a perforated colon: the extraluminal air provided a 3-dimensional mesh shape which was then smoothed across the deep surface.

The mean maximum length and width of the potential space of the peritoneal cavity was obtained using ten consecutive outpatient female abdominopelvic computed tomography (CT) scans. The length was measured from the most cranial part of the diaphragm to the parietal peritoneum lying immediately deep to the most anterior aspect of the pubic symphisis (319.5mm +/- 21.3mm); for the workspace, 25mm was added to this for

insufflatory diaphragmatic elevation[330, 331]. The width was calculated across the peritoneal cavity at the widest part of the iliac crests (235mm +/- 22.3mm). From the inferior tip of the pneumoperitoneum the posterior colpotomy for the transvaginal entry point was a mean of 20mm +/-8.2mm craniocaudally and 58mm +/-13 anteroposteriorly. The 3-dimensional mesh was then shrunk to these dimensions creating a pneumoperitoneum depth of 93mm.

6.2.4 Projection of robotic pCLE in workspace

An optimisation algorithm was developed to establish the proportion of the mesh surface that could be touched by the probe tip, to a tolerance of 1mm, at various different probe/tissue angles, using all possible robot configurations for every point on the visceral and parietal workspace surface. The software was implemented in Matlab®. In the projection, the robot was treated as having eleven degrees-of-freedom. These arose from a) the seven degrees-of-freedom shown in Figure 6.2, b) translation in and out of the patient, c) roll about the robot axis, d) 30 degrees of tilt in the sagittal plane, and e) 30 degrees of sideways yaw. Yaw and tilt were pivoted at the posterior colpotomy. The pCLE probe tip was assumed to lie 10mm beyond the distal tip of the robot.

6.2.5 Study animal and in vivo imaging procedure

An adult large white landrace crossbread female pig (70kg) was anaesthetised with intramuscular ketamine 5mg/kg and xylazine 1mg/kg. After endotracheal intubation anaesthesia was maintained with oxygen, nitrous oxide and isofluorane, and at the conclusion of the procedure, the animal was euthanized with anaesthetic overdose using sodium pentabarbitone (Lethobarb). The study protocol was approved by the home office under the Home Office Animals for Scientific Procedure Act 1986, (number 80/2297).

Intravenous fluorescein sodium 10% (Martindale's, UK) was used as a contrast agent. 0.05ml/kg body weight[73] was used with a saline flush, 5 minutes before pCLE imaging[74].

Pneumoperitoneum was created through a 10mm umbilical port and maintained at 14mmHg; this port accommodated a laparoscope which was used to record footage of the robot during the procedure. Transvaginal access was via a bespoke 30cm trocar inserted

through a posterior colpotomy. The rigid proximal end of the endoscope was manipulated by the surgeon, and the articulated distal end was navigated between pre-determined anatomical regions of the peritoneal cavity using the handheld controller. At each target, with the distal tip of the endoscope 10-20mm from the tissue surface, the axial deployment mechanism was switched on to advance the probe until tissue contact was made. pCLE videos were then recorded as the probe was translated across the tissue surface using controlled motion of the distal tip. Once acquisition was complete, the probe was retracted back into the channel using the deployment mechanism.

Cellvizio Viewer software (Mauna Kea Technologies, Paris, France) was used after the procedure to create mosaics from the video sequences. Images were compared with known histology.

6.3 Results - Robotic Manipulation Study

6.3.1 Workspace analysis

The algorithm calculated that 88% of the estimated workspace mesh surface could be reached (Table 6.1).Over half of the workspace could be contacted perpendicularly.

Contact angle between probe and tissue	Percentage of mesh surface that probe tip can touch within 1mm with transvaginal approach
0-90° (any angle)	88%
≥45°	83%
≥60°	78%
≥70°	70%
≥80°	61%
90°	53%

Table 6.1: The proportion of the workspace mesh surface that would be reached for different angles of the pCLE probe.

By examining the heatmaps generated from this analysis, it is clear that the only unreachable surfaces (12%) are within the workspace pelvis, especially on the deep visceral surface (Figure 6.3). Here, the robot is retroflexed, rendering its transvaginal forward translation unhelpful for closing in on the probe's target. It is also evident that the recesses of the workspace and some areas of the irregularly contoured visceral surface can only be reached at angles shallower than 90°.

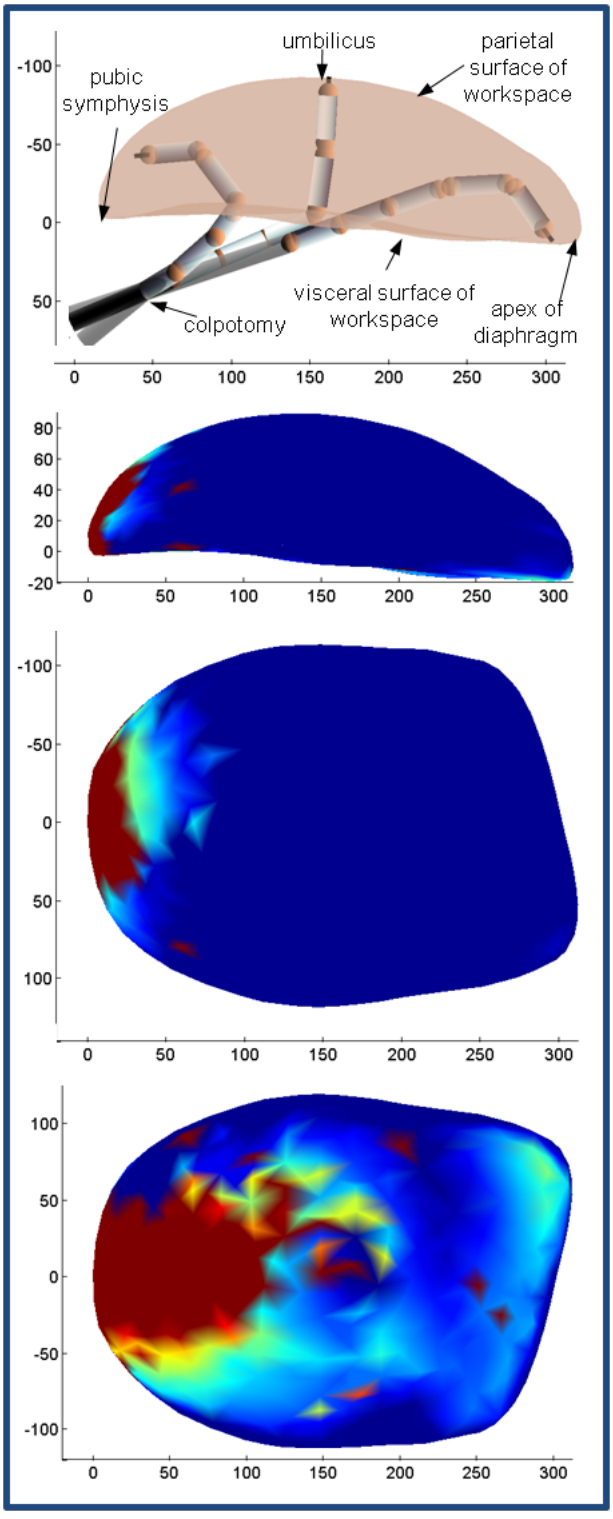


Figure 6.3: The top diagram projects the configurations required by the robot to target three regions of the pneumoperitoneum workspace during transvaginal deployment. Underneath it are heatmaps which illustrate the areas of the workspace that could be pCLE biopsied at particular angles (proceeding downwards is a lateral view from the left; a view of the parietal peritoneum from the outside; and a view of the visceral surface from below the workspace). Dark blue, lighter blue/yellow, and red areas can be abutted at a maximum of 90°, 45-90° and <45° respectively by the probe.

6.3.2 pCLE peritoneoscopy

The operator was able to systematically navigate the articulated endoscope throughout predefined regions of the abdominal cavity using the onboard camera. It took 3 minutes to provide adequate onboard views of the main viscera. After switch operated deployment of the probe, providing an optical biopsy took a further 1-2minutes for each organ. The deployed pCLE probe was able to translate sufficiently slowly under active control of the distal joint to provide artefact free videos and therefore mosaics up to 2mm in length to effectively increase the image field-of-view of parietal peritoneum, liver, and spleen (Figure 6.4). Movement from positive ventilation provided enough translation between probe and serosal surface for imaging of some areas of liver and spleen. It was necessary to increase the probe deployment length to image pelvic surfaces. Tissue deformation frequently enabled imaging at shallower angles than 90°. There was no evidence of tissue damage from the probe.

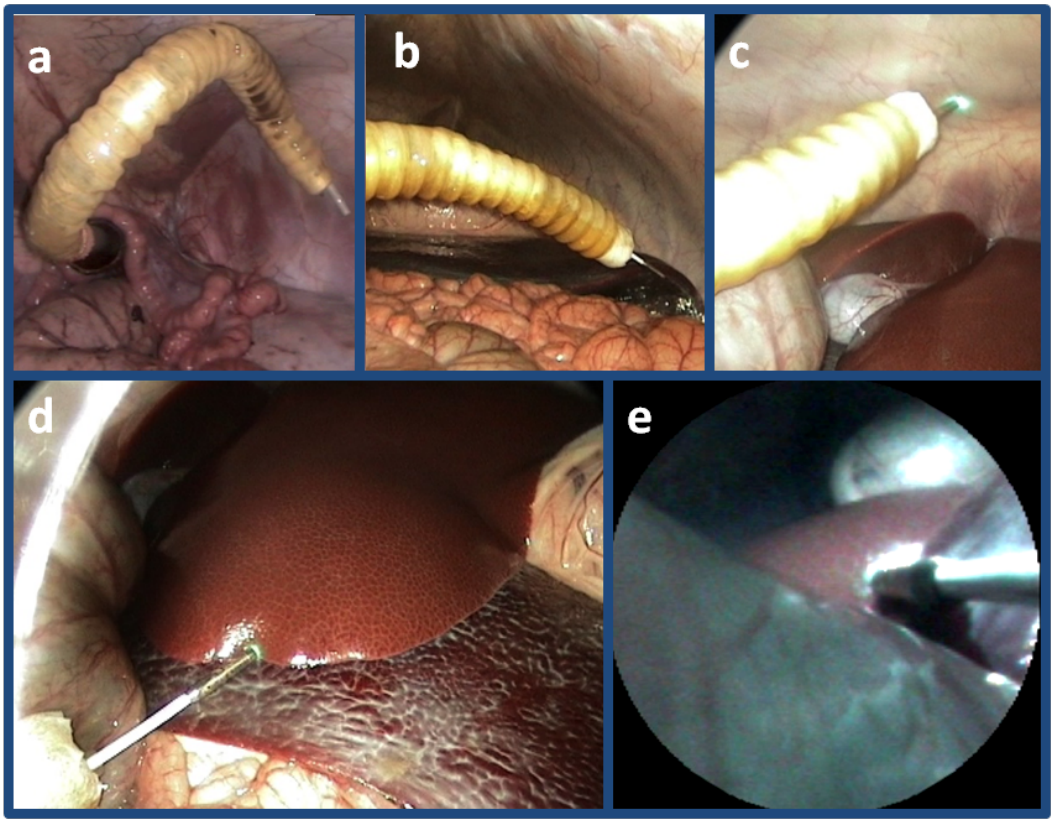


Figure 6.4: The robot was inserted transvaginally and navigated around the abdominopelvic cavity (a). Optical biopsies were obtained of spleen (b), peritoneum of anterior abdominal wall (c), and liver (d). (e) shows the onboard camera view of the liver during pCLE imaging.

6.3.3 Interpretability of robotic actuated optical biopsies

Whilst the images from the stomach surface had no recognisable features, the robot enabled recognisable stills and mosaics to be acquired of other organs (Figure 6.5).

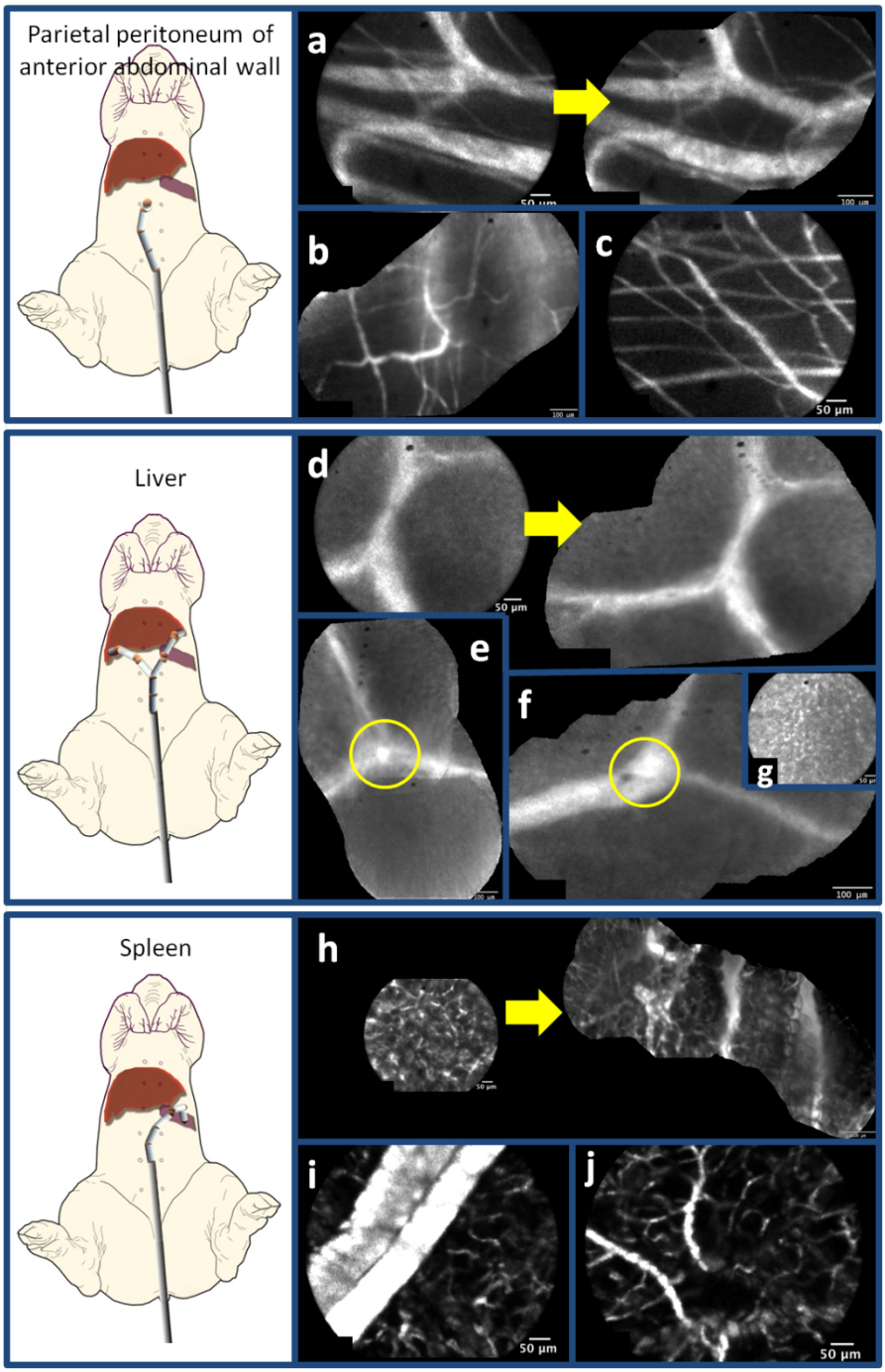


Figure 6.5 Robotically acquired pCLE optical biopsies of peritoneum, liver and spleen. Courtesy of slow and controlled movements of the distal robotic joint, it was possible to use mosaicing software to expand the field-of-view by up to 4 times (approximately 2mm) to create more representative and interpretable optical biopsies (a, d & h show the expansion). The parietal peritoneum of the anterior abdominal wall shows 10 to 100µm blood vessels (a-c). The liver images show distinct features of liver parenchyma, with mildly fluorescent hepatocytes contrasted against dark sinusoids (particularly prominent in (g)), arranged into hexagonal lobules (d-f) each surrounded by fluorescent vascular septa with highly fluorescent branches of the portal vein at the hepatic triad present at each lobule corner (marked by circles). The splenic parenchyma shows dark cords of billroth surrounded by extracellular space containing fluorescent blood. Larger diameter sinusoids are clearest in j. The 100µm vessel in i is likely to be a penicillar arteriole (a straight arteriolar branch of one of the central arteries)[333].

Peritoneum: In the parietal peritoneum of the anterior abdominal wall, fluorescein was observed to course through the straight and angularly bifurcating vessels deep to the mesothelial monolayer. These vessels ranged from 10µm (capillaries) to 100µm (arterioles and venules).

Liver: With the porcine liver capsule reported as being less than 100µm thick[334], the recognisable features of liver parenchyma deep to the capsule are compatible with the 100µm confocal imaging depth. In the porcine model, each 1-2mm hexagonal liver acinus/lobule is surrounded by thick, vascular, well developed connective tissue septa that branch from the capsule[335]. Under pCLE these were highly fluorescent and delineated the edges of the lobules. Furthermore, enhanced fluorescence was seen at the highly vascular portal triads present at each corner of the lobule, and a characteristic mottling was present within each lobule from dark sinusoids lined by mildly fluorescent hepatocytes.

Spleen: Some areas of the spleen provided minimal fluorescence and it is likely that the confocal imaging depth was within a relatively avascular area of the 50-165µm[336] splenic capsule. Elsewhere there was a unique appearance from the fluorescent blood filled spaces of the splenic parenchyma under the capsule. It can be surmised that these structures are part of the red pulp and comprise tortuous 20µm sinusoids (modified endothelial lined venules) together with a narrower network of blood filled extracellular space surrounding the cords of billroth.

6.4 Discussion - Robotic Manipulation Study

pCLE is a new in situ imaging technology where potential diagnostic tissue targets are being continually expanded. However, regardless of optical biopsy location, cellular level resolution brings the need for careful ergonomic control. Still images can be created when the probe is stationary relative to the tissue. With steady, slow movement over a couple of millimetres, a more representative area can be imaged, and the resultant increased field-of-view mosaics may enhance the interpretability for the operator[101]. The instrumentation available to perform these sometimes awkward manoeuvres is

limited[52]; the first aim of this chapter was to establish whether robotic control could be the solution.

By estimating the clinical workspace provided by a pneumoperitoneum in the average female, it was calculated that a 7 degrees-of-freedom robotic endoscope, when introduced transvaginally with the benefits of manual roll, tilt, yaw and translation movements, would allow 88% of the peritoneal cavity to be abutted by a pCLE probe that had been deployed by 10mm. If the optimisation algorithm was adjusted to permit longer deployment of the probe, it is probable that much of the unreachable pelvic region could be contacted. Perpendicular probe abutment is preferable for consistent images, but only 53% of the cavity would be abutted at a minimum of 90°. Nevertheless, deformable soft tissues tend to pucker, enabling shallower angles to often achieve adequate results.

In the subsequent feasibility study we demonstrated that control via an articulated robotic endoscope would enable simple pCLE optical biopsy in a transvaginal porcine NOTES setting. The robotic endoscope was navigated around the peritoneal cavity and after the probe had been deployed using the linear translation mechanism, small yaw movements of the distal joint enabled mosaics of up to 2mm to be constructed.

There were specific features representing the architecture of healthy liver, spleen and peritoneum. If metastatic deposits display characteristic pCLE features, clinical translation for assessment of suspicious peritoneal nodules in patients merits further evaluation. It is likely that novel fluorescent biomarkers which are switched on by malignant tissue[337], or that target specific peptides which are expressed in cancer[126] will help with this.

It should be noted that there are limitations to the workspace estimation used in this paper. For example, the shape reflected a single pathological pneumoperitoneum, where consciousness and abdominal muscular contraction secondary to peritonism may have created a different contour compared to a surgical pneumoperitoneum. During surgery, 12-16mmHg pressure is often used (though there is some evidence that the workspace is not altered by lower pressure[338]), but the pressure of the pathological pneumoperitoneum could not be measured. Nevertheless, abdominal compartment syndrome (ACS) occurs above 20mmHg, and, excluding iatrogenic endoscopic injury, acute visceral perforation is a rare cause of ACS[339], which suggests that a pathological pneumoperiteonum is at relatively low pressure, and therefore of no increased volume. In practice the workspace may well be intentionally increased and deformed intraoperatively

by intraoperative patient positioning and manipulation of the intestines, providing even more space for the robot.

If translatable, there are numerous potential clinical applications for this ergonomically enhanced intraperitoneal pCLE. For example, in chronic renal failure patients undergoing peritoneal dialysis (PD), establishing the cause of ultrafiltration failure sometimes requires a peritoneal biopsy. Encapsulating peritoneal sclerosis is a potentially fatal complication of PD with inadequate early diagnostic investigations[340]. Nevertheless, there is a correlation between decreased ultrafiltration and a submesothelial thickening with vasculopathy. These vascular changes include neovascularisation, vessel wall thickening and dilatation[341]. Experimental chapters 3, 4, and 7 confirm that pCLE provides high resolution images of the microvessels and could therefore have a role in the future in longitudinal study of the membrane, particularly if minimum invasive access could be developed – such as through NOTES, or a wide diameter PD catheter[342]. Perhaps a device such as has been described could provide rapid and simple in situ diagnosis of ultrafiltration failure in real time. However, it is likely that cancer staging, and diagnosis of liver disease would be the main targets for robotically controlled pCLE peritoneoscopy [226, 343], and its precise movements may have a role in making nCLE of solid organs safer[227, 344].

The addition of automated control of the distal probe tip contact force could potentially make the ergonomics even more straightforward, increase safety and improve image consistency. It might require the use of a distal force transducer, or a means of indirectly assessing the distal contact force by adjusting the values measured at the proximal translation device according to the conformation of the flexible endoscope.

6.5 Methods – Tracking Study

A balloon cuffed size 15 endotracheal tube was inserted into the left main bronchus of a fresh left pig lung. It was connected to a continuous positive airways pressure (CPAP) machine (Resmed Sullivan® S6 elite) and placed "supine" in a non-restrictive perspex tray secured with zip ties around the trachea (Figure 6.6). After 15 minutes of continuous flow to ensure maximum inflation, 20 radioopaque fiducial markers (3mm Suremark® V30 spheres) were attached to the visceral pleura using Loctite® superglue adhesive. The inflated lung was then imaged with HRCT using 0.5mm slices with subsequent resolution into transverse, sagittal and coronal sections.

With the lung tray then anchored at 45 degrees supine, a lubricated 6mm Olympus BF10 bronchoscope was inserted through the endotracheal tube and navigated sequentially to all of the most distally navigable bronchial branches. At each of these bronchoscope tip locations, the pCLE probe was deployed with constant gentle force until a subpleural blue glow was visible. The probe was then reinserted several times until all possible destinations had been found. Where feasible, this process incorporated different angles of approach and positions of the bronchoscope with respect to the bronchus being cannulated. For each of the probe tip's supleural terminal destinations, the straight line distance to the three nearest fiducials on the relevant pleural surface was measured by ruler.

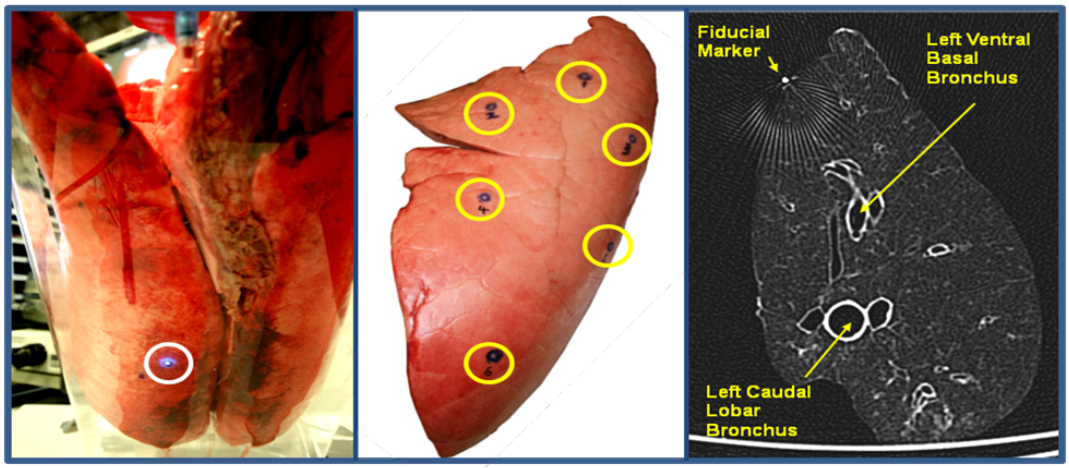


Figure 6.6 The argon blue laser light appearing subpleurally after probe deployment down a dorsal branch of the pig's left caudal lobar bronchus is circled in white (left). Fiducial markers, circled in yellow, were stuck to the inflated lung (middle). An axial slice of the mid pig lung is viewed from below (right).

The coordinates of the probe tip destinations were retrospectively estimated by iterative optimisation using Praxis software. In essence, after establishing the fiducial coordinates on the CT scan images using the MRIcroN viewer, the sum of squared differences of the unknown point to the fiducials was minimised[345, 346]. Estimates were disregarded for any further assessment if they required the algorithm to change any of the measurements to a fiducial by more than 11mm. These were regarded as a software calculation flaw. Where a bronchoscope tip location produced more than one probe tip destination, the maximum distance between these estimated points was calculated. The distance between each starting point and optimised terminal destination was measured on CT (rather than simply via length of probe deployment).

6.6 Results - Tracking Study

Whilst the size and volume of porcine lungs is comparable to human lungs[347], the anatomy differs markedly. For example, there are four lobes on the right (the right apical lobar bronchus to the right apical lobe stems from the trachea) but only two on the left[348]. This study only used the left lung and the CPAP machine inflated it with a constant 20cmH_2O. Its height was comparable to an adult human's at 489mm from the most caudal part of the caudal lobe to a point level with the apex of the apical lobe. With the stiff probe contained within the biopsy channel, it was not possible to flex the bronchoscope sufficiently to cannulate the apical lobe via the apical bronchus off the left principal bronchus.

A systematic inspection of the left caudal lobe with the bronchoscope revealed 28 tertiary and quarternary bronchi branching from the caudal lobar bronchus where the pCLE but not the bronchoscope could fit (starting points) (Figure 6.7). Awkward bronchial branch angles prevented pCLE deployment from 7 starting points, and in 2 further cases the probe stopped before its blue haze was visible. Therefore, 19 starting points yielded recordable terminal destinations of the probe. After multiple insertions from each of these starting points, it was concluded that 10 had a single possible destination and 9 had multiple destinations (3 had 2 destinations, 3 had 3 destinations, with 3 starting points even having 4 possible terminal destinations) (Table 6.2). The mean distance between the multiple terminal destinations was 33.98mm ± 21.43. The mean distance from the starting points to the terminal destinations was 57.4mm ± 15.5. There was no significant difference between this deployment distance when comparing the group comprising

starting points yielding multiple destinations with the group yielding single destinations (data not shown).

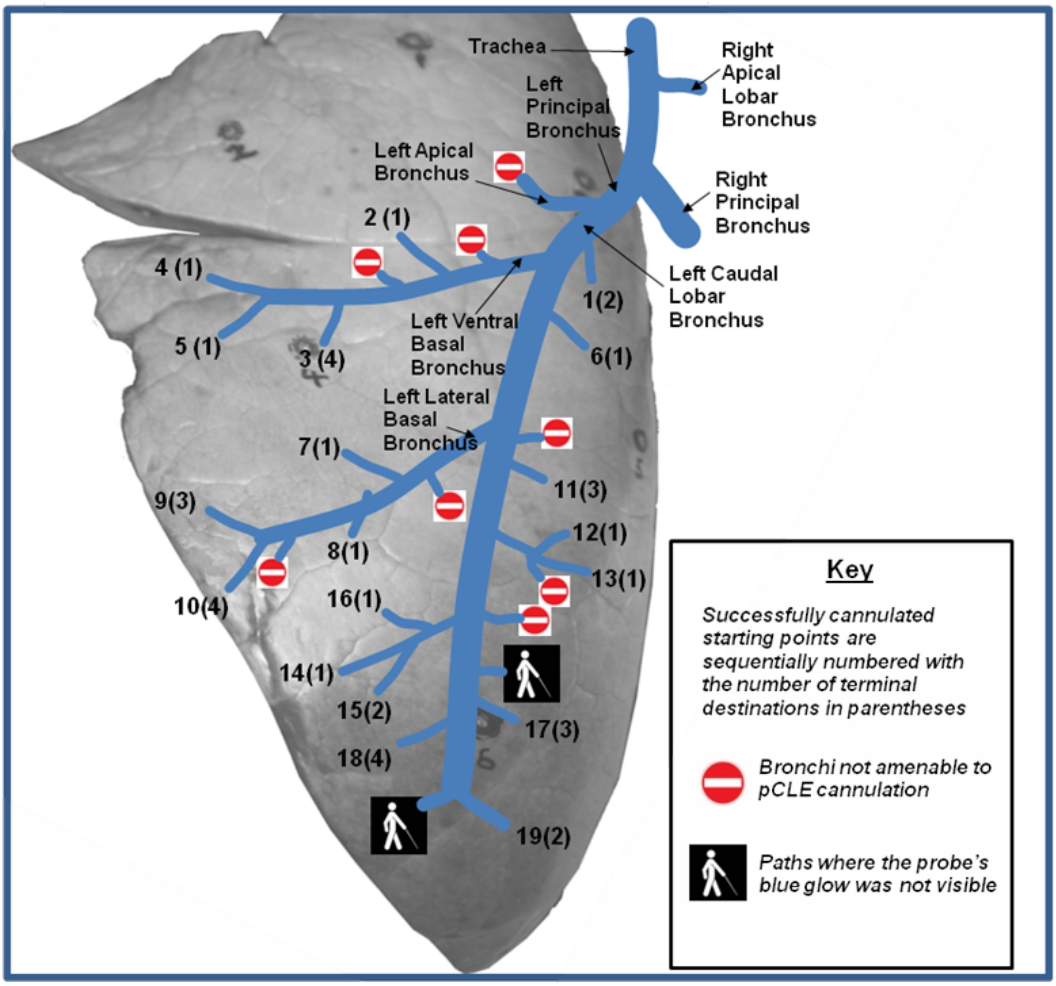


Figure 6.7: A schematic representation of the pig lung's bronchial tree at bronchoscopy with the number of terminal destinations possible (in parentheses) for each starting point 1-19.

Number of Starting Point	Resulting Number of Destinations	Distance from Starting Point to Destination(s) (mm)		Maximum Distance Between Any Two Terminal Destinations of Probe (mm)
10	4	70.1	$\bar{x}$ = 65.2	44.11
		64.2		
		52.5		
		74.19		
18	4	82.41	$\bar{x}$ = 64.6	75.03
		66.02		
		45.51		
3	4	Difficult to assuredly state starting coordinates on CT		16.62
11	3	63.15	$\bar{x}$ =63.2	35.06
		60.38		
		65.94		
17	3	21.98	$\bar{x}$ = 38.4	45.27
		38.07		
		55.28		
9	3	37.73	$\bar{x}$ = 45.6	22.63
		53.37		
1	2	72.8	$\bar{x}$ = 71.5	5.12
		70.2		
15	2	73.89	$\bar{x}$ = 63.2	28.02
		52.56		
19	2	25.33		*~11 but ignored*
2	1	43.07		N/A
6	1	77.96		N/A
7	1	47.75		N/A
8	1	80.62		N/A
12	1	53.3		N/A
4	1	Difficult to assuredly state starting coordinates on CT		N/A
5	1	Difficult to assuredly state starting coordinates on CT		N/A
13	1	62.2		N/A
14	1	72.4		N/A
16	1	44.3		N/A
		Mean ± SD = 57.4 ± 15.5		**Mean ± SD = 33.98 ± 21.43**

Table 6.2 A table outlining the length of probe deployment from each starting point to terminal destination, and the maximum distances between possible probe tip terminal destinations (the 3 destinations 9a, 18b, 19a were removed from the data table as their computed coordinates would have required their measurements to fiducials to change by ≥ 11mm).

6.7 Discussion - Tracking Study

This study supports the hypothesis that a pCLE probe will not always arrive in the same acinus after peripheral deployment into the most distally visualised part of the bronchial tree. In a simple, carefully controlled test environment of a pig lung, only about half of the most distally bronchoscopically visualised openings for pCLE deployment have a single route that the probe passes down; the other openings have two or more potential routes of passage.

For a given bronchial tree, the path of a probe of fixed diameter and stiffness will depend upon the angle and position that the probe approaches the bronchus at, as well as levels of endogenous lubrication, possible trauma from previous cannulations, and in vivo the respiratory cycle phase as the probe "chooses" its path at each bifurcation. Where there are bifurcations, branches and therefore "options" for the probe beyond the visual limit of the bronchoscopist, the maximum distance that the resultant terminal destinations will be separated was 34mm on average in this model, although the maximum was 75mm when the probe was deployed from the most caudal lateral branch of the caudal lobar bronchus (number 18).

This uncertainty compromises the reliable interpretation of attempted pCLE imaging of a) solitary pulmonary nodules (SPNs) discovered on computed tomography (CT) but not visible at bronchoscopy, as demonstrated by the case report on page 119, and b) bronchopulmonary segments heterogeneously affected by parenchymal lung diseases.

This issue of imprecise peripheral pCLE navigation mirrors the variable diagnostic yield from attempted transbronchial lung biopsy (TBB). The yield is only 19-62% for SPNs[349, 350], though positively correlated with both size and centrality[351]. For TBB of parenchymal lung diseases the yield is better, but nevertheless it diminishes where there is sparse radiographic involvement[352]. Other methods designed to improve the accuracy of lung biopsy without resorting to surgery include X-ray[353] and CT-fluoroscopy guided TBB[354], endobronchial ultrasound-guided TBB[355], TBB using an electromagnetically guided steerable bronchoscope[356] and CT guided transthoracic needle aspiration[357]. However, a diagnosis cannot always be provided by these methods and there are added issues such as pneumothorax and bleeding risks from biopsy, and the additional radiation exposure during any fluoroscopic guidance.

SPNs are by most definitions 10-30mm diameter on CT[358] and are a major target for TBB and, perhaps in the future, pCLE. Therefore, without a means of predicting and tracking its course, pCLE could easily miss an SPN if human lung starting points provide similar divergence from multiple available paths[1].

It would perhaps be logical for those starting points furthest from the pleura to have more potential for divergence of the probe but the deployment distances were no different between the single destination and multiple destination groups. This could be that the deployment distances were insufficiently dissimilar between the two groups or, perhaps less likely, that the bifurcations responsible for the multiple destinations occur distally.

There are limitations to this study beyond any inherent errors in the computations of terminal destination coordinates from the fiducial measurements and the arguable need for repetition of the results in more pig lungs. Whilst porcine and human lungs are comparably sized[359], and the subgross anatomy is similar[360], the lobes are different as previously discussed, and the mural cartilage extends more distally within the tracheobronchial tree providing the pig lung with cartilage to within three bronchiole generations of the acinus versus ten in the human lung.[361] The pig lung is susceptible to deformation from both dehydration (between the CT scan and the end of the extended bronchoscopy) and from necessary tilting of the Perspex tray to measure the terminal destinations on the posterior surface. Furthermore the probe might behave differently in continuously inflated lungs, with positive pressure, and with less external restraint than a thoracic cavity. Only two paths yielded invisible terminal destinations; fluoroscopy or adaptation of the probe with tracking technology would be required to identify them. Even with careful insertion, in this porcine model where peripheral pCLE images are poor, false passages or deployment beyond the lobules might be possible. It was certainly apparent that without careful observation, subpleural skimming of the probe could create the illusion of additional terminal destinations. This would probably create an impression of there being more divergence of the routes than is the case. With unlimited resources, tracking the nuances of the probe path would be best performed by serial CT scan.

[1] In the pig lung, the starting points were a mean of 57.4mm from the pleural destinations. This compares similarly with a mean of 82.2mm deployment in patients (data not shown in chapter 4 as only measured in 5 patients; range 65-125mm). (A longer deployment could lead to greater potential divergence, and thus error).

6.8 Conclusion

The robotic probe manipulator is projected to have the ergonomic requirements to perform pCLE peritoneoscopy. In the porcine model it enables controlled, steady contact translations of a pCLE probe for safely acquiring distortion free characteristic near-histological grade submesothelial images of viscera within the peritoneal cavity. Other future work will include assessing the device's role for pCLE via transumbilical SILS, and directly comparing its ergonomics with conventional endoscopic pCLE within the abdominal cavity[17] and eventually the gastrointestinal lumen. Currently, the linear deployment mechanism is designed to initiate contact and maintain it during extensive probe translations, but with development dynamic force control should be possible. Future work should also identify whether the actuator can help maintain image consistency and actually produce larger controlled lateral translations to rapidly mosaic larger areas.

This chapter has also addressed the significant issue of probe tracking, using the peripheral lung as an important example. It has found that if optical biopsy of the lung parenchyma with technologies such as pCLE is to develop without the targeting issues that affect TBB, a more accurate prediction of probe tip location will be required, perhaps using one of the technologies mentioned in the introduction to the chapter. A robotic manipulator such as the one employed in this chapter could be part of a more integrated approach to recording where the probe tip has been during pCLE and white light videos, and with the potential for the robot to incorporate more accurate probe contact force measurements towards its distal end, it could even have a role in parenchymal lung pCLE for predicting the route of the probe through the constantly altering resistance to deployment through the bronchial tree's bifurcations.

Chapter 7 Chronic Radiation Proctopathy Assessment with pCLE

7.1 Introduction

7.1.1 pCLE and vascularity

For pCLE to achieve its potential in terms of maximising its diagnostic accuracy and generating a clinical niche greater than that of an expensive experimental device, it is important for it to focus on its "Unique Selling Points". One of these, as investigated in chapter 4, is its ability to access relatively restricted regions. Another is its ability to delineate blood vessels and dynamic circulation in vivo. As an illustration of the importance of blood vessel morphology in tumourgenesis, it was previously described in chapter 2 that CLE using topical acriflavine can easily identify a severely dysplastic uterine cervix but, similar to conventional colposcopy, struggles to differentiate between the lesser grades of abnormality[177]. Immunohistochemical analysis shows that as the dysplasia progresses from CIN1 to CIN3, and then into microinvasive carcinoma, microvessel density increases[362-364]. Similarly, as measured by eCLE, microvessel diameter quantitatively increases by half between Barrett's oesophagus and dysplasia[163]. Measurement of the microvessel density may also help predict survival and the likelihood of recurrence in many cancers, and may also help guide treatment decisions[365]. pCLE has potential benefits over eCLE for this purpose; eCLE can identify microvessels and contrast agent leakage, but unlike pCLE, its inferior frame rate renders it incapable of assessing erythrocyte flow rate. In an in vivo animal model of pancreatic cancer, pCLE has been used to quantitatively show differences in microvessel diameter, density and fractal geometry, by developing a vessel segmentation and delineation algorithm[366]. A fluorescent agent (with molar mass nearly 700 times greater than fluorescein) was used to pool selectively within the blood vessels.

7.1.2 Radiation proctopathy

As described in chapter 3, radiotherapy for pelvic malignancies is increasingly successful, but leaves many patients with unpleasant symptoms of chronic radiation induced proctopathy such as bleeding, urgency, frequency, and tenesmus. The pathophysiology is poorly understood, but involves ischaemia, fibrosis, and neovascularisation at least in part by the formation of fragile superficial telangectasia.

There are many treatments for RP, but efficacy is less than ideal. Whilst hyperbaric oxygen may play a role in management[367], most medical therapies such as oral or rectal preparations of steroids, sucralfate, and 5-aminosalicylates have limited efficacy. Endoscopic therapies used to ablate rogue superficial vessels include formalin[368], Nd:YAG laser and argon plasma coagulation. Whilst efficacy of these treatments is currently judged upon symptom response using validated questionnaires of quality of life or symptoms, together with subjective assessment during follow-up endoscopy, a more objective assessment of the initial severity of disease and response at the tissue level is vital[270]. pCLE has the potential to provide such in vivo information, and may offer clues as to the pathophysiological processes involved. Whilst there are older technologies to quantify mucosal blood flow such as laser doppler flowmetry[369], tonometry[370], reflectance spectrophotometry[370, 371], pulse oximetry, and ultrasound flowmetry[372], pCLE may provide similar information but with morphological images at the same time.

7.1.3 Aims and hypothesis

Having demonstrated feasibility and tolerability for pCLE with marked *acute* radiation proctopathy in chapter 3, it was hypothesised that pCLE might provide insight, in vivo, into the vascular and epithelial disruption present in *chronic* radiation proctopathy, potentially enhancing longitudinal follow up of the disease and of any treatments. These pCLE morphology differences observed between healthy and diseased mucosa were correlated with conventional histology as well as white light endoscopy imaging (VRS), and symptom scores.

To benchmark pCLE against histology, histology was correlated with white light endoscopic findings (VRS) and symptom scores.

7.2 Methods

This was a prospective, non-randomised study. Recruitment was aimed at consecutive patients in an outpatient department fulfilling the inclusion criteria of adults who had finished external beam radiotherapy for a non-gastrointestinal pelvic malignancy at least six months previously that were, compared to before treatment, troubled by some degree of lower gastrointestinal symptoms assumed to be caused by radiation proctopathy. Exclusion criteria included patients with a history of previous bowel resection, inflammatory bowel disease, prostate brachytherapy, allergies to fluorescein or other intravenous contrast agent, known alternative causes for their new bowel symptoms (such as untreated bacterial overgrowth, bile-salt malabsorption or carbohydrate malabsorption), or those pregnant, breast feeding or unable to provide informed consent.

The protocol was similar to chapter 3. After a phosphate enema, patients underwent flexible sigmoidoscopy with pCLE using 5mls of 10% intravenous fluorescein.

From up to 3 areas of bowel in each patient (descending colon, upper rectum and lower rectum in an attempt to acquire sites within and outside the original radiation field), 1 minute pCLE video sequences were recorded with gentle probe apposition, and analysed. Two correlative pinch biopsies were obtained, fixed in 10% neutral buffered formalin, embedded in paraffin wax, sectioned at 4μm, and examined using haematoxylin and eosin. 16 histopathological features (imperfectly categorised into 4 vascular, 7 epithelial, and 5 glandular) were recorded for each site through blinded analysis by a single expert histopathologist; plasma cells were absent in all biopsies so eliminated as a potential discriminator or pathological feature. Parameters were graded according to a predefined scale similar to that of Hovdenak et al.[268].

Each pCLE video was blindly assessed using the Cellvizio-viewer software by a single investigator for the categorical presence of blood vessels, the diameter of the largest visible blood vessel if present, and examined for morphological changes including fluorescein leakage, glandular and lamina propria disruption. Rather than using the Hanauer grade of proctitis (G_{0-3})[280], Wachter's Vienna Rectoscopy Score of proctitis severity (VRS) was assigned via consensus opinion to each area (G_{0-5}) [373]. VRS is a means of objectively and systematically describing the severity of chronic radiation induced damage on a 0-5 scale as judged by endoscopic examination evaluating 5 factors:

- Telangiectasia: (grade 0, none; grade 1, single telangiectasia; grade 2, multiple non-confluent telangiectasia; grade 3, multiple confluent telangiectasia).

- Congested mucosa: (grade 0, none; grade 1, focal reddening of the mucosa combined with an oedematous mucosa; grade 2, diffuse non-confluent reddening of the mucosa combined with an oedematous mucosa; grade 3, diffuse confluent reddening of the mucosa combined with an oedematous mucosa).

- Ulceration: (grade 0, none; grade 1, microulceration – superficial, $<1cm^2$; grade 2; grade 2, superficial $>1cm^2$; grade 3, deep ulceration; grade 4, fistualtion or perforation.

- Stricture: 0, none; grade 1, >2/3 of regular diameter; grade 2, 1/3-2/3 of regular diameter; grade 3, <1/3 regular diameter; grade 4, complete obstruction.

- Necrosis: grade 0, none; grade 1, necrosis.

The highest grade of any one of 5 parameters provides the VRS score $G_{0\text{-}5}$ (Table 7.1):

VRS	Congested Mucosa	Telangectasia	Ulceration	Stricture	Necrosis
0	Grade 1	None	None	None	None
1	Grade 2	Grade 1	None	None	None
2	Grade 3	Grade 2	None	None	None
3	Any	Grade 3	Grade 1	None	None
4	Any	Any	Grade 2	Grade 1	None
5	Any	Any	Grade ≥3	Grade ≥2	Yes

Table 7.1: The VRS score was provided for each area of mucosa.

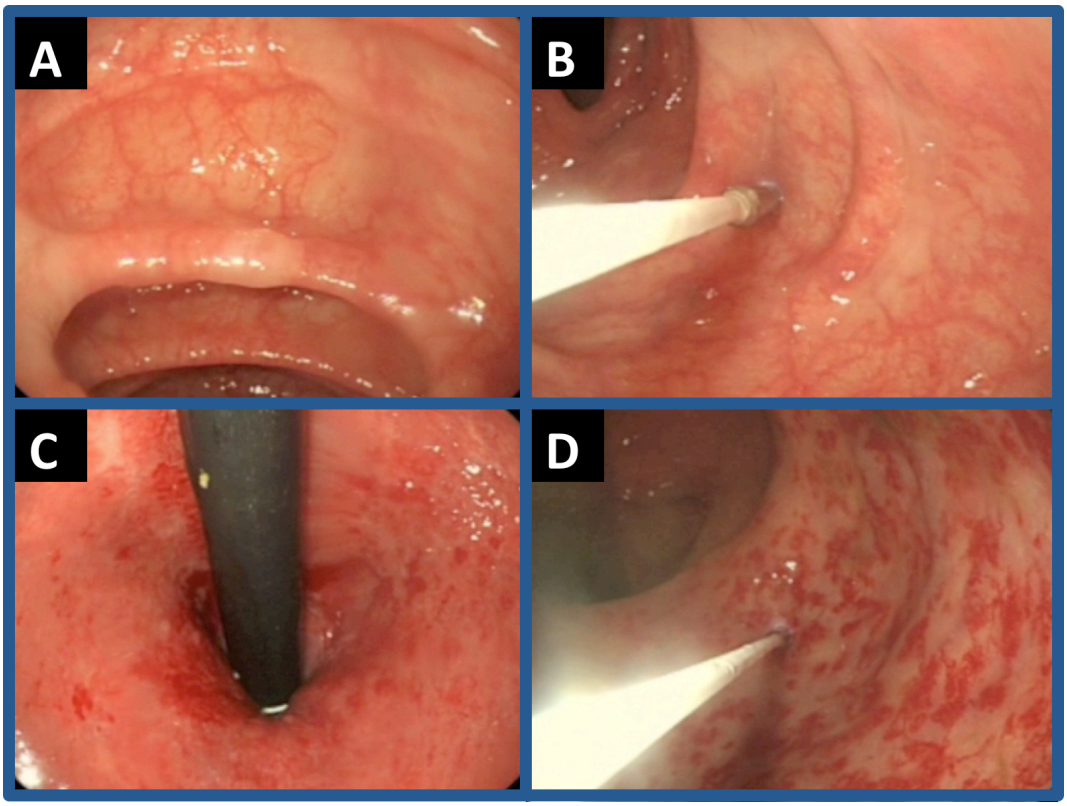


Figure 7.1 The typical vascular pattern of normal colonic mucosa (G_0) is demonstrated with normal descending colon in A, and undergoes pCLE optical biopsy in B. C shows G_2 VRS proctopathy of the lower rectum with an oedematous mucosa containing multiple non-confluent telangectasia. G_3 mucosa of the upper rectum with confluent telangectasia is shown in D.

Patients were then asked to list their main symptoms, before completing a Vaizey Incontinence score and a modified Inflammatory Bowel Disease Questionnaire (modified IBDQ), prior to their endoscopy session, similar to chapter 3. Once again, the endoscopist completed an EORTC/RTOG (Radiation Therapy Oncology Group) late proctitis score for the patient and an acceptability questionnaire was completed the day after the procedure.

7.2.1 Statistics

For categorical variables such as the presence of vessels or the observation of fluorescein leakage at progressive VRS grades, two-tailed Chi-squared test (or Fisher's exact test for small cell numbers) were used. The Kruskal-Wallis test was used to compare non-parametric measurements between groups (such as maximum vessel diameter at different VRS grades); where two groups were present the Mann-Whitney U test was employed

(for example comparing the symptom scores of patients with and without visible vessels on pCLE imaging). Spearmann's Rank Correlation Coefficient were calculated for the relationship between symptom score and widest vessel on pCLE.

The ethical approval obtained for the study was from the NHS Regional Ethics Committee (Oxford: 11/SC/0036). Written informed consent was obtained from all patients before study registration.

7.3 Results

7.3.1 Patient cohort

26 patients with symptomatic chronic radiation proctopathy participated and completed the study, with a median age of 68 (range 27-82). The main symptoms that the patients described included bleeding (16 patients); frequency, urgency or a change in bowel habit (16 patients); abdominal pain, borborygmi, flatulence or cramps (8 patients); faecal incontinence and mucus (7 patients); and tenesmus (6 patients). Their median modified IBDQ score was 180.5 (range 57 to 219), IBDQ-B score was 58.5 (range 21 to 69), Vaizey score 6.2 (range 0 to 19), and median late RTOG score 1 out of 4 (range 1 to 2) (see Table 3.2 for a recap of these classifications). They had completed external beam radiotherapy (± brachytherapy) a median of 23.5 months previously (range 7 to 73 months). The primary diagnosis was either prostate (21), cervical (4), or vaginal (1) cancer. 5 patients had undergone treatment for their proctopathy other than enemas: topical formalin application (2), topical formalin application with argon plasma coagulation (1), and blinded participation in a randomised controlled trial with hyperbaric oxygen therapy (2). 10 patients were taking anti-thrombotic medications: aspirin (7), aspirin and clopidogrel (1), warfarin (1) and low molecular weight heparin (1). Of the participants, 5 were current smokers, 6 had never smoked, with the remaining 15 patients have stopped smoking a mean of 27.0 years previously. The mean body mass index was 26.3.

The procedures were well tolerated: on the same 1-7 visual analogue scale as chapter 3 the mean score was 2.3, which is roughly midway between "very comfortable" and "uncomfortable" (range 1-6; though the "6" was by a patient who had undergone colonoscopy). Only urinary discolouration was noticed in 18 of the 26 patients which disappeared after a day or two, and there were two cases of marked nausea with no

complications. When asked within the questionnaire the day after the procedure "*If this endoscopic procedure is shown to provide useful information to guide your treatment, would you recommend it to other suitable patients?*" on a visual analogue scale from 1 (definitely recommend) to 7 (definitely advise against), there was an average score of 2.3.

7.3.2 Biopsy sites

76 pCLE sequences were obtained with corresponding pinch biopsies from a potential of 78; one descending colon and one upper rectum area were abandoned owing to apparent discomfort in two patients. Though possible, the accessibility of one lower rectum was ergonomically challenging owing to diffuse extrinsic luminal compression from pelvic fibrosis. Altogether, this produced $39G_0$, $25G_1$, $9G_2$, and $3G_3$ regions according to the VRS scale using white light endoscopy (Figure 7.2).

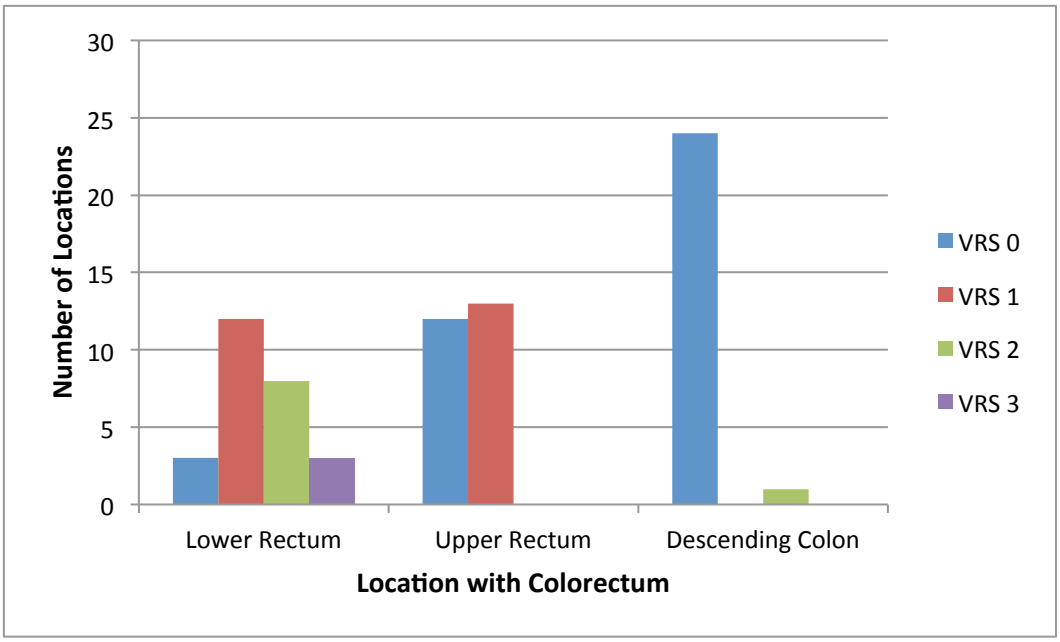


Figure 7.2 The biopsy sites in the lower rectum were generally affected by the higher VRS grades of radiation proctopathy. Only one descending colon was macroscopically unhealthy (in a very symptomatic patient 72 months post brachytherapy and external beam radiotherapy for cervical cancer).

7.3.3 pCLE correlated with VRS

Sequences from areas of higher grade VRS were more likely to have no visible vessels on pCLE: G_0, 7.7%; G_1, 8%; G_2, 55.6%; and G_3, 66.6% (p=0.0005) (Figure 7.3). Combining categories, vessels were absent in 8.47% of normal or mildly diseased sequences (G_0&G_1), versus 58.3% of more macroscopically damaged tissue (G_2&G_3 sequences) (p=0.0001). Providing dark contrast within the microvessels against the hyperfluorescent lumen, individual red blood cells were observed flowing in many of the sequences independent of VRS grade; however a reliable measurement of red blood cell translational movement per unit time was deemed unfeasible.

In those sequences where there were visible vessels, the mean (± SD) diameter of the widest vessel increased across the grades: G_0, 15.0µm ± 4.7; G_1, 20.0µm ± 11.4; G_2, 32.9µm ± 8.54; G_3 37.1µm ± N/A). Despite the convincing nature of the images and the trend in calibre this phenomenon only approached significance, perhaps due to inadequate sequences (p=0.147) (Figure 7.4). In the G_0 and G_1 sequences, the red blood cells appear to pulse down the microvessels in single file, whereas several of the larger diameter vessels from G_2 and G_3 sequences appeared to contain several red blood cells squeezed in adjacent to one another. Furthermore, there were two examples of G_3 sequences where large calibre vessels appeared to contain static red blood cells.

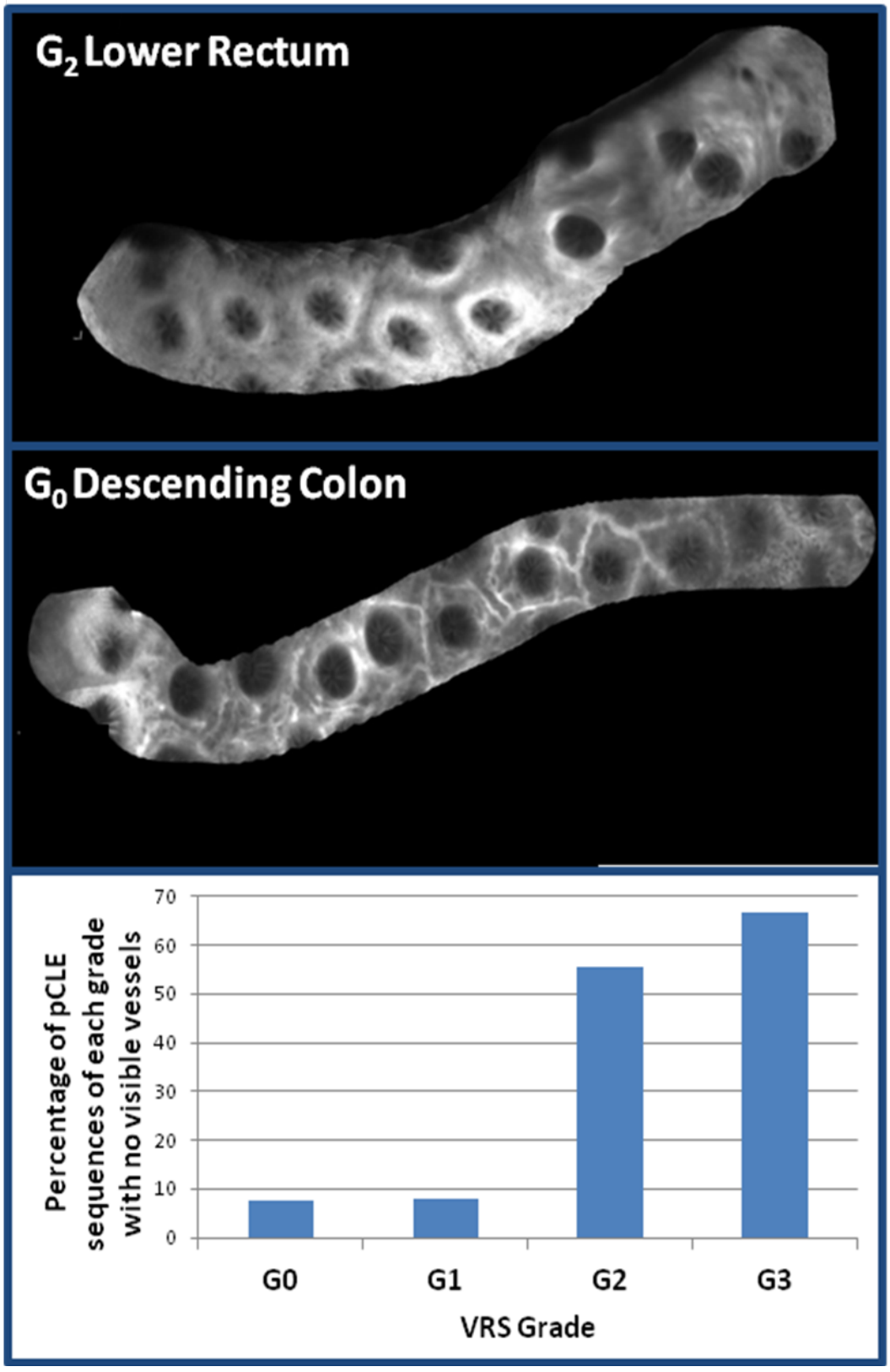


Figure 7.3 A chart demonstrating that VRS G_2 and G_3 areas were much more likely to display no obvious vessels on pCLE videos. pCLE mosaics provide examples whereby external beam radiotherapy for prostate cancer appears to have disrupted the normal vascular appearance.

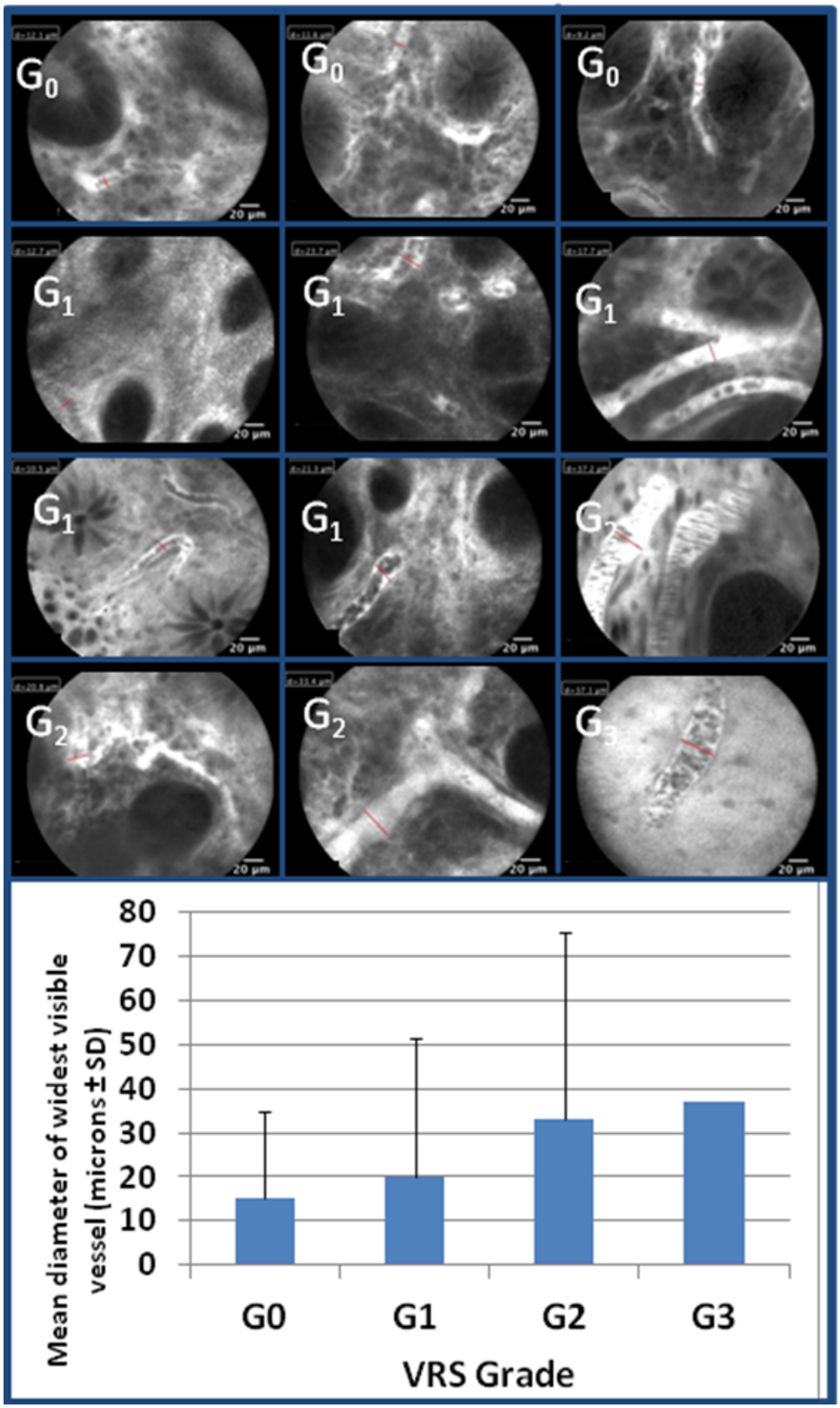


Figure 7.4 In proctopathic tissue, where vessels *are* seen, there is a (non-significant) tendency for the vessels to have a larger calibre; some examples are shown.

Morphological distortion of glandular structure and epithelium was more common in tissue affected by severe proctopathy, characterised by irregular shaped or thickened glands, a sloughy epithelium or irregular ridge-lined epithelial layer ($p<0.0001$). Marked irregular epithelial ridges were observed in all 3 of the G_3 sequences. In the sequences where glands were apparent, fluorescein leakage into the centre seemed more common in proctopathic tissue, though there was no statistically significant difference in this observation across the VRS groups ($p=0.25$).

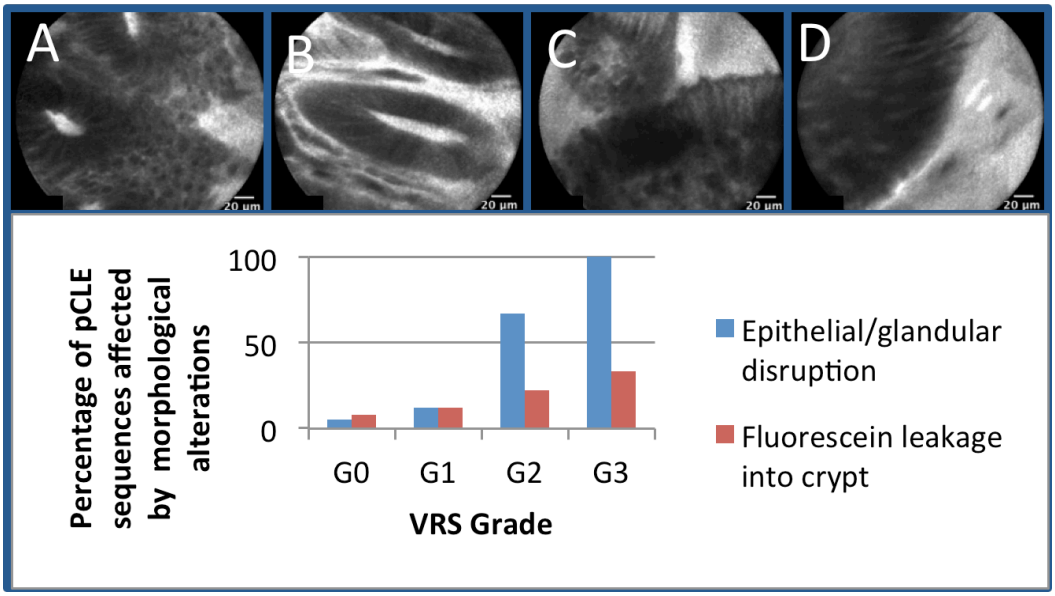


Figure 7.5 Morphological changes appear more commonly in G_2 and G_3 disease. An irregular ridge-lined epithelial layer ($p<0.0001$) is more common. Fluorescein leakage seemed particular marked in the G2/G3 disease but its categorical presence was not statistically different across the groups ($p=0.25$). Included are some examples of G_3 disease displaying fluorescein leakage into the crypt lumen (A and B) and epithelial ridges (C and D).

7.3.4 Histology

One pair of lower rectum VRS G_1 biospies did not survive processing so was removed from the analysis leaving 75 sites for histological assessment. One prostate radiotherapy patient had a macroscopically VRS G_0 descending colon that displayed borderline

features of collagenous colitis with a thickened basement membrane. Otherwise, a summary of the findings for each of the 16 histological features is found in Figure 7.6. Overall, the most common deviations from a normal appearance were at least some degree of either vessel dilatation (61.3%), superficial epithelial loss (58.7%) vessel congestion (56%), or goblet cell loss (54.7%), or the presence to some degree of mucophages (58.7%) or macrophages (57.3%). The least commonly found abnormalities were microthrombi (14.7%), crypt loss (25.3%), increased apoptosis (28%), fibrosis (29.3%), eosinophils (34.7%) or an abnormal proliferation pattern (34.7%).

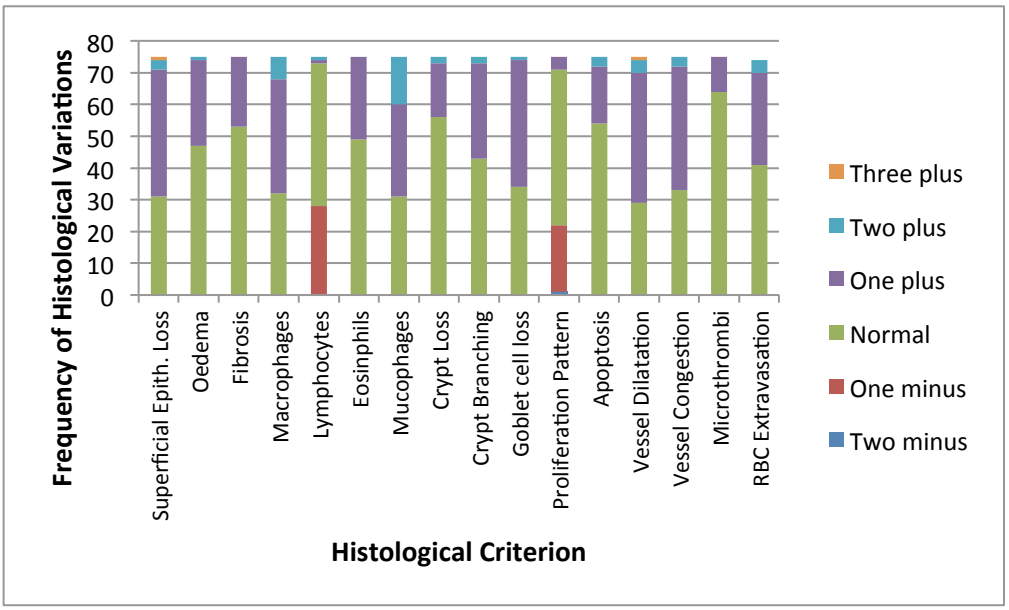


Figure 7.6: For each of the 16 histological features analysed, stacked columns showing the interpreted frequency of severity for the 75 biopsy pairs.

7.3.5 Correlation between histology and macroscopic appearance

For each VRS grade, the mean "score" attributed from histological examination was calculated; a mean absolute score was also calculated for "lymphocytes" and "proliferation pattern" where 1- was treated as 1+.

Individually, only the presence of mucophages was statistically significantly different between VRS groups (although mucophages did not steadily increase in prevalence with VRS grade). Despite not reaching significance, more convincing trends were seen with gland morphology where there was an almost universal increase at every VRS grade in

crypt loss, crypt branching, goblet cell loss, apoptosis, and altered proliferation pattern, with the mean VRS G_3 having a score 2-3 times greater than that of G_0 for each of these histological factors. For epithelial histological observations only the presence of fibrosis and altered lymphocyte concentration seemed to increase consistently across the VRS grades, with G_3 sites having a mean score 4-5 times greater than G_0 sites although statistical significance was not approached for these factors individually. Amongst the 4 vascular histological factors, only vessel dilatation convincingly increased across the VRS grades (although p=0.051).

For each VRS grade, the mean combined score from all 16 criteria (0 to a potential maximum of 31) increased steadily from 6 for G_0 to 10.33 for G_3, a small but statistically significant difference(p=0.016).

		Histological Assessment (mean value) for each VRS Category				
	Histological Observation	**VRS 0**	**VRS 1**	**VRS 2**	**VRS 3**	**P value**
Vascular	Vessel Dilatation (0, 1, 2, or 3)	0.51	0.75	1	1.7	0.051
	Vessel Congestion (0, 1 or 2)	0.54	0.75	0.56	0.33	0.29
	Microthrombi (0 or 1)	0.10	0.21	0.11	0.33	0.33
	Erythrocyte Extravasation (0, 1 or 2)	0.56	0.38	0.67	0.33	0.19
Epithelium	Superficial Epithelial Loss (0, 1, 2 or 3)	0.62	0.67	0.78	0.67	0.24
	Oedema (0, 1 or 2)	0.31	0.5	0.56	0	0.45
	Fibrosis (0 or 1)	0.18	0.29	0.56	1	0.43
	Macrophages (0, 1 or 2)	0.59	0.83	0.56	0.67	0.11
	Lymphocytes (-1, 0, 1 or 2)	-0.21	-0.38	-0.56	-1	0.36
	Lymphocytes (mean absolute value: 0, 1 or 2)	*0.26*	*0.54*	*0.55*	*1*	*0.31*
	Eosinophils (0 or 1)	0.31	0.42	0.33	0.33	0.10
	Mucophages (0, 1 or 2)	0.59	1.04	1	0.67	**0.04**
Glands	Crypt Loss (0, 1, or 2)	0.23	0.25	0.44	0.67	0.45
	Crypt Branching (0, 1, or 2)	0.36	0.42	0.78	1	0.25
	Goblet Cell Loss (0, 1 or 2)	0.41	0.71	0.56	1.33	0.58
	Proliferation Pattern (-2, -1, 0 or 1)	-0.08	-0.46	-0.56	0	0.37
	Proliferation Pattern (mean absolute value: 0, 1 or 2)	*0.18*	*0.54*	*0.56*	*0.67*	*0.44*
	Apoptosis (0, 1 or 2)	0.26	0.38	0.33	0.66	0.26
	Mean overall histological score (0-31):	**6**	**8.67**	**9.33**	**10.33**	**0.016**

Table 7.2 Normal histological appearance was designated zero. The degree of severity of any deviation from normal (-, +, ++, +++), was ascribed -1, 1, 2, 3 respectively for the purposes of a) creating an average to compare each VRS group, and b) to enable Kruskal-wallis tests to assess whether there were any trends in histological features across the four VRS groups. Averages have been tabulated with mean rather than median to avoid an excess of zeros.

7.3.6 Correlation between histology and glandular distortion on pCLE

Having shown that glandular/epithelial distortion with pCLE correlates with higher grades of VRS, this was compared for each of the 16 histological observations. 3 factors were statistically significantly different between the 2 pCLE groups: pCLE sequences

showing glandular disruption had around twice the histological vessel dilatation, fibrosis and proliferation pattern scores of those without pCLE glandular disruption. However, the observation of glandular disruption on pCLE was not a particularly sensitive predictor of any of the three factors; indeed out of the 75 sequences, 33, 14 and 17 had a normal glandular appearance on pCLE but abnormal vessel dilatation, fibrosis and proliferation pattern on histology respectively. However, the mean total histological score out of 31 is 9.5 compared to 6.64 (p=0.028) according to whether or not there is glandular disruption.

			Number of sequences with glandular disruption on pCLE			
	Histological Observation		**No**	**Yes**	**Percentage with pCLE glandular disruption**	**Mean Histological Score (not affected by pCLE glandular disruption versus affected)**
Vascular	Vessel Dilatation	0 (none)	28	1	3.45	**0.59 vs 1.14 p= 0.007**
		1(+)	30	11	26.8	
		2(++)	3	1	25	
		3(+++)	0	1	100	
	Vessel Congestion	0 (none)	27	6	27.2	0.56 vs 0.64 p= 0.76
		1(+)	32	7	17.9	
		2(++)	2	1	33.3	
	Microthrombi	0 (none)	53	11	17.2	0.13 vs 0.21 p= 0.42
		1(+)	8	3	27.3	
	Erythrocyte Extravasation	0 (none)	34	7	17.1	0.49 vs 0.57 p=0.80
		1(+)	24	6	20	
		2(++)	3	1	25	
Epithelium	Superficial Epithelial Loss	0 (none)	28	3	9.68	0.62 vs 0.93 p=0.20
		1(+)	29	11	27.5	
		2(++)	3	1	25	
		3(+++)	1	0	0	
	Oedema	0 (none)	38	9	19.1	0.38 vs 0.43 p=0.24
		1(+)	23	4	14.8	
		2(++)	0	1	100	
	Fibrosis	0 (none)	47	6	11.3	**0.23 vs 0.57 p=0.02**
		1(+)	14	8	36.4	
	Macrophages	0 (none)	24	8	32	0.69 vs 0.57 p=0.24
		1(+)	32	4	11	
		2(++)	5	2	28.6	
	Lymphocytes	*-1 (-)*	*20*	*8*	*28.6*	*-0.28 vs -0.57* p=0.43
		0 (normal conc)	*39*	*6*	*13.3*	
		1(+)	*1*	*0*	*0*	
		2(++)	*1*	*0*	*0*	
	Lymphocytes (mean absolute value)	0 (normal conc)	39	6	13.3	0.38 vs 0.57 p=0.24
		1(- or +)	21	8	27.6	
		2(++)	1	0	0	
	Eosinophils	0 (none)	40	9	18.4	0.34 vs 0.36 P=0.93
		1(+)	21	5	19.2	
	Mucophages	0 (none)	26	5	16.1	0.44 vs 0.57 p=0.47
		1(+)	5	0	0	
		2(++)	11	4	26.7	
Glands	Crypt Loss	0 (none)	47	9	16.1	0.25 vs 0.43 p=0.29
		1(+)	13	4	23.5	
		2(++)	1	1	100	
	Crypt Branching	0 (none)	37	6	14	0.43 vs 0.57 p=0.29
		1(+)	22	8	26.7	
		2(++)	2	0	0	
	Goblet Cell Loss	0 (none)	30	4	11.8	0.51 vs 0.79 p=0.08
		1(+)	31	9	22.5	
		2(++)	0	1	100	
	Proliferation Pattern	*-2 (--)*	*1*	*0*	*0*	***-0.23 vs 0.36 p=0.02***
		-1 (-)	*14*	*7*	*33.3*	
		0 (normal)	*44*	*5*	*10.2*	
		1(+)	*2*	*2*	*50*	
	Proliferation Pattern (mean absolute value)	0 (normal)	44	5	10.2	**0.30 vs 0.64 p=0.02**
		1(- or +)	16	9	36	
		2(++)	1	0	0	
	Apoptosis	0 (none)	47	7	13	0.28 vs 0.5 p=0.06
		1(+)	11	7	38.9	
		2(++)	3	0	0	
	Mean overall histological score (0-31):		**6.64**	**9.5 p=0.028**		

Table 7.3 The relationship between histological factors and glandular disruption on pCLE.

7.3.7 Correlation between histology and pCLE vascular appearance

Absence of vasculature on pCLE was not statistically significantly related to any of the four individual vascular histological observations, or the mean overall vascular histological score (Table 7.4). Individually, microscopic vessel dilatation was very close to being significantly correlated with absence on pCLE (p=0.06).

Vascular Histological Observation		Number of sequences: Vasculature evident on pCLE	Number of sequences: Vasculature absent on pCLE	Percentage with absent pCLE vasculature	Mean Histological Score (vessels evident vs absent on pCLE)
Vessel Dilatation	0 (none)	27	2	6.9	0.63 vs 1 p=0.06
	1(+)	32	9	31	
	2(++)	4	0	0	
	3(+++)	0	1	100	
Vessel Congestion	0 (none)	25	8	24.2	0.65 vs 0.33 p=0.25
	1(+)	35	4	10.3	
	2(++)	3	0	0	
Microthrombi	0 (none)	54	10	15.6	0.14 vs 0.17 p>0.99
	1(+)	9	2	18.2	
Erythrocyte Extravasation	0 (none)	34	7	17.1	0.52 vs 0.42 p>0.99
	1(+)	25	5	16.7	
	2(++)	4	0	0	
	Mean overall vascular histological score (0-8)	1.95	1.92 p=0.77		

Table 7.4 A table showing the presence or absence of visible vessels on pCLE for each grade of the four vascular histological features assessed.

For those pCLE sequences with a clearly visible vessel the largest vessel diameter was recorded. In the histological 2+ vessel dilatation group the mean largest visible vessel with pCLE imaging was nearly twice the calibre to that measured from the histologically undilated group (p=0.028) (Figure 7.7). The other vascular histology features were not statistically related to the maximum pCLE vessel diameter.

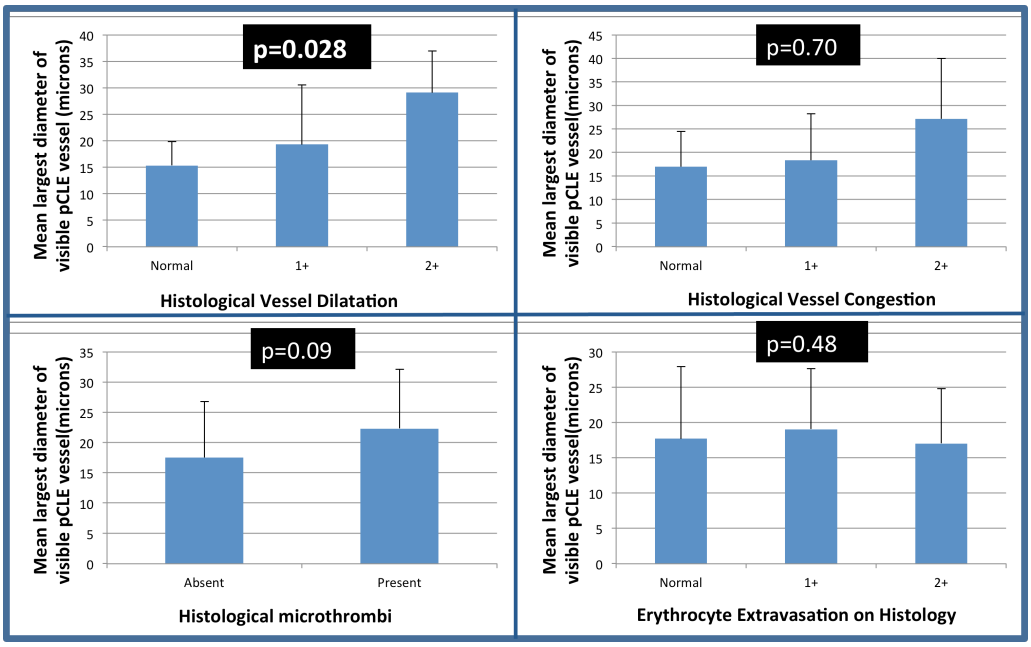


Figure 7.7 For those sequences with a visible vessel, graphs showing the mean largest vessel diameter with pCLE imaging, for each grade of the four vascular histological features assessed. Only histological vessel dilatation was significantly correlated, positively, with largest vessel diameter on pCLE.

The above two pCLE criteria of absent *or* dilated vasculature were next combined: if a pCLE sequence has no distinct vasculature, or contains a vessel with diameter equal to or greater than 25μm (this was a slightly arbitrary threshold decided upon as the midpoint between the mean pCLE diameters of G_1 and G_2 VRS), this was for brevity termed *pCLE dilabsence*. It was statistically positively correlated with 5 of the 16 histological factors: vessel dilatation, fibrosis, crypt branching, lymphocytes, and an abnormal proliferation pattern (generally a reduction in the latter two factors) (Table 7.5). Compared to sequences displaying at least one vessel less than 25μm in diameter, the histological mean "score" for each of these factors was at least twice that of sequences featuring pCLE dilabsence.

To expand, pCLE dilabsence increases from 10.3% in biopsy pairs with no histological vessel dilatation to 36.6%, 75% and 100% in those affected 1+, 2+ and 3+ respectively. For anticipating histological vessel dilatation, pCLE dilabsence has a PPV of 86.4%, a specificity of 74.3%, falling to an NPV of 49.1% and sensitivity of 41.3%. Lowering the 25μm diameter threshold for ascribing pCLE vessels as dilated would improve the sensitivity and NPV at the expense of the PPV and specificity.

The overall mean histological score (0-31) was significantly greater for sequences with dilabsence (10.05 versus 6.4).

			pCLE dilabsence (Number of sequences devoid of visible vessels or containing a vessel ≥ 25µm)			
	Histological Observation		**No**	**Yes**	**Percentage with pCLE vasculopathy**	**Mean Histological Score (no pCLE dilabsence versus pCLE dilabsence)**
Vascular	Vessel Dilatation	0 (none)	26	3	10.3	**0.528 vs 1.09 p=0.0021**
		1(+)	26	15	36.6	
		2(++)	1	3	75	
		3(+++)	0	1	100	
	Vessel Congestion	0 (none)	23	10	30.3	0.585 vs 0.545 p=0.29
		1(+)	29	10	25.6	
		2(++)	1	2	66.7	
	Microthrombi	0 (none)	47	17	26.6	0.113 vs 0.227 p=0.20
		1(+)	6	5	45.5	
	Erythrocyte Extravasation	0 (none)	30	11	26.8	0.491 vs 0.545 p=0.83
		1(+)	20	10	33.3	
		2(++)	3	1	25	
Epithelium	Superficial Epithelial Loss	0 (none)	24	7	22.6	0.623 vs 0.727 p=0.61
		1(+)	26	14	35	
		2(++)	2	1	33.3	
		3(+++)	1	0	0	
	Oedema	0 (none)	34	13	27.7	0.358 vs 0.455 p=0.42
		1(+)	19	8	37	
		2(++)	0	1	100	
	Fibrosis	0 (none)	43	10	18.9	**0.189 vs 0.545 p=0.002**
		1(+)	10	12	54.5	
	Macrophages	0 (none)	24	8	25	0.604 vs 0.818 p=0.29
		1(+)	26	10	27.8	
		2(++)	3	4	57.1	
	Lymphocytes	*-1 (-)*	*14*	*14*	*50*	*-0.208 vs -0.636 p=0.011*
		0 (normal conc)	*37*	*8*	*17.8*	
		1(+)	*1*	*0*	*0*	
		2(++)	*1*	*0*	*0*	
	Lymphocytes (mean absolute value)	0 (normal conc)	37	8	21.6	**0.321 vs 0.636 p=0.011**
		1(- or +)	15	14	48.3	
		2(++)	1	0	0	
	Eosinophils	0 (none)	36	13	26.5	0.321 vs 0.409 p=0.46
		1(+)	17	9	34.6	
	Mucophages	0 (none)	26	5	16.1	0.660 vs 1.09 p=0.07
		1(+)	19	10	34.5	
		2(++)	8	7	46.7	
Glands	Crypt Loss	0 (none)	42	14	25	0.226 vs 0.409 p=0.24
		1(+)	10	7	41.2	
		2(++)	1	1	50	
	Crypt Branching	0 (none)	36	7	16.3	**0.340 vs 0.727 p=0.008**
		1(+)	16	14	46.7	
		2(++)	1	1	50	
	Goblet Cell Loss	0 (none)	26	8	23.5	0.509 vs 0.682 p=0.22
		1(+)	27	13	32.5	
		2(++)	0	1	100	
	Proliferation Pattern	*-2 (--)*	*1*	*0*	*0*	*-0.189 vs -0.409 p=0.013*
		-1 (-)	*10*	*11*	*52.3*	
		0 (normal)	*40*	*9*	*18.4*	
		1(+)	*2*	*2*	*50*	
	Proliferation Pattern (mean absolute value)	0 (normal)	40	9	18.4	**0.264 vs 0.591 p=0.008**
		1(- or +)	12	13	52	
		2(++)	1	0	0	
	Apoptosis	0 (none)	41	13	24.1	0.264 vs 0.455 p=0.17
		1(+)	10	8	44.4	
		2(++)	2	1	33.3	
	Mean overall histological score (0-31):		**6.40**	**10.05 p=0.0033**		

Table 7.5 The relationship between histological variables and pCLE dilabsence.

7.3.8 Correlation of symptoms with pCLE and endoscopic appearance

There was little correlation between the symptom scores and either VRS grade or any postulated pCLE criteria for worse vasculopathy (vessel absence, vessel ≥25μm, or the combined pCLE *dilabsence*) (Table 7.6). The only identifiable statistically significant correlation (weakly positive) was between RTOG and maximum VRS (p=0.012).

	Endoscopic Feature		The Mean Symptom Scores Correlated with Endoscopic Features & pCLE Findings							
			IBDQ 224= asymptomatic 32=severely symptomatic		IBDQ-B 70=no bowel symptoms 10=severe bowel symptoms		Vaizey 0=perfect continence 24=total incontinence		RTOG 0=asymptomatic 5=death from DXT morbidity	
White light	VRS of patient's most proctopathic site	0	176	p=0.87	52	p=0.84	4	p=0.29	0.5	**p=0.012**
		1	178.9		54.9		6.29		1	
		2	176.8		54.9		8.13		1.5	
		3	199.3		59.7		1		1.33	
pCLE	Patient's widest Vessel Diameter	SRCC	0.33		0.35		0.03		-0.03	
		p=	0.1		0.08		0.9		0.82	
	Patient devoid of visible vessels?	No	179		55.7		5.6		1.21	
		Yes	182.5		54.9		6.9		1.36	
		p=	*0.92*		*0.7*		*0.93*		*0.47*	
	Patient devoid visible vessels or having a vessel >25μm (pCLE dilabsency)	No	164.3		50.3		5.3		1.3	
		Yes	189.1		58		6.6		1.29	
		p=	*0.06*		*0.12*		*0.8*		*0.56*	

Table 7.6 Apart from when measured by RTOG, the severity of a patient's symptoms has no correlation with their most severely proctopathic segment of colorectum as determined by VRS. Similarly, no pCLE feature was discovered that correlated with any of the four symptom scores. Kruskal-Wallis, Fisher's Exact Test, Spearman's Rank Correlation Coefficient (SRCC), and Mann-Whitney U tests were used as appropriate.

7.4 Conclusion

The primary aim of this chapter was to see if pCLE can reveal virtual histopathological differences in mucosa affected by radiation proctopathy. From the 76 sequences studied, pCLE vessel absence was associated with higher VRS grades of macroscopically proctopathic tissue. Where vessels were visible there was a non-statistically significant trend toward higher VRS grade areas yielding wider maximum vessel under pCLE imaging. Higher grade VRS areas were also associated with glandular/epithelial disruption on pCLE, characterised by slough and epithelial ridges.

Assuming that histology should be the "gold standard" for determining proctopathy characteristics and severity, vessel dilatation on histology correlated significantly with pCLE imaging for glandular disruption, size of vessel, dilabsence, and almost significantly with absent vasculature. Both histological fibrosis and an abnormal proliferation pattern (mostly attenuated) correlated positively with glandular disruption and dilabsence on pCLE. pCLE dilabsence also correlated with lymphocyte and crypt branching abnormalities. Collating the 16 histological features, a mean histological score was created which correlated significantly with both pCLE glandular disruption and with pCLE dilabsence. Whilst the endoscopic proctopathy severity using VRS grade also correlated with a collated histological score, only one individual histological observation (mucophages) was significantly related to VRS grade; this suggests that pCLE is at least as good or perhaps more powerful for predicting histological signs of proctopathy.

The extensive histological findings alone from this study require review in the context of the paucity of previous study on the subject. It has been previously suggested that chronic radiation bowel disease is predominantly a vasculopathy with intimal fibrosis and thickening of the vessel wall combined with fibrin thrombi in capillaries and larger mural vessels, and the evolution of dilated blood vessels or telangectasia[273]. The resultant effect, shown using microradiography after barium infusion into mesenteric vessels of fresh operative specimens, is that the vascular volume/capacity within the tissue is reduced[275]. (Clearly, these findings are compatible with the pCLE observation of destruction of superficial vessels with the formation of new friable dilated abnormal ones; and presumed thrombi were seen in some dilated vessels). In this current study the most common histological findings were vessel dilatation and congestion, together with loss of the superficial epithelium and goblet cells (all previously described[274, 374]), with the presence of mucophages or macrophages.

Perhaps owing to the multifactorial nature of gastrointestinal symptoms post radiotherapy[375], neither pCLE nor VRS seemed capable of reflecting the patients' symptom severity. Hovdenak et al. found that during the 6 weeks of radiotherapy treatment *mucosal* histological changes regressed despite ongoing treatment and worsening symptoms[268]; certainly the limited penetration of pCLE will prevent imaging of the submucosa, muscle, serosa, larger blood vessels and enteric nerves, damage to which may remain unrecognised but part of the proctopathy – indeed submucosal damage is much more marked in chronic than acute proctopathy, with atypical fibroblasts and collagen proliferation[376].

There are obvious limitations to the methods of this hypothesis generating study. A fuller study would require an assessment of interobserver/intraobserver agreement regarding a) pCLE factors such as the vessel presence, maximum vessel calibre, and glandular disruption, and b) the 16 histological factors. A more objective measure of vessel characteristics might be obtained using techniques employed in the studies described in *Section 2.15* CLE for the Assessment of Vasculaturesuch as bespoke software[235] or the "Vessel Detection Module™" available from Cellvizio®[236] (though this is currently only available for the laboratory based pCLE device).

Owing to the majority of patients having been treated for prostate cancer, the more severely proctopathic sequences tended to be found within the lower rectum, with seemingly healthy sequences in the descending colon; whilst differences have not been described between these mucosal areas in health, further study would need to confirm that there are no intrinsic differences independent of any radiotherapy treatment. Furthermore, the "healthy" sequences were taken from patients who had relatively recently been treated for cancer, with radiotherapy not being the only potential insult to the tissue. Only 11 of the 75 sequences were G_2 or G_3 disease; it would have been preferable to have a more equal spread of macroscopic disease severity, although it is fundamentally difficult to judge disease severity anyway; there is no "gold standard" using symptoms, macroscopic appearance or a validated histology score. There was also marked heterogeneity in the patient cohort including the primary disease, radiotherapy regimen, duration since treatment, therapies for any proctopathy. It is likely that these factors create further variation in the clinicopathologic details of what is already a highly variable disease.

This chapter shows that pCLE corroborates the evidence for radiation proctopathy being at least in part a vasculopathic condition, suggests that pCLE may be a more reliable indicator of the extent of histological damage than symptom severity or the macroscopic damage observed on endoscopy, and is the first step towards a useful optical biopsy technique to provide safe assessment of what is a severely debilitating and poorly studied condition in the era of cancer survivorship.

Chapter 8 Conclusion

8.1 The Ideal Optical Biopsy Device

The perfect clinical optical biopsy device would a) improve diagnostic accuracy beyond the standards of current pathological and imaging technologies, b) eliminate the need for conventional biopsies, or perhaps just focus them to reduce the number and improve the quality of biopsies taken, c) be safer and less invasive than current diagnostic modalities, d) provide immediate answers about tissue function and form to facilitate immediate management of clinical problems and assist these procedures by, for example, identifying the tissue margins for local treatment or resection, e) be straightforward to learn and use, f) provide consistent stable images of representative areas, and g) be cost-effective. These factors take time to achieve. To use an analogy with other technology, in 1980 endoscopic ultrasound was an experimental research tool[377], but 30 years later, it combines with FNA as a standard diagnostic procedure in many thoracic and upper gastrointestinal lesions; this transition has occurred through a combination of technical developments such as linear array and doppler, advancements in process such as on-site endocytopathology/telecytopathology, an understanding of its diagnostic limits, and improvements in training to maximise the yield and enhance safety.

As pCLE approaches its second decade of development, this thesis began by outlining the challenges it faces to achieve these goals and garner more widespread adoption. Force, accuracy, targeting and ergonomics were four themes that kept recurring: a) the role of contact force had scarcely been approached; b) despite some impressive diagnostic data pCLE's accuracy is insufficiently consistent; c) with heterogeneity in tissue microarchitecture it is imperative that the exact location of probe tissue interaction is both known and recorded; and d) current techniques for manipulation of the pCLE probe have limitations.

An examination of how the experimental chapters contribute to both an understanding of these four factors and a vision of future research requirements follows.

8.2 Achievements of this Thesis and Future Work

This thesis addressed the issues of pCLE from several directions, using laboratory experimentation both in vivo and ex vivo, as well as through clinical studies. Clearly, though much of the work was arguably very novel, much of the data was preliminary, hypothesis generating and qualitative. In general, the hypotheses generated from the clinical work would be enhanced by further prospective studies in patients from an unselected population.

8.2.1 Probe contact force – its importance in pCLE imaging

Prior to this thesis, the role of contact force in pCLE imaging had barely been touched upon. It had been suggested that alveolar morphology is affected by axial force of the probe upon the pulmonary lobule[48], and that differences in fluorescence between different regions of a pCLE image are sometimes attributable to the probe's inconsistent contact force or partial loss of contact[175].

During pCLE of the endobronchium and large bowel in chapter 3 the difficulty of controlling the distal probe contact force upon the tissue was realised (particularly during retroflexion) and there were unpredictable morphological variations within pCLE videos of in vivo endobronchial and colorectal mucosa. It was hypothesised that the contact force could contribute to these variations in the image output. In chapter 4, pCLE imaging of the peripheral lung demonstrated realtime snapping of septal walls and microvessels courtesy of uncontrolled axial pressure of the probe, suggesting that contact force *may* have safety implications (although there were no complications in the study).

In chapter 5 it was shown that force (and mucosal distension), two previously unconsidered factors, can affect image consistency. Firstly, the extent of colon inflation (in a crude in vivo porcine model) is important; compared to a hyperinflated colon a collapsed colon has three times the number of glands per FOV, and each gland is two thirds of the diameter. Secondly, and more pertinently to the topic of contact force, a pCLE probe abutting ex vivo colonic mucosa at 0.5N compared to "just touching" at 0.005N had approximately double the gland diameter but a third the number of glands per FOV. Though in clinical practice the variations in probe contact force (and bowel distension) would probably be more subtle, further work needs to be done to determine the significance in clinical practice of these findings, particularly with gland and crypt

geometry and size remaining important aspects in the interpretation of pCLE images[109, 129].

Whilst this phenomenon may mean steady contact force is required for fair image interpretation, the rest of chapter 5 explored whether this phenomenon of gland morphology alteration secondary to variable force could be exploited to gain additional information about the tissue under interrogation, similar to information gleaned with ultrasound elastography[320] or atomic force microscopy[322]. By applying a sinusoidal axial force of 0.07N via the pCLE probe to ex vivo colon it was shown that the glands cyclically expand and shrink, as well as separate. Interestingly, when the tissue was artificially stiffened with formalin to produce a simplistic disease model of fibrosis or neoplasia, the gland's percentage cyclical change in area halved, and the interglandular separation was virtually eliminated across the force cycle. Perhaps this describes the birth of pCLE elastography, although creating a similar cyclical force in a constrained gut lumen with inflated bowel wall that is not securely anchored to a firm board will be a very different exercise. In vivo a means of providing a) distal axial movement of the probe and b) stability of the tissue (perhaps with a transparent mucosectomy suction cup) would be required with a detailed understanding of any elastographic differences between healthy and diseased tissue targets. This should include hyperplastic and neoplastic colonic polyps and other gastrointestinal tract conditions, but there may be observable elastographic differences in endobronchial lesions, or between different conditions of the lung parenchyma (although the ergonomics would be more awkward here for force adjustment).

8.2.2 Assessing and trying to maximise the accuracy of pCLE

Clearly accuracy is the singlemost important characteristic in an optical biopsy device. Currently, in oesophageal and colonic neoplasia detection, reasonable accuracy is obtained from experts in high volume tertiary centres when they are given adequate time to review the pCLE video sequences; an answer from first pass visualisation will someday be the convention, though most studies conclude that offline review yields more accurate answers at present. In time, computed analysis and diagnosis will also play a key role in improving accuracy[162, 176].

Starting in colorectal endoscopy, better accuracy may lead to the redundancy of histopathology, enabling hyperplastic polyps to be left in situ, and neoplastic lesions to be

dealt with appropriately at the time of endoscopy: so called “diagnose and leave” and “resect and discard” strategies. It has been estimated that this paradigm alone will save $1 billion of histopathology costs per year in the USA[378]. Sequential endoscopic therapy during the diagnostic endoscopy procedure will become more de rigueur, avoiding the drawbacks of delays and problems of target relocation that are seen in, for example, endoscopically inapparent Barrett’s related neoplasia[172]. However, pCLE’s accuracy will need to be much improved to facilitate these shifts in management. For example, Bajbouj et al.’s multicentre study on Barrett’s oesophagus surveillance, described in chapter 2, showed that despite encouraging data on pCLE’s ability to exclude neoplasia, its sensitivity and PPV for predicting neoplasia were only 12% and 18% (for image interpretation at the time of the procedure); not only would cancer be missed if tissue biopsy was avoided, if all patients with pCLE features of neoplasia had been treated at the time of endoscopy, 82% would have been overtreated[160]. Similarly, the sensitivity and specificity were as low as 66% for colorectal neoplasia detection in Table 2.2. Establishing the grade of any dysplastic change is also imperative for the management of most neoplastic conditions including Barrett’s, but this is not straightforward with pCLE[177]. Clearly the technology alone cannot currently provide the clinician with sufficient diagnostic confidence to avoid tissue biopsy or justify a potentially morbid treatment.

A major aim of this thesis was to explore and improve the accuracy for pCLE diagnostics in novel or less well investigated niches. Chapter 3 showed feasibility and tolerability for pCLE imaging of two new areas: 1) healthy and diseased endobronchium, and 2) colorectum over five occasions during chemoradiotherapy for advanced rectal cancer. The chapter provided a library of images for both studies and demonstrated differences between 1) the endobronchial basement membrane in health, when affected by nodularity, and when affected by carcinoma/carcinoma-in-situ; and 2) rectal mucosa in both health and when affected by invasive cancer. However, pCLE specificity was inadequate to differentiate between two diseases of endobronchial nodularity (TBOP and TBA), and any differences between endobronchial dysplasia, carcinoma-in-situ and small cell lung cancer were imperceptible. There was only one patient for the rectal cancer study and further investigation would be required to confirm the suspicions of greater fluorescein leakage after two weeks of chemoradiotherapy in the tumour, and more dilated microvessels within the radiation zone after treatment.

Chapter 4 sought to evaluate the accuracy of pCLE imaging for diagnostic bronchoscopy of the diseased peripheral lung. The most noticeable and consistent finding was that parenchymal diseases (other than emphysema) create non-specific diminishment of the distinct elastin alveolar structure of the pulmonary lobule creating unrecognisable structure. This was evident in 75%, 26% and 17% of non-emphysematous peripheral diseases, healthy/normal and COPD sequences respectively. Further work is essential to establish exactly what the cause of this loss is, but whilst exciting, the finding was neither sensitive nor specific enough to even accurately and reliably indicate non-emphysematous disease. Partly because of the distinction between microvessels and alveolar septal walls being trickier in diseased lung, intravenous fluorescein was trialled in an effort to improve diagnostic accuracy; however "white-out" of the image occurred before the fluorescein could preferentially delineate structure, as it tends to in more typical epithelial surfaces. The other significant finding in the study was that severe emphysema seemed apparent from greater sparsity in the septal wall structure, with residual elastin being thickened or disrupted, and in two patients with large bullae it is highly likely that the fine reticular pattern being imaged with the pCLE probe represented the visceral pleura. However, the consistency of these findings of scanty elastin fibres was not adequate to allow some assessors (who had been briefly trained on alveolar pCLE) to accurately categorise emphysema severity according to its HRCT classification, despite there being "fair" intraassessor reliability.

Having focussed mostly on force, tracking and ergonomics in chapters 5 and 6, the final experimental chapter aimed to explore a completely new niche for pCLE, where in vivo vessel assessment (one of the device's fortes as indicated in preceding chapters) would be a key component. Thus a clinical study was conducted, endoscoping the lower bowel of 26 patients to characterise and assess the severity of chronic radiation proctopathy (a predominantly vascular pathology) with pCLE, white light imaging and conventional histology. 76 pCLE sequences were acquired and there was a plethora of encouraging associations with pCLE observations. Higher macroscopic grades of proctopathy were associated with glandular/epithelial disruption on pCLE, pCLE vessel absence, and a trend, where vessels were actually observable under pCLE imaging, towards wider maximum diameter vessels. Histology until now has provided the most in depth evaluation of proctopathic tissue and several pCLE findings correlated well with many histological features of disease in this study. Conversely only one histological feature of disease correlated with the macroscopic appearance suggesting that the accuracy of pCLE for identifying histological signs of chronic radiation proctopathy is potentially greater

than white light imaging. Interestingly, 16 histopathological features were collated to form a mean histological score; this correlated with both pCLE glandular disruption and dilabsence. Further clinical study is needed to establish if pCLE could be used for accurate longitudinal assessment of chronic radiation proctopathy therapies but the initial results are encouraging.

Acccuracy will be improved when there is better consensus and understanding of what the images represent. The speculative conclusions drawn regarding biliary tree image microstructure illustrate this well; the mucus globules and 3μm specks in parenchymal lung diseases seen in chapter 4 are other examples.

pCLE should not be seen as an expensive realtime version of histopathology; it has unique qualities and strengths over histology and other optical biopsy tools. It can be pushed into very narrow lumens such as the biliary tree, ureter and (in chapter 4) the peripheral lung. It provides in vivo information on permeability, blood flow, cell shedding and (shown for the first time in chapter 5) tissue elasticity. Fluorescent molecular imaging will play a key role in the pCLE of tomorrow. pCLE immunohistochemistry already has promising data for the identification of a) specific antigens[126], VEGF[232] and EGFR expression[125] in colorectal neoplasia; b) EGF-R, survivin and other antigens that are expressed in oesophageal cancer[166-168]; and c) pulmonary aspergillosis[213]. Other mechanisms of teasing out information from the tissue being examined include 1) combining fluorescence lifetime imaging with confocal endomicroscopy[299], and 2) especially in the lung where contrast agents are not traditionally used, to assess confocal autofluorescence from endogenous sources other than elastin (such as collagen[298]) using different wavelengths. In future, contrast agents that can safely outline the cell nucleus will undoubtedly be created or the safety of current ones such as cresyl violet and acriflavin will be confirmed. In many countries there are still (arguably unjustifiable) reservations with regards to the safe use of intravenous fluorescein, leading to clinical pCLE studies remaining in the domain of clinical trials. With fluorescein's excellent safety in ophthalmology, this will gradually change.

8.2.3 Tracking the probe

Even if pCLE becomes supremely accurate, it is essential that its operator can pinpoint where the optical biopsies have come from. This is difficult to reliably ascertain in "blind" areas such as the peripheral lung. Furthermore, pCLE leaves no trace on mucosal

surfaces, hence, a) it is difficult to confirm that pinch biopsies have come from exactly the same area as the optical biopsy, b) it may not be obvious where an earlier optical biopsy came from (for the purposes of an intervention either later in a procedure or at another procedure – this issue was evident in the pCLE of rectal cancer over several weeks in chapter 3), and c) a record of the macroscopic boundaries of pCLE identified disease for the purposes of later endoscopic intervention is not available. Future platforms may include a means of recording the exact area from where optical biopsies have been taken. Simlilar to the work of Mountney et al.[248], this could be a bright semi-translucent icon (circle, or even the path the probe translated across) overlaid on the dynamic white light endoscope video sequences or upon a 3D or holographic representation of the organ undergoing assessment.

Chapter 4 underlined the requirement for better understanding of the probe whereabouts, during pCLE video capture. It highlighted the scenarios of a) imperceptible autofluorescence on probe deployment towards emphysematous peripheral lung either representing a large bullous or the probe not having reached a lobule, and b) a patient who had two very different pCLE appearances stemming from sequential cannulations of the same segmental bronchus (Figure 6.1). This led to the question of whether or not the final location of an alveoflex pCLE probe is ever pre-determinable if it is blindly inserted to a specific length into the most distally accessible generation of bronchiole. Therefore the second part of chapter 6 used an ex vivo porcine lung to demonstrate that approximately half of these probe deployment starting points can physically only lead to one possible terminal destination, and that half would yield obvious multiple terminal destinations of the probe (between 2 and 4 destinations) depending on the exact mechanics of deployment (angle, respiratory cycle etc.). However, with the greatest maximum separation between multiple terminal destinations arising from a single starting point being 75mm (average maximum 34mm) half the time in clinical practice there is likely to be major guesswork as to the probe's position. Clearly the work ideally needs to be repeated in ex vivo human lungs, with factors such as the degree of lung inflation being carefully controlled to mimic more closely the conditions of a bronchoscopy. Nevertheless, it suggests that, assuming it is not possible to identify the starting points that have only one route to the periphery, reliable tracking may require fluoroscopy or the other imaging modalities thus far used for TBB which were described in chapter 6 [353-357].

8.2.4 Ergonomics of probe manipulation

By manipulating the shaft and the twin control wheels, the flexible video endoscope has several degrees of freedom at the operator's disposal, and it has traditionally provided adequate stability for intraluminal white light imaging and pinch biopsy. However it is now used for procedures that it was not originally destined for. The endoscope requires considerable stability for the more highly magnified imaging it now incorporates, and requires fine dexterity for endolumenal interventions such as submucosal resections, and extralumenal interventions; for example in NOTES surgery. There is a drive to improve the ergonomics with, for example, master and slave devices[379] or nanobots. Similarly, pCLE has thusfar been almost exclusively delivered via the operating channel of endoscopes; these are not designed to enable perpendicular optical biopsy probe apposition with constant pressure at a specific point in the presence of tissue flaccidity, peristalsis and respiratory movement, let alone facilitate slow controlled translation in an ordered fashion to create mosaics. pCLE particularly struggles with pedunculated lesions, and any resultant movement artefact has been logically shown to diminish interpretability and accuracy[108]. pCLE also slows down the workflow as an attempt is made to obtain good quality reproducible images. In this thesis, manipulation of the probe was found particularly challenging in chapter 3, during imaging of the narrowest of bronchi and during retroflexion within the lower rectum.

Furthermore, fragile tissues require careful handling, and any clumsiness at the probe tissue interface will damage epithelium and affect the image output[175]. Therefore to improve the delivery of confocal endomicroscopy in terms of manoeuvrability, stability and targeting, its safety, and the predictability of contact pressure, multiple alternative devices to the flexible eCLE and pCLE have been devised. These include a prototype confocal microlaparoscope employed to image the ovary and uterine cervix[175, 177], a smaller device for percutaenous imaging of the liver[226], and a rigid distal scanning CLE device for use in the lung[201].

The in vivo experiment in chapter 6 was an attempt to improve the ergonomics of pCLE delivery by integrating the probe into a flexible endoscopic robot. Having predicted that the robot should be capable transvaginally of acquiring pCLE optical biopsies of 88% of a human pneumperitoneum workspace (the rest of the pelvis may have been reachable if the algorithm was adjusted for greater than 10mm of probe deployment), the actual

flexible endoscopic robot was inserted into a pig and with a handheld controller navigated around the pig's abdominopelvic cavity. The probe was deployed and, using intravenous fluorescein, interpretable pCLE optical biopsies were acquired from the liver, spleen and peritoneal lining. Translational yaw movements of the distal degree of movement enabled mosaics up to 2mm to be acquired. For clinical practice, the robot would need to move more quickly and be more robust (especially for the gastrointestinal lumen). Nevertheless, the concept of highly precise thumbstick control pCLE navigation is an exciting one, especially if a distal force-torque sensor could facilitate constant contact and pressure with the tissue (such as has been done with a handheld device in our laboratory[243]. It may even enable a dynamic force to extract elastographic properties (as has been discussed).

As regards mosaicing, a fivefold increase in the FOV has been previously demonstrable on the urothelium; a relatively unbound epithelial surface [59]. In this thesis, with current standard endoscopic techniques, mosaics up to 2.5mm in length were seen in healthy colorectal mucosa, essentially a tenfold increase in the 240μm diameter FOV of the UHD Coloflex Probe (Figure 3.5). By incorporating the 600μm diameter probe within the flexible endoscopic robot in chapter 6, 2mm long mosaics of peritoneal structures were possible (Figure 6.5). The longest mosaics from the pulmonary lobule in chapter 4 were only 1mm (from a 600μm FOV probe) owing to more restricted movement, and endobronchial mosaics were even more limited probably owing to more difficult translational movements and less feature distinctiveness within the images. In the future, improved ergonomics of pCLE delivery will enable more effective mosaicing as the probe is able to translate in an automated predetermined path to rapidly construct larger, more representative depictions of the tissue. Perhaps a means of displaying the dynamic information such as vascular flow will eventually be possible on a large mosaic. The device used to generate these mosaics may resemble the robot employed in chapter 6, or may use octopus inspired suction cups such as the "heartlander" cardiac robot[380].

8.3 Closing Comments

Currently pCLE increases both the cost of and time taken to perform procedures. As the technology develops, there will be more choice in hardware, bringing down its significant cost (currently >€100K initial capital outlay with probes costing in the region of €6K and programmed to only last for 20 patients). These time and financial implications will be

offset when optical biopsy either abrogates the need for pinch biopsy, or enables more selective biopsies to be taken (smart biopsies). Fresh niches will also appear; in the last few months alone there have first publications on potential roles for pCLE in the diagnosis of gastric ischaemia in critical care[381], microcirculatory changes in sepsis[382], colonic clostridium difficile infection[383], irritable bowel syndrome[384], and neurosurgical treatment of brain tumours[385]. It is exciting to imagine the endoscopy suite of 2030. Perhaps, drawing parallels with PET-CT where the co-registration of two imaging modalities provides complementary information, a fully integrated multimodality robotic imaging device will use a wide field technique such as NBI to alert the endoscopist to a suspicious mucosal lesion, force controlled pCLE will then be deployed from the device to interrogate the epithelium and basement membrane using a combination of fluorescent molecular markers and elastography, and OCT will assess the depth of invasion of any neoplastic lesion.

The pCLE machine not only plunges man more deeply into the problems of nature but also into the solutions to nature's problems.

References

1. Rajadhyaksha M, Anderson RR, Webb RH (1999) Video-rate confocal scanning laser microscope for imaging human tissues in vivo. Appl Opt 38**:**2105-2115

2. Paul N, Ghassemi KA (2011) Uses of probe-based confocal laser endomicroscopy: responses to a question to practitioners. World J Gastroenterol 17**:**4739-4740

3. Anderson JB, Webb AJ (1987) Fine-needle aspiration biopsy and the diagnosis of thyroid cancer. British Journal of Surgery 74**:**292-296

4. Puls L, Heidtman E, Hunter JE, Crane M, Stafford J (1997) The Accuracy of Frozen Section by Tumor Weight for Ovarian Epithelial Neoplasms. Gynecologic Oncology 67**:**16-19

5. Snook KL, Layer GT, Jackson PA, de Vries CS, Shousha S, Sinnett HD, Nigar E, Singhal H, Chia Y, Cunnick G, Kissin MW (2011) Multicentre evaluation of intraoperative molecular analysis of sentinel lymph nodes in breast carcinoma. Br J Surg 98**:**527-535

6. Selvaggi SM (2004) Biliary brushing cytology. Cytopathology 15**:**74-79

7. Gilmore IT, Burroughs A, Murray-Lyon IM, Williams R, Jenkins D, Hopkins A (1995) Indications, methods, and outcomes of percutaneous liver biopsy in England and Wales: an audit by the British Society of Gastroenterology and the Royal College of Physicians of London. Gut 36**:**437-441

8. Van Leeuwen DJ, Balabaud C, Crawford JM, Bioulac-Sage P, Dhillon AP (2008) A clinical and histopathologic perspective on evolving noninvasive and invasive alternatives for liver biopsy. Clin Gastroenterol Hepatol 6**:**491-496

9. Bozzini P (1807) Der Lichtleiter oder die Beschreibung einer einfachen Vorrichtung und ihrer Anwendung zur Erleuchtung innerer Höhlen und Zwischenräume des lebenden animalischen Körpers, Landes-Industrie-Comptoir

10. Jacques Van D (2004) Optical Biopsy. Gastrointestinal endoscopy clinics of North America 14**:**xv-xvi

11. Vincent BD, Fraig M, Silvestri GA (2007) A pilot study of narrow-band imaging compared to white light bronchoscopy for evaluation of normal airways and premalignant and malignant airways disease. Chest 131**:**1794-1799

12. Shibuya K, Hoshino H, Chiyo M, Iyoda A, Yoshida S, Sekine Y, Iizasa T, Saitoh Y, Baba M, Hiroshima K, Ohwada H, Fujisawa T (2003) High magnification bronchovideoscopy combined with narrow band imaging could detect capillary loops of angiogenic squamous dysplasia in heavy smokers at high risk for lung cancer. Thorax 58**:**989-995

13. Pohl J, Lotterer E, Balzer C, Sackmann M, Schmidt KD, Gossner L, Schaab C, Frieling T, Medve M, Mayer G, Nguyen-Tat M, Ell C (2009) Computed virtual chromoendoscopy versus standard colonoscopy with targeted indigocarmine chromoscopy: a randomised multicentre trial. Gut 58**:**73-78

14. Beamis JF, Jr., Ernst A, Simoff M, Yung R, Mathur P (2004) A multicenter study comparing autofluorescence bronchoscopy to white light bronchoscopy using a non-laser light stimulation system. Chest 125**:**148S-149S

15. Edell E, Lam S, Pass H, Miller YE, Sutedja T, Kennedy T, Loewen G, Keith RL (2009) Detection and localization of intraepithelial neoplasia and invasive carcinoma using fluorescence-reflectance bronchoscopy: an international, multicenter clinical trial. J Thorac Oncol 4**:**49-54

16. Haussinger K, Becker H, Stanzel F, Kreuzer A, Schmidt B, Strausz J, Cavaliere S, Herth F, Kohlhaufl M, Muller KM, Huber RM, Pichlmeier U, Bolliger Ch T (2005) Autofluorescence bronchoscopy with white light bronchoscopy compared with white light bronchoscopy alone for the detection of precancerous lesions: a European randomised controlled multicentre trial. Thorax 60**:**496-503

17. Yamada G, Takahashi H, Shijubo N, Itoh T, Abe S (2005) Subepithelial microvasculature in large airways observed by high-magnification bronchovideoscope. Chest 128**:**876-880

18. Huang Z, Teh SK, Zheng W, Mo J, Lin K, Shao X, Ho KY, Teh M, Yeoh KG (2009) Integrated Raman spectroscopy and trimodal wide-field imaging techniques for real-time in vivo tissue Raman measurements at endoscopy. Opt Lett 34**:**758-760

19. Testoni PA, Mangiavillano B (2008) Optical coherence tomography in detection of dysplasia and cancer of the gastrointestinal tract and bilio-pancreatic ductal system. World J Gastroenterol 14**:**6444-6452

20. Chen J, Lee L (2007) Clinical applications and new developments of optical coherence tomography: an evidence-based review. Clin Exp Optom 90**:**317-335

21. Gambichler T, Moussa G, Sand M, Sand D, Altmeyer P, Hoffmann K (2005) Applications of optical coherence tomography in dermatology. J Dermatol Sci 40**:**85-94

22. Farooq MU, Khasnis A, Majid A, Kassab MY (2009) The role of optical coherence tomography in vascular medicine. Vasc Med 14**:**63-71

23. Kubo T, Akasaka T (2008) Recent advances in intracoronary imaging techniques: focus on optical coherence tomography. Expert Rev Med Devices 5**:**691-697

24. Yang Y, Whiteman S, Gey van Pittius D, He Y, Wang RK, Spiteri MA (2004) Use of optical coherence tomography in delineating airways microstructure: comparison of OCT images to histopathological sections. Phys Med Biol 49**:**1247-1255

25. Tearney GJ, Brezinski ME, Bouma BE, Boppart SA, Pitris C, Southern JF, Fujimoto JG (1997) In vivo endoscopic optical biopsy with optical coherence tomography. Science 276:2037-2039

26. Kurimoto N, Murayama M, Yoshioka S, Nishisaka T (2002) Analysis of the internal structure of peripheral pulmonary lesions using endobronchial ultrasonography. Chest 122:1887-1894

27. Lam S, Standish B, Baldwin C, McWilliams A, leRiche J, Gazdar A, Vitkin AI, Yang V, Ikeda N, MacAulay C (2008) In vivo optical coherence tomography imaging of preinvasive bronchial lesions. Clin Cancer Res 14:2006-2011

28. Whiteman SC, Yang Y, Gey van Pittius D, Stephens M, Parmer J, Spiteri MA (2006) Optical coherence tomography: real-time imaging of bronchial airways microstructure and detection of inflammatory/neoplastic morphologic changes. Clin Cancer Res 12:813-818

29. Tsuboi M, Hayashi A, Ikeda N, Honda H, Kato Y, Ichinose S, Kato H (2005) Optical coherence tomography in the diagnosis of bronchial lesions. Lung Cancer 49:387-394

30. Michel RG, Kinasewitz GT, Fung KM, Keddissi JI (2010) Optical coherence tomography as an adjunct to flexible bronchoscopy in the diagnosis of lung cancer: a pilot study. Chest 138:984-988

31. Hamou J (1981) Microhysteroscopy. A new procedure and its original applications in gynecology. J Reprod Med 26:375-382

32. Tomizawa Y, Abdulla HM, Prasad GA, Wong Kee Song LM, Lutzke LS, Borkenhagen LS, Wang KK (2009) Endocytoscopy in esophageal cancer. Gastrointest Endosc Clin N Am 19:273-281

33. Cipolletta L, Bianco MA, Rotondano G, Piscopo R, Meucci C, Prisco A, Cipolletta F, de Gregorio A, Salvati A (2009) Endocytoscopy can identify dysplasia in aberrant crypt foci of the colorectum: a prospective in vivo study. Endoscopy 41:129-132

34. Fasoli A, Pugliese V, Furnari M, Gatteschi B, Truini M, Meroni E (2009) Signet ring cell carcinoma of the stomach: correlation between endocytoscopy and histology. Endoscopy 41 Suppl 2:E65-66

35. Ohigashi T, Kozakai N, Mizuno R, Miyajima A, Murai M (2006) Endocytoscopy: novel endoscopic imaging technology for in-situ observation of bladder cancer cells. J Endourol 20:698-701

36. Fujishiro M, Kodashima S, Takubo K, Kakushima N, Omata M (2008) Detailed comparison between endocytoscopy and horizontal histology of an esophageal intraepithelial squamous cell carcinoma. Dis Esophagus 21:181-185

37. Inoue H, Kazawa T, Sato Y, Satodate H, Sasajima K, Kudo SE, Shiokawa A (2004) In vivo observation of living cancer cells in the esophagus, stomach, and colon using catheter-type contact endoscope, "Endo-Cytoscopy system". Gastrointest Endosc Clin N Am 14:589-594, x-xi

38. Kodashima S, Fujishiro M, Takubo K, Kammori M, Nomura S, Kakushima N, Muraki Y, Tateishi A, Kaminishi M, Omata M (2006) Ex-vivo study of high-magnification chromoendoscopy in the gastrointestinal tract to determine the optimal staining conditions for endocytoscopy. Endoscopy 38**:**1115-1121

39. Shibuya K, Yasufuku K, Chiyo M, Nakajima T, Fujiwara T, Nagato K, Suzuki H, Iyoda A, Yoshida S, Suzuki M, Sekine Y, Hiroshima K, Nakatani Y, Yoshino I (2008) Endo-cytoscopy system is a novel endoscopic technology to visualize microscopic imaging of the tracheobronchial tree ERS, Berlin

40. Shibuya K, Fujiwara T, Yasufuku K, Alaa Rm M, Chiyo M, Nakajima T, Hoshino H, Hiroshima K, Nakatani Y, Yoshino I (2011) In vivo microscopic imaging of the bronchial mucosa using an endo-cytoscopy system. Lung Cancer 72**:**184-190

41. Neumann H, Vieth M, Neurath MF, Fuchs FS (2011) In Vivo Diagnosis of Small-Cell Lung Cancer by Endocytoscopy. J Clin Oncol 29**:**e31-32

42. Kiesslich R, Goetz M, Lammersdorf K, Schneider C, Burg J, Stolte M, Vieth M, Nafe B, Galle PR, Neurath MF (2007) Chromoscopy-guided endomicroscopy increases the diagnostic yield of intraepithelial neoplasia in ulcerative colitis. Gastroenterology 132**:**874-882

43. Minsky M (1988) Memoir on inventing the confocal scanning microscope. Scanning 10**:**128-138

44. Pawley JB (2006) Handbook of biological confocal microscopy, 3rd ed. edn, Springer, New York, NY

45. Sakashita M, Inoue H, Kashida H, Tanaka J, Cho JY, Satodate H, Hidaka E, Yoshida T, Fukami N, Tamegai Y, Shiokawa A, Kudo S (2003) Virtual histology of colorectal lesions using laser-scanning confocal microscopy. Endoscopy 35**:**1033-1038

46. Goetz M, Kiesslich R (2008) Confocal endomicroscopy: in vivo diagnosis of neoplastic lesions of the gastrointestinal tract. Anticancer Res 28**:**353-360

47. Thiberville L, Moreno-Swirc S, Vercauteren T, Peltier E, Cave C, Bourg Heckly G (2007) In vivo imaging of the bronchial wall microstructure using fibered confocal fluorescence microscopy. Am J Respir Crit Care Med 175**:**22-31

48. Thiberville L, Salaun M, Lachkar S, Dominique S, Moreno-Swirc S, Vever-Bizet C, Bourg-Heckly G (2009) Human in vivo fluorescence microimaging of the alveolar ducts and sacs during bronchoscopy. Eur Respir J 33**:**974-985

49. Tearney GJ, Wang TD (2008) Endoscopic microscopy III : 20-21 January 2008, San Jose, California, USA, SPIE, Bellingham, Wash.

50. Tan J, Delaney P, McLaren WJ (2007) Confocal endomicroscopy: a novel imaging technique for in vivo histology of cervical intraepithelial neoplasia. Expert Review of Medical Devices 4**:**863-871

51. Sonn GA, Jones SN, Tarin TV, Du CB, Mach KE, Jensen KC, Liao JC (2009) Optical biopsy of human bladder neoplasia with in vivo confocal laser endomicroscopy. J Urol 182**:**1299-1305

52. von Delius S, Feussner H, Wilhelm D, Karagianni A, Henke J, Schmid RM, Meining A (2007) Transgastric in vivo histology in the peritoneal cavity using miniprobe-based confocal fluorescence microscopy in an acute porcine model. Endoscopy 39**:**407-411

53. Karen JK, Gareau DS, Dusza SW, Tudisco M, Rajadhyaksha M, Nehal KS (2009) Detection of basal cell carcinomas in Mohs excisions with fluorescence confocal mosaicing microscopy. British Journal of Dermatology 160**:**1242-1250

54. Thong PS, Olivo M, Kho KW, Zheng W, Mancer K, Harris M, Soo KC (2007) Laser confocal endomicroscopy as a novel technique for fluorescence diagnostic imaging of the oral cavity. J Biomed Opt 12**:**014007

55. Kiesslich R, Burg J, Vieth M, Gnaendiger J, Enders M, Delaney P, Polglase A, McLaren W, Janell D, Thomas S, Nafe B, Galle PR, Neurath MF (2004) Confocal laser endoscopy for diagnosing intraepithelial neoplasias and colorectal cancer in vivo. Gastroenterology 127**:**706-713

56. Viellerobe B, Osdoit A, Cave C, Lacombe F, Loiseau S, Abrat B (2006) Mauna Kea technologies' F400 prototype: a new tool for in vivo microscopic imaging during endoscopy. Endoscopic Microscopy 6082**:**C820-885

57. Vercauteren T, Perchant A, Malandain G, Pennec X, Ayache N (2006) Robust mosaicing with correction of motion distortions and tissue deformations for in vivo fibered microscopy. Med Image Anal 10**:**673-692

58. Becker V, Vercauteren T, von Weyhern CH, Prinz C, Schmid RM, Meining A (2007) High-resolution miniprobe-based confocal microscopy in combination with video mosaicing (with video). Gastrointestinal Endoscopy 66**:**1001-1007

59. Wu K, Liu JJ, Adams W, Sonn GA, Mach KE, Pan Y, Beck AH, Jensen KC, Liao JC (2011) Dynamic real-time microscopy of the urinary tract using confocal laser endomicroscopy. Urology 78**:**225-231

60. Tumlinson AR, Hariri LP, Utzinger U, Barton JK (2004) Miniature endoscope for simultaneous optical coherence tomography and laser-induced fluorescence measurement. Applied optics 43**:**113-121

61. Ferrer-Roca O (2009) Telepathology and optical biopsy. Int J Telemed Appl 2009**:**740712

62. Kerkhof M, van Dekken H, Steyerberg EW, Meijer GA, Mulder AH, de Bruine A, Driessen A, ten Kate FJ, Kusters JG, Kuipers EJ, Siersema PD (2007) Grading of dysplasia in Barrett's oesophagus: substantial interobserver variation between general and gastrointestinal pathologists. Histopathology 50**:**920-927

63. Meining A, Saur D, Bajbouj M, Becker V, Peltier E, Hufler H, von Weyhern CH, Schmid RM, Prinz C (2007) In Vivo Histopathology for Detection of

Gastrointestinal Neoplasia With a Portable, Confocal Miniprobe: An Examiner Blinded Analysis. Clinical Gastroenterology and Hepatology 5:1261-1267

64. Kuiper T, Kiesslich R, Ponsioen C, Fockens P, Dekker E (2012) The learning curve, accuracy, and interobserver agreement of endoscope-based confocal laser endomicroscopy for the differentiation of colorectal lesions. Gastrointest Endosc 75:1211-1217

65. Pittayanon R, Rerknimitr R, Wisedopas N, Khemnark S, Thanapirom K, Thienchanachaiya P, Norrasetwanich N, Charoensuk K, Ridtitid W, Treeprasertsuk S, Kongkam P, Kullavanijaya P (2012) The learning curve of gastric intestinal metaplasia interpretation on the images obtained by probe-based confocal laser endomicroscopy. Diagn Ther Endosc 2012:278045

66. Buchner AM, Gomez V, Heckman MG, Shahid MW, Achem S, Gill KR, Laith J, Kahaleh M, Lo SK, Picco M, Riegert-Johnson D, Raimondo M, Sciemeca D, Wolfsen H, Woodward T, Wallace MB (2011) The learning curve of in vivo probe-based confocal laser endomicroscopy for prediction of colorectal neoplasia. Gastrointestinal Endoscopy 73:556-560

67. Becker V, Wallace MB, Fockens P, von Delius S, Woodward TA, Raimondo M, Voermans RP, Meining A (2010) Needle-based confocal endomicroscopy for in vivo histology of intra-abdominal organs: first results in a porcine model (with videos). Gastrointest Endosc 71:1260-1266

68. Kwan AS, Barry C, McAllister IL, Constable I (2006) Fluorescein angiography and adverse drug reactions revisited: the Lions Eye experience. Clin Experiment Ophthalmol 34:33-38

69. Wallace M, Meining A, Miehlke S (2009) Safety of intravenous fluorescein for probe-based Confocal Laser Endomicroscopy (pCLE): a multicenter study. Gastrointestinal Endoscopy 69:AB367-AB368

70. Wallace MB, Meining A, Canto MI, Fockens P, Miehlke S, Roesch T, Lightdale CJ, Pohl H, Carr-Locke D, Lohr M, Coron E, Filoche B, Giovannini M, Moreau J, Schmidt C, Kiesslich R (2010) The safety of intravenous fluorescein for confocal laser endomicroscopy in the gastrointestinal tract. Aliment Pharmacol Ther 31:548-552

71. Emmart EW (1958) Observations on the absorption spectra of fluorescein, fluorescein derivatives and conjugates. Archives of Biochemistry and Biophysics 73:1-8

72. Shahid MW, Crook JE, Meining A, Perchant A, Buchner A, Gomez V, Wallace MB (2012) Exploring the optimal fluorescein dose in probe-based confocal laser endomicroscopy for colonic imaging. J Interv Gastroenterol 1:166-171

73. Becker V, van den Broek FJ, Buchner AM, Dekker E, Wallace MB, von Delius S, Schneider A, Schmid RM, Meining A (2010) Optimal fluorescein dose for intravenous application in miniprobe-based confocal laser scanning microscopy in pigs. J Biophotonics 4:108-113

74. Becker V, von Delius S, Bajbouj M, Karagianni A, Schmid RM, Meining A (2008) Intravenous application of fluorescein for confocal laser scanning microscopy: evaluation of contrast dynamics and image quality with increasing injection-to-imaging time. Gastrointest Endosc 68**:**319-323

75. Northern_Ireland_Cancer_Registry (2008) Cancer incidence and mortality.

76. Office_for_National_Statistics (2011) Cancer statistics registrations: registrations of cancer diagnosed in 2008, England.

77. ISD_Scotland (2010) Colorectal Cancer: Annual Incidence.

78. Welsh_cancer_and_intelligence_surveillance_unit (2011) Cancer incidence in wales 2005-2009.

79. Heald RJ, Ryall RDH (1986) Recurrence and Survival after Total Mesorectal Excision for Rectal Cancer. The Lancet 327**:**1479-1482

80. Kapiteijn E, Marijnen CAM, Nagtegaal ID, Putter H, Steup WH, Wiggers T, Rutten HJT, Pahlman L, Glimelius B, van Krieken JHJM, Leer JWH, van de Velde CJH (2001) Preoperative Radiotherapy Combined with Total Mesorectal Excision for Resectable Rectal Cancer. New England Journal of Medicine 345**:**638-646

81. André T, Boni C, Mounedji-Boudiaf L, Navarro M, Tabernero J, Hickish T, Topham C, Zaninelli M, Clingan P, Bridgewater J (2004) Oxaliplatin, fluorouracil, and leucovorin as adjuvant treatment for colon cancer. New England Journal of Medicine 350**:**2343-2351

82. Office_for_National_Statistics (2009) Cancer survival rates, Survival Rates in England, patients diagnosed 2001-2006 followed up to 2007.

83. Moreaux J, Catala M (1987) Carcinoma of the colon: long-term survival and prognosis after surgical treatment in a series of 798 patients. World journal of surgery 11**:**804-808

84. Muto T, Bussey HJ, Morson BC (1975) The evolution of cancer of the colon and rectum. Cancer 36**:**2251-2270

85. Morson BC (1968) Precancerous and early malignant lesions of the large intestine. Br J Surg 55**:**725-731

86. Saito Y, Uraoka T, Matsuda T, Emura F, Ikehara H, Mashimo Y, Kikuchi T, Fu K-I, Sano Y, Saito D (2007) Endoscopic treatment of large superficial colorectal tumors: a case series of 200 endoscopic submucosal dissections (with video). Gastrointestinal Endoscopy 66**:**966-973

87. Weller D, Coleman D, Robertson R, Butler P, Melia J, Campbell C, Parker R, Patnick J, Moss S (2007) The UK colorectal cancer screening pilot: results of the second round of screening in England. British journal of cancer 97**:**1601-1605

88. Lieberman DA, Harford WV, Ahnen DJ, Provenzale D, Sontag SJ, Schnell TG, Chejfec G, Campbell DR, Durbin TE, Bond JH, Nelson DB, Ewing SL,

Triadafilopoulos G, Ramirez FC, Lee JG, Collins JF, Fennerty MB, Johnston TK, Corless CL, McQuaid KR, Garewal H, Sampliner RE, Morales TG, Fass R, Smith RE, Maheshwari Y, Weiss DG (2001) One-Time Screening for Colorectal Cancer with Combined Fecal Occult-Blood Testing and Examination of the Distal Colon. New England Journal of Medicine 345:555-560

89. Lieberman DA, Weiss DG, Bond JH, Ahnen DJ, Garewal H, Harford WV, Provenzale D, Sontag S, Schnell T, Durbin TE, Nelson DB, Ewing SL, Triadafilopoulos G, Ramirez FC, Lee JG, Collins JF, Fennerty MB, Johnston TK, Corless CL, McQuaid KR, Sampliner RE, Morales TG, Fass R, Smith R, Maheshwari Y, Chejfec G (2000) Use of Colonoscopy to Screen Asymptomatic Adults for Colorectal Cancer. New England Journal of Medicine 343:162-168

90. Pickhardt PJ, Choi JR, Hwang I, Butler JA, Puckett ML, Hildebrandt HA, Wong RK, Nugent PA, Mysliwiec PA, Schindler WR (2003) Computed Tomographic Virtual Colonoscopy to Screen for Colorectal Neoplasia in Asymptomatic Adults. New England Journal of Medicine 349:2191-2200

91. Atkin WS, Edwards R, Kralj-Hans I, Wooldrage K, Hart AR, Northover JMA, Parkin DM, Wardle J, Duffy SW, Cuzick J (2010) Once-only flexible sigmoidoscopy screening in prevention of colorectal cancer: a multicentre randomised controlled trial. The Lancet 375:1624-1633

92. Huang CS, O'Brien M J, Yang S, Farraye FA (2004) Hyperplastic polyps, serrated adenomas, and the serrated polyp neoplasia pathway. Am J Gastroenterol 99:2242-2255

93. Hoff G, Foerster A, Vatn MH, Sauar J, Larsen S (1986) Epidemiology of Polyps in the Rectum and Colon: Recovery and Evaluation of Unresected Polyps 2 Years after Detection. Scandinavian Journal of Gastroenterology 21:853-862

94. van Rijn JC, Reitsma JB, Stoker J, Bossuyt PM, van Deventer SJ, Dekker E (2006) Polyp Miss Rate Determined by Tandem Colonoscopy: A Systematic Review. Am J Gastroenterol 101:343-350

95. Lecomte T, Cellier C, Meatchi T, Barbier JP, Cugnenc PH, Jian R, Laurent-Puig P, Landi B (2005) Chromoendoscopic colonoscopy for detecting preneoplastic lesions in hereditary nonpolyposis colorectal cancer syndrome. Clinical Gastroenterology and Hepatology 3:897-902

96. Kudo S-e, Tamura S, Nakajima T, Yamano H-o, Kusaka H, Watanabe H (1996) Diagnosis of colorectal tumorous lesions by magnifying endoscopy. Gastrointestinal Endoscopy 44:8-14

97. Hurlstone DP, Cross SS, Adam I, Shorthouse AJ, Brown S, Sanders DS, Lobo AJ (2004) Efficacy of high magnification chromoscopic colonoscopy for the diagnosis of neoplasia in flat and depressed lesions of the colorectum: a prospective analysis. Gut 53:284-290

98. Rabeneck L, Paszat LF, Hilsden RJ, Saskin R, Leddin D, Grunfeld E, Wai E, Goldwasser M, Sutradhar R, Stukel TA (2008) Bleeding and perforation after outpatient colonoscopy and their risk factors in usual clinical practice. Gastroenterology 135:1899-1906, 1906 e1891

99. Buchner AM, Ghabril MS, Krishna M, Wolfsen HC, Wallace MB (2008) High-Resolution Confocal Endomicroscopy Probe System for In Vivo Diagnosis of Colorectal Neoplasia. Gastroenterology 135:295

100. Shahid MW, Buchner AM, Heckman MG, Krishna M, Raimondo M, Woodward T, Wallace MB (2012) Diagnostic Accuracy of Probe-Based Confocal Laser Endomicroscopy and Narrow Band Imaging for Small Colorectal Polyps: A Feasibility Study. Am J Gastroenterol 107:231-239

101. De Palma GD, Staibano S, Siciliano S, Persico M, Masone S, Maione F, Siano M, Mascolo M, Esposito D, Salvatori F, Persico G (2010) In vivo characterisation of superficial colorectal neoplastic lesions with high-resolution probe-based confocal laser endomicroscopy in combination with video-mosaicing: A feasibility study to enhance routine endoscopy. Digestive and Liver Disease 42:791-797

102. Kuiper T, van den Broek FJ, van Eeden S, Wallace MB, Buchner AM, Meining A, van Hee K, Fockens P, Dekker E (2011) New classification for probe-based confocal laser endomicroscopy in the colon. Endoscopy 43:1076-1081

103. Hlavaty T, Huorka M, Koller T, Zita P, Kresanova E, Rychly B, Toth J (2011) Colorectal cancer screening in patients with ulcerative and Crohn's colitis with use of colonoscopy, chromoendoscopy and confocal endomicroscopy. Eur J Gastroenterol Hepatol 23:680-689

104. Gunther U, Kusch D, Heller F, Burgel N, Leonhardt S, Daum S, Siegmund B, Loddenkemper C, Grunbaum M, Buhr HJ, Schulzke JD, Zeitz M, Bojarski C (2011) Surveillance colonoscopy in patients with inflammatory bowel disease: comparison of random biopsy vs. targeted biopsy protocols. Int J Colorectal Dis 26:667-672

105. Xie XJ, Li CQ, Zuo XL, Yu T, Gu XM, Li Z, Ji R, Wang Q, Li YQ (2011) Differentiation of colonic polyps by confocal laser endomicroscopy. Endoscopy 43:87-93

106. van den Broek FJ, van Es JA, van Eeden S, Stokkers PC, Ponsioen CY, Reitsma JB, Fockens P, Dekker E (2011) Pilot study of probe-based confocal laser endomicroscopy during colonoscopic surveillance of patients with longstanding ulcerative colitis. Endoscopy 43:116-122

107. Sanduleanu S, Driessen A, Gomez-Garcia E, Hameeteman W, de Bruine A, Masclee A (2009) In Vivo Diagnosis and Classification of Colorectal Neoplasia by Chromoendoscopy-Guided Confocal Laser Endomicroscopy. Clinical gastroenterology and hepatology : the official clinical practice journal of the American Gastroenterological Association 8:371-378

108. Gomez V, Buchner AM, Dekker E, van den Broek FJC, Meining A, Shahid MW, Ghabril MS, Fockens P, Heckman MG, Wallace MB (2010) Interobserver agreement and accuracy among international experts with probe-based confocal laser endomicroscopy in predicting colorectal neoplasia. Endoscopy 42:286-291

109. Buchner AM, Shahid MW, Heckman MG, Krishna M, Ghabril M, Hasan M, Crook JE, Gomez V, Raimondo M, Woodward T, Wolfsen HC, Wallace MB (2009) Comparison of probe-based confocal laser endomicroscopy with virtual chromoendoscopy for classification of colon polyps. Gastroenterology 138**:**834-842

110. Hurlstone DP, Baraza W, Brown S, Thomson M, Tiffin N, Cross SS (2008) In vivo real-time confocal laser scanning endomicroscopic colonoscopy for the detection and characterization of colorectal neoplasia. British Journal of Surgery 95**:**636-645

111. Shahid MW, Buchner AM, Raimondo M, Woodward TA, Krishna M, Wallace MB (2012) Accuracy of real-time vs. blinded offline diagnosis of neoplastic colorectal polyps using probe-based confocal laser endomicroscopy: a pilot study. Endoscopy 44**:**343-348

112. Lim LG, Yeoh KG, Srivastava S, Chan YH, Teh M, Ho KY (2013) Comparison of probe-based confocal endomicroscopy with virtual chromoendoscopy and white-light endoscopy for diagnosis of gastric intestinal metaplasia. Surg Endosc

113. Su P, Liu Y, Lin S, Xiao K, Chen P, An S, He J, Bai Y (2012) Efficacy of confocal laser endomicroscopy for discriminating colorectal neoplasms from non-neoplasms: a systematic review and meta-analysis. Colorectal Dis 15**:**e1-e12

114. Andre B, Vercauteren T, Buchner AM, Krishna M, Ayache N, Wallace MB (2012) Software for automated classification of probe-based confocal laser endomicroscopy videos of colorectal polyps. World J Gastroenterol 18**:**5560-5569

115. Winawer SJ, Zauber AG, Fletcher RH, Stillman JS, O'Brien M J, Levin B, Smith RA, Lieberman DA, Burt RW, Levin TR, Bond JH, Brooks D, Byers T, Hyman N, Kirk L, Thorson A, Simmang C, Johnson D, Rex DK (2006) Guidelines for colonoscopy surveillance after polypectomy: a consensus update by the US Multi-Society Task Force on Colorectal Cancer and the American Cancer Society. CA Cancer J Clin 56**:**143-159; quiz 184-145

116. Gomez V, Shahid MW, Krishna M, Heckman MG, Crook JE, Wallace MB (2013) Classification criteria for advanced adenomas of the colon by using probe-based confocal laser endomicroscopy: a preliminary study. Dis Colon Rectum 56**:**967-973

117. Wallace MB, Fockens P (2009) Probe-based confocal laser endomicroscopy. Gastroenterology 136**:**1509-1513

118. Wang TD, Friedland S, Sahbaie P, Soetikno R, Hsiung PL, Liu JT, Crawford JM, Contag CH (2007) Functional imaging of colonic mucosa with a fibered confocal microscope for real-time in vivo pathology. Clin Gastroenterol Hepatol 5**:**1300-1305

119. Goetz M, Toermer T, Vieth M, Dunbar K, Hoffman A, Galle PR, Neurath MF, Delaney P, Kiesslich R (2009) Simultaneous confocal laser endomicroscopy and chromoendoscopy with topical cresyl violet. Gastrointest Endosc 70**:**959-968

120. (1977) IARC monographs on the evaluation of the carcinogenic risk of chemicals to man: some miscellaneous pharmaceutical substances. IARC Monogr Eval Carcinog Risk Chem Man 13:1-255

121. Yoshida S, Tanaka S, Hirata M, Mouri R, Kaneko I, Oka S, Yoshihara M, Chayama K (2007) Optical biopsy of GI lesions by reflectance-type laser-scanning confocal microscopy. Gastrointest Endosc 66:144-149

122. Anikijenko P, Vo LT, Murr ER, Carrasco J, McLaren WJ, Chen Q, Thomas SG, Delaney PM, King RG (2001) In Vivo Detection of Small Subsurface Melanomas in Athymic Mice Using Noninvasive Fiber Optic Confocal Imaging. 117:1442-1448

123. Spano J-P, Lagorce C, Atlan D, Milano G, Domont J, Benamouzig R, Attar A, Benichou J, Martin A, Morere J-F, Raphael M, Penault-Llorca F, Breau J-L, Fagard R, Khayat D, Wind P (2005) Impact of EGFR expression on colorectal cancer patient prognosis and survival. Annals of Oncology 16:102-108

124. Goetz M, Ziebart A, Foersch S, Vieth M, Waldner MJ, Delaney P, Galle PR, Neurath MF, Kiesslich R (2010) In Vivo Molecular Imaging of Colorectal Cancer With Confocal Endomicroscopy by Targeting Epidermal Growth Factor Receptor. Gastroenterology 138:435-446

125. Liu J, Zuo X, Li C, Yu T, Gu X, Zhou C, Li Z, Goetz M, Kiesslich R, Li Y (2013) In vivo molecular imaging of epidermal growth factor receptor in patients with colorectal neoplasia using confocal laser endomicroscopy. Cancer Lett 330:200-207

126. Hsiung PL, Hardy J, Friedland S, Soetikno R, Du CB, Wu AP, Sahbaie P, Crawford JM, Lowe AW, Contag CH, Wang TD (2008) Detection of colonic dysplasia in vivo using a targeted heptapeptide and confocal microendoscopy. Nat Med 14:454-458

127. Cartana T, Saftoiu A, Gruionu LG, Gheonea DI, Pirici D, Georgescu CV, Ciocalteu A, Gruionu G (2012) Confocal Laser Endomicroscopy for the Morphometric Evaluation of Microvessels in Human Colorectal Cancer Using Targeted Anti-CD31 Antibodies. PLoS One 7:e52815

128. Shahid MW, Buchner AM, Coron E, Woodward TA, Raimondo M, Dekker E, Fockens P, Wallace MB (2012) Diagnostic accuracy of probe-based confocal laser endomicroscopy in detecting residual colorectal neoplasia after EMR: a prospective study. Gastrointestinal Endoscopy 75:525-533.e521

129. Li C-Q, Xie X-J, Yu T, Gu X-M, Zuo X-L, Zhou C-J, Huang W-Q, Chen H, Li Y-Q (2010) Classification of Inflammation Activity in Ulcerative Colitis by Confocal Laser Endomicroscopy. Am J Gastroenterol 105:1391-1396

130. Liu JJ, Wong K, Thiesen AL, Mah SJ, Dieleman LA, Claggett B, Saltzman JR, Fedorak RN (2011) Increased epithelial gaps in the small intestines of patients with inflammatory bowel disease: density matters. Gastrointestinal Endoscopy 73:1174-1180

131. Kiesslich R, Duckworth CA, Moussata D, Gloeckner A, Lim LG, Goetz M, Pritchard DM, Galle PR, Neurath MF, Watson AJ (2012) Local barrier dysfunction identified by confocal laser endomicroscopy predicts relapse in inflammatory bowel disease. Gut 61:1146-1153

132. Turcotte JF, Wong K, Mah SJ, Dieleman LA, Kao D, Kroeker K, Claggett B, Saltzman JR, Wine E, Fedorak RN, Liu JJ (2013) Increased epithelial gaps in the small intestine are predictive of hospitalization and surgery in patients with inflammatory bowel disease. Clin Transl Gastroenterol 3:e19

133. Hundorfean G, Chiriac MT, Mudter J, Neurath MF (2013) Confocal laser endomicroscopy provides potential differentiation criteria between Crohn's disease and ulcerative colitis. Inflammatory Bowel Diseases 19:E61-64

134. Bojarski C, Gunther U, Rieger K, Heller F, Loddenkemper C, Grunbaum M, Uharek L, Zeitz M, Hoffmann JC (2009) In vivo diagnosis of acute intestinal graft-versus-host disease by confocal endomicroscopy. Endoscopy 41:433-438

135. Hundorfean G, Agaimy A, Chiriac MT, Rosler W, Mackensen A, Siebler J, Neurath MF (2013) Highlighting Crypt Necrosis by Using Confocal Laser Endomicroscopy for the In Vivo and Real-Time Diagnosis of GI Graft-Versus-Host Disease. J Clin Oncol 30:e368-369

136. Sumiyama K, Kiesslich R, Ohya TR, Goetz M, Tajiri H (2012) In vivo imaging of enteric neuronal networks in humans using confocal laser endomicroscopy. Gastroenterology 143:1152-1153

137. Ohya TR, Sumiyama K, Takahashi-Fujigasaki J, Dobashi A, Saito S, Tajiri H (2012) In vivo histologic imaging of the muscularis propria and myenteric neurons with probe-based confocal laser endomicroscopy in porcine models (with videos). Gastrointest Endosc 75:405-410

138. Jailwala J, Fogel EL, Sherman S, Gottlieb K, Flueckiger J, Bucksot LG, Lehman GA (2000) Triple-tissue sampling at ERCP in malignant biliary obstruction. Gastrointestinal Endoscopy 51:383-390

139. Baron TH, Harewood GC, Rumalla A, Pochron NL, Stadheim LM, Gores GJ, Therneau TM, De Groen PC, Sebo TJ, Salomao DR, Kipp BR (2004) A prospective comparison of digital image analysis and routine cytology for the identification of malignancy in biliary tract strictures. Clinical Gastroenterology and Hepatology 2:214-219

140. Kipp BR, Stadheim LM, Halling SA, Pochron NL, Harmsen S, Nagorney DM, Sebo TJ, Therneau TM, Gores GJ, Groen PCd, Baron TH, Levy MJ, Halling KC, Roberts LR (2004) A Comparison of Routine Cytology and Fluorescence in situ Hybridization for the Detection of Malignant Bile Duct Strictures. Am J Gastroenterol 99:1675-1681

141. Meining A, Frimberger E, Becker V, Von Delius S, Von Weyhern CH, Schmid RM, Prinz C (2008) Detection of cholangiocarcinoma in vivo using miniprobe-based confocal fluorescence microscopy. Clin Gastroenterol Hepatol 6:1057-1060

142. Loeser CS, Robert ME, Mennone A, Nathanson MH, Jamidar P (2011) Confocal endomicroscopic examination of malignant biliary strictures and histologic correlation with lymphatics. J Clin Gastroenterol 45:246-252

143. Giovannini M, Bories E, Monges G, Pesenti C, Caillol F, Delpero JR (2011) Results of a phase I-II study on intraductal confocal microscopy (IDCM) in patients with common bile duct (CBD) stenosis. Surg Endosc 25:2247-2253

144. Chennat J, Konda VJ, Madrigal-Hoyos E, Fernandez-Sordo J, Xiao SY, Hart J, Waxman I (2011) Biliary confocal laser endomicroscopy real-time detection of cholangiocarcinoma. Dig Dis Sci 56:3701-3706

145. Meining A, Shah RJ, Slivka A, Pleskow D, Chuttani R, Stevens PD, Becker V, Chen YK (2012) Classification of probe-based confocal laser endomicroscopy findings in pancreaticobiliary strictures. Endoscopy 44:251-257

146. Caillol F, Filoche B, Gaidhane M, Kahaleh M (2013) Refined Probe-Based Confocal Laser Endomicroscopy Classification for Biliary Strictures: The Paris Classification. Dig Dis Sci 58:1784-1789

147. Bakhru MR, Sethi A, Jamidar PA, Singh SK, Kwon RS, Siddiqui UD, Sawhney M, Talreja JP, Kline P, Malik U, Gaidhane M, Sauer BG, Kahaleh M (2013) Interobserver Agreement for Confocal Imaging of Ampullary Lesions: A Multicenter Single-blinded Study. J Clin Gastroenterol 47:440-442

148. Talreja J, Sethi A, Jamidar P, Singh S, Kwon R, Siddiqui U, Sawhney M, Bakhru M, Gaidhane M, Kline P, Sauer B, Kahaleh M (2012) Interpretation of Probe-Based Confocal Laser Endomicroscopy of Indeterminate Biliary Strictures: Is There Any Interobserver Agreement? Digestive Diseases and Sciences 57:3299-3302

149. Enzinger PC, Mayer RJ (2003) Esophageal cancer. New England Journal of Medicine 349:2241-2252

150. UK_Office_For_National_Statistics (2005) Cancer trends in england and wales - smps no. 66.

151. Portale G, Hagen JA, Peters JH, Chan LS, DeMeester SR, Gandamihardja TAK, DeMeester TR (2006) Modern 5-Year Survival of Resectable Esophageal Adenocarcinoma: Single Institution Experience with 263 Patients. Journal of the American College of Surgeons 202:588-596

152. Wang KK, Sampliner RE (2008) Updated Guidelines 2008 for the Diagnosis, Surveillance and Therapy of Barrett's Esophagus. Am J Gastroenterol 103:788-797

153. Egger K, Werner M, Meining A, Ott R, Allescher H, Hofler H, Classen M, Rosch T (2003) Biopsy surveillance is still necessary in patients with Barrett's oesophagus despite new endoscopic imaging techniques. Gut 52:18-23

154. Kiesslich R, Gossner L, Goetz M, Dahlmann A, Vieth M, Stolte M, Hoffman A, Jung M, Nafe B, Galle PR (2006) In vivo histology of Barrett's esophagus and

associated neoplasia by confocal laser endomicroscopy. Clinical Gastroenterology and Hepatology 4:979-987

155. Dunbar KB, Okolo P, 3rd, Montgomery E, Canto MI (2009) Confocal laser endomicroscopy in Barrett's esophagus and endoscopically inapparent Barrett's neoplasia: a prospective, randomized, double-blind, controlled, crossover trial. Gastrointest Endosc 70:645-654

156. Guo YT, Li YQ, Yu T, Zhang TG, Zhang JN, Liu H, Liu FG, Xie XJ, Zhu Q, Zhao YA (2008) Diagnosis of gastric intestinal metaplasia with confocal laser endomicroscopy in vivo: a prospective study. Endoscopy 40:547-553

157. Pohl H, Rosch T, Vieth M, Koch M, Becker V, Anders M, Khalifa AC, Meining A (2008) Miniprobe confocal laser microscopy for the detection of invisible neoplasia in patients with Barrett's oesophagus. Gut 57:1648-1653

158. Wallace MB, Sharma P, Lightdale C, Wolfsen H, Coron E, Buchner A, Bajbouj M, Bansal A, Rastogi A, Abrams J, Crook JE, Meining A (2010) Preliminary accuracy and interobserver agreement for the detection of intraepithelial neoplasia in Barrett's esophagus with probe-based confocal laser endomicroscopy. Gastrointest Endosc 72:19-24

159. Gaddam S, Mathur SC, Singh M, Arora J, Wani SB, Gupta N, Overhiser A, Rastogi A, Singh V, Desai N, Hall SB, Bansal A, Sharma P (2011) Novel probe-based confocal laser endomicroscopy criteria and interobserver agreement for the detection of dysplasia in Barrett's esophagus. Am J Gastroenterol 106:1961-1969

160. Bajbouj M, Vieth M, Rosch T, Miehlke S, Becker V, Anders M, Pohl H, Madisch A, Schuster T, Schmid RM, Meining A (2010) Probe-based confocal laser endomicroscopy compared with standard four-quadrant biopsy for evaluation of neoplasia in Barrett's esophagus. Endoscopy 42:435-440

161. Sharma P, Meining AR, Coron E, Lightdale CJ, Wolfsen HC, Bansal A, Bajbouj M, Galmiche JP, Abrams JA, Rastogi A, Gupta N, Michalek JE, Lauwers GY, Wallace MB (2011) Real-time increased detection of neoplastic tissue in Barrett's esophagus with probe-based confocal laser endomicroscopy: final results of an international multicenter, prospective, randomized, controlled trial. Gastrointest Endosc 74:465-472

162. Becker V, Vieth M, Bajbouj M, Schmid RM, Meining A (2008) Confocal laser scanning fluorescence microscopy for in vivo determination of microvessel density in Barrett's esophagus. Endoscopy 40:888-891

163. Iguchi Y, Niwa Y, Miyahara R, Nakamura M, Banno K, Nagaya T, Nagasaka T, Watanabe O, Ando T, Kawashima H, Ohmiya N, Itoh A, Hirooka Y, Goto H (2009) Pilot study on confocal endomicroscopy for determination of the depth of squamous cell esophageal cancer in vivo. J Gastroenterol Hepatol 24:1733-1739

164. Thekkek N, Maru DM, Polydorides AD, Bhutani MS, Anandasabapathy S, Richards-Kortum R (2011) Pre-clinical evaluation of fluorescent deoxyglucose as a topical contrast agent for the detection of Barrett's-associated neoplasia during confocal imaging. Technol Cancer Res Treat 10:431-441

165. Gorospe EC, Leggett CL, Sun G, Anderson MA, Gupta M, Penfield JD, Lutzke L, Lewis JT, Wong Kee Song LM, Wang KK (2012) Diagnostic performance of two confocal endomicroscopy systems in detecting Barrett's dysplasia: a pilot study using a novel bioprobe in ex vivo tissue. Gastrointest Endosc 76**:**933-938

166. Nakai Y, Shinoura S, Ahluwalia A, Tarnawski AS, Chang KJ (2012) Molecular imaging of epidermal growth factor-receptor and survivin in vivo in porcine esophageal and gastric mucosae using probe-based confocal laser-induced endomicroscopy: proof of concept. J Physiol Pharmacol 63**:**303-307

167. Li M, Anastassiades CP, Joshi B, Komarck CM, Piraka C, Elmunzer BJ, Turgeon DK, Johnson TD, Appelman H, Beer DG, Wang TD (2010) Affinity Peptide for Targeted Detection of Dysplasia in Barrett's Esophagus. Gastroenterology 139**:**1472-1480

168. Sturm MB, Piraka C, Elmunzer BJ, Kwon RS, Joshi BP, Appelman HD, Turgeon DK, Wang TD (2013) In Vivo Molecular Imaging of Barrett's Esophagus With Confocal Laser Endomicroscopy. Gastroenterology 145**:**56-58

169. Bisschops R, Bergman J (2010) Probe-based confocal laser endomicroscopy: scientific toy or clinical tool? Endoscopy 42**:**487-489

170. Ell C, May A, Gossner L, Pech O, Gunter E, Mayer G, Henrich R, Vieth M, Muller H, Seitz G (2000) Endoscopic mucosal resection of early cancer and high-grade dysplasia in Barrett's esophagus. Gastroenterology 118**:**670-677

171. Leung KK, Maru D, Abraham S, Hofstetter WL, Mehran R, Anandasabapathy S (2009) Optical EMR: confocal endomicroscopy-targeted EMR of focal high-grade dysplasia in Barrett's esophagus. Gastrointest Endosc 69**:**170-172

172. Konda VJ, Chennat JS, Hart J, Waxman I (2010) Confocal laser endomicroscopy: potential in the management of Barrett's esophagus. Dis Esophagus 23**:**E21-31

173. Chang TC, Liu JJ, Hsiao ST, Pan Y, Mach KE, Leppert JT, McKenney JK, Rouse RV, Liao JC (2013) Interobserver Agreement of Confocal Laser Endomicroscopy for Bladder Cancer. J Endourol 27**:**598-603

174. Bonnal JL, Rock A, Jr., Gagnat A, Papadopoulos S, Filoche B, Mauroy B (2012) Confocal laser endomicroscopy of bladder tumors associated with photodynamic diagnosis: an ex vivo pilot study. Urology 80**:**1162 e1161-1165

175. Tanbakuchi AA, Udovich JA, Rouse AR, Hatch KD, Gmitro AF (2009) In vivo imaging of ovarian tissue using a novel confocal microlaparoscope. Am J Obstet Gynecol 202**:**90 e91-99

176. Srivastava S, Rodriguez JJ, Rouse AR, Brewer MA, Gmitro AF (2008) Computer-aided identification of ovarian cancer in confocal microendoscope images. J Biomed Opt 13**:**024021

177. Tan J, Quinn MA, Pyman JM, Delaney PM, McLaren WJ (2009) Detection of cervical intraepithelial neoplasia in vivo using confocal endomicroscopy. BJOG 116

178. Lam S, Hung JY, Kennedy SM, Leriche JC, Vedal S, Nelems B, Macaulay CE, Palcic B (1992) Detection of dysplasia and carcinoma in situ by ratio fluorometry. Am Rev Respir Dis 146**:**1458-1461

179. Bard MP, Amelink A, Skurichina M, Noordhoek Hegt V, Duin RP, Sterenborg HJ, Hoogsteden HC, Aerts JG (2006) Optical spectroscopy for the classification of malignant lesions of the bronchial tree. Chest 129**:**995-1001

180. Chao TY, Lie CH, Chung YH, Wang JL, Wang YH, Lin MC (2006) Differentiating peripheral pulmonary lesions based on images of endobronchial ultrasonography. Chest 130**:**1191-1197

181. Baba M, Sekine Y, Suzuki M, Yoshida S, Shibuya K, Iizasa T, Saitoh Y, Onuma EK, Ohwada H, Fujisawa T (2002) Correlation between endobronchial ultrasonography (EBUS) images and histologic findings in normal and tumor-invaded bronchial wall. Lung Cancer 35**:**65-71

182. Tanaka M, Takizawa H, Satoh M, Okada Y, Yamasawa F, Umeda A (1994) Assessment of an ultrathin bronchoscope that allows cytodiagnosis of small airways. Chest 106**:**1443-1447

183. (2005) The Diagnosis and Treatment of Lung Cancer: Methods, Evidence and Guidance. In: Evidence NIfC (ed)

184. Elston WJ, Whittaker AJ, Khan LN, Flood-Page P, Ramsay C, Jeffery PK, Barnes NC (2004) Safety of research bronchoscopy, biopsy and bronchoalveolar lavage in asthma. Eur Respir J 24**:**375-377

185. Dhillon DP, Haslam PL, Townsend PJ, Primett Z, Collins JV, Turner-Warwick M (1986) Bronchoalveolar lavage in patients with interstitial lung diseases: side effects and factors affecting fluid recovery. Eur J Respir Dis 68**:**342-350

186. Flaherty KR, King TE, Jr., Raghu G, Lynch JP, 3rd, Colby TV, Travis WD, Gross BH, Kazerooni EA, Toews GB, Long Q, Murray S, Lama VN, Gay SE, Martinez FJ (2004) Idiopathic interstitial pneumonia: what is the effect of a multidisciplinary approach to diagnosis? Am J Respir Crit Care Med 170**:**904-910

187. Zhang D, Liu Y (2010) Surgical lung biopsies in 418 patients with suspected interstitial lung disease in China. Intern Med 49**:**1097-1102

188. Wells AU (2004) Histopathologic Diagnosis in Diffuse Lung Disease. American Journal of Respiratory and Critical Care Medicine 170**:**828-829

189. Izbicki G, Shitrit D, Yarmolovsky A, Bendayan D, Miller G, Fink G, Mazar A, Kramer MR (2006) Is routine chest radiography after transbronchial biopsy necessary?: A prospective study of 350 cases. Chest 129**:**1561-1564

190. Hanson RR, Zavala DC, Rhodes ML, Keim LW, Smith JD (1976) Transbronchial biopsy via flexible fiberoptic bronchoscope; results in 164 patients. Am Rev Respir Dis 114**:**67-72

191. Smyth CM, Stead RJ (2002) Survey of flexible fibreoptic bronchoscopy in the United Kingdom. Eur Respir J 19:458-463

192. Andersen HA (1978) Transbronchoscopic lung biopsy for diffuse pulmonary diseases. Results in 939 patients. Chest 73:734-736

193. O'Brien JD, Ettinger NA, Shevlin D, Kollef MH (1997) Safety and yield of transbronchial biopsy in mechanically ventilated patients. Crit Care Med 25:440-446

194. Herth FJ, Becker HD, Ernst A (2002) Aspirin does not increase bleeding complications after transbronchial biopsy. Chest 122:1461-1464

195. Silva CI, Muller NL, Hansell DM, Lee KS, Nicholson AG, Wells AU (2008) Nonspecific interstitial pneumonia and idiopathic pulmonary fibrosis: changes in pattern and distribution of disease over time. Radiology 247:251-259

196. Jimenez MF (2001) Prospective study on video-assisted thoracoscopic surgery in the resection of pulmonary nodules: 209 cases from the Spanish Video-Assisted Thoracic Surgery Study Group. Eur J Cardiothorac Surg 19:562-565

197. Yick CY, von der Thusen JH, Bel EH, Sterk PJ, Kunst PW (2011) In vivo imaging of the airway wall in asthma: fibered confocal fluorescence microscopy in relation to histology and lung function. Respiratory Research 12

198. Lane PM, Lam S, McWilliams A, Leriche JC, Anderson MW, Macaulay CE (2009) Confocal fluorescence microendoscopy of bronchial epithelium. J Biomed Opt 14:024008

199. Fuchs FS, Zirlik S, Hildner K, Frieser M, Ganslmayer M, Schwarz S, Uder M, Neurath MF (2010) Fluorescein-aided confocal laser endomicroscopy of the lung. Respiration 81:32-38

200. Thiberville L, Salaun M, Moreno-Swirc S, Bourg-Heckly G (2007) In vivo endoscopic microimaging of the bronchial epithelial layer using 660nm fibered confocal fluorescence microscopy and topical methylene blue. European Respiratory Society Meeting; Stockholm European Respiratory Journal 7125

201. Musani AI, Sims M, Sareli C, Russell W, McLaren WJ, Delaney PM, Litzky LA, Panettieri RAJ (2010) A Pilot Study of the Feasibility of Confocal Endomicroscopy for Examination of the Human Airway. Journal of Bronchology & Interventional Pulmonology 17:126-130

202. Prakash UB, Fontana RS (1984) Functional classification of bronchial carinae. Chest 86:770-772

203. Skold CM, Hed J, Eklund A (1992) Smoking cessation rapidly reduces cell recovery in bronchoalveolar lavage fluid, while alveolar macrophage fluorescence remains high. Chest 101:989-995

204. Salaun M, Roussel F, Hauss PA, Lachkar S, Thiberville L (2010) In vivo imaging of pulmonary alveolar proteinosis using confocal endomicroscopy. Eur Respir J 36:451-453

205. Thiberville L, Salaun M, Lachkar S, Moreno-Swirc S, Bourg-Heckly G (2008) In-vivo confocal endomicroscopy of peripheral lung nodules using 488nm/660nm induced fluorescence and topical methylene blue. European Respiratory Society, Berlin, pp 263s-264s

206. Thiberville L, Salaun M, Moreno-Swirc S, Bourg-Heckly G (2007) Alveoscopy in diffuse interstitial lung disease. European Respiratory Journal:712S

207. Keller C, Erasmus D, Alvarez F, Wallace M (2010) Preliminary observations in the use of confocal alveolar endomicroscopy in recipients of single lung transplantation. Am J Respir Crit Care Med 181:A4316

208. Salaun M, Roussel F, Bourg-Heckly G, Vever-Bizet C, Dominique S, Genevois A, Jounieaux V, Zalcman G, Bergot E, Jean-Michel V, Thiberville L (2012) In vivo probe-based confocal laser endomicroscopy in amiodarone-related pneumonia. Eur Respir J in press

209. Yserbyt J, Alame T, Dooms C, Ninane V (2013) Pulmonary alveolar microlithiasis and probe-based confocal laser endomicroscopy. J Bronchology Interv Pulmonol 20:159-163

210. Bickenbach J, Czaplik M, Dembinski R, Pelosi P, Schroeder W, Marx G, Rossaint R (2010) In vivo microscopy in a porcine model of acute lung injury. Respir Physiol Neurobiol 172:192-200

211. Namati E, Thiesse J, de Ryk J, McLennan G (2008) In vivo assessment of alveolar morphology using a flexible catheter-based confocal microscope. Computer Vision, IET 2:228-235

212. Chagnon F, Fournier C, Charette PG, Moleski L, Payet MD, Dobbs LG, Lesur O (2010) In vivo intravital endoscopic confocal fluorescence microscopy of normal and acutely injured rat lungs. Laboratory Investigation 90:824-834

213. Morisse H, Heyman L, Salaun M, Favennec L, Picquenot JM, Bohn P, Thiberville L (2013) In vivo molecular microimaging of pulmonary aspergillosis. Med Mycol 51:352-360

214. Sutton C, Ewen S, Whitelaw N, Haines P (1994) Prospective, randomized, double-blind, controlled trial of laser laparoscopy in the treatment of pelvic pain associated with minimal, mild, and moderate endometriosis. Fertility and sterility 62:696

215. Swank DJ, Swank-Bordewijk SCG, Hop WCJ, van Erp WFM, Janssen IMC, Bonjer HJ, Jeekel J (2003) Laparoscopic adhesiolysis in patients with chronic abdominal pain: a blinded randomised controlled multi-centre trial. The Lancet 361:1247-1251

216. Brandt CP, Priebe PP, Eckhauser ML (1993) Diagnostic laparoscopy in the intensive care patient. Surgical Endoscopy 7:168-172

217. Hariharan D, Constantinides VA, Froeling FE, Tekkis PP, Kocher HM (2010) The role of laparoscopy and laparoscopic ultrasound in the preoperative staging of pancreatico-biliary cancers: a meta-analysis. Eur J Surg Oncol 36:941-948

218. Hazey J, Narula V, Renton D, Reavis K, Paul C, Hinshaw K, Muscarella P, Ellison E, Melvin W (2008) Natural-orifice transgastric endoscopic peritoneoscopy in humans: Initial clinical trial. Surgical Endoscopy 22:16-20

219. Voermans RP, Sheppard B, van Berge Henegouwen MI, Fockens P, Faigel DO (2009) Comparison of Transgastric NOTES and laparoscopic peritoneoscopy for detection of peritoneal metastases. Ann Surg 250:255-259

220. Steele K, Schweitzer MA, Lyn-Sue J, Kantsevoy SV (2008) Flexible transgastric peritoneoscopy and liver biopsy: a feasibility study in human beings (with videos). Gastrointest Endosc 68:61-66

221. Voermans RP, van Berge Henegouwen MI, Bemelman WA, Fockens P (2009) Feasibility of transgastric and transcolonic natural orifice transluminal endoscopic surgery peritoneoscopy combined with intraperitoneal EUS. Gastrointestinal Endoscopy 69:e61-e67

222. Mieog J, Hutteman M, van der Vorst J, Kuppen P, Que I, Dijkstra J, Kaijzel E, Prins F, Lowik C, Smit V, van de Velde C, Vahrmeijer A (2011) Image-guided tumor resection using real-time near-infrared fluorescence in a syngeneic rat model of primary breast cancer. Breast Cancer Research and Treatment 128:679-689

223. Cahill RA, Asakuma M, Trunzo J, Schomisch S, Wiese D, Saha S, Dallemagne B, Marks J, Marescaux J (2010) Intraperitoneal virtual biopsy by fibered optical coherence tomography (OCT) at natural orifice transluminal endoscopic surgery (NOTES). J Gastrointest Surg 14:732-738

224. Rao G, Mansard M, Rebala P, Sekaran A, Reddy D (2009) Endocytoscopy assisted laparoscopic intraoperative diagnosis of disseminated malignancy. Surgical Endoscopy 23:2395-2396

225. McKinlay R, Sanfiel F, Roth JS (2005) The current role of laparoscopy in staging upper gastrointestinal malignancies. Current Surgery 62:35-37

226. Goetz M, Deris I, Vieth M, Murr E, Hoffman A, Delaney P, Galle PR, Neurath MF, Kiesslich R (2010) Near-infrared confocal imaging during mini-laparoscopy: a novel rigid endomicroscope with increased imaging plane depth. J Hepatol 53:84-90

227. Konda VJ, Aslanian HR, Wallace MB, Siddiqui UD, Hart J, Waxman I (2011) First assessment of needle-based confocal laser endomicroscopy during EUS-FNA procedures of the pancreas (with videos). Gastrointest Endosc 74:1049-1060

228. Brugge WR, Lewandrowski K, Lee-Lewandrowski E, Centeno BA, Szydlo T, Regan S, del Castillo CF, Warshaw AL (2004) Diagnosis of pancreatic cystic neoplasms: a report of the cooperative pancreatic cyst study. Gastroenterology 126:1330-1336

229. DelMaschio A, Vanzulli A, Sironi S, Castrucci M, Mellone R, Staudacher C, Carlucci M, Zerbi A, Parolini D, Faravelli A (1991) Pancreatic cancer versus chronic pancreatitis: diagnosis with CA 19-9 assessment, US, CT, and CT-guided fine-needle biopsy. Radiology 178**:**95-99

230. Oh HC, Seo DW, Song TJ, Moon SH, Park DH, Soo Lee S, Lee SK, Kim MH, Kim J (2011) Endoscopic ultrasonography-guided ethanol lavage with paclitaxel injection treats patients with pancreatic cysts. Gastroenterology 140**:**172-179

231. Bergers G, Benjamin LE (2003) Tumorigenesis and the angiogenic switch. Nat Rev Cancer 3**:**401-410

232. Foersch S, Kiesslich R, Waldner MJ, Delaney P, Galle PR, Neurath MF, Goetz M (2010) Molecular imaging of VEGF in gastrointestinal cancer in vivo using confocal laser endomicroscopy. Gut 59**:**1046-1055

233. Laemmel E, Genet M, Le Goualher G, Perchant A, Le Gargasson JF, Vicaut E (2004) Fibered confocal fluorescence microscopy (Cell-vizio) facilitates extended imaging in the field of microcirculation. A comparison with intravital microscopy. J Vasc Res 41**:**400-411

234. Meining A, Bajbouj M, Schmid RM (2007) Confocal fluorescence microscopy for detection of gastric angiodysplasia. Endoscopy 39 Suppl 1**:**E145

235. Dietrich A, Stewart J, Huether M, Helm M, Schuetze C, Schnittler HJ, Jaffray DA, Kunz-Schughart LA (2013) Macromolecule Extravasation-Xenograft Size Matters: A Systematic Study Using Probe-Based Confocal Laser Endomicroscopy (pCLE). Mol Imaging Biol 15(6)**:**693-702

236. Schwitalla S, Ziegler P, Horst D, Becker V, Kerle I, Begus-Nahrmann Y, Lechel A, Rudolph L, Langer R, Slotta-Huspenina J, Bader F, Prazeres da Costa O, Neurath M, Meining A, Kirchner T, Greten F (2013) Loss of p53 in Enterocytes Generates an Inflammatory Microenvironment Enabling Invasion and Lymph Node Metastasis of Carcinogen-Induced Colorectal Tumors. Cancer Cell 23**:**93-106

237. Polglase AL, McLaren WJ, Skinner SA, Kiesslich R, Neurath MF, Delaney PM (2005) A fluorescence confocal endomicroscope for in vivo microscopy of the upper- and the lower-GI tract. Gastrointestinal Endoscopy 62**:**686-695

238. Zuo XL, Li Z, Liu XP, Li CQ, Ji R, Wang P, Zhou CJ, Liu H, Li YQ (2012) Propofol vs midazolam plus fentanyl for upper gastrointestinal endomicroscopy: a randomized trial. World J Gastroenterol 18**:**1814-1821

239. Liu H, Li YQ, Yu T, Zhao YA, Zhang JP, Zhang JN, Guo YT, Xie XJ, Zhang TG, Desmond PV (2008) Confocal endomicroscopy for in vivo detection of microvascular architecture in normal and malignant lesions of upper gastrointestinal tract. J Gastroenterol Hepatol 23**:**56-61

240. Xu C, Ussui V, Staggs EG, Hardee DJ, Wallace MB (2013) Tu1956 Use of Distal Attachment CAP to Enhance Image Stabilization in Probe-Based Confocal Laser

Endomicroscopy: A Randomized Double Blind Trial. Gastroenterology 144:S-890

241. Pogorzelski B, Hanenkamp U, Goetz M, Kiesslich R, Gosepath J (2012) Systematic intraoperative application of confocal endomicroscopy for early detection and resection of squamous cell carcinoma of the head and neck: a preliminary report. Arch Otolaryngol Head Neck Surg 138:404-411

242. Nguyen NQ, Biankin AV, Leong RW, Chang DK, Cosman PH, Delaney P, Kench JG, Merrett ND (2009) Real time intraoperative confocal laser microscopy-guided surgery. Ann Surg 249:735-737

243. Latt WT, Newton RC, Visentini-Scarzanella M, Payne CJ, Noonan DP, Shang J, Yang GZ (2011) A hand-held instrument to maintain steady tissue contact during probe-based confocal laser endomicroscopy. IEEE Trans Biomed Eng 58:2694-2703

244. Ti Y, Lin WC (2008) Effects of probe contact pressure on in vivo optical spectroscopy. Opt Express 16:4250-4262

245. Newton RC, Noonan D, Payne C, Andreyev J, Di Marco A, Scarzanella MV, Darzi A, Yang G-Z (2011) Probe tip contact force and bowel distension affect crypt morphology during confocal endomicroscopy. Gut 60:A12-A13

246. Rosa B, Erden M, Vercauteren T, Herman B, Szewczyk J, Morel G (2013) Building large mosaics of confocal endomicroscopic images using visual servoing. IEEE Trans Biomed Eng 60:1041-1049

247. Atasoy S, Mateus D, Meining A, Yang G-Z, Navab N, Fichtinger G, Martel A, Peters T (2011) Targeted Optical Biopsies for Surveillance Endoscopies. Medical Image Computing and Computer-Assisted Intervention - MICCAI 2011, Springer Berlin / Heidelberg, pp 83-90

248. Mountney P, Giannarou S, Elson D, Yang G-Z, Hawkes D, Rueckert D, Noble A, Taylor C (2009) Optical Biopsy Mapping for Minimally Invasive Cancer Screening. Medical Image Computing and Computer-Assisted Intervention - MICCAI 2009, Springer Berlin / Heidelberg, pp 483-490

249. Jeffery PK (2001) Remodeling in asthma and chronic obstructive lung disease. Am J Respir Crit Care Med 164:S28-38

250. Wilks S (1857) Ossific deposits in the larynx, trachea and bronchi. Transactions of the Pathological Society of London 8:88

251. Lesser A (1877) Ein Fall von Enchondroma osteiodes mixtum der Lunge mit partieller amyloid Entortung. Virchows Arch (Path Anat) 69:404-408

252. Leske V, Lazor R, Coetmeur D, Crestani B, Chatte G, Cordier JF (2001) Tracheobronchopathia osteochondroplastica: a study of 41 patients. Medicine (Baltimore) 80:378-390

253. Puchtler H, Sweat F, Levine M (1962) On the Binding of Congo Red by Amyloid. J Histochem Cytochem 10:355-364

254. Camus P, Piard F, Ashcroft T, Gal AA, Colby TV (1993) The lung in inflammatory bowel disease. Medicine (Baltimore) 72:151-183

255. Meisamy S, Bolan PJ, Baker EH, Bliss RL, Gulbahce E, Everson LI, Nelson MT, Emory TH, Tuttle TM, Yee D, Garwood M (2004) Neoadjuvant chemotherapy of locally advanced breast cancer: predicting response with in vivo (1)H MR spectroscopy--a pilot study at 4 T. Radiology 233:424-431

256. Hiotis SP, Weber SM, Cohen AM, Minsky BD, Paty PB, Guillem JG, Wagman R, Saltz LB, Wong WD (2002) Assessing the predictive value of clinical complete response to neoadjuvant therapy for rectal cancer: an analysis of 488 patients. J Am Coll Surg 194:131-135; discussion 135-136

257. Habr-Gama A (2006) Assessment and management of the complete clinical response of rectal cancer to chemoradiotherapy. Colorectal Dis 8 Suppl 3:21-24

258. Wynn GR, Bhasin N, Macklin CP, George ML (2009) Complete clinical response to neoadjuvant chemoradiotherapy in patients with rectal cancer: opinions of British and Irish specialists. Colorectal Dis

259. Kuremsky JG, Tepper JE, McLeod HL (2009) Biomarkers for response to neoadjuvant chemoradiation for rectal cancer. Int J Radiat Oncol Biol Phys 74:673-688

260. Brettingham-Moore KH, Duong CP, Greenawalt DM, Heriot AG, Ellul J, Dow CA, Murray WK, Hicks RJ, Tjandra J, Chao M, Bui A, Joon DL, Thomas RJ, Phillips WA (2011) Pretreatment transcriptional profiling for predicting response to neoadjuvant chemoradiotherapy in rectal adenocarcinoma. Clin Cancer Res 17:3039-3047

261. Shanmugan S, Arrangoiz R, Nitzkorski JR, Yu JQ, Li T, Cooper H, Konski A, Farma JM, Sigurdson ER (2012) Predicting pathological response to neoadjuvant chemoradiotherapy in locally advanced rectal cancer using 18FDG-PET/CT. Ann Surg Oncol 19:2178-2185

262. Goldberg N, Kundel Y, Purim O, Bernstine H, Gordon N, Morgenstern S, Idelevich E, Wasserberg N, Sulkes A, Groshar D, Brenner B (2012) Early prediction of histopathological response of rectal tumors after one week of preoperative radiochemotherapy using 18 F-FDG PET-CT imaging. A prospective clinical study. Radiat Oncol 7:124

263. Luxton G, Hancock SL, Boyer AL (2004) Dosimetry and radiobiologic model comparison of IMRT and 3D conformal radiotherapy in treatment of carcinoma of the prostate. International Journal of Radiation Oncology Biology Physics 59:267-284

264. Zelefsky MJ, Levin EJ, Hunt M, Yamada Y, Shippy AM, Jackson A, Amols HI (2008) Incidence of Late Rectal and Urinary Toxicities After Three-Dimensional Conformal Radiotherapy and Intensity-Modulated Radiotherapy for Localized Prostate Cancer. International Journal of Radiation Oncology, Biology and Physics 70:1124-1129

265. Gelber RD, Goldhirsch A, Cole BF, Wieand HS, Schroeder G, Krook JE (1996) A quality-adjusted time without symptoms or toxicity (Q-TWiST) analysis of adjuvant radiation therapy and chemotherapy for resectable rectal cancer. J Natl Cancer Inst 88:1039-1045

266. Dahlberg M, Glimelius B, Graf W, Pahlman L (1998) Preoperative irradiation affects functional results after surgery for rectal cancer: results from a randomized study. Dis Colon Rectum 41:543-549; discussion 549-551

267. Rubin P, Casarett GW (1968) Clinical radiation pathology as applied to curative radiotherapy. Cancer 22:767-778

268. Hovdenak N, Fajardo LF, Hauer-Jensen M (2000) Acute radiation proctitis: a sequential clinicopathologic study during pelvic radiotherapy. Int J Radiat Oncol Biol Phys 48:1111-1117

269. Hovdenak N, SÃ¸rbye H, Dahl O (2005) Sucralfate Does Not Ameliorate Acute Radiation Proctitis: Randomised Study and Meta-analysis. Clinical Oncology 17:485-491

270. Denton AS, Andreyev HJ, Forbes A, Maher EJ (2002) Systematic review for non-surgical interventions for the management of late radiation proctitis. Br J Cancer 87:134-143

271. Gami B, Harrington K, Blake P, Dearnaley D, Tait D, Davies J, Norman AR, Andreyev HJ (2003) How patients manage gastrointestinal symptoms after pelvic radiotherapy. Aliment Pharmacol Ther 18:987-994

272. Warren S (1980) Effects of radiation on normal tissues. CA: A Cancer Journal for Clinicians 30:350-355

273. Hasleton PS, Carr N, Schofield PF (1985) Vascular changes in radiation bowel disease. Histopathology 9:517-534

274. Haboubi NY, Schofield PF, Rowland PL (1988) The light and electron microscopic features of early and late phase radiation-induced proctitis. Am J Gastroenterol 83:1140-1144

275. Carr ND, Pullen BR, Hasleton PS, Schofield PF (1984) Microvascular studies in human radiation bowel disease. Gut 25:448-454

276. Covington JA, Wedlake L, Andreyev J, Ouaret N, Thomas MG, Nwokolo CU, Bardhan KD, Arasaradnam RP (2013) The detection of patients at risk of gastrointestinal toxicity during pelvic radiotherapy by electronic nose and FAIMS: a pilot study. Sensors (Basel) 12:13002-13018

277. Pilepich MV, Asbell SO, Krall JM, Baerwald WH, Sause WT, Rubin P, Emami BN, Pidcock GM (1987) Correlation of radiotherapeutic parameters and treatment related morbidity--analysis of RTOG study 77-06. International Journal of Radiation Oncology Biology Physics 13:1007-1012

278. Khalid U, McGough C, Hackett C, Blake P, Harrington KJ, Khoo VS, Tait D, Norman AR, Andreyev HJN (2006) A modified inflammatory bowel disease

questionnaire and the Vaizey Incontinence questionnaire are more sensitive measures of acute gastrointestinal toxicity during pelvic radiotherapy than RTOG grading. International Journal of Radiation Oncology Biology Physics 64:1432-1441

279. Guyatt G, Mitchell A, Irvine EJ, Singer J, Williams N, Goodacre R, Tompkins C (1989) A new measure of health status for clinical trials in inflammatory bowel disease. Gastroenterology 96:804-810

280. Hanauer SB, Robinson M, Pruitt R, Lazenby AJ, Persson T, Nilsson LG, Walton-Bowen K, Haskell LP, Levine JG (1998) Budesonide enema for the treatment of active, distal ulcerative colitis and proctitis: a dose-ranging study. U.S. Budesonide enema study group. Gastroenterology 115:525-532

281. Bergin C, Müller N, Nichols D, Lillington G, Hogg J, Mullen B, Grymaloski M, Osborne S, Pare P (1986) The diagnosis of emphysema. A computed tomographic-pathologic correlation. The American review of respiratory disease 133:541

282. Newton RC, Kemp SV, Yang G-Z, Darzi A, Sheppard MN, Shah PL (2011) Tracheobronchial Amyloidosis and Confocal Endomicroscopy. Respiration 82:209-211

283. Lesur O, Thiberville L (2009) Vers une évaluation in vivo, en temps réel, de la réparation pulmonaire dans le SDRA : une place pour la micro-imagerie de fluorescence par laser confocal ? Réanimation 18:111-113

284. Horsfield K, Cumming G (1968) Morphology of the bronchial tree in man. J Appl Physiol 24:373-383

285. Leslie KO, Gruden JF, Parish JM, Scholand MB (2007) Transbronchial biopsy interpretation in the patient with diffuse parenchymal lung disease. Arch Pathol Lab Med 131:407-423

286. Raghu G, Nicholson AG, Lynch D (2008) The classification, natural history and radiological/histological appearance of idiopathic pulmonary fibrosis and the other idiopathic interstitial pneumonias. European Respiratory Review 17:108-115

287. Honda T, Ota H, Arai K, Hayama M, Fujimoto K, Yamazaki Y, Haniuda M (2002) Three-dimensional analysis of alveolar structure in usual interstitial pneumonia. Virchows Arch 441:47-52

288. Mariani TJ, Crouch E, Roby JD, Starcher B, Pierce RA (1995) Increased elastin production in experimental granulomatous lung disease. Am J Pathol 147:988-1000

289. Deslee G, Woods JC, Moore CM, Liu L, Conradi SH, Milne M, Gierada DS, Pierce J, Patterson A, Lewit RA, Battaile JT, Holtzman MJ, Hogg JC, Pierce RA (2009) Elastin expression in very severe human COPD. Eur Respir J 34:324-331

290. Hoff CR, Perkins DR, Davidson JM (1999) Elastin gene expression is upregulated during pulmonary fibrosis. Connect Tissue Res 40:145-153

291. Black PN, Ching PS, Beaumont B, Ranasinghe S, Taylor G, Merrilees MJ (2008) Changes in elastic fibres in the small airways and alveoli in COPD. Eur Respir J 31:998-1004

292. Rabe KF, Hurd S, Anzueto A, Barnes PJ, Buist SA, Calverley P, Fukuchi Y, Jenkins C, Rodriguez-Roisin R, van Weel C, Zielinski J (2007) Global strategy for the diagnosis, management, and prevention of chronic obstructive pulmonary disease: GOLD executive summary. Am J Respir Crit Care Med 176:532-555

293. Toshima M, Ohtani Y, Ohtani O (2004) Three-dimensional architecture of elastin and collagen fiber networks in the human and rat lung. Arch Histol Cytol 67:31-40

294. Liebow AA (1959) Pulmonary emphysema with special reference to vascular changes. The American review of respiratory disease 80:67-93

295. Wiebe BM, Laursen H (1998) Lung morphometry by unbiased methods in emphysema: bronchial and blood vessel volume, alveolar surface area and capillary length. APMIS 106:651-656

296. Peinado VI, Pizarro S, Barbera JA (2008) Pulmonary vascular involvement in COPD. Chest 134:808-814

297. Ghio AJ, Sangani RG, Brighton LE, Carson JL (2009) MRT letter: Auto-fluorescence by human alveolar macrophages after in vitro exposure to air pollution particles. Microsc Res Tech

298. Jean F, Bourg-Heckly G, Viellerobe B (2007) Fibered confocal spectroscopy and multicolor imaging system for in vivo fluorescence analysis. Opt Express 15:4008-4017

299. Kennedy GT, Manning HB, Elson DS, Neil MA, Stamp GW, Viellerobe B, Lacombe F, Dunsby C, French PM (2009) A fluorescence lifetime imaging scanning confocal endomicroscope. J Biophotonics 3:103-107

300. Shahab L, Jarvis MJ, Britton J, West R (2006) Prevalence, diagnosis and relation to tobacco dependence of chronic obstructive pulmonary disease in a nationally representative population sample. Thorax 61:1043-1047

301. (Summer 2006) Health statistics quarterly 30, London : Stationery Office, 1999-

302. (2004) Chronic obstructive pulmonary disease. National clinical guideline on management of chronic obstructive pulmonary disease in adults in primary and secondary care. Thorax 59 Suppl 1:1-232

303. Mclean AN, Sproule MW, Cowan MD, Thomson NC (1998) High resolution computed tomography in asthma. Thorax 53::308-314

304. Newton R, Yang G-Z (2010) In vivo imaging for cell therapy. In: Polak J (ed) Cell Therapy for Lung Disease, Imperial College Press, London

305. Cohen J (1960) A Coefficient of Agreement for Nominal Scales. Educational and Psychological Measurement 20:37-46

306. Landis JR, Koch GG (1977) An application of hierarchical kappa-type statistics in the assessment of majority agreement among multiple observers. Biometrics 33:363-374

307. Randolph JJ ((2008)) Online Kappa Calculator.

308. Krippendorff K (1980) Content analysis : an introduction to its methodology, 3rd ed. edn, SAGE, Los Angeles ; London

309. Yserbyt J, Dooms C, Decramer M, Verleden GM (2013) Probe-based confocal laser endomicroscopy of the respiratory tract: A data consistency analysis. Respir Med 107:1234-1240

310. Tous R, Delgado J, Zinkl T, Toran P, Alcalde G, Goetz M, Ferrer Roca O (2012) The Anatomy of an Optical Biopsy Semantic Retrieval System. MultiMedia, IEEE 19:16-27

311. Noonan D, Payne CJ, Shang J, Sauvage V, Newton R, Elson D, Darzi A, Yang G-Z (2010) Force Adaptive Multi-spectral Imaging with an Articulated Robotic Endoscope. Med Image Comput Comput Assist Interv 13:245-252

312. Fung YC, Zweifach BW (1971) Microcirulation - mechanics of blood flow in capillaries. Annu Rev Fluid Mech 3:181-192

313. Zimmerman LM, Veith I (1993) Great ideas in the history of surgery. Norman surgery series no. 7, Norman Pub., San Francisco, pp xii, 587 p.

314. Carter FJ, Frank TG, Davies PJ, McLean D, Cuschieri A (2001) Measurements and modelling of the compliance of human and porcine organs. Med Image Anal 5:231-236

315. Klaesner JW, Hastings MK, Zou D, Lewis C, Mueller MJ (2002) Plantar tissue stiffness in patients with diabetes mellitus and peripheral neuropathy. Arch Phys Med Rehabil 83:1796-1801

316. Phipps S, Yang THJ, Habib FK, Reuben RL, McNeill SA (2005) Measurement of the mechanical characteristics of benign prostatic tissue: A Novel method for assessing benign prostatic disease. Urology 65:1024-1028

317. Phipps S, Yang THJ, Habib FK, Reuben RL, McNeill SA (2005) Measurement of tissue mechanical characteristics to distinguish between benign and malignant prostatic disease. Urology 66:447-450

318. Dobrev H (2000) Use of Cutometer to assess epidermal hydration. Skin Research and Technology 6:239-244

319. Yamamoto Y, Kawai K (1999) Development of measuring method for softness of epidermis using rotational step response. Instrumentation and Measurement Technology Conference, 1999. IMTC/99. Proceedings of the 16th IEEE, pp 359-364 vol.351

320. Ophir J, Céspedes I, Ponnekanti H, Yazdi Y, Li X (1991) Elastography: A quantitative method for imaging the elasticity of biological tissues. Ultrasonic Imaging 13**:**111-134

321. Waage JER, Havre RF, Ødegaard S, Leh S, Eide GE, Baatrup G (2011) Endorectal elastography in the evaluation of rectal tumours. Colorectal Disease 13**:**1130-1137

322. Binnig G, Quate CF, Gerber C (1986) Atomic Force Microscope. Physical Review Letters 56**:**930

323. Lekka M, Laidler P, Gil D, Lekki J, Stachura Z, Hrynkiewicz AZ (1999) Elasticity of normal and cancerous human bladder cells studied by scanning force microscopy. European Biophysics Journal 28**:**312-316

324. Cross SE, Jin Y-S, Rao J, Gimzewski JK (2007) Nanomechanical analysis of cells from cancer patients. Nat Nano 2**:**780-783

325. Paszek MJ, Weaver VM (2004) The Tension Mounts: Mechanics Meets Morphogenesis and Malignancy. Journal of Mammary Gland Biology and Neoplasia 9**:**325-342

326. Paszek MJ, Zahir N, Johnson KR, Lakins JN, Rozenberg GI, Gefen A, Reinhart-King CA, Margulies SS, Dembo M, Boettiger D, Hammer DA, Weaver VM (2005) Tensional homeostasis and the malignant phenotype. Cancer Cell 8**:**241-254

327. Netti PA, Berk DA, Swartz MA, Grodzinsky AJ, Jain RK (2000) Role of Extracellular Matrix Assembly in Interstitial Transport in Solid Tumors. Cancer Research 60**:**2497-2503

328. Clark J, Sodergren M, Noonan D, Shang J, Payne C, James D, Athanasiou T, Teare J, Darzi A, Yang GZ (2010) A novel articulated robotic laparoscope for single incision and natural orifice surgical applications: preliminary usability trials in a live porcine model. Surgical Endoscopy 24(1)**:**690

329. Shang J, Noonan D, Payne C, Clark J, Sodergren M, Darzi A, Yang G-Z (2011) An Articulated Universal Joint Based Flexible Access Robot for Minimally Invasive Surgery. International Conference on Robotics and Automation, IEEE, Shanghai, China, pp 1147-1152

330. Sánchez-Margallo F, Moyano-Cuevas J, Latorre R, Maestre J, Correa L, Pagador J, Sánchez-Peralta L, Sánchez-Margallo J, Usón-Gargallo J Anatomical changes due to pneumoperitoneum analyzed by MRI: an experimental study in pigs. Surgical and Radiologic Anatomy 33**:**389-396

331. Andersson LE, Baath M, Thorne A, Aspelin P, Odeberg-Wernerman S (2005) Effect of carbon dioxide pneumoperitoneum on development of atelectasis during anesthesia, examined by spiral computed tomography. Anesthesiology 102**:**293-299

332. Shamiyeh A, Glaser K, Kratochwill H, Hörmandinger K, Fellner F, Wayand W, Zehetner J (2009) Lifting of the umbilicus for the installation of pneumoperitoneum with the Veress needle increases the distance to the retroperitoneal and intraperitoneal structures. Surgical Endoscopy 23:313-317

333. Henrikson RC, Kaye GI, Mazurkiewicz JE (1997) Histology, 1st edn, Williams & Wilkins, Baltimore

334. Hollenstein M, Nava A, Valtorta D, Snedeker J, Mazza E (2006) Mechanical Characterization of the Liver Capsule and Parenchyma. Biomedical Simulation, Springer Berlin / Heidelberg, pp 150-158

335. Kuntz E, Kuntz H-D (2006) Hepatology : principles and practice : history, morphology, biochemistry, diagnostics, clinic, therapy, 2nd edn, Springer, Heidelberg ;

336. Tehver J, Grahame T (1931) The Capsule and Trabeculae of the Spleens of Domestic Mammals. J Anat 65:473-481

337. Ignat M, Aprahamian M, Lindner V, Altmeyer A, Perretta S, Dallemagne B, Mutter D, Marescaux J (2009) Feasibility and reliability of pancreatic cancer staging using fiberoptic confocal fluorescence microscopy in rats. Gastroenterology 137:1584-1592 e1581

338. von Delius S, Schorn A, Grimm M, Schneider A, Wilhelm D, Schuster T, Stangassinger M, Feussner H, Schmid RM, Meining A (2011) Natural-orifice transluminal endoscopic surgery: low-pressure pneumoperitoneum is sufficient and is associated with an improved cardiopulmonary response (PressurePig Study). Endoscopy 43:808-815

339. Sugrue M (2005) Abdominal compartment syndrome. Current Opinion in Critical Care 11:333-338

340. Summers AM, Clancy MJ, Syed F, Harwood N, Brenchley PE, Augustine T, Riad H, Hutchison AJ, Taylor P, Pearson R, Gokal R (2005) Single-center experience of encapsulating peritoneal sclerosis in patients on peritoneal dialysis for end-stage renal failure. Kidney Int 68:2381-2388

341. Williams JD, Craig KJ, Topley N, Von Ruhland C, Fallon M, Newman GR, Mackenzie RK, Williams GT (2002) Morphologic changes in the peritoneal membrane of patients with renal disease. J Am Soc Nephrol 13:470-479

342. Mettang T, Krumme B, Wilhelm A, Duschka L (2010) Endoscopic transluminal insertion of a peritoneal dialysis catheter. Perit Dial Int 30:63-65

343. Goetz M, Vieth M, Kanzler S, Galle PR, Delaney P, Neurath MF, Kiesslich R (2008) In vivo confocal laser laparoscopy allows real time subsurface microscopy in animal models of liver disease. J Hepatol 48:91-97

344. Konda VJ, Meining A, Jamil LH, Giovannini M, Hwang JH, Wallace MB, Chang KJ, Siddiqui UD, Hart J, Lo SK, Saunders MD, Aslanian HR, Wroblewski K, Waxman I (2013) A pilot study of in vivo identification of pancreatic cystic

neoplasms with needle-based confocal laser endomicroscopy under endosonographic guidance. Endoscopy 45:1006-1013

345. Powell MJD (1964) An efficient method for finding the minimum of a function of several variables without calculating derivatives. The Computer Journal 7:155-162

346. Brent RP (1973) Algorithms for minimization without derivatives, Prentice-Hall, Englewood Cliffs ; [Hemel Hempstead]

347. Rudolph A, Markstaller K, Gast KK, David M, Schreiber WG, Eberle B (2009) Visualization of alveolar recruitment in a porcine model of unilateral lung lavage using 3He-MRI. Acta Anaesthesiol Scand 53:1310-1316

348. Sisson S, Grossman JD, Getty R (1975) Sisson and Grossman's The anatomy of the domestic animals, 5th edn, Saunders, Philadelphia

349. Wallace JM, Deutsch AL (1982) Flexible fiberoptic bronchoscopy and percutaneous needle lung aspiration for evaluating the solitary pulmonary nodule. Chest 81:665-671

350. Lai RS, Lee SS, Ting YM, Wang HC, Lin CC, Lu JY (1996) Diagnostic value of transbronchial lung biopsy under fluoroscopic guidance in solitary pulmonary nodule in an endemic area of tuberculosis. Respir Med 90:139-143

351. Baaklini WA, Reinoso MA, Gorin AB, Sharafkaneh A, Manian P (2000) Diagnostic yield of fiberoptic bronchoscopy in evaluating solitary pulmonary nodules. Chest 117:1049-1054

352. de Boer S, Milne DG, Zeng I, Wilsher ML (2009) Does CT scanning predict the likelihood of a positive transbronchial biopsy in sarcoidosis? Thorax 64:436-439

353. Tachihara M, Ishida T, Kanazawa K, Sugawara A, Watanabe K, Uekita K, Moriya H, Yamazaki K, Asano F, Munakata M (2007) A virtual bronchoscopic navigation system under X-ray fluoroscopy for transbronchial diagnosis of small peripheral pulmonary lesions. Lung Cancer 57:322-327

354. Ost D, Shah R, Anasco E, Lusardi L, Doyle J, Austin C, Fein A (2008) A randomized trial of CT fluoroscopic-guided bronchoscopy vs conventional bronchoscopy in patients with suspected lung cancer. Chest 134:507-513

355. Herth FJ, Eberhardt R, Becker HD, Ernst A (2006) Endobronchial ultrasound-guided transbronchial lung biopsy in fluoroscopically invisible solitary pulmonary nodules: a prospective trial. Chest 129:147-150

356. Makris D, Scherpereel A, Leroy S, Bouchindhomme B, Faivre JB, Remy J, Ramon P, Marquette CH (2007) Electromagnetic navigation diagnostic bronchoscopy for small peripheral lung lesions. Eur Respir J 29:1187-1192

357. Geraghty PR, Kee ST, McFarlane G, Razavi MK, Sze DY, Dake MD (2003) CT-guided transthoracic needle aspiration biopsy of pulmonary nodules: needle size and pneumothorax rate. Radiology 229:475-481

358. Austin JH, Muller NL, Friedman PJ, Hansell DM, Naidich DP, Remy-Jardin M, Webb WR, Zerhouni EA (1996) Glossary of terms for CT of the lungs: recommendations of the Nomenclature Committee of the Fleischner Society. Radiology 200:327-331

359. Jones R, Baskerville A, Reid L (1975) Histochemical identification of glycoproteins in pig bronchial epithelium: (a) normal and (b) hypertrophied from enzootic pneumonia. J Pathol 116:1-11

360. Rogers CS, Abraham WM, Brogden KA, Engelhardt JF, Fisher JT, McCray PB, Jr., McLennan G, Meyerholz DK, Namati E, Ostedgaard LS, Prather RS, Sabater JR, Stoltz DA, Zabner J, Welsh MJ (2008) The porcine lung as a potential model for cystic fibrosis. Am J Physiol Lung Cell Mol Physiol 295:L240-263

361. Haworth SG, Hislop AA (1981) Adaptation of the pulmonary circulation to extra-uterine life in the pig and its relevance to the human infant. Cardiovasc Res 15:108-119

362. Smith-McCune KK, Weidner N (1994) Demonstration and characterization of the angiogenic properties of cervical dysplasia. Cancer Res 54:800-804

363. Guidi AJ, Abu-Jawdeh G, Berse B, Jackman RW, Tognazzi K, Dvorak HF, Brown LF (1995) Vascular permeability factor (vascular endothelial growth factor) expression and angiogenesis in cervical neoplasia. J Natl Cancer Inst 87:1237-1245

364. Tjalma W, Sonnemans H, Weyler J, Van Marck E, Van Daele A, van Dam P (1999) Angiogenesis in cervical intraepithelial neoplasia and the risk of recurrence. Am J Obstet Gynecol 181:554-559

365. Hlatky L, Hahnfeldt P, Folkman J (2002) Clinical Application of Antiangiogenic Therapy: Microvessel Density, What It Does and Doesn't Tell Us. Journal of the National Cancer Institute 94:883-893

366. Lin KY, Maricevich M, Bardeesy N, Weissleder R, Mahmood U (2008) In vivo quantitative microvasculature phenotype imaging of healthy and malignant tissues using a fiber-optic confocal laser microprobe. Transl Oncol 1:84-94

367. Woo TC, Joseph D, Oxer H (1997) Hyperbaric oxygen treatment for radiation proctitis. Int J Radiat Oncol Biol Phys 38:619-622

368. Chautems RC, Delgadillo X, Rubbia-Brandt L, Deleaval JP, Marti MC, Roche B (2003) Formaldehyde application for haemorrhagic radiation-induced proctitis: a clinical and histological study. Colorectal Dis 5:24-28

369. Emmanuel A, Kamm M (1999) Laser Doppler measurement of rectal mucosal blood flow. Gut 45:64

370. Larson MV, Ahlquist DA, Karlstrom L, Sarr MG (1994) Intraluminal measurement of enteric mucosal perfusion: relationship to superior mesenteric artery flow during basal and postprandial states in the dog. Surgery 115:118-126

371. Leung FW, Wong DN, Lau J, Bondoc EM, Hsu R, Leung JW (1994) Endoscopic assessment of blood flow in duodenal ulcers. Gastrointest Endosc 40:334-341

372. Gardner GP, LaMorte WW, Obi-Tabot ET, Menzoian JO (1994) Transanal intracolonic pulse oximetry as a means of monitoring the adequacy of colonic perfusion. J Surg Res 57:537-540

373. Wachter S, Gerstner N, Goldner G, Pötzi R, Wambersie A, Pötter R (2000) Endoscopic scoring of late rectal mucosal damage after conformal radiotherapy for prostatic carcinoma. Radiotherapy and Oncology 54:11-19

374. Berthrong M (1986) Pathologic changes secondary to radiation. World J Surg 10:155-170

375. Andreyev J (2007) Gastrointestinal symptoms after pelvic radiotherapy: a new understanding to improve management of symptomatic patients. Lancet Oncol 8:1007-1017

376. Coia LR, Myerson RJ, Tepper JE (1995) Late effects of radiation therapy on the gastrointestinal tract. Int J Radiat Oncol Biol Phys 31:1213-1236

377. Dimagno E, Regan P, Wilson D, Buxton J, Hattery R, Suarez J, Green P (1980) Ultrasonic Endoscope. The Lancet 315:629-631

378. Kessler WR, Imperiale TF, Klein RW, Wielage RC, Rex DK (2011) A quantitative assessment of the risks and cost savings of forgoing histologic examination of diminutive polyps. Endoscopy 43:683-691

379. Ho K-Y, Phee SJ, Shabbir A, Low SC, Huynh VA, Kencana AP, Yang K, Lomanto D, So BYJ, Wong YYJ, Chung SCS Endoscopic submucosal dissection of gastric lesions by using a Master and Slave Transluminal Endoscopic Robot (MASTER). Gastrointestinal Endoscopy 72:593-599

380. Barillot C, Haynor D, Hellier P, Patronik N, Zenati M, Riviere C (2004) Crawling on the Heart: A Mobile Robotic Device for Minimally Invasive Cardiac Interventions. Medical Image Computing and Computer-Assisted Intervention MICCAI 2004, Springer Berlin Heidelberg, pp 9-16

381. Beltran NE, Garcia LE, Garcia-Lorenzana M (2013) Gastric tissue damage analysis generated by ischemia: bioimpedance, confocal endomicroscopy, and light microscopy. Biomed Res Int 2013:824682

382. Schmidt C, Lautenschlager C, Petzold B, Sakr Y, Marx G, Stallmach A (2013) Confocal laser endomicroscopy reliably detects sepsis-related and treatment-associated changes in intestinal mucosal microcirculation. Br J Anaesth In press

383. Neumann H, Gunther C, Vieth M, Grauer M, Wittkopf N, Mudter J, Becker C, Schoerner C, Atreya R, Neurath MF (2013) Confocal laser endomicroscopy for in vivo diagnosis of Clostridium difficile associated colitis - a pilot study. PLoS One 8:e58753

384. Turcotte JF, Kao D, Mah SJ, Claggett B, Saltzman JR, Fedorak RN, Liu JJ (2013) Breaks in the wall: increased gaps in the intestinal epithelium of irritable

bowel syndrome patients identified by confocal laser endomicroscopy (with videos). Gastrointest Endosc 77**:**624-630

385. Breuskin D, Divincenzo J, Kim YJ, Urbschat S, Oertel J (2013) Confocal laser endomicroscopy in neurosurgery: a new technique with much potential. Minim Invasive Surg 2013**:**851819